Chapter

7 THEORY AND APPLICATION OF SYMMETRY REPRESENTATION PRODUCTS (CONTINUOUS ROTATION GROUPS)

7.1 Introduction to R_3 and U_2 Coupling Coefficients / 553
- A. Two-Particle Spin States: Hydrogen Hyperfine Structure / 554
- B. Two-Electron Atomic Configurations / 561
- C. Spin-Orbital Coupling / 564
- D. Geometrical Interpretation of Angular-Momentum Coupling / 567

7.2 Mathematical Relations for Coupling and Wigner 3j Coefficients / 570
- A. Scalars, Vectors, and Tensors / 570
- B. General R_3 Scalar Coupling / 573
- C. Fundamental Coupling Definitions and Symmetry Relations: The Wigner 3j Coefficient / 574
- D. Clebsch-Gordon and Wigner Coefficient Formulas / 578

7.3 Rotational Tensor Operators and the Wigner-Eckart Theorem / 584
- A. Construction of R_3 Tensor Operators / 585
- B. The Wigner-Eckart Theorem for R_3 / 597
- C. Evaluation of Crystal Field Splitting / 598
- D. Evaluation of Reduced Matrix Elements / 603

7.4 Rotational Level Splitting for High J: Semiclassical Angular Momentum Mechanics / 608
- A. Rigid Rotors ($D_\infty \supset D_2$ Symmetry) / 609
- B. Semirigid Spherical Tops Octahedral (O) Symmetry / 618

7.5 Rotating Spinor Systems and Two-Dimensional Oscillator Analogies / 628
- A. Euler-Angle Definition of Spinor States / 630
- B. Axis-Angle Definition of Spinor Operators / 631
- C. Rotational Angle Parameterization for a Classical two-dimensional Harmonic Oscillator / 634
- D. Polarization Ellipsometry Coordinates / 636
- E. Generalized Lissajous Trajectories and Related Dynamics / 641
- F. Rotational Energy (RE) Surface Description of Anharmonic Vibrations / 649

7.6 Molecular Electronic Structure / 654
- A. Electronic Models for Diatomic Molecules / 654
- B. How to "Point" Electronic Orbitals / 674

Additional Reading / 682

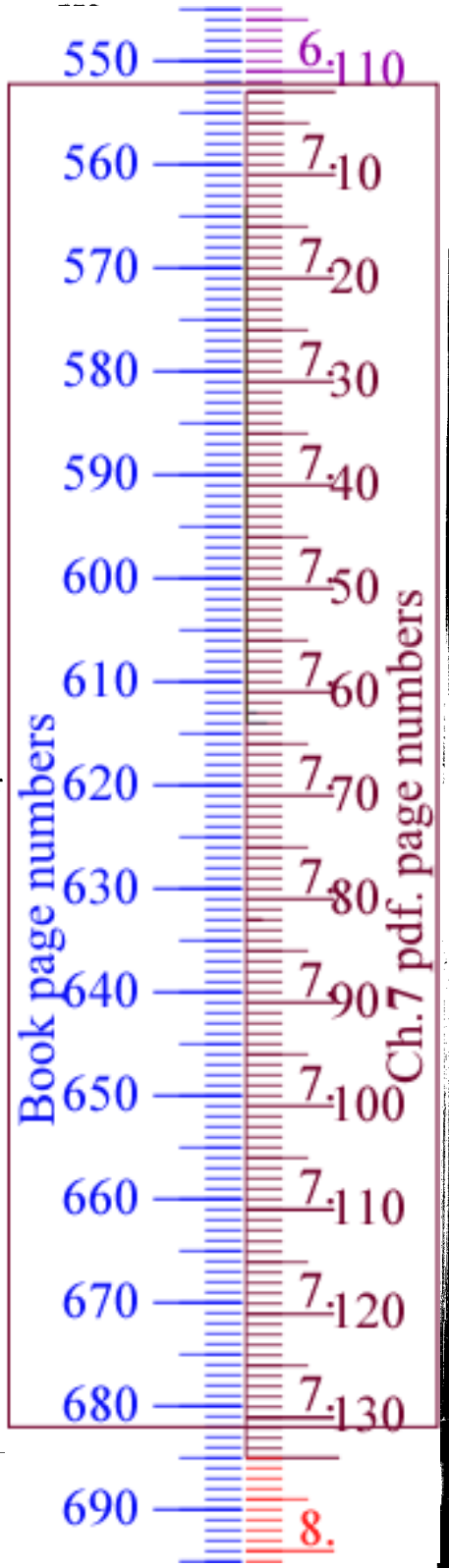

CHAPTER 7

THEORY AND APPLICATION OF SYMMETRY REPRESENTATION PRODUCTS (CONTINUOUS ROTATION GROUPS)

In many ways the basic symmetry analysis with continuous Lie groups R_3, O_3, R_4, U_2, and U_3 is similar to that of finite groups. In either case there exist irreducible representations (irreps) of finite dimension l^α which correspond to l^α-fold degenerate energy levels of a symmetric physical system. It will now be shown that the basic structure and application of irrep outer products of the continuous groups is similar to that of finite groups which was described in Chapter 6. In fact, it will not be necessary to repeat many of the details and motivation which were given in Sections 6.1 and 6.2.

The main difference between the finite and continuous symmetry analyses lies in the methods used to derive and record their structures. For the rotation group R_3 or the closely related SU_2 there exist formulas for the group structure (recall (Eqs. 5.5.10)], irreps [(Eq. 5.4.45)], characters [(Eq. 5.6.4)], and now, as we will see, the coupling coefficients. The finite group theory, on the other hand, does not always provide such convenient formulas, but then there are only a finite number of things to compute.

7.1 INTRODUCTION TO R_3 AND U_2 COUPLING COEFFICIENTS

The R_3 and U_2 coupling coefficients are introduced in this section by reviewing the simplest problems which use angular-momentum coupling. These and other problems which involve coupling will be discussed in detail, later, after a more complete mathematical treatment has been given.

A. Two-Particle Spin States: Hydrogen Hyperfine Structure

The electron and the proton each have spin-$\frac{1}{2}$ and a magnetic moment. The qualitative effects of the electron-proton spin-spin interaction in atomic hydrogen will be discussed as an example of coupling and symmetry. The spin-spin interaction is very weak compared to the Coulomb interaction, so one may assume the electron is fixed in a zero-orbit ($1s$) ground state and consider only the spin states of the electron and the proton nucleus.

If no spin-spin interaction existed the following four outer product states

$$\left|\begin{matrix}\frac{1}{2}\\ \frac{1}{2}\end{matrix}\right\rangle^{\text{proton}}\left|\begin{matrix}\frac{1}{2}\\ \frac{1}{2}\end{matrix}\right\rangle^{\text{electron}} \rightarrow \begin{pmatrix}1\\0\\0\\0\end{pmatrix}, \qquad \left|\begin{matrix}\frac{1}{2}\\ \frac{1}{2}\end{matrix}\right\rangle^{\text{proton}}\left|\begin{matrix}\frac{1}{2}\\ -\frac{1}{2}\end{matrix}\right\rangle^{\text{electron}} \rightarrow \begin{pmatrix}0\\1\\0\\0\end{pmatrix},$$

$$\left|\begin{matrix}\frac{1}{2}\\ -\frac{1}{2}\end{matrix}\right\rangle^{\text{proton}}\left|\begin{matrix}\frac{1}{2}\\ \frac{1}{2}\end{matrix}\right\rangle^{\text{electron}} \rightarrow \begin{pmatrix}0\\0\\1\\0\end{pmatrix}, \qquad \left|\begin{matrix}\frac{1}{2}\\ -\frac{1}{2}\end{matrix}\right\rangle^{\text{proton}}\left|\begin{matrix}\frac{1}{2}\\ -\frac{1}{2}\end{matrix}\right\rangle^{\text{electron}} \rightarrow \begin{pmatrix}0\\0\\0\\1\end{pmatrix}$$

would be degenerate eigenstates. As explained in Section 6.1, one could rotate either particle independently without changing the energy if the interaction is zero. All pairs of rotations $(R(\alpha_p\beta_p\gamma_p), R(\alpha_e\beta_e\gamma_e))$ form a symmetry group $G = R_3(\text{proton}) \times R_3(\text{electron})$. The base states $\left|\begin{matrix}\frac{1}{2}\\ m_1\end{matrix}\right\rangle\left|\begin{matrix}\frac{1}{2}\\ m_2\end{matrix}\right\rangle \equiv \left|\begin{matrix}\frac{1}{2} & \frac{1}{2}\\ m_1 & m_2\end{matrix}\right\rangle$ are a basis of the irrep $\mathscr{D}^{\frac{1}{2}} \otimes \mathscr{D}^{\frac{1}{2}} = \mathscr{D}^{\frac{1}{2}\frac{1}{2}}$ of G as shown by the following:

$$\begin{aligned}
&\left(R(\alpha_p\beta_p\gamma_p), R(\alpha_e\beta_e\gamma_e)\right)\left|\begin{matrix}\frac{1}{2} & \frac{1}{2}\\ m_1 & m_2\end{matrix}\right\rangle \\
&\quad = R(\alpha_p\beta_p\gamma_p)\left|\begin{matrix}\frac{1}{2}\\ m_1\end{matrix}\right\rangle R(\alpha_e\beta_e\gamma_e)\left|\begin{matrix}\frac{1}{2}\\ m_2\end{matrix}\right\rangle \\
&\quad = \sum_{m_1'} \mathscr{D}^{\frac{1}{2}}_{m_1' m_1}(\alpha_p\beta_p\gamma_p)\left|\begin{matrix}\frac{1}{2}\\ m_1'\end{matrix}\right\rangle \sum_{m_2'} \mathscr{D}^{\frac{1}{2}}_{m_2' m_2}(\alpha_p\beta_p\gamma_p)\left|\begin{matrix}\frac{1}{2}\\ m_2'\end{matrix}\right\rangle \\
&\quad = \sum_{m_1'}\sum_{m_1'} \mathscr{D}^{\frac{1}{2}}_{m_1' m_1}(\alpha_p\beta_p\gamma_p)\mathscr{D}^{\frac{1}{2}}_{m_2' m_2}(\alpha_e\beta_e\gamma_e)\left|\begin{matrix}\frac{1}{2} & \frac{1}{2}\\ m_1' & m_2'\end{matrix}\right\rangle \\
&\quad = \sum_{m_1' m_2'} \mathscr{D}^{\frac{1}{2}\frac{1}{2}}_{m_1' m_2';\, m_1 m_2}(\alpha_p\beta_p\gamma_p;\, \alpha_e\beta_e\gamma_e)\left|\begin{matrix}\frac{1}{2} & \frac{1}{2}\\ m_1' & m_2'\end{matrix}\right\rangle.
\end{aligned}$$

Using the notation of Eq. (6.1.8) the representation $\mathscr{D}^{\frac{1}{2}\frac{1}{2}}$ is written as

follows:

$$\mathscr{D}^{\frac{1}{2}\frac{1}{2}}(0\beta_p 00\beta_e 0) = \begin{pmatrix} \mathscr{D}_{\frac{1}{2}\frac{1}{2}}(0\beta_p 0)\mathscr{D}_{\frac{1}{2}\frac{1}{2}}(0\beta_e 0) & \mathscr{D}_{\frac{1}{2}\frac{1}{2}}\mathscr{D}_{\frac{1}{2}-\frac{1}{2}} & \mathscr{D}_{\frac{1}{2}-\frac{1}{2}}\mathscr{D}_{\frac{1}{2}\frac{1}{2}} & \mathscr{D}_{\frac{1}{2}-\frac{1}{2}}\mathscr{D}_{\frac{1}{2}-\frac{1}{2}} \\ \mathscr{D}_{\frac{1}{2}\frac{1}{2}}\mathscr{D}_{\frac{1}{2}\frac{1}{2}} & \mathscr{D}_{\frac{1}{2}\frac{1}{2}}\mathscr{D}_{-\frac{1}{2}-\frac{1}{2}} & \mathscr{D}_{\frac{1}{2}-\frac{1}{2}}\mathscr{D}_{-\frac{1}{2}\frac{1}{2}} & \mathscr{D}_{\frac{1}{2}-\frac{1}{2}}\mathscr{D}_{-\frac{1}{2}-\frac{1}{2}} \\ \mathscr{D}_{-\frac{1}{2}\frac{1}{2}}\mathscr{D}_{\frac{1}{2}\frac{1}{2}} & \mathscr{D}_{-\frac{1}{2}\frac{1}{2}}\mathscr{D}_{\frac{1}{2}-\frac{1}{2}} & \mathscr{D}_{-\frac{1}{2}-\frac{1}{2}}\mathscr{D}_{\frac{1}{2}\frac{1}{2}} & \mathscr{D}_{-\frac{1}{2}-\frac{1}{2}}\mathscr{D}_{\frac{1}{2}-\frac{1}{2}} \\ \mathscr{D}_{-\frac{1}{2}\frac{1}{2}}\mathscr{D}_{-\frac{1}{2}\frac{1}{2}} & \mathscr{D}_{-\frac{1}{2}\frac{1}{2}}\mathscr{D}_{-\frac{1}{2}-\frac{1}{2}} & \mathscr{D}_{-\frac{1}{2}-\frac{1}{2}}\mathscr{D}_{-\frac{1}{2}\frac{1}{2}} & \mathscr{D}_{-\frac{1}{2}-\frac{1}{2}}\mathscr{D}_{-\frac{1}{2}-\frac{1}{2}} \end{pmatrix}$$

$$= \begin{pmatrix} \cos\frac{\beta_p}{2}\cos\frac{\beta_e}{2} & -\cos\frac{\beta_p}{2}\sin\frac{\beta_e}{2} & -\sin\frac{\beta_p}{2}\cos\frac{\beta_e}{2} & \sin\frac{\beta_p}{2}\sin\frac{\beta_e}{2} \\ \cos\frac{\beta_p}{2}\sin\frac{\beta_e}{2} & \cos\frac{\beta_p}{2}\cos\frac{\beta_e}{2} & -\sin\frac{\beta_p}{2}\sin\frac{\beta_e}{2} & -\sin\frac{\beta_p}{2}\cos\frac{\beta_e}{2} \\ \sin\frac{\beta_p}{2}\cos\frac{\beta_e}{2} & -\sin\frac{\beta_p}{2}\sin\frac{\beta_e}{2} & \cos\frac{\beta_p}{2}\cos\frac{\beta_e}{2} & -\cos\frac{\beta_p}{2}\sin\frac{\beta_e}{2} \\ \sin\frac{\beta_p}{2}\sin\frac{\beta_e}{2} & \sin\frac{\beta_p}{2}\cos\frac{\beta_e}{2} & \cos\frac{\beta_p}{2}\sin\frac{\beta_e}{2} & \cos\frac{\beta_p}{2}\cos\frac{\beta_e}{2} \end{pmatrix}. \quad (7.1.2)$$

Here all Euler angles are zero except β_p and β_e. (In this section we shall not need to distinguish between representations and ray representations. We call either one an irreducible representation or irrep.)

However, with a nonzero interaction we see that $(R(\alpha_p\beta_p\gamma_p), R(\alpha_e\beta_e\gamma_e))$ is not a symmetry operator unless $\alpha_p = \alpha_e$, $\beta_p = \beta_e$, and $\gamma_p = \gamma_e$. Only the "rigid" rotations which preserve the relative orientation of the two spins are still symmetry operators. Rotation operators such as

$$\big(R(0\beta_p 0), R(0\beta_e 0)\big) = e^{\beta_p J_y^{\text{proton}}/i\hbar} e^{\beta_e J_y^{\text{electron}}/i\hbar} \quad (7.1.3)$$

generated by individual angular-momentum operators J_y^{proton} and J_y^{electron} must have equal angles ($\beta_p = \beta_e \equiv \beta$). When the angles are equal one may write the rigid rotation

$$\big(R(0\beta 0), R(0\beta 0)\big) = e^{(\beta/i\hbar)(J_y^{\text{proton}} + J_y^{\text{electron}})} = e^{(\beta/i\hbar)J_y^{\text{total}}} \quad (7.1.4)$$

in terms of the *total* angular momentum

$$\mathbf{J}^{\text{total}} = \mathbf{J}^{\text{proton}} + \mathbf{J}^{\text{electron}}. \quad (7.1.5)$$

In other words, the individual angular momenta of the proton or the electron may not be conserved when the interaction is on, but the total momentum is constant. By total momentum we mean here total spin angular momentum $\mathbf{J} = \mathbf{S}$. The orbital momentum of an s-state electron is zero. Spin-orbit interactions will be introduced in Section 7.1.C.

The irrep $\mathscr{D}^{\frac{1}{2}} \otimes \mathscr{D}^{\frac{1}{2}}$ of $R_3 \times R_3$ is a reducible representation of the rigid rotation symmetry $R_3^{\text{rigid}} = \{\cdots (R(0\beta 0), R(0\beta 0))\cdots\}$ generated by J^{total} operators. The following transformation (which we derive shortly) of the

matrix $\mathscr{D}^{\frac{1}{2}} \otimes \mathscr{D}^{\frac{1}{2}}$ gives a reduced representation:

$$\begin{pmatrix} 1 & 0 & 0 & 0 \\ 0 & \frac{1}{\sqrt{2}} & \frac{1}{\sqrt{2}} & 0 \\ 0 & 0 & 0 & 1 \\ 0 & \frac{1}{\sqrt{2}} & -\frac{1}{\sqrt{2}} & 0 \end{pmatrix} \begin{pmatrix} \cos^2\frac{\beta}{2} & -\sin\frac{\beta}{2}\cos\frac{\beta}{2} & -\sin\frac{\beta}{2}\cos\frac{\beta}{2} & \sin^2\frac{\beta}{2} \\ \sin\frac{\beta}{2}\cos\frac{\beta}{2} & \cos^2\frac{\beta}{2} & -\sin^2\frac{\beta}{2} & -\sin\frac{\beta}{2}\cos\frac{\beta}{2} \\ \sin\frac{\beta}{2}\cos\frac{\beta}{2} & -\sin^2\frac{\beta}{2} & \cos^2\frac{\beta}{2} & -\sin\frac{\beta}{2}\cos\frac{\beta}{2} \\ \sin^2\frac{\beta}{2} & \sin\frac{\beta}{2}\cos\frac{\beta}{2} & \sin\frac{\beta}{2}\cos\frac{\beta}{2} & \cos^2\frac{\beta}{2} \end{pmatrix} \begin{pmatrix} 1 & 0 & 0 & 0 \\ 0 & \frac{1}{\sqrt{2}} & 0 & \frac{1}{\sqrt{2}} \\ 0 & \frac{1}{\sqrt{2}} & 0 & -\frac{1}{\sqrt{2}} \\ 0 & 0 & 1 & 0 \end{pmatrix}$$

$$= \begin{pmatrix} \sin^2\frac{\beta}{2} & \frac{-\sin\beta}{\sqrt{2}} & \sin^2\frac{\beta}{2} & 0 \\ \frac{\sin\beta}{\sqrt{2}} & \cos\beta & \frac{-\sin\beta}{\sqrt{2}} & 0 \\ \sin^2\frac{\beta}{2} & \frac{\sin\beta}{\sqrt{2}} & \cos^2\frac{\beta}{2} & 0 \\ 0 & 0 & 0 & 1 \end{pmatrix}. \tag{7.1.6a}$$

Writing this in matrix notation, we have the following:

$$C^{\dagger}\mathscr{D}^{\frac{1}{2}}(0\beta 0) \otimes \mathscr{D}^{\frac{1}{2}}(0\beta 0)C = \left(\begin{array}{ccc|c} & \mathscr{D}^1(0\beta 0) & & \begin{matrix}0\\0\\0\end{matrix} \\ \hline 0 & 0 & 0 & \mathscr{D}^0 \end{array}\right) = \mathscr{D}^1 \oplus \mathscr{D}^0. \tag{7.1.6b}$$

The standard index notation for this is

$$\sum_{m_1 m_1'} \sum_{m_2 m_2'} C^{\frac{1}{2}\,\frac{1}{2}\,J}_{m_1 m_1' M} \mathscr{D}^{\frac{1}{2}}_{m_1 m_2} \mathscr{D}^{\frac{1}{2}}_{m_1' m_2'} C^{\frac{1}{2}\,\frac{1}{2}\,J'}_{m_2 m_2' M'} = \delta^{JJ'} \mathscr{D}^{J}_{mm'}, \tag{7.1.6c}$$

where the transformation coefficients

$$C^{\frac{1}{2}\,\frac{1}{2}\,J}_{mm'M} \equiv \left\langle \begin{matrix} \frac{1}{2} & \frac{1}{2} \\ m & m' \end{matrix} \middle| \begin{matrix} J \\ M \end{matrix} \right\rangle \tag{7.1.6d}$$

give states of definite total momentum J

$$\left| \begin{matrix} J \\ M \end{matrix} \quad \left(\tfrac{1}{2} \times \tfrac{1}{2}\right) \right\rangle = \sum_{m,m'} \left| \begin{matrix} \frac{1}{2} & \frac{1}{2} \\ m & m' \end{matrix} \right\rangle \left\langle \begin{matrix} \frac{1}{2} & \frac{1}{2} \\ m & m' \end{matrix} \middle| \begin{matrix} J \\ M \end{matrix} \right\rangle$$

$$= \sum_{m,m'} C^{\frac{1}{2}\,\frac{1}{2}\,J}_{mm'M} \left| \begin{matrix} \frac{1}{2} & \frac{1}{2} \\ m & m' \end{matrix} \right\rangle. \tag{7.1.6e}$$

At the same time it reduces the product representation $\mathscr{D}^{\frac{1}{2}} \otimes \mathscr{D}^{\frac{1}{2}}$ of the R_3^{Rigid} symmetry as shown in Eqs. (7.1.6a) and (7.1.6b)).

The $C^{\frac{1}{2}\ \frac{1}{2}\ J}_{m m' M}$ are examples of CLEBSCH-GORDON or COUPLING COEFFICIENTS of the rotation group R_3. Coupling coefficients are usually tabulated as they appear in the transformation matrix [see Eq. (7.1.6a)] by arrays of the following form:

$$\left\langle C^{\frac{1}{2}\ \frac{1}{2}\ \cdot}_{\cdot\ \cdot\ \cdot} \right\rangle_{\cdot} = \begin{array}{c|cc|ccc|c} & \frac{1}{2} & \otimes & \frac{1}{2} & 1 & 1 & 1 & 0 \\ & & & & 1 & 0 & -1 & 0 \\ \hline \frac{1}{2} & & & \frac{1}{2} & 1 & \cdot & \cdot & \cdot \\ \frac{1}{2} & & & -\frac{1}{2} & \cdot & \frac{1}{\sqrt{2}} & \cdot & \frac{1}{\sqrt{2}} \\ -\frac{1}{2} & & & \frac{1}{2} & \cdot & \frac{1}{\sqrt{2}} & \cdot & -\frac{1}{\sqrt{2}} \\ -\frac{1}{2} & & & -\frac{1}{2} & \cdot & \cdot & 1 & \cdot \end{array} . \tag{7.1.7}$$

The derivation of the coupling coefficients can be done by appealing to the generators $J_z^{\text{total}} = J_z^{\text{proton}} + J_z^{\text{electron}}$ and $J_{\pm}^{\text{total}} = J_{\pm}^{\text{proton}} + J_{\pm}^{\text{electron}}$. Applying J_z^{total} to the state

$$\left| \begin{matrix} J \\ M \end{matrix} \quad (j_1 \otimes j_2) \right\rangle = \sum_{m_1, m_2} C^{j_1\ j_2\ J}_{m_1 m_2 M} \left| \begin{matrix} j_1 & j_2 \\ m_1 & m_2 \end{matrix} \right\rangle \tag{7.1.8}$$

yields the following:

$$\begin{aligned} J_z^{\text{total}} \left| \begin{matrix} J \\ M \end{matrix} \quad (j_1 \otimes j_2) \right\rangle &= M \left| \begin{matrix} J \\ M \end{matrix} \quad (j_1 \otimes j_2) \right\rangle \\ &= \sum_{m_1, m_2} C^{j_1\ j_2\ J}_{m_1 m_2 M} \left(J_z^{\text{proton}} \left| \begin{matrix} j_1 \\ m_1 \end{matrix} \right\rangle \left| \begin{matrix} j_2 \\ m_2 \end{matrix} \right\rangle + \left| \begin{matrix} j_1 \\ m_1 \end{matrix} \right\rangle J_z^{\text{electron}} \left| \begin{matrix} j_2 \\ m_2 \end{matrix} \right\rangle \right) \\ &= \sum_{m_1, m_2} C^{j_1\ j_2\ J}_{m_1 m_2 M} (m_1 + m_2) \left| \begin{matrix} j_1 & j_2 \\ m_1 & m_2 \end{matrix} \right\rangle . \end{aligned}$$

(Here we assume general values j_1 and j_2 of spin for the proton and electron, respectively.) Using Eq. (7.1.6d) and the usual orthonormality

$$\left\langle \begin{matrix} j_1 & j_2 \\ m_1' & m_2' \end{matrix} \middle| \begin{matrix} j_1 & j_2 \\ m_1 & m_2 \end{matrix} \right\rangle = \delta_{m_1' m_1} \delta_{m_2' m_2}$$

we see that this implies that either $M = m_1 + m_2$ or $C^{j_1\ j_2\ J}_{m_1 m_2 M} = 0$. The total z

component must be the sum of the z components of the factor states. Therefore the state with the highest z component involving the two factors j_1 and j_2 must be

$$\left|\begin{matrix} j_1 & j_2 \\ j_1 & j_2 \end{matrix}\right\rangle = \left|\begin{matrix} J = j_1 + j_2 \\ \\ M = j_1 + j_2 \end{matrix} \quad (j_1 \otimes j_2)\right\rangle. \tag{7.1.9}$$

Then we apply the total lowering operator J_-^{total} to this highest state to give

$$J_-^{\text{total}} \left|\begin{matrix} J \\ \\ J \end{matrix} \quad (j_1 \otimes j_2)\right\rangle = J_-^{\text{proton}} \left|\begin{matrix} j_1 \\ j_1 \end{matrix}\right\rangle \left|\begin{matrix} j_2 \\ j_2 \end{matrix}\right\rangle + \left|\begin{matrix} j_1 \\ j_1 \end{matrix}\right\rangle J_-^{\text{electron}} \left|\begin{matrix} j_2 \\ j_2 \end{matrix}\right\rangle,$$

$$\sqrt{2(j_1+j_2)} \left|\begin{matrix} J \\ \\ J-1 \end{matrix} \quad (j_1 \otimes j_2)\right\rangle = \sqrt{2j_1} \left|\begin{matrix} j_1 & j_2 \\ j_1 - 1 & j_2 \end{matrix}\right\rangle + \sqrt{2j_2} \left|\begin{matrix} j_1 & j_2 \\ j_1 & j_2 - 1 \end{matrix}\right\rangle,$$

$$\left|\begin{matrix} J \\ \\ J-1 \end{matrix} \quad (j_1 \otimes j_2)\right\rangle = \sqrt{\frac{j_1}{j_1+j_2}} \left|\begin{matrix} j_1 & j_2 \\ j_1 - 1 & j_2 \end{matrix}\right\rangle + \sqrt{\frac{j_2}{j_1+j_2}} \left|\begin{matrix} j_1 & j_2 \\ j_1 & j_2 - 1 \end{matrix}\right\rangle, \tag{7.1.10}$$

where Eq. (5.4.23b) was used. For the proton-electron problem with $j_1 = \frac{1}{2} = j_2$, we have

$$\left|\begin{matrix} J = 1 \\ \\ M = 0 \end{matrix} \quad (\tfrac{1}{2} \otimes \tfrac{1}{2})\right\rangle = \sqrt{\frac{1}{2}} \left|\begin{matrix} \frac{1}{2} & \frac{1}{2} \\ -\frac{1}{2} & \frac{1}{2} \end{matrix}\right\rangle + \sqrt{\frac{1}{2}} \left|\begin{matrix} \frac{1}{2} & \frac{1}{2} \\ \frac{1}{2} & -\frac{1}{2} \end{matrix}\right\rangle, \tag{7.1.10}_x$$

which is the second column of the table of (7.1.7). Lowering this state again gives the third column,

$$\left|\begin{matrix} J = 1 \\ \\ M = -1 \end{matrix} \quad (\tfrac{1}{2} \otimes \tfrac{1}{2})\right\rangle = \left|\begin{matrix} \frac{1}{2} & \frac{1}{2} \\ -\frac{1}{2} & -\frac{1}{2} \end{matrix}\right\rangle.$$

Finally, the fourth column state is obtained by orthogonalizing with the other $M = 0$ state we just derived. The result is

$$\left|\begin{matrix} J = 0 \\ \\ M = 0 \end{matrix} \quad (\tfrac{1}{2} \otimes \tfrac{1}{2})\right\rangle = \sqrt{\frac{1}{2}} \left|\begin{matrix} \frac{1}{2} & \frac{1}{2} \\ \frac{1}{2} & -\frac{1}{2} \end{matrix}\right\rangle - \sqrt{\frac{1}{2}} \left|\begin{matrix} \frac{1}{2} & \frac{1}{2} \\ -\frac{1}{2} & \frac{1}{2} \end{matrix}\right\rangle. \tag{7.1.11}$$

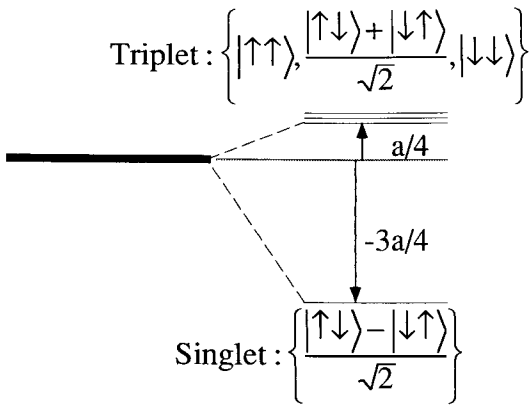

Figure 7.1.1 Singlet-triplet splitting of levels for two interacting spin-$\frac{1}{2}$ particles.

This reduction of a four-by-four representation to a three-by-three and a one-by-one representation implies a splitting of the four spin energy levels of hydrogen into a "triplet" and a "singlet," as shown in Figure 7.1.1.

The observed magnitude of this splitting is small, but very important to radio astronomers. It is one of the more accurately measured quantities: 1,420,405,751.8 $\pm$ 0.03 Hz or approximate equivalents 5.88×10^{-5} eV; 0.0474 cm^{-1}, or 1/(21.1 cm). It is the well known 21-cm line which is used to locate atomic hydrogen in intergalactic space.

The spin-spin interaction Hamiltonian which approximately gives this splitting is the Fermi contact interaction.

$$H_{\text{contact}} = aJ^{\text{proton}} \cdot J^{\text{electron}}. \tag{7.1.12a}$$

The name "contact" refers to the dependence of the interaction constant

$$a = (8\pi/3) g_e \beta_e g_p \beta_p |\psi(0)|^2 \tag{7.1.12b}$$

on the value $\psi(0)$ of the electronic wave function at the proton. For a $(1s)$ wave function one has

$$|\psi_{1s}(0)|^2 = 1/(\pi a_0^3), \tag{7.1.12c}$$

where $a_0 = \hbar^2/me^2 = 0.5292 \times 10^{-8}$ cm is the Bohr radius. The other constants are the gyromagnetic ratios g_e (= 2.0023) and g_p (= 5.585) and magneton moments β_e ($= e\hbar/2m_e c = 0.9273 \times 10^{-20}$ erg/gauss) and β_p ($= e\hbar/2m_p c = 0.50504 \times 10^{-23}$ erg/gauss) of the electron and proton, respectively. The derivation of the contact interaction follows from the Dirac equation. This may be found in most advanced quantum theory texts.

The eigenvalues of the contact interaction are easy to find if it is rewritten in terms of operators that are diagonal in the bases of triplet and singlet

states $(7.1.10)_x$ and (7.1.11):

$$aJ^{\text{proton}} \cdot J^{\text{electron}} = \frac{a}{2}\left[(J^{\text{proton}} + J^{\text{electron}})^2 - (J^{\text{proton}})^2 - (J^{\text{electron}})^2\right]$$
$$= \frac{a}{2}\left[(J^{\text{total}})^2 - (J^{\text{proton}})^2 - (J^{\text{electron}})^2\right]. \qquad (7.1.13)$$

This trick will be used again many times to evaluate the eigenvalues of interaction operators. The contact eigenvalues are

$$\left\langle \begin{matrix} J \\ M \end{matrix} \middle| H_{\text{contact}} \middle| \begin{matrix} J \\ M \end{matrix} \right\rangle = \frac{a}{2}\left[J(J+1) - \tfrac{1}{2}(\tfrac{1}{2}+1) - \tfrac{1}{2}(\tfrac{1}{2}+1)\right]$$
$$= \begin{cases} a/4 & \text{for the } (J=1) \text{ triplet state,} \\ -3a/4 & \text{for the } (J=0) \text{ singlet state.} \end{cases} \qquad (7.1.14)$$

This implies that the magnitude of the singlet-triplet splitting is equal to that of the interaction constant (a). Substituting the magnetic constants given with Eq. (7.1.12) yields the following value:

$$a(\text{calculated}) = 1.500 \times 10^{-18} \text{ erg} = 1422.74 \text{ MHz}. \qquad (7.1.15)$$

This agrees with the observed value up to the third decimal place. Further theory of relativistic spin-$\frac{1}{2}$ particles is needed to get more accuracy. However, so far no theory has the 10- or 11-place accuracy of the experiment. At the very least this is beyond our present accuracy of knowledge of most fundamental constants.

To continue the coupling analysis for more general values of angular momentum, one needs to finish the lowering job started in Eq. (7.1.10). After N lowerings the result is

$$(J_-)^N \left| \begin{matrix} J = j_1 + j_2 \\ M = j_1 + j_2 \end{matrix} \right\rangle = \sum_{n_1, n_2 = 0}^{N} \frac{N!}{n_1! n_2!} (J_-^{\text{proton}})^{n_1} \left| \begin{matrix} j_1 \\ j_1 \end{matrix} \right\rangle (J_-^{\text{electron}})^{n_2} \left| \begin{matrix} j_2 \\ j_2 \end{matrix} \right\rangle,$$

where $N = n_1 + n_2$. Using Eq. (5.4.23b) repeatedly one obtains

$$(J_-)^n \left| \begin{matrix} j \\ m \end{matrix} \right\rangle = \sqrt{\frac{(j+m)!(j-m+n)!}{(j-m)!(j+m-n)!}} \left| \begin{matrix} j \\ m-n \end{matrix} \right\rangle. \qquad (7.1.16)$$

This gives the desired result

$$\left| \begin{matrix} J = j_1 + j_2 \\ M = m_1 + m_2 \end{matrix} \right\rangle = \sum_{m_1, m_2} C^{j_1\, j_2\, J}_{m_1 m_2 M} \left| \begin{matrix} j_1 & j_2 \\ m_1 & m_2 \end{matrix} \right\rangle,$$

where $J = j_1 + j_2$ and $M = m_1 + m_2$ are maximal.

$$C^{j_1\, j_2\, J}_{m_1 m_2 M} = \sqrt{\frac{(J-M)!}{(j_1-m_1)!(j_2-m_2)!} \frac{(J+M)!}{(j_1+m_1)!(j_1+m_2)!} \frac{(2j_1)!(2j_2)!}{(2J)!}}. \qquad (7.1.17)$$

These are the coupling coefficients for the cases of highest total momentum $J = j_1 + j_2$. The coefficients for the other possibilities, $J = j_1 + j_2 - 1, j_1 + j_2 - 2, \ldots, |j_1 - j_2|$ are obtained by orthogonalization, or by a generalization of Eq. (7.1.17) which is derived in Section 7.2.D.

B. Two-Electron Atomic Configurations

Consider the elementary electronic structure of the carbon atom which has six electrons in a configuration $(1s)^2(2s)^2(2p)^2$. A very good approximate model can be made by ignoring, at first, the two pairs of electrons in the "closed" $1s$ and $2s$ shells, and treating the atom as though it had only the two $2p$ electrons. The orbital basis of this model is a ninefold product basis $\left|\begin{matrix}1\\m_1\end{matrix}\right\rangle\left|\begin{matrix}1\\m_2\end{matrix}\right\rangle$ made from the individual $2p$ orbitals.

If no electrostatic repulsion or interaction of any kind existed between the electrons then these nine states would be degenerate in energy. However, in the presence of electrostatic repulsion one takes the coupled states

$$\left|\begin{matrix}L\\M\end{matrix}\quad (2p)^2\right\rangle = \sum_{m_1, m_2} C^{1\,1\,L}_{m_1 m_2 M}\left|\begin{matrix}1\\m_1\end{matrix}\right\rangle\left|\begin{matrix}1\\m_2\end{matrix}\right\rangle \tag{7.1.18}$$

to be model eigenstates. They will generally have different energy for different values of total orbit momentum L.

Using Eq. (7.1.17) we find the $L = 2$ coupling coefficients $C^{1\,1\,2}_{m_1 m_2 M}$ shown in the left-hand block of the following table:

$$\left\langle C^{1\ 1\ \cdot}_{\cdot\ \cdot\ \cdot}\right\rangle =$$

$1 \otimes 1$	$\begin{matrix}2\\2\end{matrix}$	$\begin{matrix}2\\1\end{matrix}$	$\begin{matrix}2\\0\end{matrix}$	$\begin{matrix}2\\-1\end{matrix}$	$\begin{matrix}2\\-2\end{matrix}$	$\begin{matrix}1\\1\end{matrix}$	$\begin{matrix}1\\0\end{matrix}$	$\begin{matrix}1\\-1\end{matrix}$	$\begin{matrix}0\\0\end{matrix}$
$1\ \ 1$	1	$\cdot$	$\cdot$	$\cdot$	$\cdot$	$\cdot$	$\cdot$	$\cdot$	$\cdot$
$1\ \ 0$	$\cdot$	$\frac{1}{\sqrt{2}}$	$\cdot$	$\cdot$	$\cdot$	$\frac{1}{\sqrt{2}}$	$\cdot$	$\cdot$	$\cdot$
$1\ -1$	$\cdot$	$\cdot$	$\frac{1}{\sqrt{6}}$	$\cdot$	$\cdot$	$\cdot$	$\frac{1}{\sqrt{2}}$	$\cdot$	$\frac{1}{\sqrt{3}}$
$0\ \ 1$	$\cdot$	$\frac{1}{\sqrt{2}}$	$\cdot$	$\cdot$	$\cdot$	$-\frac{1}{\sqrt{2}}$	$\cdot$	$\cdot$	$\cdot$
$0\ \ 0$	$\cdot$	$\cdot$	$\sqrt{\frac{2}{3}}$	$\cdot$	$\cdot$	$\cdot$	$\cdot$	$\cdot$	$-\frac{1}{\sqrt{3}}$
$0\ -1$	$\cdot$	$\cdot$	$\cdot$	$\frac{1}{\sqrt{2}}$	$\cdot$	$\cdot$	$\cdot$	$\frac{1}{\sqrt{2}}$	$\cdot$
$-1\ \ 1$	$\cdot$	$\cdot$	$\frac{1}{\sqrt{6}}$	$\cdot$	$\cdot$	$\cdot$	$-\frac{1}{\sqrt{2}}$	$\cdot$	$\frac{1}{\sqrt{3}}$
$-1\ \ 0$	$\cdot$	$\cdot$	$\cdot$	$\frac{1}{\sqrt{2}}$	$\cdot$	$\cdot$	$\cdot$	$-\frac{1}{\sqrt{2}}$	$\cdot$
$-1\ -1$	$\cdot$	$\cdot$	$\cdot$	$\cdot$	1	$\cdot$	$\cdot$	$\cdot$	$\cdot$

(7.1.19)

Using the $L = 2$ results one may orthogonalize and lower to obtain the

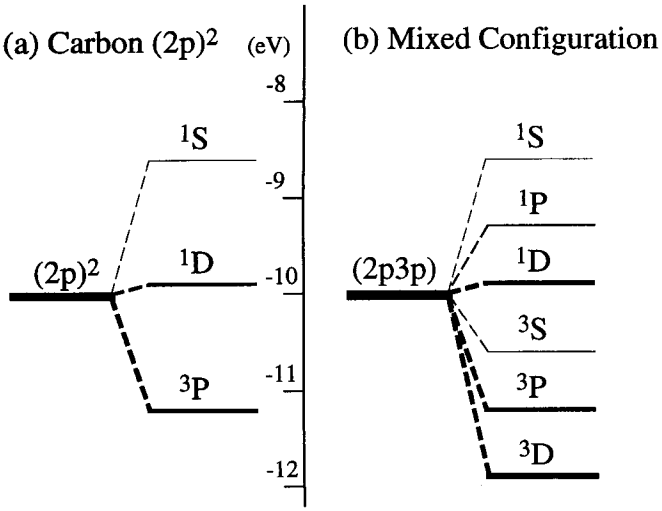

Figure 7.1.2 Atomic ^{2S+1}L multiplet levels for two ($l = 1$) p electrons. (a) Two equivalent electrons. Pauli exclusion principle allows only ^1S, ^1D, and ^3D levels for two p-electrons with the same radial quantum number. (b) Two inequivalent electrons. All combinations of spin and orbit states are allowed.

$L = 1$ and $L = 0$ states. The electrostatic interaction causes a splitting of the nine $\left|\begin{smallmatrix}1\\m_1\end{smallmatrix}\right\rangle\left|\begin{smallmatrix}1\\m_2\end{smallmatrix}\right\rangle$ levels and it results in $L = 2$, 1, and 0 levels. These are labeled by D, P, and S, respectively, in Figure 7.1.2(a), which shows the observed energies for carbon.

Now we should also consider the spins of each $2p$ electron. The correct total spin states have the same form as those derived in Eqs. (7.1.10) and (7.1.11) or Figure 7.1.1. There is a triplet set

$$\left|\begin{matrix}S=1\\M_S=1\end{matrix}\right\rangle = \left|\begin{matrix}\frac{1}{2} & \frac{1}{2}\\ \frac{1}{2} & \frac{1}{2}\end{matrix}\right\rangle, \quad \left|\begin{matrix}S=1\\M_S=0\end{matrix}\right\rangle = \left(\left|\begin{matrix}\frac{1}{2} & \frac{1}{2}\\ \frac{1}{2} & -\frac{1}{2}\end{matrix}\right\rangle + \left|\begin{matrix}\frac{1}{2} & \frac{1}{2}\\ -\frac{1}{2} & \frac{1}{2}\end{matrix}\right\rangle\right)\Big/\sqrt{2},$$

$$\left|\begin{matrix}S=1\\M_S=-1\end{matrix}\right\rangle = \left|\begin{matrix}\frac{1}{2} & \frac{1}{2}\\ -\frac{1}{2} & -\frac{1}{2}\end{matrix}\right\rangle, \tag{7.1.20a}$$

and a singlet state

$$\left|\begin{matrix}S=0\\M_S=0\end{matrix}\right\rangle = \left(\left|\begin{matrix}\frac{1}{2} & \frac{1}{2}\\ \frac{1}{2} & -\frac{1}{2}\end{matrix}\right\rangle - \left|\begin{matrix}\frac{1}{2} & \frac{1}{2}\\ -\frac{1}{2} & \frac{1}{2}\end{matrix}\right\rangle\right)\Big/\sqrt{2}. \tag{7.1.20b}$$

The model atomic states are a product of an $\left|\begin{matrix} L \\ M \end{matrix}\right\rangle$ orbital state with a triplet spin state to give a triplet atomic term state

$$\left|{}^3LM_LM_S\right\rangle \equiv \left|\begin{matrix} L \\ M_L \end{matrix}\right\rangle \left|\begin{matrix} S=1 \\ M_S \end{matrix}\right\rangle, \tag{7.1.21a}$$

and a product of $\left|\begin{matrix} L \\ M \end{matrix}\right\rangle$ with a singlet spin state to give a singlet term state

$$\left|{}^1LM_L0\right\rangle \equiv \left|\begin{matrix} L \\ M_L \end{matrix}\right\rangle \left|\begin{matrix} S=0 \\ 0 \end{matrix}\right\rangle. \tag{7.1.21b}$$

However, it is necessary to consider a rule called the PAULI EXCLUSION PRINCIPLE, which plays an important role. Here it prevents some of these states from existing.

This mysterious principle allows only states which are antisymmetric to permutation of electrons. Note that the orbital states $\left|\begin{matrix} 2 \\ M \end{matrix}\right\rangle$ and $\left|\begin{matrix} 0 \\ 0 \end{matrix}\right\rangle$ in the table of (7.1.19) are symmetric to the interchange $\left|\begin{matrix} 1 & 1 \\ m_1 & m_2 \end{matrix}\right\rangle \rightarrow \left|\begin{matrix} 1 & 1 \\ m_2 & m_1 \end{matrix}\right\rangle$ of the *orbital* states of the electrons. Therefore they can be matched only with the *anti*symmetric $S = 0$ singlet *spin* state. Hence, the term states $|{}^1L = 2\rangle$ or $({}^1D)$ and $|{}^1L = 0\rangle$ or $({}^1S)$ obey the Pauli principle, and occur in Figure 7.1.2(a). Similarly, the antisymmetric orbital states $\left|\begin{matrix} L=1 \\ M_L \end{matrix}\right\rangle$ must be matched with the symmetric triplet spin states to give the ${}^3P$ term shown in Figure 7.1.2(a). This accounts for all the terms in the ground $(2p)^2$ configuration. In excited configurations like $(2p)(3p)$ other terms can exist, as shown in Figure 7.1.2(b).

Now it is possible to estimate the ordering of ${}^{2S+1}L$ terms. Note that the orbital wave function

$$\left\langle \mathbf{x}_1\mathbf{x}_2 \left| \begin{matrix} L=1 \\ M_L \end{matrix} \quad (2p)^2 \right\rangle = -\left\langle \mathbf{x}_2\mathbf{x}_1 \left| \begin{matrix} L=1 \\ M_L \end{matrix} \quad (2p)^2 \right\rangle \right.$$

must go to zero as $\mathbf{x}_1 \rightarrow \mathbf{x}_2$ because of the antisymmetry of $\left|\begin{matrix} 1 \\ M_L \end{matrix}\right\rangle$. Therefore, the two electrons in this triplet spin state are never at the same point, and seldom near each other. Therefore, electrostatic repulsion should be less for triplet states than singlets. Indeed ${}^3P$ is the ground state of carbon.

Now a classical argument can be made to tell which ${}^{2S+1}L$ for a given S should be lowest. One may imagine that to make the greatest L the electrons must orbit in more or less the same direction. Thus they have less chance of colliding and raising the electrostatic energy. Indeed, ${}^1D$ is lower than ${}^1S$. These arguments give what are known as HUND'S RULES: The ground

state has the highest possible spin and orbital momentum allowed by the Pauli principle.

C. Spin-Orbital Coupling

The outer product is used to describe states corresponding to two properties of a single electron, such as spin and orbit. The states of a single electron in hydrogen can be written

$$\left|\begin{matrix} l \\ m_l \end{matrix}\right\rangle \left|\begin{matrix} \frac{1}{2} \\ m_s \end{matrix}\right\rangle \equiv \left|\begin{matrix} l & \frac{1}{2} \\ m_l & m_s \end{matrix}\right\rangle, \tag{7.1.22}$$

and the same coupling formalism can be used to give states

$$\left|\begin{matrix} j \\ m \end{matrix} \quad (l \otimes \tfrac{1}{2})\right\rangle = \sum_{m_l, m_s} C^{l\ \frac{1}{2}\ j}_{m_l m_s m} \left|\begin{matrix} l & \frac{1}{2} \\ m_l & m_s \end{matrix}\right\rangle \tag{7.1.23}$$

of definite total angular momentum j.

Before discussing the spin-orbit interaction, one may predict the form of the splitting of an l level. Several levels of hydrogen are plotted in Figure 7.1.3. They are seen to conform to the reduction

$$\mathscr{C}^{\dagger}\mathscr{D}^{l} \otimes \mathscr{D}^{\frac{1}{2}}\mathscr{C} = \mathscr{D}^{l+\frac{1}{2}} \oplus \mathscr{D}^{l-\frac{1}{2}} \qquad (l > 0). \tag{7.1.24}$$

The splittings are quite small compared to the $(1s)$ energy of -13.6 eV. The shifts and splittings of the excited levels are less than the shift of the

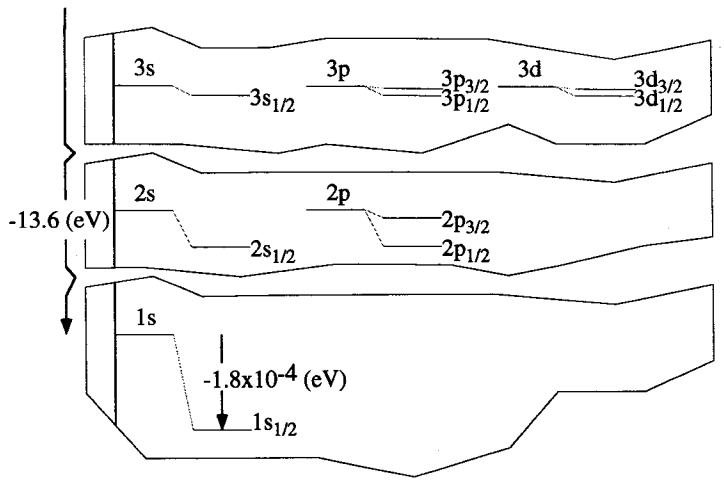

Figure 7.1.3 Fine-structure levels for atomic hydrogen. Hyperfine splittings are not shown.

ground ($1s$) level which is 1.8×10^{-4} eV. The spectral structure which arises from transitions between these levels is called FINE STRUCTURE. Note that splittings are large compared to the hyperfine splittings given by Eq. (7.1.15) in Section 7.1.A. Indeed, each of the fine-electron spin-orbit levels is slightly split into electron spin-nuclear spin or hyperfine levels. Hyperfine splitting is extremely small for p levels, however, since p electrons spend less time near the nucleus.

The spin-orbit Hamiltonian is

$$H_{\text{s.o.}} = a_{\text{s.o.}}(\mathbf{S} \cdot \mathbf{l}), \tag{7.1.25a}$$

where the interaction constant is the following:

$$a_{\text{s.o.}} = \frac{Z\alpha^2}{2}\langle 1/r^3 \rangle = \frac{Z^4\alpha^2}{2n^3(l+1)(l+\frac{1}{2})l}, \tag{7.1.25b}$$

where $\alpha = e^2/\hbar c \sim \frac{1}{137}$ is the fine-structure constant. (Atomic units $\varepsilon = e^2/a_0 = me^4/\hbar^2 \sim 27.21$ eV are used here.) The expectation values for the spin-orbit energies are

$$\left\langle \begin{matrix} j \\ m \end{matrix} \quad (l \otimes \tfrac{1}{2}) \middle| H_{\text{s.o.}} \middle| \begin{matrix} j \\ m \end{matrix} \quad (l \otimes \tfrac{1}{2}) \right\rangle$$
$$= a_{\text{s.o.}}\left[j(j+1) - l(l+1) - \tfrac{3}{4}\right] \qquad \left(j = l \pm \tfrac{1}{2}\right), \tag{7.1.26}$$

where the total angular momentum $j = l + s$ has been used in the same manner as in the preceding section.

The spin-orbit effects, like most spin interactions, are derived most elegantly using the Dirac equation. This includes all relativistic effects and leads to a very simple expression for energy eigenvalues:

$$\varepsilon_{n,j} = -\frac{Z^2}{2n^2} - \frac{\alpha^2 Z^4}{2n^3}\left(\frac{1}{j+\frac{1}{2}} - \frac{3}{4n}\right). \tag{7.1.27}$$

The Dirac formula predicts that a degeneracy remains between pairs of fine levels such as $(2s_{1/2} - 2p_{1/2})$ and $(3p_{3/2} - 3d_{3/2})$. This degeneracy is lifted by a small quantum electrodynamic perturbation and the splitting is called the Lamb shift. The degeneracy between nl_j and nl'_j states can also be understood in terms of a relativistic generalization of the eccentricity symmetry discussed in Section 5.8.

Fine structure is more easily observed in multielectron configurations. In fact, it dominates the electrostatic energies in some larger atoms since the spin-orbit term in Eq. (7.1.25) varies as Z^4. Model states such as those for

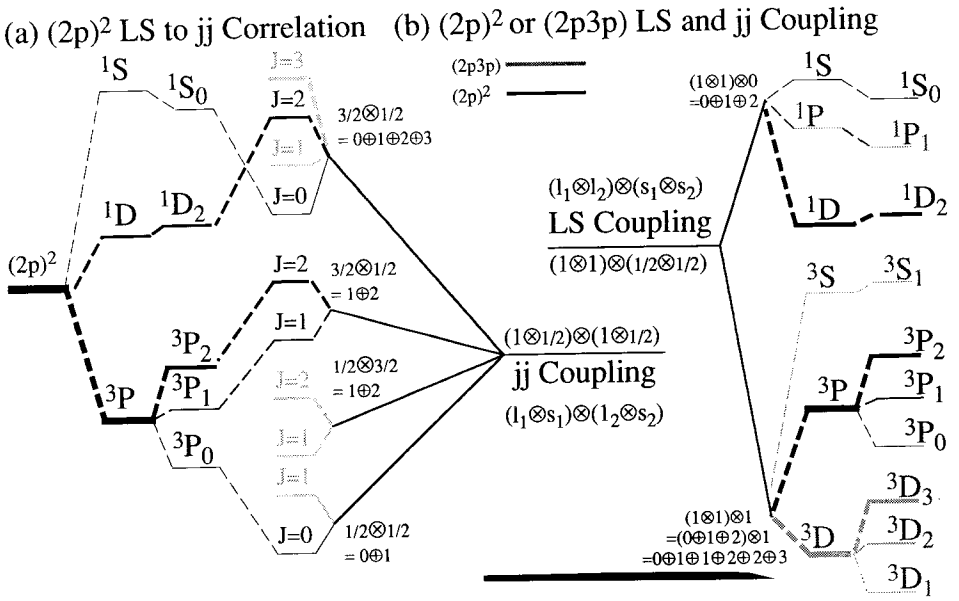

Figure 7.1.4 Fine-structure levels for configurations involving two p electrons. (a) $(2p)^2$ configuration in LS coupling case. (b) Comparison between jj- and LS-coupling cases. In the LS case L and S are good approximate quantum labels and the splitting between levels of different J and the same (L, S) is relative small. In the jj case j and j' are good approximate quantum labels.

carbon can be coupled as follows

$$\left|{}^{2S+1}L_J \quad M\right\rangle = \sum_{M_L, M_S} C^{L\ S\ J}_{M_L M_S M} \left|\begin{matrix} L \\ M_L \end{matrix}\right\rangle \left|\begin{matrix} S \\ M_S \end{matrix}\right\rangle. \tag{7.1.28}$$

This gives, finally, states of definite total electronic angular momentum J. In general, a given ${}^{2S+1}L$ term will split into $2S + 1$ J-states for each $S \leq L$. For example, the triplet levels of carbon split into three, as shown in Figure 7.1.4(a) on the lower right-hand side.

Note that there are *four* angular-momentum factors $(1 \otimes \frac{1}{2} \otimes 1 \otimes \frac{1}{2})$ associated with two p electrons, and one may couple them in different orders. The ordering

$$\begin{aligned}(1 \otimes 1) \otimes \left(\tfrac{1}{2} \otimes \tfrac{1}{2}\right) &= (2 \oplus 1 \oplus 0) \otimes (1 \oplus 0) \\ &= (\cdots \oplus L \cdots) \otimes (\cdots \oplus S \cdots) = (\cdots \oplus J \oplus \cdots)\end{aligned}$$

corresponds to what is called LS coupling, and the resulting levels are drawn on the right-hand sides of Figures 7.1.4(a) and 7.1.4(b). [The grayed lines in Figure 7.1.4(b) indicate levels that are present in an $(npn'p)$ configuration but are ruled out of an $(np)^2$ configuration by the Pauli principle.] If spin-orbit

splittings are small compared to the electrostatic splittings between ^{2S+1}L terms, then L and S are still useful quantum labels.

On the other hand, a strong spin-orbit perturbation may make the following coupling ordering more appropriate:

$$\begin{aligned}\left(1 \otimes \tfrac{1}{2}\right) \otimes \left(1 \otimes \tfrac{1}{2}\right) &= \left(\tfrac{3}{2} \oplus \tfrac{1}{2}\right) \otimes \left(\tfrac{3}{2} \oplus \tfrac{1}{2}\right) \\ &= (\cdots \oplus j \cdots) \otimes (\cdots \oplus j' \cdots) = (\cdots \oplus J \oplus \cdots).\end{aligned}$$

This corresponds to what is called jj coupling, and the resulting levels are indicated on the left-hand side of Figure 7.1.4(b). For each J term that comes out of the jj combination, there must be a corresponding term with the same J in the LS combination. This is indicated by correlation lines between Figures 7.1.4(a) and 7.1.4(b).

D. Geometrical Interpretation of Angular-Momentum Coupling

In general it is possible to couple two separate angular momenta j_1 and j_2 to make a total momentum equal to $j_3 = j_1 + j_2, j_1 + j_2 - 1, \ldots,$ or $|j_1 - j_2|$.

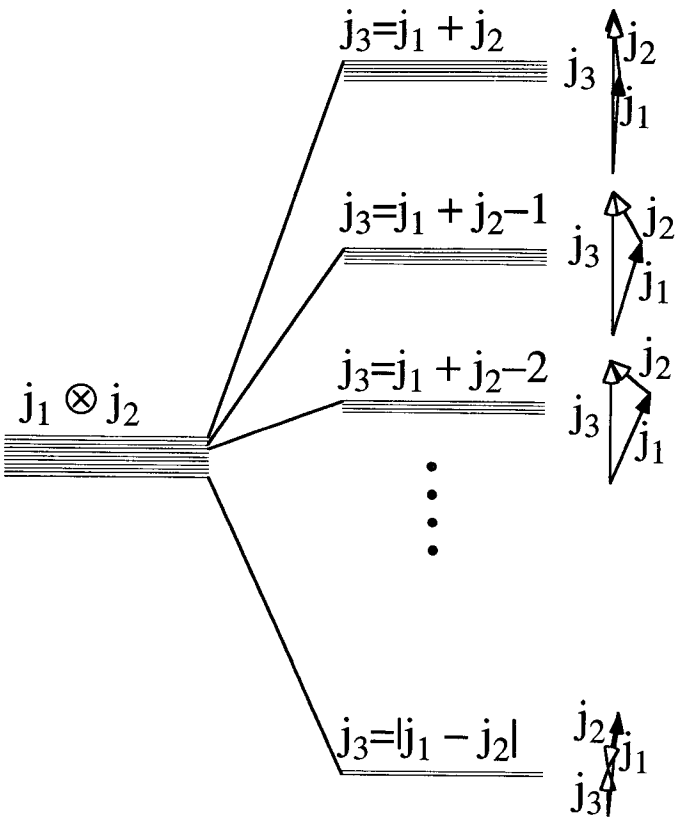

Figure 7.1.5 Vector-addition picture of angular-momentum coupling.

The level diagram corresponding to these coupling possibilities is shown in Figure 7.1.5. Beside each level is sketched a vector triangle composed of sides j_1, j_2, and j_3. The inequality $j_1 + j_2 \geq j_3 \geq |j_1 - j_2|$ is called the TRIANGULAR CONDITION and it must hold in order to have a nonzero coupling coefficient.

It is interesting to look at the vector addition model in terms of the angular-momentum cones which we discussed in Sections 5.4 and 5.5.B. (See Figures 5.4.4 and 5.5.3.) We may imagine that the $C^{j_1\, j_2\, j_3}_{m_1 m_2 m_3}$ is the amplitude for the angular-momentum cone and vector arrangement pictured in Figure 7.1.6.

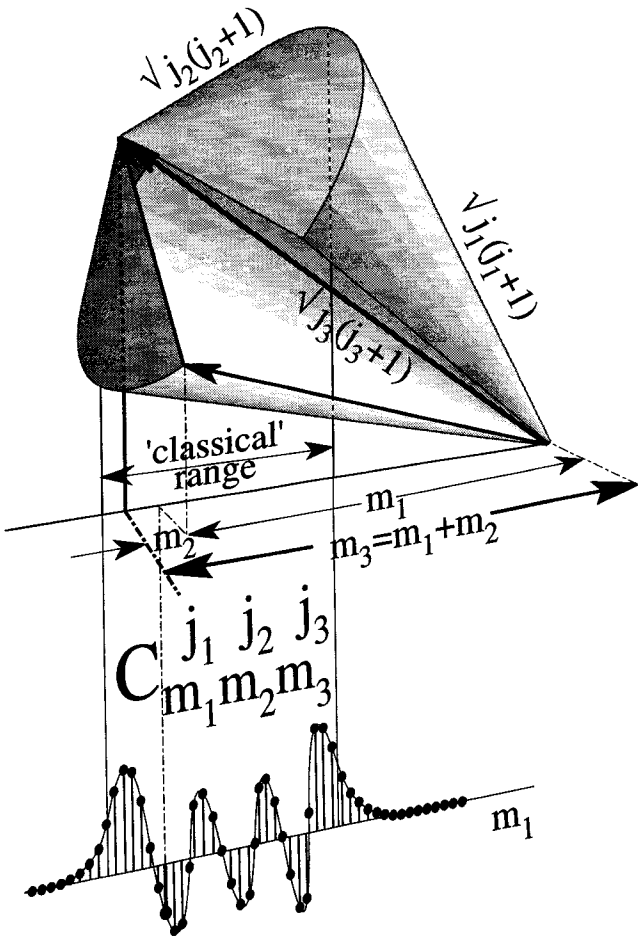

Figure 7.1.6 Angular-momentum cone picture of coupling.

Since z-component conservation requires that $m_1 + m_2 = m_3$ we may plot $C^{j_1\, j_2\, j_3}_{m_1 m_2 m_3}$, as a function of a single variable $m_1 = m$ for fixed j_1, j_2, j_3 and m_3. This is done in Figure 7.1.7 for $j_1 = j_2 = 9$ and select values of j_3 and m_3. The plots are quite similar to the ones of $\mathscr{D}^j_{mm'}(0\beta 0)$, which were shown in Figure 5.5.5. Once again we note that the projection of an angular-momentum cone base on the m or z axis defines the "classical" limits, or external inflection points of a "discrete wave." The number of "nodes" of this wave is $j_1 + j_2 - j_3$. We also note that the discrete quantum number m_3 plays the role of the continuous angle β in Figure 5.5.5. Regge and Schulten and Gordon have derived Schrödinger-like differential equations which give solu-

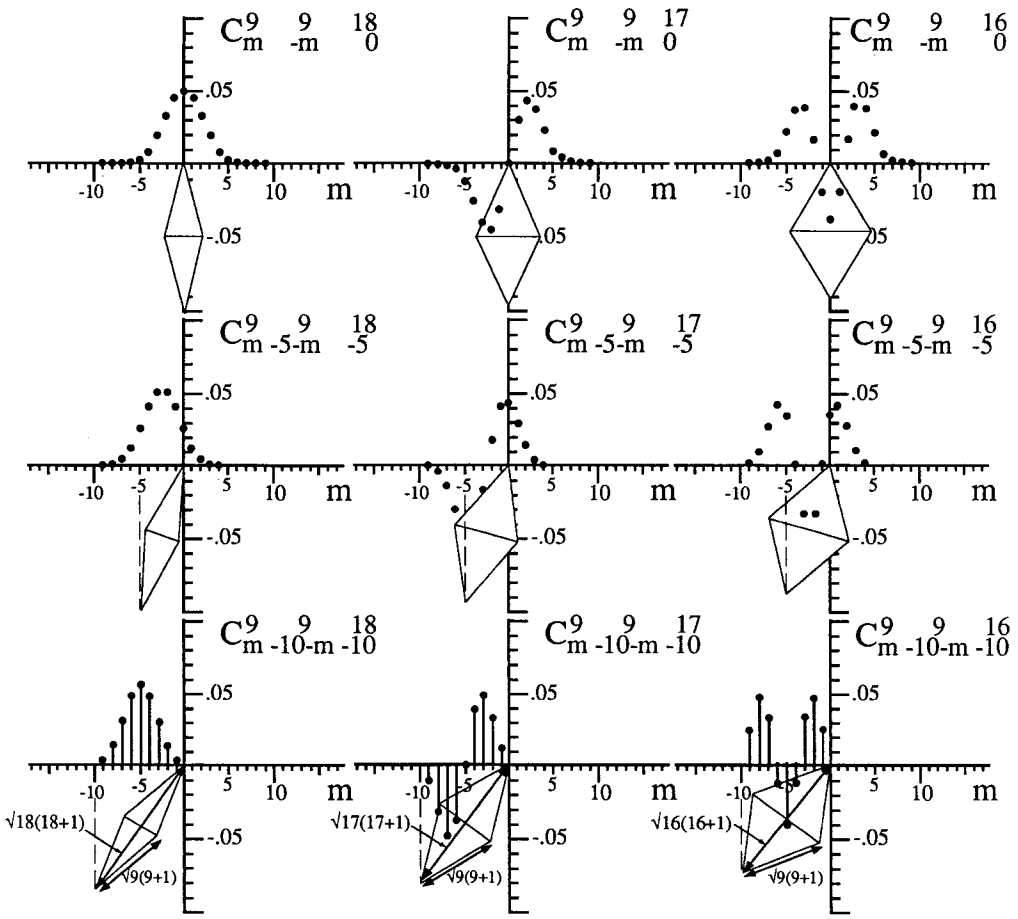

Figure 7.1.7 Plots of coupling coefficients $C^{9\ \ 9\ \ J}_{m\ -m-k\ -k}$ for $J = 18, 17, 16, \ldots$ and $k = 0, -5, -10, \ldots$.

tions that pass near or through those points. (See Additional Reading lists at the end of this chapter and Chapter 5.)

7.2 MATHEMATICAL RELATIONS OF COUPLING AND WIGNER 3j COEFFICIENTS

Before treating more applications of the coupling coefficients we should review the mathematical properties of them. First, the angular-momentum products will be related to common products in vector analysis. Then the fundamental relations between the C coefficients and the D irreps will be derived and used to define symmetry relations. This will lead naturally to the definition of the Wigner 3j coefficients.

A. Scalars, Vectors, and Tensors

Consider two ordinary three-dimensional vectors

$$\mathbf{A} \rightarrow \begin{pmatrix} \mathscr{A}_x \\ \mathscr{A}_y \\ \mathscr{A}_z \end{pmatrix} \quad \text{and} \quad \mathbf{B} \rightarrow \begin{pmatrix} \mathscr{B}_x \\ \mathscr{B}_y \\ \mathscr{B}_z \end{pmatrix}. \tag{7.2.1}$$

From the theory of vector analysis there are three different types of products between them. There is a SCALAR, DOT, or INNER PRODUCT

$$\mathbf{A} \cdot \mathbf{B} = \mathscr{A}_x \mathscr{B}_x + \mathscr{A}_y \mathscr{B}_y + \mathscr{A}_z \mathscr{B}_z, \tag{7.2.2a}$$

a VECTOR, or CROSS-PRODUCT

$$\mathbf{A} \times \mathbf{B} \rightarrow \begin{pmatrix} \mathscr{A}_y \mathscr{B}_z - \mathscr{A}_z \mathscr{B}_y \\ \mathscr{A}_z \mathscr{B}_x - \mathscr{A}_x \mathscr{B}_z \\ \mathscr{A}_x \mathscr{B}_y - \mathscr{A}_y \mathscr{B}_x \end{pmatrix}, \tag{7.2.2b}$$

and a TENSOR, DYADIC, or OUTER PRODUCT

$$\mathbf{AB} \rightarrow \begin{pmatrix} \mathscr{A}_x \mathscr{B}_x & \mathscr{A}_x \mathscr{B}_y & \mathscr{A}_x \mathscr{B}_z \\ \mathscr{A}_y \mathscr{B}_x & \mathscr{A}_y \mathscr{B}_y & \mathscr{A}_y \mathscr{B}_z \\ \mathscr{A}_z \mathscr{B}_x & \mathscr{A}_z \mathscr{B}_y & \mathscr{A}_z \mathscr{B}_z \end{pmatrix}. \tag{7.2.2c}$$

It is instructive to note that these three products correspond directly with the three reductions of products between $l = 1(p)$ states which give total $L = 0$, 1, and 2 states, respectively.

The only complication in making this correspondence comes from using two different types of coordinates, namely, CARTESIAN or PLANE-POLARIZATION components $(\mathscr{A}_x, \mathscr{A}_y, \mathscr{A}_z)$ on one hand, and R_3 symmetry-defined or circular-polarization components $(\mathscr{A}^1_1, \mathscr{A}^1_0, \mathscr{A}^1_{-1})$ on the other. Let us define the following relations between these sets:

$$\mathscr{A}^1_1 = -(\mathscr{A}_x + i\mathscr{A}_y)/\sqrt{2}\,, \qquad \mathscr{A}^1_{-1} = (\mathscr{A}_x - i\mathscr{A}_y)/\sqrt{2}\,,$$
$$\mathscr{A}_x = (\mathscr{A}^1_{-1} - \mathscr{A}^1_1)/\sqrt{2}\,, \qquad \mathscr{A}_y = i(\mathscr{A}^1_{-1} + \mathscr{A}^1_1)/\sqrt{2}\,, \qquad \mathscr{A}_z = \mathscr{A}^1_0, \quad (7.2.3)$$

so that they conform to those between (x, y, z) and the harmonics or multipole functions $(rY^1_1, rY^1_0, rY^1_{-1})$ given in Appendix F or Eq. (5.6.19). Then it follows using the table of (7.1.15) that the symmetry-defined product

$$[\mathscr{A}^1 \times \mathscr{B}^1]^0_0 \equiv \sum_{m_1, m_2} C^{1\ 1\ 0}_{m_1 m_2 0} \mathscr{A}^1_{m_1} \mathscr{B}^1_{m_2} \quad (7.2.4a)$$

is proportional to the scalar product in Eq. (7.2.2a):

$$\begin{aligned}[\mathscr{A}^1 \times \mathscr{B}^1]^0_0 &= 1/\sqrt{3}\,\mathscr{A}^1_1\mathscr{B}^1_{-1} - 1/\sqrt{3}\,\mathscr{A}^1_0\mathscr{B}^1_0 + 1/\sqrt{3}\,\mathscr{A}^1_{-1}\mathscr{B}^1_1 \\ &= 1/\sqrt{3}\,(-\mathscr{A}_x - i\mathscr{A}_y)(\mathscr{B}_x - i\mathscr{B}_y)/2 - 1/\sqrt{3}\,\mathscr{A}_z\mathscr{B}_z \\ &\quad + 1/\sqrt{3}\,(\mathscr{A}_x - i\mathscr{A}_y)(-\mathscr{B}_x - i\mathscr{B}_y)/2 \\ &= -(\mathscr{A}_x\mathscr{B}_x + \mathscr{A}_y\mathscr{B}_y + \mathscr{A}_z\mathscr{B}_z)/\sqrt{3} = -\mathbf{A}\cdot\mathbf{B}/\sqrt{3}\,. \quad (7.2.4b)\end{aligned}$$

The R_3 symmetry-defined product with $L = 1$ and $M = 0$,

$$[\mathscr{A}^1 \times \mathscr{B}^1]^1_0 \equiv \sum_{m_1, m_2} C^{1\ 1\ 1}_{m_1 m_2 0} \mathscr{A}^1_{m_1} \mathscr{B}^1_{m_2}, \quad (7.2.5a)$$

is proportional to the $\begin{pmatrix}1\\0\end{pmatrix}$ or z component of the vector product in Eq. (7.2.2b):

$$\begin{aligned}[\mathscr{A}^1 \times \mathscr{B}^1]^1_0 &= 1/\sqrt{2}\,\mathscr{A}^1_1\mathscr{B}^1_{-1} - 1/\sqrt{2}\,\mathscr{A}^1_{-1}\mathscr{B}^1_1 \\ &= i(-\mathscr{A}_y\mathscr{B}_x + \mathscr{A}_x\mathscr{B}_y)/\sqrt{2} = i(\mathbf{A}\times\mathbf{B})_z/\sqrt{2}\,. \quad (7.2.5b)\end{aligned}$$

Finally, the $L = 2$ products are made of second-rank tensor components:

$$[\mathscr{A}^1 \times \mathscr{B}^1]^2_m \equiv \sum_{m_1, m_2} C^{1\ 1\ 2}_{m_1 m_2 m}\, \mathscr{A}^1_{m_1} \mathscr{B}^1_{m_2}, \quad (7.2.6a)$$

$$[\mathscr{A}^1 \times \mathscr{B}^1]^2_2 = (\mathscr{A}_x\mathscr{B}_x - \mathscr{A}_y\mathscr{B}_y + i\mathscr{A}_x\mathscr{B}_y + i\mathscr{A}_y\mathscr{B}_x)/2, \quad (7.2.6b)$$

$$[\mathscr{A}^1 \times \mathscr{B}^1]^2_1 = -(\mathscr{A}_x\mathscr{B}_z + \mathscr{A}_z\mathscr{B}_x + i\mathscr{A}_y\mathscr{B}_z + i\mathscr{A}_z\mathscr{B}_y)/2,$$

$$[\mathscr{A}^1 \times \mathscr{B}^1]^2_0 = (-\mathscr{A}_x\mathscr{B}_x - \mathscr{A}_y\mathscr{B}_y + 2\mathscr{A}_z\mathscr{B}_z)/\sqrt{6}\,.$$

All these products are summarized in the following matrix:

$$\mathcal{T}\left\langle xyz\middle|{}^{k}_{q}\right\rangle =$$

	$[\ ]^2_2$	$[\ ]^2_1$	$[\ ]^2_0$	$[\ ]^2_{-1}$	$[\ ]^2_{-2}$	$[\ ]^1_1$	$[\ ]^1_0$	$[\ ]^1_{-1}$	$[\ ]^0_0$
$\mathscr{A}_x\mathscr{B}_x$	$\frac{1}{2}$	·	$-\frac{1}{\sqrt{6}}$	·	$\frac{1}{2}$	·	·	·	$-\frac{1}{\sqrt{3}}$
$x\ y$	$\frac{i}{2}$	·	·	·	$-\frac{1}{2}$	·	$\frac{i}{\sqrt{2}}$	·	·
$x\ z$	·	$-\frac{1}{2}$	·	$\frac{1}{2}$	·	$-\frac{1}{2}$	·	$-\frac{1}{2}$	·
$y\ x$	$\frac{i}{2}$	·	·	·	$-\frac{i}{2}$	·	$-\frac{i}{\sqrt{2}}$	·	·
$y\ y$	$-\frac{1}{2}$	·	$-\frac{1}{\sqrt{6}}$	·	$-\frac{1}{2}$	·	·	·	$-\frac{1}{\sqrt{3}}$
$y\ z$	·	$-\frac{i}{2}$	·	$-\frac{i}{2}$	·	$-\frac{i}{2}$	·	$\frac{i}{2}$	·
$z\ x$	·	$-\frac{1}{2}$	·	$\frac{1}{2}$	·	$\frac{1}{2}$	·	$\frac{1}{2}$	·
$z\ y$	·	$-\frac{i}{2}$	·	$-\frac{i}{2}$	·	$\frac{i}{2}$	·	$-\frac{i}{2}$	·
$z\ z$		·	$\frac{2}{\sqrt{6}}$	·	·	·	·	·	$-\frac{1}{\sqrt{3}}$

(7.2.7)

This matrix represents a unitary transformation between Cartesian components $\mathcal{T}_{ij} = \mathscr{A}_i\mathscr{B}_j$ and symmetry-defined components $\mathcal{T}^k_q = [\mathscr{A} \times \mathscr{B}]^k_q$ of a second-rank tensor:

$$\vec{\vec{T}} = \sum_{ij} \mathcal{T}_{ij}\hat{x}_i\hat{x}_j = \sum_{k,g} \mathcal{T}^k_q [xx]^k_q. \tag{7.2.8}$$

Note that if the two vectors **A** and **B** are the radius vector (i.e., **A** = **B** = **r**) in Eqs. (7.2.4)–(7.2.7), then one obtains the elementary multipole functions such as the following:

$$\begin{aligned} [r^1r^1]^2_2 &= (x^2 - y^2 + 2ixy)/2, & [r^1r^1]^2_1 &= -(x - iy)z, \ldots \text{ etc.} \\ &= \sqrt{\tfrac{2}{3}}\, X^2_2 & &= \sqrt{\tfrac{2}{3}}\, X^2_1 \end{aligned} \tag{7.2.9}$$

These polynomial relations were discussed in Section 5.6.C.

Tensor or polynomial algebra can easily be continued up to arbitrary rank or order k, by attaching more vector factors. If we just want the new tensor or polynomial at each stage, i.e., the one which has the highest $L = k$, the necessary coupling formulas are quite simple. For example, to make the kth-order product,

$$\begin{aligned} \left[\left[[\mathscr{A}^1 \times \mathscr{B}^1]^2 \times C^1 \cdots\right]^{k-1} \times \mathscr{H}^1\right]^k_q &= C^{k\,-\,11k}_{q\,-\,11q}[[[\cdots]^{k-1}_{q-1}\mathscr{H}^1_1 \\ &+ C^{k\,-\,11k}_{q\ \ 0q}[[[\cdots]^{k-1}_{q}\mathscr{H}^1_0 \\ &+ C^{k\,-\,1\ 1\ k}_{q\,+\,1\,-1q}[[[\cdots]^{k-1}_{q+1}\mathscr{H}^1_{-1}, \end{aligned} \tag{7.2.10}$$

from the $(k-1)$th products one requires the following coupling coefficients:

$$C^{k-11k}_{q-11q} = \left(\frac{(k+q-1)(k+q)}{(2k-1)(2k)}\right)^{\frac{1}{2}}, \qquad C^{k-11k}_{q\ 0q} = \left(\frac{k^2-q^2}{k(2k-1)}\right)^{\frac{1}{2}},$$
$$C^{k-11k}_{q+11q} = \left(\frac{(k-q)(k-q-1)}{2k(2k-1)}\right)^{\frac{1}{2}}. \tag{7.2.11}$$

These are derived from Eq. (7.1.17).

B. The General R_3 Scalar Coupling

If there is any type of coupling coefficients which should be memorized, it is the ones which make the scalar ($l = 0$) irrep:

$$C^{j_1\ j_2\ 0}_{m_1 m_2 0} = \delta_{j_1, j_2}\delta_{m_1, -m_2}(-1)^{j_1-m_1}\Big/\sqrt{2j_j+1}\,. \tag{7.2.12}$$

The product of any two bases belonging to the *same j* can be made combined in the form

$$\left|\begin{matrix}0\\0\end{matrix}\right\rangle = \sum_m \frac{(-1)^{j-m}}{\sqrt{2j+1}}\left|\begin{matrix}j\\m\end{matrix}\right\rangle\left|\begin{matrix}j\\-m\end{matrix}\right\rangle, \tag{7.2.13}$$

so the result has zero total J and belongs to the scalar irrep $\mathscr{D}^0(R) \equiv 1$. The derivation of this coupling is a little more complicated than it was for real irreps in Section 6.2.A, since the phase is variable.

The derivation is made by using the relation between an irrep $\mathscr{D}^j$, which serves to transform ket vectors:

$$R(\alpha\beta\gamma)\left|\begin{matrix}j\\m\end{matrix}\right\rangle = \sum_{m'}\mathscr{D}^j_{m'm}(\alpha\beta\gamma)\left|\begin{matrix}j\\m'\end{matrix}\right\rangle, \tag{7.2.14}$$

and its complex conjugate $\mathscr{D}^{j*}$, which does the transformation of bra vectors:

$$\left(R(\alpha\beta\gamma)\left|\begin{matrix}j\\m\end{matrix}\right\rangle\right)^\dagger = \left\langle\begin{matrix}j\\m\end{matrix}\right|R^\dagger(\alpha\beta\gamma) = \sum_{m'}\mathscr{D}^{j*}_{m'm}(\alpha\beta\gamma)\left\langle\begin{matrix}j\\m'\end{matrix}\right|. \tag{7.2.15}$$

Note that the ket-bra product completeness relation

$$1 = \sum_m \left|\begin{matrix}j\\m\end{matrix}\right\rangle\left\langle\begin{matrix}j\\m\end{matrix}\right| \tag{7.2.16}$$

is clearly a scalar. One needs to find which combinations of bras $\left\langle\begin{matrix}j\\m'\end{matrix}\right|$ transform like a given ket $\left|\begin{matrix}j\\m\end{matrix}\right\rangle$. This will yield the coefficients that make scalars out of ket-ket products.

To this end let us examine the transpose conjugate,

$$\mathscr{D}^{j\dagger}(\alpha\beta\gamma) = \mathscr{D}^{j^{-1}}(\alpha\beta\gamma) = \mathscr{D}^{j}(-\gamma, -\beta, -\alpha), \tag{7.2.17}$$

of $\mathscr{D}^j$ and use the fact that it is unitary. By making the substitutions $\alpha \to -\gamma$, $\gamma \to -\alpha$, $m \to -m'$, $m' \to -m$ in Eq. (5.4.45) one finds the following:

$$\mathscr{D}^{j}_{m'm}(\alpha\beta\gamma) = \mathscr{D}^{j}_{-m-m'}(-\gamma, \beta, -\alpha). \tag{7.2.18}$$

Also, by substituting $\beta \to -\beta$ one obtains

$$\mathscr{D}^{j}_{m'm}(\alpha - \beta\gamma) = (-1)^{-m+m'}\mathscr{D}^{j}_{m'm}(\alpha\beta\gamma). \tag{7.2.19}$$

Combining the last three equations in turn gives

$$\begin{aligned}
&\mathscr{D}^{j\dagger}_{mm'}(\alpha\beta\gamma) = \mathscr{D}^{j}_{mm'}(-\gamma - \beta - \alpha),\\
&\mathscr{D}^{j*}_{m'm}(\alpha\beta\gamma) = \mathscr{D}^{j}_{-m'-m}(\alpha - \beta\gamma) = \mathscr{D}^{j}_{-m'-m}(\alpha\beta\gamma)(-1)^{-m+m'}.
\end{aligned} \tag{7.2.20a}$$

This is substituted into Eq. (7.2.15):

$$\begin{aligned}
\left\langle \begin{matrix} j \\ m \end{matrix} \right| R^{\dagger}(\alpha\beta\gamma) &= \sum_{m'} \mathscr{D}^{j}_{-m'-m}(\alpha\beta\gamma)(-1)^{-m+m'}\left\langle \begin{matrix} j \\ m' \end{matrix} \right|,\\
(-1)^{-m}\left\langle \begin{matrix} j \\ -m \end{matrix} \right| R^{\dagger}(\alpha\beta\gamma) &= \sum_{m'} \mathscr{D}^{j}_{m'm}(\alpha\beta\gamma)(-1)^{-m'}\left\langle \begin{matrix} j \\ -m' \end{matrix} \right|.
\end{aligned} \tag{7.2.20b}$$

The resulting equation proves that the bra bases

$$(-1)^{-m}\left\langle \begin{matrix} j \\ -m \end{matrix} \right| \text{ or } (-1)^{j-m}\left\langle \begin{matrix} j \\ -m \end{matrix} \right|$$

transform exactly like the ket bases $\left| \begin{matrix} j \\ m \end{matrix} \right\rangle$. The extra overall phase factor $(-1)^j$ does not affect the transformation. It is conventional to choose $(-1)^{j-m}$ as the phase factor since it is real even when j is half-integral. This completes the proof of Eq. (7.2.12) for scalar coupling.

C. Fundamental Coupling Definitions and Symmetry Relations: The Wigner 3*j* Coefficient

The R_3 coupling coefficients are defined to be components of orthogonal transformation matrices:

$$\sum_{m_1=-j_1}^{j_1}\sum_{m_2=-j_2}^{j_2} C^{j_1\, j_2\, j_3}_{m_1 m_2 m_3} C^{j_1\, j_2\, j'_3}_{m_1 m_2 m'_3} = \delta_{j_3 j'_3}\delta_{m_3 m'_3}. \tag{7.2.21}$$

They therefore satisfy completeness relations, too:

$$\sum_{j_3=|j_1-j_2|}^{j_1+j_2} \sum_{m_3=-j_3}^{j_3} C^{j_1\ j_2\ j_3}_{m_1 m_2 m_3} C^{j_1\ j_2\ j_3}_{m_1' m_2' m_3} = \delta_{m_1 m_1'} \delta_{m_2 m_2'}. \tag{7.2.22}$$

We shall use these relations with the fundamental irrep orthogonality relation (5.5.28):

$$\int d(\alpha\beta\gamma) \mathscr{D}^{j'*}_{m'n'}(\alpha\beta\gamma) \mathscr{D}^{j}_{mn}(\alpha\beta\gamma) = \delta_{jj'} \delta_{mm'} \delta_{nn'}/2j + 1.$$

Also, we need the reduction equation for $\mathscr{D}^{j_1} \otimes \mathscr{D}^{j_2}$:

$$\sum_{m_1 m_2} \sum_{m_1' m_2'} C^{j_1\ j_2\ j_3}_{m_1 m_2 m_3} \mathscr{D}^{j_1}_{m_1 m_1'}(\alpha\beta\gamma) \mathscr{D}^{j_2}_{m_2 m_2'}(\alpha\beta\gamma) C^{j_1\ j_2\ j_3'}_{m_1' m_2' m_3'} = \delta_{j_3 j_3'} \mathscr{D}^{j_3}_{m_3 m_3'}(\alpha\beta\gamma). \tag{7.2.23}$$

[Recall Eq. (7.1.6c) for an example of this.] The inverse reduction equation,

$$\mathscr{D}^{j_1}_{m_1 m_1'}(\alpha\beta\gamma) \mathscr{D}^{j_2}_{m_2 m_2'}(\alpha\beta\gamma) = \sum_{j_3=|j_1-j_2|}^{j_1+j_2} \sum_{m_3=-j_3}^{j_3} C^{j_1\ j_2\ j_3}_{m_1 m_2 m_3} \mathscr{D}^{j_3}_{m_3 m_3'}(\alpha\beta\gamma) C^{j_1\ j_2\ j_3}_{m_1' m_2' m_3'}, \tag{7.2.24}$$

follows from Eq. (7.2.22). Finally, by applying the irrep orthogonality relation one obtains

$$\int d(\alpha\beta\gamma) \mathscr{D}^{j_3*}_{m_3 m_3'}(\alpha\beta\gamma) \mathscr{D}^{j_2}_{m_1 m_1'}(\alpha\beta\gamma) \mathscr{D}^{j_2}_{m_2 m_2'}(\alpha\beta\gamma) = C^{j_1\ j_2\ j_3}_{m_1 m_2 m_3} C^{j_1\ j_2\ j_3}_{m_1' m_2' m_3'}/2j_3 + 1. \tag{7.2.25}$$

This is an extremely useful result. It is sometimes called the FACTORIZATION LEMMA.

Our first use of this equation will be to suggest a more symmetric form of coupling coefficient. We shall need the conjugation relation,

$$\mathscr{D}^{j_3*}_{m_3 m_3'} = (-1)^{j_3 - m_3 - j_3 + m_3'} \mathscr{D}^{j_3}_{-m_3 - m_3'} = (-1)^{-j_3 + m_3 - j_3 + m_3'} \mathscr{D}^{j_3}_{-m_3 - m_3'}, \tag{7.2.26}$$

from Eq. (7.2.20a). We also need to become familiar with some of the tricks of phase arithmetic. For example, one can often use the fact that the factor

$$(-1)^{j_3 - m_3} = (-1)^{-j_3 + m_3} \tag{7.2.27}$$

is positive or negative unity even if j_3 is half-integral. The point is that if j_3 is half-integral then so is m_3, and this means that $j_3 \pm m_3$ is an integer. Also, we will use the fact that for any $\{j_1 j_2 j_3\}$ in $C^{j_1 j_2 j_3}$ one must have

$$1 = (-1)^{2j_1+2j_2+2j_3} = (-1)^{2j_1+2j_2-2j_3} = (-1)^{2j_1-2j_2+2j_3}, \text{ etc.} \quad (7.2.28)$$

This follows since there cannot be an odd number of half-integral j's in $C^{j_1 j_2 j_3}$. Finally, we obtain

$$\begin{aligned}
&\int d(\alpha\beta\gamma)\mathscr{D}^{j_3}_{m_3 m_3'}(\alpha\beta\gamma)\mathscr{D}^{j_1}_{m_1 m_1'}(\alpha\beta\gamma)\mathscr{D}^{j_2}_{m_2 m_2'}(\alpha\beta\gamma) \\
&\quad = \left(\frac{(-1)^{-j_3-m_3} C^{j_1\ j_2\ j_3}_{m_1 m_2 -m_3}}{\sqrt{2j_3+1}}\right)\left(\frac{(-1)^{-j_3-m_3'} C^{j_1\ j_2\ j_3}_{m_1' m_2' -m_3'}}{\sqrt{2j_3+1}}\right) \\
&\quad = \left(\frac{(-1)^{j_1-j_2-m_3} C^{j_1\ j_2\ j_3}_{m_1 m_2 -m_3}}{\sqrt{2j_3+1}}\right)\left(\frac{(-1)^{j_1-j_2-m_3'} C^{j_1\ j_2\ j_3}_{m_1' m_2' -m_3'}}{\sqrt{2j_3+1}}\right). \quad (7.2.29)
\end{aligned}$$

The last line includes a factor $(-1)^{2j_1-2j_2+2j_3}$ which is always unity. This leads to the conventional WIGNER $3j$ COEFFICIENT:

$$\begin{pmatrix} j_1 & j_2 & j_3 \\ m_1 & m_2 & m_3 \end{pmatrix} \equiv (-1)^{j_1-j_2-m_3} C^{j_1\ j_2\ j_3}_{m_1 m_2 -m_3} \Big/ \sqrt{2j_3+1}, \quad (7.2.30a)$$

which satisfies

$$\begin{aligned}
&\int d(\alpha\beta\gamma)\mathscr{D}^{j_1}_{m_1 m_1'}(\alpha\beta\gamma)\mathscr{D}^{j_2}_{m_2 m_2'}(\alpha\beta\gamma)\mathscr{D}^{j_3}_{m_3 m_3'}(\alpha\beta\gamma) \\
&\quad = \begin{pmatrix} j_1 & j_2 & j_3 \\ m_1 & m_2 & m_3 \end{pmatrix}\begin{pmatrix} j_1 & j_2 & j_3 \\ m_1' & m_2' & m_3' \end{pmatrix}. \quad (7.2.30b)
\end{aligned}$$

The idea of this definition is to make a coupling coefficient that has convenient symmetry relations with respect to permutations of the j_1, j_2, and j_3 parts. From Eq. (7.2.30) a number of symmetry relations follow. For example, we have

$$\begin{pmatrix} j_1 & j_2 & j_3 \\ m_1 & m_2 & m_3 \end{pmatrix}^2 = \begin{pmatrix} j_2 & j_1 & j_3 \\ m_2 & m_1 & m_3 \end{pmatrix}^2 = \begin{pmatrix} j_3 & j_2 & j_1 \\ m_3 & m_2 & m_1 \end{pmatrix}^2,$$

$$\begin{aligned}
\begin{pmatrix} j_1 & j_2 & j_3 \\ m_1 & m_2 & m_3 \end{pmatrix}\begin{pmatrix} j_1 & j_2 & j_3 \\ 0 & 0 & 0 \end{pmatrix} &= \begin{pmatrix} j_2 & j_1 & j_3 \\ m_1 & m_2 & m_3 \end{pmatrix}\begin{pmatrix} j_2 & j_1 & j_3 \\ 0 & 0 & 0 \end{pmatrix} \\
&= \begin{pmatrix} j_3 & j_2 & j_1 \\ m_3 & m_2 & m_1 \end{pmatrix}\begin{pmatrix} j_3 & j_2 & j_1 \\ 0 & 0 & 0 \end{pmatrix}.
\end{aligned}$$

However, the phase relations for the individual coefficients are not so obvious, since they depend on the detailed definition of $C^{j_1\, j_2\, j_3}_{m_1 m_2 m_3}$ for different products. Wigner's definition is made so the following permutation properties hold:

$$\begin{aligned}\begin{pmatrix} j_1 & j_2 & j_3 \\ m_1 & m_2 & m_3 \end{pmatrix} &= (-1)^{j_1+j_2+j_3}\begin{pmatrix} j_2 & j_1 & j_3 \\ m_2 & m_1 & m_3 \end{pmatrix} \\ &= (-1)^{j_1+j_2+j_3}\begin{pmatrix} j_3 & j_2 & j_1 \\ m_3 & m_2 & m_1 \end{pmatrix} \\ &= (-1)^{j_1+j_2+j_3}\begin{pmatrix} j_1 & j_3 & j_2 \\ m_1 & m_3 & m_2 \end{pmatrix} \\ &= \begin{pmatrix} j_3 & j_1 & j_2 \\ m_3 & m_1 & m_2 \end{pmatrix} = \begin{pmatrix} j_2 & j_3 & j_1 \\ m_2 & m_3 & m_1 \end{pmatrix}. \end{aligned} \tag{7.2.31}$$

Also, we have from Eqs. (7.2.30) and (7.2.20b),

$$\begin{pmatrix} j_1 & j_2 & j_3 \\ m_1 & m_2 & m_3 \end{pmatrix} = (-1)^{j_1+j_2+j_3}\begin{pmatrix} j_1 & j_2 & j_3 \\ -m_1 & -m_2 & -m_3 \end{pmatrix}. \tag{7.2.32}$$

The $3-j$ coefficients have easily remembered properties, and one may quickly find various permutation relations for the $C^{j_1\, j_2\, j_3}_{m_1 m_2 m_3}$. For example, transposing the first two factors gives the following:

$$\begin{aligned} C^{j_2\, j_1\, j_3}_{m_2 m_1 m_3} &= (-1)^{j_2-j_1+m_3}\sqrt{2j_3+1}\begin{pmatrix} j_2 & j_1 & j_3 \\ m_2 & m_1 & -m_3 \end{pmatrix} \\ &= (-1)^{j_2-j_1+m_3}\sqrt{2j_3+1}\,(-1)^{j_1+j_2+j_3}\begin{pmatrix} j_1 & j_2 & j_3 \\ m_1 & m_2 & -m_3 \end{pmatrix} \\ &= (-1)^{j_1+j_2-j_3}C^{j_1\, j_2\, j_3}_{m_1 m_2 m_3}. \end{aligned} \tag{7.2.33}$$

For $j_1 = j_2 = j$ this gives an important special case of this relation:

$$C^{j\ j\ j_3}_{m_2 m_1 m_3} = (-1)^{2j-j_3}C^{j\ j\ j_3}_{m_1 m_2 m_3}. \tag{7.2.34}$$

This is very useful to have when applying the Pauli principle. Note that when two integral momenta $j_1 = j_2 = n$ are coupled, the even total j_3 states are symmetric, while the odd j_3 states are antisymmetric. For half-integral $j_1 = j_2 = n/2$ the reverse is true.

A permutation of the second two factors gives the following relation:

$$C^{j_1\, j_3\, j_2}_{m_1 m_3 m_2} = (-1)^{j_2-j_3+m_1}\sqrt{\frac{2j_2+1}{2j_3+1}}\,C^{\,j_1\, j_2\, j_3}_{-m_1 m_2 m_3}. \tag{7.2.35}$$

D. Clebsch-Gordon and Wigner Coefficient Formulas

In Section 5.4.C the connection between two-dimensional oscillator operators (SU_2) and three-dimensional rotation operators (R_3) was introduced. [Recall Eqs. (5.4.37).] The creation operator algebra of Schwinger and Jordan was used to derive the irrep formula (5.4.45). Now the same methods can be extended to derive coupling coefficient formulas. The methods described here are due to the combined works of many researchers who are developing similar formulas for higher unitary groups $U_3, U_4, \ldots$. [The principal pioneers in this field include Baird, Biedenharn, Bincer, Gelfand, Louck, and Moshinsky. See Additional Reading list at the end of the Chapter.)

Let us begin by representing the product state $\left|\begin{matrix} j_1 \\ m_1 \end{matrix}\right\rangle_A \left|\begin{matrix} j_2 \\ m_2 \end{matrix}\right\rangle_B$ using two pairs of oscillator operators. One pair $\{a^\dagger_\uparrow \equiv a^1_1, a^\dagger_\downarrow \equiv a^1_2\}$ includes the creation operators for momentum j_1 of particle A while the second pair $\{b^\dagger_\uparrow \equiv a^2_1, b^\dagger_\downarrow \equiv a^2_2\}$ includes the creation operators for momentum j_2 of particle B. Note the change in notation in which creation operators a^j_i are indicated without the dagger (†). Destruction operators are denoted by $(a^j_i)^\dagger \equiv \bar{a}^j_i$ in this notation. The product state consists of generalization of Eq. (5.4.38) in which the oscillator analogy is used once for the angular-momentum j_1 state of particle A and then again for the j_2 state of particle B:

$$\left|\begin{matrix} j_1 & j_2 \\ m_1 & m_2 \end{matrix}\right\rangle = \frac{(a^1_1)^{j_1+m_1}(a^1_2)^{j_1-m_1}(a^2_1)^{j_2+m_2}(a^2_2)^{j_2-m_2} \mid \rangle}{[(j_1+m_1)!(j_1-m_1)!(j_2+m_2)!(j_2-m_2)!]^{\frac{1}{2}}} \tag{7.2.36}$$
$$= |j_1+m_1 j_1-m_1, j_2+m_2 j_2-m_2\rangle.$$

The empty ket $\mid \rangle = |00,00\rangle$ denotes the vacuum state in which each particle has zero angular momentum.

The problem is to construct the states which are eigenvectors of definite total angular momentum. This may be done by appealing to a generalization of the $\mathscr{D}$-matrix derivation by creation operators. Let us begin with a generalization of Eq. (5.4.41):

$$a^{j'}_1 = u_{11}a^j_1 + u_{21}a^j_2,$$
$$a^{j'}_2 = u_{12}a^j_1 + u_{22}a^j_2 \qquad (j = 1, 2 \text{ or } A, B). \tag{7.2.37}$$

Here, u_{ij} are components of a general unitary ($u^\dagger = u^{-1}$) unimodular (det u = 1) two-by-two matrix. That is, u is an element of SU_2. This transformation of creation operators may be substituted in Eq. (5.4.42) and the entire analysis of the resulting expansion carried out as it was in Section 5.4. The result is an expression for the general irrep $\mathscr{D}^j(u)$ of SU_2:

$$\mathscr{D}^j_{mn}\begin{pmatrix} u_{11} & u_{12} \\ u_{21} & u_{22} \end{pmatrix} = \sum_k \frac{[(j+n)!(j-n)!(j+m)!(j-m)!]^{\frac{1}{2}}}{(j-k+m)!(k-m+n)!k!(j-n-k)!}$$
$$\times (u_{11})^{j-k+m}(u_{21})^{k-m+n}(u_{12})^k(u_{22})^{j-n-k}. \tag{7.2.38}$$

Since products of representations must be a representation of products we must have $\mathscr{D}^j(u)\mathscr{D}^j(v) = \mathscr{D}^j(uv) \equiv \mathscr{D}^j(w)$, or

$$\sum_n \mathscr{D}^j_{mn}\begin{pmatrix} u_{11} & u_{12} \\ u_{21} & u_{23} \end{pmatrix} \mathscr{D}^j_{nl}\begin{pmatrix} v_{11} & v_{12} \\ v_{21} & v_{22} \end{pmatrix} = \mathscr{D}^j_{ml}\begin{pmatrix} w_{11} & w_{12} \\ w_{21} & w_{22} \end{pmatrix}, \quad (7.2.39a)$$

where

$$w_{ik} = \sum_{j=1}^{2} u_{ij} v_{jk}. \quad (7.2.39b)$$

Now a useful operator results if each u_{ij} component is replaced by a creation operator a^j_i. Let us define a boson polynomial

$$B^j_{mn}(a) = \sum_k \frac{[(j+n)!(j-n)!(j+m)!(j-m)!/(2j)!]^{\frac{1}{2}}}{(j-k+m)!(k-m+n)!k!(j-n-k)!} \times (a^1_1)^{j-k+m}(a^1_2)^{k-m+n}(a^2_1)^k(a^2_2)^{j-n-k}, \quad (7.2.40)$$

which is the same as $\mathscr{D}^j_{mn}(a)$ with (a) replacing (u) except for an extra normalization factor $(2j)!$. We will explain the normalization factor shortly. In any case the result is a polynomial that has the correct transformation properties of a total angular-momentum state. To see this consider the same polynomial made of transformed (a') operators given by Eq. (7.2.37). Rewriting this equation as a matrix product, one has

$$a' = \tilde{u} \cdot a, \quad (7.2.41)$$

where

$$\tilde{u}_{ij} = u_{ji}. \quad (7.2.42)$$

Then the representation equation $\mathscr{D}^j(\tilde{u}a) = \mathscr{D}^j(\tilde{u})\mathscr{D}^j(a)$ becomes

$$B^j_{mn}(\tilde{u}a) = \sum_{m'} \mathscr{D}^j_{mm'}(\tilde{u}) B^j_{m'n}(a) \quad (7.2.43a)$$

or

$$B^j_{mn}(a') = \sum_{m'} \mathscr{D}^j_{m'm}(u) B^j_{m'n}(a), \quad (7.2.43b)$$

where the unitarity $(\mathscr{D}^j(u^\dagger) = \mathscr{D}^j(u)^\dagger)$ and conjugation $(\mathscr{D}^j(u^*) = \mathscr{D}^j(u)^*)$ properties of $\mathscr{D}^j$ have been used to write $\mathscr{D}^j_{mn}(\tilde{u})$ as $\mathscr{D}^j_{nm}(u)$. The result shows that the polynomial has correct $\mathscr{D}^j$-transformation properties when the 1 (spin $\uparrow$) and 2 (spin $\downarrow$) components of the two types of bosons are

mixed simultaneously according to Eq. (7.2.37). The transformation corresponds to the rigid rotations of the coupled A and B particles.

The same polynomial also transforms irreducibly under all transformations which mix "A-ness" and "B-ness" of the two different particles. Consider a transformation

$$\begin{aligned} a_i^{1''} &= v_{11}a_i^1 + v_{21}a_i^2, \\ a_i^{2''} &= v_{12}a_i^1 + v_{22}a_i^2 \qquad (i = 1,2 \text{ or } \uparrow, \downarrow), \end{aligned} \tag{7.2.44a}$$

which can be written in matrix notation as follows:

$$a'' = a \cdot v. \tag{7.2.44b}$$

The representation multiplication rules (7.2.39) lead to the following transformation properties:

$$B^j_{mn}(a'') = B^j_{mn}(a \cdot v) = \sum_{n'} \mathscr{D}^j_{n'n}(v) B^j_{mn'}(a). \tag{7.2.45}$$

This is another example which has two commuting groups of transformations for one system. The right- and left-transformation laws (7.2.43) and (7.2.45) are analogous to "laboratory" and "body" transformations (5.5.31) and (5.5.40). Here we have a transformation group $SU_2 = \{ \cdots u \cdots \}$ of states which commutes with a transformation group $SU_2 = \{ \cdots v \cdots \}$ of particles. The combination is often labeled $SU_2 \times SU_2$ or $SU_2 * SU_2$. [The modified cross-product $(*)$ notation is used to indicate that the two groups share a common irrep $\mathscr{D}^j$.]

A normalized state results if the boson creation operator (7.2.40) is applied to the vacuum:

$$\begin{aligned} \left| \begin{matrix} j \\ mn \end{matrix} \right\rangle &= B^j_{mn}(a)|00,00\rangle \\ &= \left[\frac{(j+m)!(j-m)!}{(2j)!} \right]^{\frac{1}{2}} \\ &\quad \times \sum_k \left[\frac{(j+n)!}{(n_1^1)!(n_2^1)!} \frac{(j-n)!}{(n_1^2)!(n_2^2)!} \right]^{\frac{1}{2}} |n_1^1 n_2^1, n_1^2 n_2^2\rangle. \end{aligned} \tag{7.2.46a}$$

Here the occupation numbers are

$$n_1^1 = j + m - k, \quad n_2^1 = n - m + k, \quad n_1^2 = k, \quad \text{and} \quad n_2^2 = j - n - k. \tag{7.2.46b}$$

The usual oscillator creation rules

$$(a_1^1)^{n_1^1}(a_2^1)^{n_2^1}(a_1^2)^{n_1^2}(a_2^2)^{n_2^2}|00,00\rangle = \sqrt{(n_1^1)!(n_2^1)!(n_1^2)!(n_2^2)!}\,|n_1^1 n_2^1, n_1^2 n_2^2\rangle$$

have been used. [Recall Eqs. (4.4.62).] To check the normalization one may evaluate the scalar product

$$\left\langle \begin{matrix} j \\ mn \end{matrix} \middle| \begin{matrix} j \\ mn \end{matrix} \right\rangle = \frac{(j+m)!(j-m)!}{2j!} \times \sum_k \frac{(j+n)!}{(j+m-k)!(n-m+k)!} \frac{(j-n)!}{k!(j-n-k)!},$$

where the orthonormality relations

$$\langle a'b', c'd'|ab, cb\rangle = \delta_{a'a}\delta_{b'b}\delta_{c'c}\delta_{d'd}$$

for oscillator eigenstates are assumed. Then the relation

$$\sum_m \binom{p}{m}\binom{q}{s-m} = \binom{p+q}{s} \tag{7.2.47}$$

for binomial coefficients $\binom{p}{m} \equiv p!/m!(p-m)!$ may be used. This relation is obtained by equating terms of binomial expansions:

$$(x+y)^{p+q} = \sum_s \binom{p+q}{s} x^s x^{p+q-s} = (x+y)^p (x+y)^q.$$

The desired normalization is then proven.

$$\left\langle \begin{matrix} j \\ mn \end{matrix} \middle| \begin{matrix} j \\ mn \end{matrix} \right\rangle = \frac{(j+m)!(j-m)!}{(2j)!} \sum_k \binom{j+n}{j+m-k}\binom{j-n}{k}$$
$$= \frac{(j+m)!(j-m)!}{(2j)!}\binom{2j}{j+m} = 1.$$

The boson state (7.2.46) is composed of exactly $(2j)$ bosons. This is the minimum number of bosons needed to make a state of total angular momentum j.

Another boson polynomial of interest is the determinantal combination

$$\det(a) \equiv D(a) \equiv a_1^1 a_2^2 - a_2^1 a_1^2. \tag{7.2.48}$$

This combination is invariant to all $SU_2 \times SU_2$ transformations because of

the unimodularity conditions (det $u = 1 = \det v$). The invariance then follows from the elementary properties of determinants:

$$\begin{aligned}\det(\tilde{u}av) &= \det(u)\det(v)\det(a)\\ &= \det(a).\end{aligned} \tag{7.2.49}$$

A totally scalar ($j = 0$) state of ($N = 2d$) bosons has the form

$$\begin{aligned}|j = 0 \quad N = 2d\rangle &= [(2d)!(2d+1)!]^{-\frac{1}{2}}\left(a_1^2a_2^2 - a_2^1a_1^2\right)^{2d}|00,00\rangle\\ &= [(2d)!(2d+1)!]^{-\frac{1}{2}}\\ &\quad\times\sum_r\binom{2d}{r}(a_1^1a_2^2)^r(-a_2^1a_1^2)^{2d-r}|00,00\rangle\\ &= [(2d)!(2d+1)!]^{-\frac{1}{2}}\\ &\quad\times\sum_r(2d)!(-1)^r|rr,\quad 2d-r\quad 2d-r\rangle\\ &= (2d+1)^{-\frac{1}{2}}\sum_r(-1)^r|rr,\quad 2d-r\quad 2d-r\rangle.\end{aligned} \tag{7.2.50}$$

The sum over r contains exactly $(2d + 1)$ terms, so the normalization of the scalar state is seen to be correctly chosen so that $\langle j = 0|j = 0\rangle = 1$.

The Clebsch-Gordon coefficient is the scalar product

$$C^{j_1\,j_2\,j}_{m_1m_2m} = \left\langle \begin{matrix} j_1 & j_2 \\ m_1 & m_2 \end{matrix}\middle|\, \begin{matrix} j \\ mn \end{matrix}\right\rangle$$

between the uncoupled state (7.2.36) and a coupled state similar to the one in Eq. (7.2.46). However, the scalar product of boson states will vanish unless three criteria are met. First, the eigenvalues of m components of momentum determined by

$$J(m) \equiv J_z^A + J_z^B = \hbar/2\left(\bar{a}_1^1a_1^1 - \bar{a}_2^1a_2^1 + \bar{a}_1^2a_1^2 - \bar{a}_2^2a_2^2\right) \tag{7.2.51a}$$

must be equal; i.e.,

$$m_1 + m_2 = m. \tag{7.2.51b}$$

Second, the eigenvalues of

$$J(n) = \hbar/2\left(\bar{a}_1^1a_1^1 + \bar{a}_2^1a_2^1 - \bar{a}_1^2a_1^2 - \bar{a}_2^2a_2^2\right) \tag{7.2.52a}$$

for the other commuting SU_2 generator must be equal, i.e.,

$$j_1 - j_2 = n. \tag{7.2.52b}$$

Finally, the total number

$$N = 2(j_1 + j_2) \tag{7.2.53}$$

of bosons must be the same for the states $\left|\begin{matrix} j_1 & j_2 \\ m_1 & m_2 \end{matrix}\right\rangle$ and $\left|\begin{matrix} j \\ mn \end{matrix}\right\rangle$. The last requirement generally means that some number $(N - 2j)$ of bosons in scalar determinantal combinations must be added to $\left|\begin{matrix} j \\ mn \end{matrix}\right\rangle$ to give the following general coupled state:

$$\left|\begin{matrix} j \\ mn \end{matrix} \quad N\right\rangle = \left[\frac{(2j+1)(j+m)!(j-m)!}{(N/2-j)!(N/2+j+1)!}\right]^{\frac{1}{2}} \times \sum_k \left[\frac{(j+n)!}{(n_1^1)!(n_2^1)!}\frac{(j-n)!}{(n_1^2)!(n_2^2)!}\right](a_1^1 a_2^2 - a_2^1 a_1^2)^{N/2-j}\left|n_1^1 n_2^2, n_1^2 n_2^2\right\rangle. \tag{7.2.54}$$

Here the occupation numbers n_j^i from Eq. (7.2.46b) are used. The normalization factors for this state are difficult to prove, and we refer to the work by A. Bincer for their derivation. Expansion of determinantal expression gives

$$(a_1^1 a_2^2 - a_2^1 a_1^2)^{N/2-j} = \sum_r (-1)^r \frac{(N/2-j)!}{r!(N/2-j-r)!}(a_1^1 a_2^2)^{N/2-r}(a_2^1 a_1^2)^r.$$

Insertion of this into the coupled state gives

$$\left|\begin{matrix} j \\ mn \end{matrix} \quad N\right\rangle = \left[\frac{(2j+1)(j+m)!(j-m)!}{(N/2-j)!(N/2+j+1)!}\right]^{\frac{1}{2}} \times \sum_{k,r} (-1)^r \frac{\left[(j+n)!(j-n)!(m_1^1)!(m_2^1)!(m_1^2)!(m_2^2)!\right]^{\frac{1}{2}}}{r!(N/2-j-r)!(n_1^1)!(n_2^1)!(n_1^2)!(n_2^2)!}(N/2-j)! \times \left|m_1^1 m_2^1, m_1^2 m_2^2\right\rangle, \tag{7.2.55a}$$

where the new occupation numbers are as follows, according to Eqs.

(7.2.51)–(7.2.53):

$$\begin{aligned} m_1^1 &= n_1^1 + \frac{N}{2} - j - r = j_1 + j_2 + m - k - r && (= j_1 + m_1), \\ m_2^1 &= n_2^1 + r = j_1 - j_2 - m + k + r && (= j_1 - m_1), \\ m_1^2 &= n_1^2 + r = k + r && (= j_2 + m_2), \\ m_2^2 &= n_2^2 + \frac{N}{2} - j - r = 2j_2 - r - k && (= j_2 - m_2). \end{aligned} \quad (7.2.55b)$$

The equalities written in parentheses on the right must hold when this state is matched with (7.2.36) to derive the coupling coefficient. The r sum is eliminated then, since

$$r = j_2 - k + m - m_1 = j_2 + m_2 - k. \quad (7.2.56)$$

The resulting coupling coefficient formula has $m_3 = m_1 + m_2$, $n = j_1 - j_2$, and $N = 2j_1 + 2j_2$.

$$\begin{aligned} C^{j_1\, j_2\, j_3}_{m_1 m_2 m_3} &= \left\langle \begin{matrix} j_1 & j_2 \\ m_1 & m_2 \end{matrix} \middle| \begin{matrix} j & \\ m_3 n & N \end{matrix} \right\rangle \\ &= (-1)^{j_2+m_2} \left[\frac{(2j_3+1)(j_1+j_2-j_3)!(j_3+j_1-j_2)!(j_2+j_3-j_1)!}{(j_1+j_2+j_3+1)!} \right]^{\frac{1}{2}} \\ &\cdot [(j_1+m_1)!(j_1-m_1)!(j_2+m_2)!(j_2-m_2)!(j_3+m_3)!(j_3-m_3)!]^{\frac{1}{2}} \\ &\cdot \sum_k \frac{(-1)^k}{(j_2+m_2-k)!(j_1-j_3-m_2+k)!(j_3+m_3-k)!(j_1-j_2-m_3+k)!k!(j_3-j_1+j_2-k)!}. \end{aligned} \quad (7.2.57)$$

The standard formula for the Wigner coefficient

$$\begin{pmatrix} j_1 & j_2 & j_3 \\ m_1 & m_2 & m_3 \end{pmatrix} = (-1)^{j_1-j_2-m_3} C^{j_1\, j_2\, j_3}_{m_1 m_2 -m_3} / (2j_3+1)^{\frac{1}{2}}$$

follows and is given in Appendix F.

7.3 ROTATIONAL TENSOR OPERATORS AND THE WIGNER-ECKART THEOREM

The theory and application of R_3 tensor operators will be introduced in this section. The development will be similar to that of Section 6.4, where the tensor operators of finite symmetry were introduced. First, the construction of tensor operators from bra and ket bases will be shown using simple

examples. Then the Wigner-Eckart theorem will be discussed and applied to atomic crystal field problems which were first encountered in Section 5.6. Racah coefficients will be introduced in a treatment of a two-electron crystal field splitting.

A. Construction of R_3 Tensor Operators

For each set of irrep bases $\left|{}^{j}_{m}\right\rangle$: $\left\{\left|{}^{j}_{j}\right\rangle, \left|{}^{j}_{j-1}\right\rangle, \ldots, \left|{}^{j}_{-j}\right\rangle\right\}$ of $2j+1$ ket vectors there is an equal number of bra vectors

$$(-1)^{j-m}\left\langle {}^{j}_{-m}\right|: \quad \left\{\left\langle {}^{j}_{-j}\right|, -\left\langle {}^{j}_{-j+1}\right|, \ldots, (-1)^{2j}\left\langle {}^{j}_{j}\right|\right\},$$

which belong to the same irrep $\mathscr{D}^j$. (Recall Section 7.2.B.) By combining them using coupling coefficients one may construct the IRREDUCIBLE TENSORIAL OPERATORS,

$$T(jj)^k_q = \sum_{m,m'} C^{j\,j\,k}_{mm'q}\left|{}^{j}_{m}\right\rangle\left\langle {}^{j}_{-m'}\right|(-1)^{j-m'}, \tag{7.3.1a}$$

which transform according to irrep $\mathscr{D}^k$ $(2j \geq k \geq 0)$ as follows:

$$R(\alpha\beta\gamma)T(jj)^k_q R^{\dagger}(\alpha\beta\gamma) = \sum_{q'} \mathscr{D}^k_{q'q}(\alpha\beta\gamma)T(jj)^k_{q'}. \tag{7.3.1b}$$

This is similar to the construction which was introduced in Section 6.4.A for finite-group irreps. The only difference is that now we must account for the different transformation behavior of the bra vectors.

If two or more sets $\left\{\left|{}^{j_1}_{j_1}\right\rangle, \ldots, \left|{}^{j_1}_{m_1}\right\rangle, \ldots\right\}, \left\{\left|{}^{j_2}_{j_2}\right\rangle, \ldots, \left|{}^{j_2}_{m_2}\right\rangle, \ldots\right\}, \ldots$ of angular-momentum states need to be considered, then one may make combinations

$$T(j_1 j_2)^k_q = \sum_{m_1, m_2} C^{j_1\,j_2\,k}_{m_1 m_2 q}\left|{}^{j_1}_{m_1}\right\rangle\left\langle {}^{j_2}_{-m_2}\right|(-1)^{j_2-m_2}, \tag{7.3.2}$$

where

$$j_1 + j_2 \geq k \geq |j_1 - j_2|.$$

All combinations are needed to make a complete set of irreducible tensor operators acting on the bases. The first few examples treated in the following will be based on a single set $\{|^{j}_{m}\rangle\}$ of angular-momentum states, and so there will only be one combination $T^k_q(jj) = T^k_q$ for each $k = 0, 1, \ldots, 2j$, and q. $(k \geq q \geq -k)$.

(a) Tensor Operators for Spin $-\frac{1}{2}$ States From the spin-$\frac{1}{2}$ states $\left\{\left|\begin{smallmatrix}\frac{1}{2}\\ \frac{1}{2}\end{smallmatrix}\right\rangle, \left|\begin{smallmatrix}\frac{1}{2}\\ -\frac{1}{2}\end{smallmatrix}\right\rangle\right\}$ one may construct the tensor operators

$$T_q^k = \sum_{m_1} C^{\frac{1}{2}\,\frac{1}{2}\,k}_{m_1 m_2 q} \left|\begin{matrix}\frac{1}{2}\\ m_1\end{matrix}\right\rangle\left\langle\begin{matrix}\frac{1}{2}\\ -m_2\end{matrix}\right| (-1)^{\frac{1}{2}-m_2}, \tag{7.3.3}$$

using $\frac{1}{2} \otimes \frac{1}{2}$ coupling coefficients (7.1.7). The results are given in the following with their representations in the spin-$\frac{1}{2}$ basis:

$$\begin{aligned}
T^1_{-1} &= \begin{pmatrix} 0 & 0 \\ -1 & 0 \end{pmatrix} & T^1_0 &= \frac{1}{\sqrt{2}}\begin{pmatrix} -1 & 0 \\ 0 & 1 \end{pmatrix} & T^1_1 &= \begin{pmatrix} 0 & 1 \\ 0 & 0 \end{pmatrix} \\
&= -\left|\begin{matrix}\frac{1}{2}\\ -\frac{1}{2}\end{matrix}\right\rangle\left\langle\begin{matrix}\frac{1}{2}\\ -\frac{1}{2}\end{matrix}\right|, & &= -\frac{1}{\sqrt{2}}\left[\left|\begin{matrix}\frac{1}{2}\\ \frac{1}{2}\end{matrix}\right\rangle\left\langle\begin{matrix}\frac{1}{2}\\ \frac{1}{2}\end{matrix}\right| - \left|\begin{matrix}\frac{1}{2}\\ -\frac{1}{2}\end{matrix}\right\rangle\left\langle\begin{matrix}\frac{1}{2}\\ -\frac{1}{2}\end{matrix}\right|\right], & &= \left|\begin{matrix}\frac{1}{2}\\ \frac{1}{2}\end{matrix}\right\rangle\left\langle\begin{matrix}\frac{1}{2}\\ -\frac{1}{2}\end{matrix}\right|,
\end{aligned}$$

$$\begin{aligned}
T^0_0 &= -\frac{1}{\sqrt{2}}\begin{pmatrix} 1 & 0 \\ 0 & 1 \end{pmatrix} \\
&= -\frac{1}{\sqrt{2}}\left[\left|\begin{matrix}\frac{1}{2}\\ \frac{1}{2}\end{matrix}\right\rangle\left\langle\begin{matrix}\frac{1}{2}\\ \frac{1}{2}\end{matrix}\right| + \left|\begin{matrix}\frac{1}{2}\\ -\frac{1}{2}\end{matrix}\right\rangle\left\langle\begin{matrix}\frac{1}{2}\\ -\frac{1}{2}\end{matrix}\right|\right].
\end{aligned} \tag{7.3.3}_x$$

The first three operators form a vector set. Consider the following Cartesian combinations:

$$\begin{aligned}
T_x &\equiv -\frac{T^1_{-1} - T^1_1}{\sqrt{2}} & T_y &\equiv -i\frac{T^1_{-1} + T^1_1}{\sqrt{2}} & T_z &\equiv -T^1_0 \\
&= \frac{1}{\sqrt{2}}\begin{pmatrix} 0 & 1 \\ 1 & 0 \end{pmatrix} & &= \frac{1}{\sqrt{2}}\begin{pmatrix} 0 & -i \\ i & 0 \end{pmatrix} & &= \frac{1}{\sqrt{2}}\begin{pmatrix} 1 & 0 \\ 0 & -1 \end{pmatrix} \\
&\equiv \frac{1}{\sqrt{2}}\sigma_x & &\equiv \frac{1}{\sqrt{2}}\sigma_y & &\equiv \frac{1}{\sqrt{2}}\sigma_z \\
&\equiv \sqrt{2}J_x & &\equiv \sqrt{2}J_y & &\equiv \sqrt{2}J_z.
\end{aligned} \tag{7.3.4}$$

Except for an overall minus phase, these relations correspond to Eq. (7.2.3). The resulting Cartesian tensors are proportional to the Pauli spinor operators:

$$\sigma_x \to \begin{pmatrix} 0 & 1 \\ 1 & 0 \end{pmatrix}, \qquad \sigma_y \to \begin{pmatrix} 0 & -i \\ i & 0 \end{pmatrix}, \qquad \sigma_z \to \begin{pmatrix} 1 & 0 \\ 0 & -1 \end{pmatrix}, \tag{7.3.5}$$

or the spin-$\frac{1}{2}$ angular-momentum operators [recall the original definitions in Eq. (5.5.3)]:

$$J_x = \sigma_x/2, \qquad J_y = \sigma_y/2, \qquad J_z = \sigma_z/2. \tag{7.3.6}$$

An explicit example of the transformation behavior required by Eq. (7.3.1b)

is represented in the following:

$$
\begin{array}{ccccc}
R(0\beta 0) & & T_0^1 & & R^\dagger(0\beta 0) \quad = \quad T_0^{1'} \\
\downarrow & & \downarrow & & \downarrow \qquad\qquad \downarrow \\
\begin{pmatrix} \cos\frac{\beta}{2} & -\sin\frac{\beta}{2} \\ \sin\frac{\beta}{2} & \cos\frac{\beta}{2} \end{pmatrix} & & \begin{pmatrix} -1/\sqrt{2} & 0 \\ 0 & 1/\sqrt{2} \end{pmatrix} & & \begin{pmatrix} \cos\frac{\beta}{2} & \sin\frac{\beta}{2} \\ -\sin\frac{\beta}{2} & \cos\frac{\beta}{2} \end{pmatrix} = -\frac{1}{\sqrt{2}}\begin{pmatrix} \cos\beta & \sin\beta \\ \sin\beta & -\cos\beta \end{pmatrix}
\end{array}
$$

$$
= \mathscr{D}^1_{10}(0\beta 0)\,T_1^1 \quad + \mathscr{D}^1_{00}(0\beta 0)\,T_0^1 \quad + \mathscr{D}^1_{-10}(0\beta 0)\,T_{-1}^1
$$

$$
\downarrow \qquad\qquad \downarrow \qquad\qquad \downarrow
$$

$$
= \frac{-\sin\beta}{\sqrt{2}}\begin{pmatrix} 0 & 1 \\ 0 & 0 \end{pmatrix} + \cos\beta\begin{pmatrix} -1/\sqrt{2} & 0 \\ 0 & 1/\sqrt{2} \end{pmatrix} + \frac{\sin\beta}{\sqrt{2}}\begin{pmatrix} 0 & 0 \\ -1 & 0 \end{pmatrix}. \tag{7.3.7}
$$

The Cartesian form of this equation is simpler. Multiplying the angular-momentum form by $-1/\sqrt{2}$ and using Eq. (7.3.4) yields

$$J_z(\text{rotated}) \equiv R(0\beta 0)J_zR^\dagger(0\beta 0) = \sin\beta J_x + \cos\beta J_z. \tag{7.3.8}$$

It should be clear now that products of spinor bases form operator quantities that behave like ordinary vectors in 3-space. In this sense spinors are "square roots" of vectors. In order to appreciate the physical meaning of Eq. (7.3.8) one may take its expectation value in an arbitrary state $|\psi\rangle$:

$$\langle\psi|J_z(\text{rotated})|\psi\rangle = \sin\beta\langle\psi|J_x|\psi\rangle + \cos\beta\langle\psi|J_z|\psi\rangle. \tag{7.3.9}$$

Figure 7.3.1 shows how the average or expectation value of the component of J on the (z-rotated) axis is given by Eq. (7.3.9). However, one should remember that the *actual* values for the component in a Stern-Gerlach spin-$\frac{1}{2}$ analyzer will be $\hbar/2$ for some fraction for events and $-\hbar/2$ for the rest. (Recall discussions at the beginning of Chapter 1 and in Section 5.5.B.) By expanding the expectation matrix, one obtains the result in terms of the fractions or probabilities $\left|\left\langle\psi|R\middle|\begin{smallmatrix}\frac{1}{2}\\ m\end{smallmatrix}\right\rangle\right|^2$ (as usual, let $\hbar = 1$):

$$
\begin{aligned}
\langle\psi|R(\alpha\beta\gamma)J_zR^\dagger(\alpha\beta\gamma)|\psi\rangle &= \sum_m\sum_{m'}\left\langle\psi|R\middle|\begin{smallmatrix}\frac{1}{2}\\ m\end{smallmatrix}\right\rangle\left\langle\begin{smallmatrix}\frac{1}{2}\\ m\end{smallmatrix}\middle|J_z\middle|\begin{smallmatrix}\frac{1}{2}\\ m'\end{smallmatrix}\right\rangle\left\langle\begin{smallmatrix}\frac{1}{2}\\ m'\end{smallmatrix}\middle|R^\dagger\middle|\psi\right\rangle \\
&= \sum_m\left|\left\langle\psi|R\middle|\begin{smallmatrix}\frac{1}{2}\\ m\end{smallmatrix}\right\rangle\right|^2 m \\
&= \tfrac{1}{2}\left|\left\langle\psi|R\middle|\begin{smallmatrix}\frac{1}{2}\\ \frac{1}{2}\end{smallmatrix}\right\rangle\right|^2 - \tfrac{1}{2}\left|\left\langle\psi|R\middle|\begin{smallmatrix}\frac{1}{2}\\ -\frac{1}{2}\end{smallmatrix}\right\rangle\right|^2.
\end{aligned} \tag{7.3.10a}
$$

Each quantum amplitude $\left\langle\psi|R\middle|\begin{smallmatrix}\frac{1}{2}\\ m\end{smallmatrix}\right\rangle$ depends upon the initial unrotated ampli-

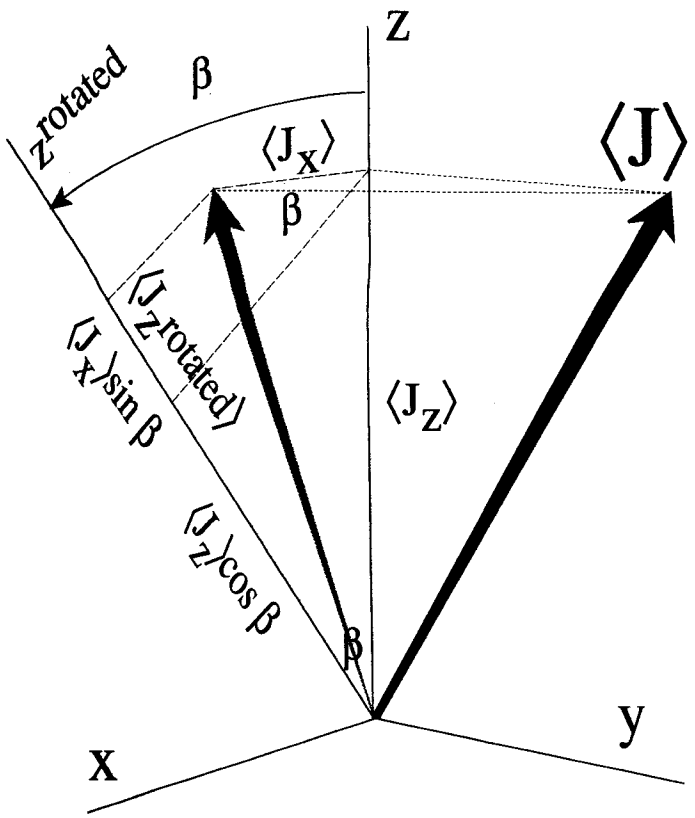

Figure 7.3.1 Geometry of expectation vector $\langle J \rangle$. Component on rotated z axis is determined by ordinary vector geometry. This picture collaborates the tensor equation (7.3.9).

tudes $\psi_{m'} = \left\langle \psi \middle| \begin{matrix} \frac{1}{2} \\ m' \end{matrix} \right\rangle$ and the rotation matrices:

$$\left\langle \psi | R(\alpha\beta\gamma) \middle| \begin{matrix} \frac{1}{2} \\ m \end{matrix} \right\rangle = \sum_{m'} \psi_{m'} \mathscr{D}^{\frac{1}{2}}_{m'm}(\alpha\beta\gamma). \tag{7.3.10b}$$

The well-known classical behavior of the angular-momentum vector emerges after many spin-$\frac{1}{2}$ states have passed the analyzer. The "expectation vector" for $|\psi\rangle$ states has components

$$\langle J_x \rangle = \langle \psi | J_x | \psi \rangle, \qquad \langle J_y \rangle = \langle \psi | J_y | \psi \rangle, \qquad \langle J_z \rangle = \langle \psi | J_z | \psi \rangle, \tag{7.3.11}$$

as indicated in Figure 7.3.1. This vector provides a useful picture of the properties of particles in a given pure spin-$\frac{1}{2}$ state. The vector picture will be studied in detail in Section 7.4.

(b) Tensor Operators for Higher Spin States ($j = 1, \frac{3}{2}, 2, \ldots, 4$) The $1 \otimes 1$ coupling coefficients (7.1.19) may be used to construct a complete set of nine tensor operators for the $j = 1$ basis. The tensor operators and their representations are given in the following, using Eq. (7.3.1a):

$$T^2_{-2} = \left|\begin{matrix}1\\-1\end{matrix}\right\rangle\left\langle\begin{matrix}1\\1\end{matrix}\right|, \quad T^2_{-1} = \frac{\left|\begin{matrix}1\\0\end{matrix}\right\rangle\left\langle\begin{matrix}1\\1\end{matrix}\right| - \left|\begin{matrix}1\\-1\end{matrix}\right\rangle\left\langle\begin{matrix}1\\0\end{matrix}\right|}{\sqrt{2}}, \quad T^2_0 = \frac{\left|\begin{matrix}1\\1\end{matrix}\right\rangle\left\langle\begin{matrix}1\\1\end{matrix}\right| - 2\left|\begin{matrix}1\\0\end{matrix}\right\rangle\left\langle\begin{matrix}1\\0\end{matrix}\right| + \left|\begin{matrix}1\\-1\end{matrix}\right\rangle\left\langle\begin{matrix}1\\-1\end{matrix}\right|}{\sqrt{6}}, \quad T^2_1 = \frac{-\left|\begin{matrix}1\\1\end{matrix}\right\rangle\left\langle\begin{matrix}1\\0\end{matrix}\right| + \left|\begin{matrix}1\\0\end{matrix}\right\rangle\left\langle\begin{matrix}1\\-1\end{matrix}\right|}{\sqrt{2}},$$

$$\to \begin{pmatrix}0&0&0\\0&0&0\\1&0&0\end{pmatrix} \quad \to \begin{pmatrix}0&0&0\\1/\sqrt{2}&0&0\\0&-1/\sqrt{2}&0\end{pmatrix} \quad \to \begin{pmatrix}1/\sqrt{6}&0&0\\0&-2/\sqrt{6}&0\\0&0&1/\sqrt{6}\end{pmatrix} \quad \to \begin{pmatrix}0&-1/\sqrt{2}&0\\0&0&1/\sqrt{2}\\0&0&0\end{pmatrix}$$

$$T^2_2 = \left|\begin{matrix}1\\1\end{matrix}\right\rangle\left\langle\begin{matrix}1\\-1\end{matrix}\right|, \quad T^1_{-1} = \frac{\left|\begin{matrix}1\\0\end{matrix}\right\rangle\left\langle\begin{matrix}1\\1\end{matrix}\right| + \left|\begin{matrix}1\\-1\end{matrix}\right\rangle\left\langle\begin{matrix}1\\0\end{matrix}\right|}{\sqrt{2}}, \quad T^1_0 = \frac{\left|\begin{matrix}1\\1\end{matrix}\right\rangle\left\langle\begin{matrix}1\\1\end{matrix}\right| - \left|\begin{matrix}1\\-1\end{matrix}\right\rangle\left\langle\begin{matrix}1\\-1\end{matrix}\right|}{\sqrt{2}}, \quad T^1_1 = \frac{-\left|\begin{matrix}1\\0\end{matrix}\right\rangle\left\langle\begin{matrix}1\\0\end{matrix}\right| - \left|\begin{matrix}1\\0\end{matrix}\right\rangle\left\langle\begin{matrix}1\\-1\end{matrix}\right|}{\sqrt{2}},$$

$$\to \begin{pmatrix}0&0&1\\0&0&0\\0&0&0\end{pmatrix} \quad \to \begin{pmatrix}0&0&0\\1/\sqrt{2}&0&0\\0&1/\sqrt{2}&0\end{pmatrix} \quad \to \begin{pmatrix}1/\sqrt{2}&0&0\\0&0&0\\0&0&-1/\sqrt{2}\end{pmatrix} \quad \to \begin{pmatrix}0&-1/\sqrt{2}&0\\0&0&-1/\sqrt{2}\\0&0&0\end{pmatrix}$$

$$T^0_0 = \frac{\left|\begin{matrix}1\\1\end{matrix}\right\rangle\left\langle\begin{matrix}1\\1\end{matrix}\right| + \left|\begin{matrix}1\\0\end{matrix}\right\rangle\left\langle\begin{matrix}1\\0\end{matrix}\right| + \left|\begin{matrix}1\\-1\end{matrix}\right\rangle\left\langle\begin{matrix}1\\-1\end{matrix}\right|}{\sqrt{3}}$$

$$\to \begin{pmatrix}1/\sqrt{3}&0&0\\0&1/\sqrt{3}&0\\0&0&1/\sqrt{3}\end{pmatrix}. \tag{7.3.12}$$

The lower four operators are the scalar ($k = 0$) and vector ($k = 1$) operators. T^0_0 is proportional to the identity (1), and T^1_{-1}, T^1_0, and T^1_1 are proportional to the angular-momentum operators J_-, J_z, and J_+, respectively. This follows from a comparison with the original $\mathscr{D}^{j=1}$ representations given by Eqs. (5.4.21)–(5.4.25):

$$\begin{aligned} T^1_{-1} &= J_-/2 & T^1_0 &= J_z/\sqrt{2} & T^1_1 &= -J_+/2, \\ &= (J_x - iJ_y)/2 & & & &= -(J_x + iJ_y)/2. \end{aligned} \tag{7.3.13}$$

The three tensor operators (T^1_{-1}, T^1_0, T^1_1) or (J_x, J_y, J_z) have the same tranformation properties as the corresponding vector operators constructed in the spin-$\frac{1}{2}$ basis. Of course, the scalar operator T^0_0 is invariant.

Beyond the scalar and vector operators in Eq. (7.3.12) there are five more ($k = 2$) operators $\{T^2_{-2}, T^2_{-1}, T^2_0, T^2_1, T^2_2\}$ known as unit quadrupole operators. These are the "tensor" operators which deserve this old-fashioned name. To label a ($j = 1$) state completely one needs a set of quadrupole tensor expectation values $\langle T^2_q \rangle$ as well as the $\langle T^1_q \rangle$ or $\langle J_a \rangle$ vector expectation values. The significance of these values will be discussed when we introduce irreducible density matrices.

Similarly, the quantum mechanics of higher j-states will require in general a complete set of $(2j+1)^2$ tensor operators. Let us define new tensor operators which differ by an overall phase factor $(-1)^{2j}$:

$$v_q^k = \sum_{m,m'} C^{j\ j\ k}_{m\ -m'q}(-1)^{j-m'}\left|\begin{matrix} j \\ m \end{matrix}\right\rangle\left\langle\begin{matrix} j \\ m' \end{matrix}\right| = (-1)^{2j}T_q^k. \quad (7.3.14a)$$

The $3-j$ definition (7.2.30a) and symmetry relations (7.2.31) and (7.2.32) yield the following alternative form:

$$v_q^k = \sum_{m,m'} (-1)^{j-m}\sqrt{2k+1}\begin{pmatrix} k & j & j \\ q & m' & -m \end{pmatrix}\left|\begin{matrix} j \\ m \end{matrix}\right\rangle\left\langle\begin{matrix} j \\ m' \end{matrix}\right|. \quad (7.3.14b)$$

The phase eliminates the annoying minus sign that occurs in T^k for half-integral j. [Recall Eqs. $(7.3.3)_x$.] The v_q^k representations are recorded in Tables 7.1–3 in a condensed form. To understand the condensed form, compare the $(j=1)$ tensor derived in Eq. (7.3.12) with the $j=l=1$ tables in Table 7.2(p). Note that each T_q^k has nonzero entries only in particular super- or subdiagonals of the matrix. Each superdiagonal is labeled by a number $q=1,\ldots,k$ in the tables. The main or center diagonal belongs to $q=0$ and the subdiagonals belong to $q=-1,-2,\ldots,-k$. At the end of each superdiagonal is a normalization denominator.

Note that each qth superdiagonal in a set of $v_q^q, v_q^{q+1},\ldots$ matrices gives a set of orthonormal vectors. For example, with $j=2$ the $q=2$ superdiagonals of Table 7.2(d) are

$$\left|\begin{matrix} \frac{\sqrt{3}}{\sqrt{14}} & \cdot & \cdot \\ \cdot & -\frac{\sqrt{8}}{\sqrt{14}} & \cdot \\ \cdot & \cdot & \frac{\sqrt{3}}{\sqrt{14}} \end{matrix}\right|, \quad \left|\begin{matrix} \frac{1}{\sqrt{2}} & \cdot & \cdot \\ \cdot & 0 & \cdot \\ \cdot & \cdot & -\frac{1}{\sqrt{2}} \end{matrix}\right|, \quad \left|\begin{matrix} \frac{\sqrt{2}}{\sqrt{7}} & \cdot & \cdot \\ \cdot & \frac{\sqrt{3}}{\sqrt{7}} & \cdot \\ \cdot & \cdot & \frac{\sqrt{2}}{\sqrt{7}} \end{matrix}\right|$$

(for $k=4$) (for $k=3$) (for $k=2$).

Because of orthonormality of coupling coefficients these diagonals are orthonormal vectors. This makes it easy to express any $(2j+1)$ by $(2j+1)$ matrix in terms of the v_q^k. For example, using the second numbers from the $q=2$ superdiagonals we easily find the following elementary matrix or operator:

$$\begin{pmatrix} 0 & 0 & 0 & 0 & 0 \\ 0 & 0 & 0 & 1 & 0 \\ 0 & 0 & 0 & 0 & 0 \\ 0 & 0 & 0 & 0 & 0 \\ 0 & 0 & 0 & 0 & 0 \end{pmatrix} \rightarrow -\frac{\sqrt{8}}{\sqrt{14}}v_2^4 + 0v_2^3 + \frac{\sqrt{3}}{\sqrt{7}}v_2^2 = E_{24}. \quad (7.3.15)$$

TABLE 7.1 (j) Subshell Tensors

(a) $j = \frac{1}{2}$

$q = 0 \quad 1$

$$v_q^1 = \begin{matrix} 1 & -1 & 1 \\ 1 & -1 & 1 \end{matrix} \quad \begin{matrix} \\ \\ \sqrt{2} \end{matrix}$$

(b) $j = \frac{3}{2}$

$q = 0 \quad 1 \quad 2 \quad 3$

$$v_q^1 = \begin{matrix} 3 & -\sqrt{3} & \cdot & \cdot \\ \sqrt{3} & 1 & -2 & \cdot \\ \cdot & 2 & -1 & -\sqrt{3} \\ \cdot & \cdot & \sqrt{3} & -3 \end{matrix} \quad \begin{matrix} \\ \\ \\ \sqrt{10} \\ \sqrt{20} \end{matrix}$$

$$v_q^2 = \begin{matrix} 1 & -1 & 1 & \cdot \\ 1 & -1 & 0 & 1 \\ 1 & 0 & -1 & 1 \\ \cdot & 1 & -1 & 1 \end{matrix} \quad \begin{matrix} \\ \sqrt{2} \\ \sqrt{2} \\ \sqrt{4} \end{matrix}$$

$$v_q^3 = \begin{matrix} 1 & -1 & 1 & -1 \\ 1 & -3 & \sqrt{3} & -1 \\ 1 & -\sqrt{3} & 3 & -1 \\ 1 & -1 & 1 & -1 \end{matrix} \quad \begin{matrix} 1 \\ \sqrt{2} \\ \sqrt{5} \\ \sqrt{20} \end{matrix}$$

(c) $j = \frac{5}{2}$

$q = 0 \quad 1 \quad 2 \quad 3 \quad 4 \quad 5$

$$v^1 q = \begin{matrix} 5 & -\sqrt{5} & \cdot & \cdot & \cdot & \cdot \\ \sqrt{5} & 3 & -\sqrt{8} & \cdot & \cdot & \cdot \\ \cdot & \sqrt{8} & 1 & -3 & \cdot & \cdot \\ \cdot & \cdot & 3 & -1 & -\sqrt{8} & \cdot \\ \cdot & \cdot & \cdot & \sqrt{8} & -3 & -\sqrt{5} \\ \cdot & \cdot & \cdot & \cdot & \sqrt{5} & -5 \end{matrix} \quad \begin{matrix} \\ \\ \\ \\ \sqrt{35} \\ \sqrt{70} \end{matrix}$$

$$v_q^2 = \begin{matrix} 5 & -\sqrt{5} & \sqrt{5} & \cdot & \cdot & \cdot \\ \sqrt{5} & -1 & -\sqrt{2} & 3 & \cdot & \cdot \\ \sqrt{5} & \sqrt{2} & -4 & 0 & 3 & \cdot \\ \cdot & 3 & 0 & -4 & \sqrt{2} & \sqrt{5} \\ \cdot & \cdot & 3 & -\sqrt{2} & -1 & \sqrt{5} \\ \cdot & \cdot & \cdot & \sqrt{5} & -\sqrt{5} & 5 \end{matrix} \quad \begin{matrix} \\ \\ \\ \sqrt{28} \\ \sqrt{14} \\ \sqrt{84} \end{matrix}$$

$$v_q^3 = \begin{matrix} 5 & -\sqrt{10} & \sqrt{5} & -\sqrt{5} & \cdot & \cdot \\ \sqrt{10} & -7 & 1 & 1 & -\sqrt{8} & \cdot \\ \sqrt{5} & -1 & -4 & \sqrt{8} & -1 & -\sqrt{5} \\ \sqrt{5} & 1 & -\sqrt{8} & 4 & 1 & -\sqrt{5} \\ \cdot & \sqrt{8} & -1 & -1 & 7 & -\sqrt{10} \\ \cdot & \cdot & \sqrt{5} & -\sqrt{5} & \sqrt{10} & -5 \end{matrix} \quad \begin{matrix} \\ \sqrt{18} \\ \sqrt{12} \\ \sqrt{30} \\ \sqrt{180} \end{matrix}$$

$$v_q^4 = \begin{matrix} 1 & -\sqrt{2} & 3 & -1 & 1 & \cdot \\ \sqrt{2} & -3 & \sqrt{5} & -\sqrt{5} & 0 & 1 \\ 3 & -\sqrt{5} & 2 & 0 & -\sqrt{5} & 1 \\ 1 & -\sqrt{5} & 0 & 2 & -\sqrt{5} & 3 \\ 1 & 0 & -\sqrt{5} & \sqrt{5} & -3 & \sqrt{2} \\ \cdot & 1 & -1 & 3 & -\sqrt{2} & 1 \end{matrix} \quad \begin{matrix} \\ \sqrt{2} \\ \sqrt{2} \\ \sqrt{28} \\ \sqrt{14} \\ \sqrt{28} \end{matrix}$$

$$v_q^5 = \begin{matrix} 1 & -1 & 1 & -\sqrt{2} & 1 & -1 \\ 1 & -5 & \sqrt{10} & -\sqrt{5} & \sqrt{5} & -1 \\ 1 & -\sqrt{10} & 10 & -\sqrt{20} & \sqrt{5} & -\sqrt{2} \\ \sqrt{2} & -\sqrt{5} & \sqrt{20} & -10 & \sqrt{10} & -1 \\ 1 & -\sqrt{5} & \sqrt{5} & -\sqrt{10} & 5 & -1 \\ 1 & -1 & \sqrt{2} & -1 & 1 & -1 \end{matrix} \quad \begin{matrix} 1 \\ \sqrt{2} \\ \sqrt{9} \\ \sqrt{12} \\ \sqrt{42} \\ \sqrt{252} \end{matrix}$$

Linear relations between the irreducible tensor operators v_q^k and the elementary unitary operators $E_{m,m+q}$ will be used in later chapters. A simple example of such a relation involves the $q = 0$ operators for ($j = 1$). From Eq. (7.3.12) [or the diagonals of Table 7.2(p)] one may write

$$\begin{aligned} v_0^2 &= (E_{11} - 2E_{22} + E_{33})/\sqrt{6}\,, \\ v_0^1 &= (E_{11} - E_{33})/\sqrt{2}\,, \\ v_0^0 &= (E_{11} + E_{22} + E_{33})/\sqrt{3}\,. \end{aligned} \tag{7.3.16}$$

TABLE 7.2 (l) Subshell Tensors

$v_q^6 =$

$q=0$	1	2	3	4	5	6	
−1	1	$-\sqrt{2}$	1	$-\sqrt{2}$	$\sqrt{5}$	−1	1
	$\sqrt{2}$	−6	$\sqrt{30}$	$-\sqrt{8}$	3	$-\sqrt{12}$	1
	1	$-\sqrt{30}$	15	−10	$\sqrt{15}$	−3	$\sqrt{5}$
	$\sqrt{2}$	$-\sqrt{8}$	10	−20	10	$-\sqrt{8}$	$\sqrt{2}$
	$\sqrt{5}$	−3	$\sqrt{15}$	−10	15	$-\sqrt{30}$	1
	1	$-\sqrt{12}$	3	$-\sqrt{8}$	$\sqrt{30}$	−6	$\sqrt{2}$
	1	−1	$\sqrt{5}$	$-\sqrt{2}$	1	$-\sqrt{2}$	1

	1	$-\sqrt{5}$	1	$-\sqrt{2}$	1	−1	·
	$\sqrt{5}$	−4	$\sqrt{27}$	$-\sqrt{2}$	1	0	−1
	1	$-\sqrt{27}$	5	$-\sqrt{10}$	0	1	−1
	$\sqrt{2}$	$-\sqrt{2}$	$\sqrt{10}$	0	$-\sqrt{10}$	$\sqrt{2}$	$-\sqrt{2}$
	1	−1	0	$\sqrt{10}$	−5	$\sqrt{27}$	−1
	1	0	−1	$\sqrt{2}$	$-\sqrt{27}$	4	$-\sqrt{5}$
	·	1	−1	$\sqrt{2}$	−1	$\sqrt{5}$	−1

$v_q^5 =$

	3	$-\sqrt{30}$	$\sqrt{54}$	−3	$\sqrt{3}$	·	·
	$\sqrt{30}$	−7	$\sqrt{32}$	$-\sqrt{3}$	$-\sqrt{2}$	$\sqrt{5}$	·
	$\sqrt{54}$	$-\sqrt{32}$	1	$\sqrt{15}$	$-\sqrt{40}$	$\sqrt{2}$	$\sqrt{3}$
	3	$-\sqrt{3}$	$-\sqrt{15}$	6	$-\sqrt{15}$	$-\sqrt{3}$	3
	$\sqrt{3}$	$\sqrt{2}$	$-\sqrt{40}$	$\sqrt{15}$	1	$-\sqrt{32}$	$\sqrt{54}$
	·	$\sqrt{5}$	$-\sqrt{2}$	$-\sqrt{3}$	$\sqrt{32}$	−7	$\sqrt{30}$
	·	·	$\sqrt{3}$	−3	$\sqrt{54}$	$-\sqrt{30}$	3

$v_q^4 =$

	1	$-\sqrt{2}$	$\sqrt{2}$	−1	·	·	·
	$\sqrt{2}$	−1	0	1	$-\sqrt{2}$	·	·
	$\sqrt{2}$	0	−1	1	0	$-\sqrt{2}$	·
	1	1	−1	0	1	−1	−1
	·	$\sqrt{2}$	0	−1	1	0	$-\sqrt{2}$
	·	·	$\sqrt{2}$	−1	0	1	$-\sqrt{2}$
	·	·	·	1	$-\sqrt{2}$	$\sqrt{2}$	−1

$v_q^3 =$

	5	−5	$\sqrt{5}$	·	·	·	·
	5	0	$-\sqrt{15}$	$\sqrt{10}$	·	·	·
	$\sqrt{5}$	$\sqrt{15}$	−3	$-\sqrt{2}$	$\sqrt{12}$	·	·
	·	$\sqrt{10}$	$\sqrt{2}$	−4	$\sqrt{2}$	$\sqrt{10}$	·
	·	·	$\sqrt{12}$	$-\sqrt{2}$	−3	$\sqrt{15}$	$\sqrt{5}$
	·	·	·	$\sqrt{10}$	$-\sqrt{15}$	0	5
	·	·	·	·	$\sqrt{5}$	−5	5

$v_q^2 =$

	3	$-\sqrt{3}$	·	·	·	·	·
	$\sqrt{3}$	2	$-\sqrt{5}$	·	·	·	·
	·	$\sqrt{5}$	1	$-\sqrt{6}$	·	·	·
	·	·	$\sqrt{6}$	0	$-\sqrt{6}$	·	·
	·	·	·	$\sqrt{6}$	−1	$-\sqrt{5}$	·
	·	·	·	·	$\sqrt{5}$	−2	$-\sqrt{3}$
	·	·	·	·	·	$\sqrt{3}$	−3

$v_q^1 =$

(f) $l = 3$

$q=0$	1	2	3	4	
	1	−1	$\sqrt{3}$	−1	1
	1	−4	$\sqrt{6}$	$-\sqrt{8}$	1
	$\sqrt{3}$	$-\sqrt{6}$	6	$-\sqrt{6}$	$\sqrt{3}$
	1	$-\sqrt{8}$	$\sqrt{6}$	−4	1
	1	−1	$\sqrt{3}$	−1	1

	1	$-\sqrt{3}$	1	−1	·
	$\sqrt{3}$	−2	$\sqrt{2}$	0	−1
	1	$-\sqrt{2}$	0	$\sqrt{2}$	−1
	1	0	$-\sqrt{2}$	2	$-\sqrt{3}$
	·	1	−1	$\sqrt{3}$	−1

	2	$-\sqrt{6}$	$\sqrt{2}$	·	·
	$\sqrt{6}$	−1	−1	$\sqrt{3}$	·
	$\sqrt{2}$	1	−2	1	$\sqrt{2}$
	·	$\sqrt{3}$	−1	−1	$\sqrt{6}$
	·	·	$\sqrt{2}$	$-\sqrt{6}$	2

	2	$-\sqrt{2}$	·	·	·
	$\sqrt{2}$	1	$-\sqrt{3}$	·	·
	·	$\sqrt{3}$	0	$-\sqrt{3}$	·
	·	·	$\sqrt{3}$	−1	$-\sqrt{2}$
	·	·	·	$\sqrt{2}$	−2

(d) $l = 2$

$q=0$	1	2	
	1	−1	1
	1	−2	1
	1	−1	1

	1	−1	·
	1	0	−1
	·	1	−1

(p) $l = 1$

[Here the row-column indices of the elementary operators are simply numbers (1, 2, and 3) rather than angular-momentum quanta ($m = 1$, 0, and -1).] These operators are proportional to the diagonal U_3 operators introduced in Eq. (5.8.41).

The $(2j+1)^2$ tensor operators $v_q^k(jj)$ are a complete set of generators of the group U_{2j+1}, and so are the elementary operators $E_{m,n}$. Every operator that acts on a $(2j+1)$-dimensional angular-momentum basis $\{|{}^j_j\rangle, |{}^j_{j-1}\rangle, \ldots, |{}^j_{-j}\rangle\}$ is a linear combination of elementary operators $E_{m,n}$, and hence, also a combination of v_q^k's.

(c) Mixed Angular-Momentum Bases Two or more sets

$$\left\{\left|\begin{matrix} j_1 \\ j_1 \end{matrix}\right\rangle, \left|\begin{matrix} j_1 \\ j_1 - 1 \end{matrix}\right\rangle, \ldots\right\}, \left\{\left|\begin{matrix} j_2 \\ j_2 \end{matrix}\right\rangle, \ldots\right\}, \ldots$$

of angular-momentum bases are connected by generalized tensor operators of the following form:

$$v(j_1 j_2)^k_q = (-1)^{2j_1} \sum_{m_1 m_2} C^{j_1\ j_2\ k}_{m_1 -m_2 q} \left|\begin{matrix} j_1 \\ m_1 \end{matrix}\right\rangle \left\langle\begin{matrix} j_2 \\ m_2 \end{matrix}\right| (-1)^{j_2+m_2} \tag{7.3.17a}$$

$$= \sum_{m_1 m_2} (-1)^{j_1-m_1} \sqrt{2k+1} \begin{pmatrix} k & j_2 & j_1 \\ q & m_2 & -m_1 \end{pmatrix} \left|\begin{matrix} j_1 \\ m_1 \end{matrix}\right\rangle \left\langle\begin{matrix} j_2 \\ m_2 \end{matrix}\right|. \tag{7.3.17b}$$

This differs only by a phase $(-1)^{2j_1}$ from the T operator given in Eq. (7.3.2). For $j_1 = j_2$ it reduces to the definition of Eq. (7.3.14). For nonzero "shift" Δ, where

$$\Delta = j_1 - j_2, \tag{7.3.18}$$

the matrix representations of the operators are rectangular. Some examples are shown in Table 7.4 for integral $j_1, j_2 = 1 - 3$. Two explicit examples are the following:

$$\sqrt{10}\, V^1_1(pd) = \begin{bmatrix} \cdot & \cdot & 1 & \cdot & \cdot \\ \cdot & \cdot & \cdot & \sqrt{3} & \cdot \\ \cdot & \cdot & \cdot & \cdot & \sqrt{6} \end{bmatrix}$$

$$= E_{63} + \sqrt{3}\, E_{74} + \sqrt{6}\, E_{85}$$

$$\sqrt{10}\, V^1_{-1}(dp) = \begin{bmatrix} \cdot & \cdot & \cdot \\ \cdot & \cdot & \cdot \\ 1 & \cdot & \cdot \\ \cdot & \sqrt{3} & \cdot \\ \cdot & \cdot & \sqrt{6} \end{bmatrix}$$

$$= E_{36} + \sqrt{3}\, E_{47} + \sqrt{6}\, E_{58}.$$

TABLE 7.3 (g) $l = 4$

$q = 0 \quad 1 \quad 2 \quad 3 \quad 4 \quad 5 \quad 6 \quad 7 \quad 8$

$V_q^8 =$

1	-1	1	-1	$\sqrt{5}$	-1	$\sqrt{7}$	-1	1	
1	-8	$\sqrt{28}$	-4	$\sqrt{10}$	$-\sqrt{32}$	2	-4	1	1
1	$-\sqrt{28}$	28	-14	$\sqrt{70}$	$-\sqrt{28}$	$\sqrt{56}$	-2	$\sqrt{7}$	$\sqrt{2}$
1	-4	14	-56	$\sqrt{490}$	$-\sqrt{112}$	$\sqrt{28}$	$-\sqrt{32}$	1	$\sqrt{30}$
$\sqrt{5}$	$-\sqrt{10}$	$\sqrt{70}$	$-\sqrt{490}$	70	$-\sqrt{490}$	$\sqrt{70}$	$-\sqrt{10}$	$\sqrt{5}$	$\sqrt{10}$
1	$-\sqrt{32}$	$\sqrt{28}$	$-\sqrt{112}$	$\sqrt{490}$	-56	14	-4	1	$\sqrt{130}$
$\sqrt{7}$	-2	$\sqrt{56}$	$-\sqrt{28}$	$\sqrt{70}$	-14	28	$-\sqrt{28}$	1	$\sqrt{78}$
1	-4	2	$-\sqrt{32}$	$\sqrt{10}$	-4	$\sqrt{28}$	-8	1	$\sqrt{286}$
1	-1	$\sqrt{7}$	-1	$\sqrt{5}$	-1	1	-1	1	$\sqrt{1430}$

$V_q^7 =$

1	$-\sqrt{7}$	3	-5	$\sqrt{5}$	-3	1	-1	·	$\sqrt{12870}$
$\sqrt{7}$	-6	10	-8	$\sqrt{90}$	$-\sqrt{8}$	2	0	-1	
3	-10	14	$-\sqrt{252}$	$\sqrt{70}$	$-\sqrt{28}$	0	2	-1	$\sqrt{2}$
5	-8	$\sqrt{252}$	-14	$\sqrt{70}$	0	$-\sqrt{28}$	$\sqrt{8}$	-3	$\sqrt{2}$
$\sqrt{5}$	$-\sqrt{90}$	$\sqrt{70}$	$-\sqrt{70}$	0	$\sqrt{70}$	$-\sqrt{70}$	$\sqrt{90}$	$-\sqrt{5}$	$\sqrt{26}$
3	$-\sqrt{8}$	$\sqrt{28}$	0	$-\sqrt{70}$	14	$-\sqrt{252}$	8	-5	$\sqrt{26}$
1	-2	0	$\sqrt{28}$	$-\sqrt{70}$	$\sqrt{252}$	-14	10	-3	$\sqrt{286}$
1	0	-2	$\sqrt{8}$	$-\sqrt{90}$	8	-10	6	$-\sqrt{7}$	$\sqrt{286}$
·	1	-1	3	$-\sqrt{5}$	5	-3	$\sqrt{7}$	-1	$\sqrt{858}$

$V_q^6 =$

4	$-\sqrt{28}$	2	-4	$\sqrt{40}$	-2	2	·	·	$\sqrt{858}$
$\sqrt{28}$	-17	13	-3	$\sqrt{10}$	-1	-1	$\sqrt{7}$	·	
2	-13	22	$-\sqrt{63}$	0	$\sqrt{7}$	$-\sqrt{28}$	1	2	
4	-3	$\sqrt{63}$	1	$-\sqrt{70}$	$\sqrt{7}$	$-\sqrt{7}$	-1	2	$\sqrt{15}$
$\sqrt{40}$	$-\sqrt{10}$	0	$\sqrt{70}$	-20	$\sqrt{70}$	0	$-\sqrt{10}$	$\sqrt{40}$	$\sqrt{10}$
2	-1	$-\sqrt{7}$	$\sqrt{7}$	$-\sqrt{70}$	1	$\sqrt{63}$	-3	4	$\sqrt{110}$
2	1	$-\sqrt{28}$	$\sqrt{7}$	0	$-\sqrt{63}$	22	-13	2	$\sqrt{66}$
·	$\sqrt{7}$	-1	-1	$\sqrt{10}$	-3	13	-17	$\sqrt{28}$	$\sqrt{33}$
·	·	2	-2	$\sqrt{40}$	-4	2	$-\sqrt{28}$	4	$\sqrt{660}$

$V_q^5 =$

4	$-\sqrt{20}$	$\sqrt{20}$	$-\sqrt{80}$	$\sqrt{8}$	-2	·	·	·	$\sqrt{1980}$
$\sqrt{20}$	-11	$\sqrt{35}$	$-\sqrt{5}$	$-\sqrt{2}$	$\sqrt{5}$	-3	·	·	
$\sqrt{20}$	$-\sqrt{35}$	4	$\sqrt{5}$	$-\sqrt{14}$	$\sqrt{35}$	0	-3	·	
$\sqrt{80}$	$-\sqrt{5}$	$-\sqrt{5}$	9	$-\sqrt{18}$	0	$\sqrt{35}$	$-\sqrt{5}$	-2	
$\sqrt{8}$	$\sqrt{2}$	$-\sqrt{14}$	$\sqrt{18}$	0	$-\sqrt{18}$	$\sqrt{14}$	$-\sqrt{2}$	$-\sqrt{8}$	$\sqrt{26}$
2	$\sqrt{5}$	$-\sqrt{35}$	0	$\sqrt{18}$	-9	$\sqrt{5}$	$\sqrt{5}$	$-\sqrt{80}$	$\sqrt{26}$
·	3	0	$-\sqrt{35}$	$\sqrt{14}$	$-\sqrt{5}$	-4	$\sqrt{35}$	$-\sqrt{20}$	$\sqrt{234}$
·	·	3	$-\sqrt{5}$	$\sqrt{2}$	$\sqrt{5}$	$-\sqrt{35}$	11	$-\sqrt{20}$	$\sqrt{78}$
·	·	·	2	$-\sqrt{8}$	$\sqrt{80}$	$-\sqrt{20}$	$\sqrt{20}$	-4	$\sqrt{156}$
									$\sqrt{468}$

$q = 0 \quad 1 \quad 2 \quad 3 \quad 4 \quad 5 \quad 6 \quad 7 \quad 8$

$$V_q^4 = \begin{array}{|ccccccccc|l}
\hline
14 & -\sqrt{490} & \sqrt{630} & -\sqrt{70} & \sqrt{14} & \cdot & \cdot & \cdot & \cdot & \\
\sqrt{490} & -21 & \sqrt{70} & \sqrt{70} & -\sqrt{63} & \sqrt{35} & \cdot & \cdot & \cdot & \\
\sqrt{630} & -\sqrt{70} & -11 & \sqrt{360} & -11 & -\sqrt{10} & \sqrt{45} & \cdot & \cdot & \\
\sqrt{70} & \sqrt{70} & -\sqrt{360} & 9 & 9 & -\sqrt{360} & \sqrt{10} & \sqrt{35} & \cdot & \\
\sqrt{14} & \sqrt{63} & -11 & -9 & 18 & -9 & -11 & \sqrt{63} & \sqrt{14} & \\
\cdot & \sqrt{35} & \sqrt{10} & -\sqrt{360} & 9 & 9 & -\sqrt{360} & \sqrt{70} & \sqrt{70} & \sqrt{143} \\
\cdot & \cdot & \sqrt{45} & -\sqrt{10} & -11 & \sqrt{360} & -11 & -\sqrt{70} & \sqrt{630} & \sqrt{286} \\
\cdot & \cdot & \cdot & \sqrt{35} & -\sqrt{63} & \sqrt{70} & \sqrt{70} & -21 & \sqrt{490} & \sqrt{2002} \\
\cdot & \cdot & \cdot & \cdot & \sqrt{14} & -\sqrt{70} & \sqrt{630} & -\sqrt{490} & 14 & \sqrt{2002} \\
\hline
\end{array}$$

$$V_q^3 = \begin{array}{|ccccccccc|l}
\hline
14 & -\sqrt{98} & \sqrt{14} & -\sqrt{14} & \cdot & \cdot & \cdot & \cdot & \cdot & \\
\sqrt{98} & -7 & -\sqrt{14} & \sqrt{14} & -\sqrt{35} & \cdot & \cdot & \cdot & \cdot & \\
\sqrt{14} & \sqrt{14} & -13 & \sqrt{8} & \sqrt{5} & -\sqrt{50} & \cdot & \cdot & \cdot & \\
\sqrt{14} & \sqrt{14} & -\sqrt{8} & -9 & \sqrt{45} & 0 & -\sqrt{50} & \cdot & \cdot & \\
\cdot & \sqrt{35} & \sqrt{5} & -\sqrt{45} & 0 & \sqrt{45} & -\sqrt{5} & -\sqrt{35} & \cdot & \\
\cdot & \cdot & \sqrt{50} & 0 & -\sqrt{45} & 9 & \sqrt{8} & -\sqrt{14} & -\sqrt{14} & \sqrt{198} \\
\cdot & \cdot & \cdot & \sqrt{50} & -\sqrt{5} & -\sqrt{8} & 13 & -\sqrt{14} & -\sqrt{14} & \sqrt{66} \\
\cdot & \cdot & \cdot & \cdot & \sqrt{35} & -\sqrt{14} & \sqrt{14} & 7 & -\sqrt{98} & \sqrt{330} \\
\cdot & \cdot & \cdot & \cdot & \cdot & \sqrt{14} & -\sqrt{14} & \sqrt{98} & -14 & \sqrt{990} \\
\hline
\end{array}$$

$$V_q^2 = \begin{array}{|ccccccccc|l}
\hline
28 & -14 & \sqrt{28} & \cdot & \cdot & \cdot & \cdot & \cdot & \cdot & \\
14 & 7 & -\sqrt{175} & \sqrt{63} & \cdot & \cdot & \cdot & \cdot & \cdot & \\
\sqrt{28} & \sqrt{175} & -8 & -9 & \sqrt{90} & \cdot & \cdot & \cdot & \cdot & \\
\cdot & \sqrt{63} & 9 & -17 & -\sqrt{10} & 10 & \cdot & \cdot & \cdot & \\
\cdot & \cdot & \sqrt{90} & \sqrt{10} & -20 & \sqrt{10} & \sqrt{90} & \cdot & \cdot & \\
\cdot & \cdot & \cdot & 10 & -\sqrt{10} & -17 & 9 & \sqrt{63} & \cdot & \\
\cdot & \cdot & \cdot & \cdot & \sqrt{90} & -9 & -8 & \sqrt{175} & \sqrt{28} & \\
\cdot & \cdot & \cdot & \cdot & \cdot & \sqrt{63} & -\sqrt{175} & 7 & 14 & \sqrt{462} \\
\cdot & \cdot & \cdot & \cdot & \cdot & \cdot & \sqrt{28} & -14 & 28 & \sqrt{924} \\
\hline
\end{array}$$

$$V_q^1 = \begin{array}{|ccccccccc|l}
\hline
4 & -2 & \cdot & \cdot & \cdot & \cdot & \cdot & \cdot & \cdot & \\
2 & 3 & -\sqrt{7} & \cdot & \cdot & \cdot & \cdot & \cdot & \cdot & \\
\cdot & \sqrt{7} & 2 & -3 & \cdot & \cdot & \cdot & \cdot & \cdot & \\
\cdot & \cdot & 3 & 1 & -\sqrt{10} & \cdot & \cdot & \cdot & \cdot & \\
\cdot & \cdot & \cdot & \sqrt{10} & 0 & -\sqrt{10} & \cdot & \cdot & \cdot & \\
\cdot & \cdot & \cdot & \cdot & \sqrt{10} & -1 & -3 & \cdot & \cdot & \\
\cdot & \cdot & \cdot & \cdot & \cdot & 3 & -2 & -\sqrt{7} & \cdot & \\
\cdot & \cdot & \cdot & \cdot & \cdot & \cdot & \sqrt{7} & -3 & -2 & \sqrt{60} \\
\cdot & \cdot & \cdot & \cdot & \cdot & \cdot & \cdot & 2 & -4 & \sqrt{60} \\
\hline
\end{array}$$

TABLE 7.4 Mixed Subshell Tensonrs

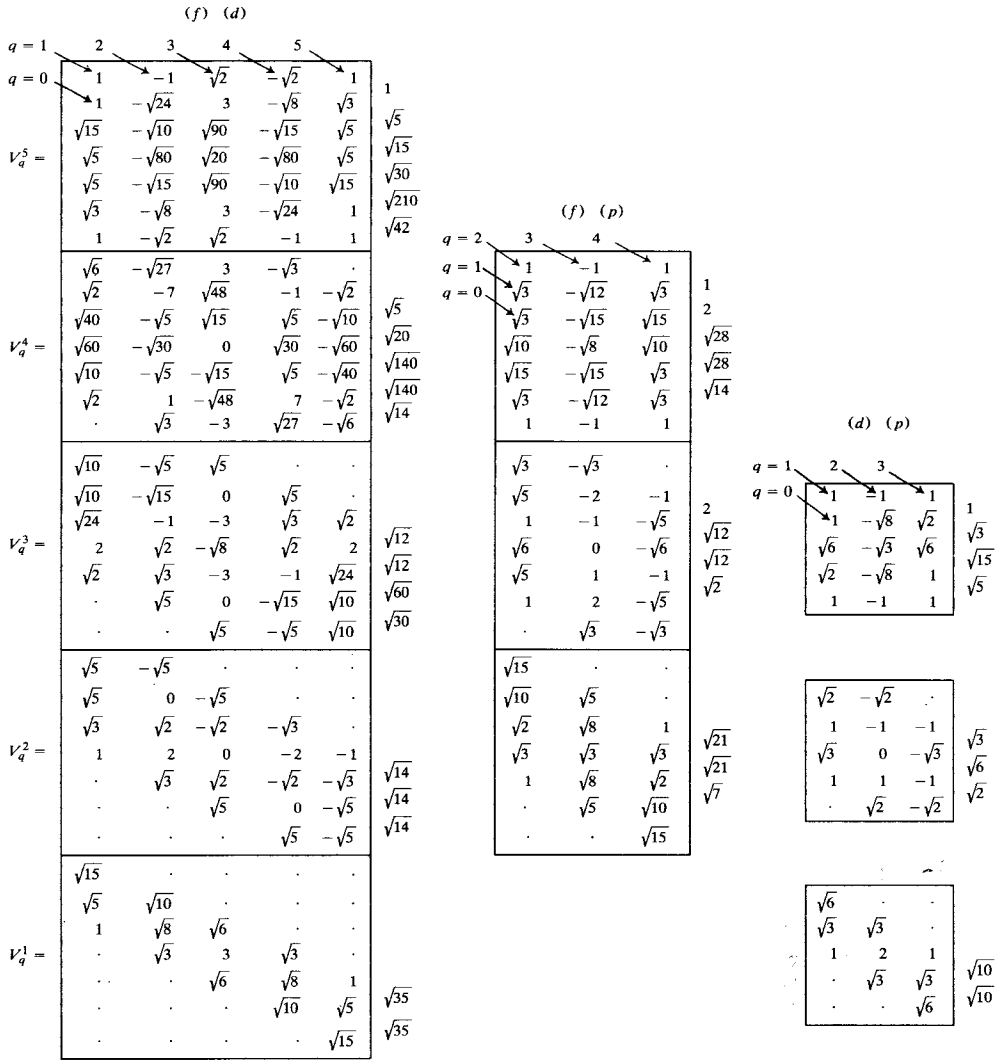

The numbering for E_{ij} reflects the choice of numbers 1 to 5 for d states ($|1\rangle = |^2_2\rangle, |2\rangle = |^2_1\rangle, \ldots, |5\rangle = |^2_{-2}\rangle$) and 6 to 8 for the p states ($|6\rangle = |^1_1\rangle, |7\rangle = |^1_0\rangle, |8\rangle = |^1_{-1}\rangle$. The tables exhibit the $v^k_q(l_1l_2)$ matrices for $l_1 - l_2 \equiv \Delta > 0$, and the transpose is found using the symmetry relation

$$v^k_q(l_2l_1) = (-1)^{l+q}\tilde{v}^k_{-q}(l_1l_2). \tag{7.3.19}$$

B. Wigner-Eckart Theorem for R_3

The Wigner-Eckart theorem for finite groups was proved in Section 6.4.B, and the same proof works for R_3 representations, too. It is only necessary to replace the sum over group elements $(1/{}^oG\Sigma_g)$ by the R_3 integral $(\int d(\alpha\beta\gamma))$ and apply the R_3-factorization lemma (Eq. 7.2.25) instead of Eq. (6.2.15). In fact, the R_3 problem is simpler, since there is no repetition of any irrep $\mathscr{D}^{j_3}$ in the reduction of a product $\mathscr{D}^{j_1} \otimes \mathscr{D}^{j_2}$. We now restate the theorem as it applies to R_3.

R_3 Wigner-Eckart Theorem If an operator $T^k_{q_{j_1}}$ belongs to a set $\{T^k_{-q}, \ldots, T^k_q\}$ which transforms according to R_3 rotation matrices as follows:

$$R(\alpha\beta\gamma)T^k_q R^\dagger(\alpha\beta\gamma) = \sum_{m'_1=-j_1}^{j_1} T^k_{q'}\mathscr{D}^k_{q'q}(\alpha\beta\gamma),$$

then matrix elements of T^k_q in angular-momentum basis are of the form

$$\left\langle \begin{matrix} j_1 \\ m_1 \end{matrix} \middle| T^k_q \middle| \begin{matrix} j_2 \\ m_2 \end{matrix} \right\rangle = C^{k\,j_2\,j_3}_{q m_2 m_1} \langle j_1| \, |T^k| \, |j_2\rangle, \tag{7.3.20a}$$

where the $C^{k\,j_2\,j_1}_{q m_2 m_1}$ are coupling coefficients, and the constants

$$\langle j_1| \, |T^k| \, |j_2\rangle \equiv \frac{1}{2j_3+1} \sum_{q'=-k} \sum_{m'_2=-j_2} \sum_{m'_1=-j_1} C^{k\,j_2\,j_1}_{q' m'_2 m'_1} \left\langle \begin{matrix} j_1 \\ m'_1 \end{matrix} \middle| T^k_{q'} \middle| \begin{matrix} j_2 \\ m'_2 \end{matrix} \right\rangle \tag{7.3.20b}$$

are independent of q, m_2, or m_1.

The theorem implies that the representations of different tensor operators which transform according to a given irrep $\mathscr{D}^k$ must be proportional to each other. The proportionality constants $\langle j_1| \, |T^k| \, |j_2\rangle$ are called REDUCED MATRIX ELEMENTS.

In particular, a representation of any tensor operator T^k_q must be proportional to the unit tensor v^k_q defined by Eq. (7.3.17):

$$\begin{aligned} v^k_q &= (-1)^{2j_1} \sum C^{j_1\ j_2\ k}_{m_1 -m_2 q} (-1)^{j_2+m_2} \left| \begin{matrix} j_1 \\ m_1 \end{matrix} \right\rangle \left\langle \begin{matrix} j_2 \\ m_2 \end{matrix} \right| \\ &= \sum (-1)^{j_1-m_1} \sqrt{2k+1} \begin{pmatrix} k & j_2 & j_1 \\ q & m_2 & -m_1 \end{pmatrix} \left| \begin{matrix} j_1 \\ m_1 \end{matrix} \right\rangle \left\langle \begin{matrix} j_2 \\ m_2 \end{matrix} \right|. \end{aligned}$$

Indeed, the $3j$ definitions (7.2.30a) and symmetry relations (7.2.31) and

(7.3.32) yield the following:

$$\left\langle \begin{matrix} j_1 \\ m_1 \end{matrix} \middle| V_q^k \middle| \begin{matrix} j_2 \\ m_2 \end{matrix} \right\rangle = (-1)^{2j_1} C^{j_1\ j_2\ k}_{m_1 - m_2 q} (-1)^{j_2 + m_2}$$

$$= C^{k\ j_2\ j_1}_{q m_2 m_1} (-1)^{k + j_1 - j_2} \sqrt{(2k+1)/(2j_1+1)}\,. \quad (7.3.21)$$

This has the Wigner-Eckart form (7.3.20a) with the following reduced matrix element:

$$\langle j_1 | \, | v^k | \, | j_2 \rangle = (-1)^{k + j_1 - j_2} \sqrt{(2k+1)/(2j_1+1)}\,. \quad (7.3.22)$$

Therefore, we may replace matrix representations of general tensor operators T_q^k with the $\langle | v_q^k | \rangle$ (recall tables 7.1–7.4) multiplied by a constant:

$$\left\langle \begin{matrix} j_1 \\ m_1 \end{matrix} \middle| T_q^k \middle| \begin{matrix} j_2 \\ m_2 \end{matrix} \right\rangle = \left\langle \begin{matrix} j_1 \\ m_1 \end{matrix} \middle| v_q^k \middle| \begin{matrix} j_2 \\ m_2 \end{matrix} \right\rangle \frac{\langle j_1 | \, | T^k | \, | j_2 \rangle}{\langle j_1 | \, | v^k | \, | j_2 \rangle}. \quad (7.3.23)$$

Each representation of T_q^k in angular-momentum bases $|j_1\rangle$ and $|j_2\rangle$ equals a v_q^k matrix multiplied by the following factor:

$$\langle j_1 | \, | T^k | \, | j_2 \rangle / \langle j_1 | \, | v^k | \, | j_2 \rangle = \langle j_1 | \, | T^k | \, | j_2 \rangle (-1)^{k + j_1 - j_2} \left(\frac{2j_1 + 1}{2k+1} \right)^{\frac{1}{2}}. \quad (7.3.24)$$

This factor is proportional to the reduced matrix element of T^k. We now see some applications of the Wigner-Eckart theorem.

C. Evaluation of Crystal Field Splitting

Let us consider an elementary octahedral potential having the form

$$V^{(4)} = D\left[x^4 + y^4 + z^4 - \tfrac{3}{5} r^4 \right] = D\left[2\left(X_4^4 + X_{-4}^4 \right)/\sqrt{70} + \tfrac{2}{5} X_0^4 \right]. \quad (7.3.25)$$

This form was derived first in Eq. (5.6.28) using the multipole expansion. It also follows from the form of the elementary multipole functions (5.6.17) of fourth degree which are tabulated in Appendix F. The $V^{(4)}$ is the fourth-rank octahedral scalar (A_{1g}) function. [See Eq. (5.6.18).]

Let us consider the effect of this potential on a d orbital, i.e., orbitals belonging to total angular momentum $j = 2$. Setting $j_1 = j_2 = 2$ in Eqs. (7.3.23) and (7.3.24) gives

$$\langle V^{(4)} \rangle_{j=2} = D\left(2\left(v_4^4 + v_{-4}^4 \right)/\sqrt{70} + \tfrac{2}{5} v_0^4 \right) (\sqrt{5}/3) \langle 2 | \, | X^4 | \, | 2 \rangle. \quad (7.3.26)$$

From the ($j = 2$) tables [Tables 7.2(d)] the following representation of the potential is derived:

$$\langle V^{(4)}\rangle_{j=2} = (D/\sqrt{70})\begin{pmatrix} \frac{2}{5} & \cdot & \cdot & \cdot & 2 \\ \cdot & -\frac{8}{5} & \cdot & \cdot & \cdot \\ \cdot & \cdot & \frac{12}{5} & \cdot & \cdot \\ \cdot & \cdot & \cdot & -\frac{8}{5} & \cdot \\ 2 & \cdot & \cdot & \cdot & \frac{2}{5} \end{pmatrix}(\sqrt{5}/3)\langle 2|\,|X^4|\,|2\rangle. \tag{7.3.27}$$

The eigenvectors and eigenvalues of this matrix are easy to find. In fact we derived the eigenvectors $\left\{\left|\begin{smallmatrix}T_2\\1\end{smallmatrix}\right\rangle, \left|\begin{smallmatrix}T_2\\2\end{smallmatrix}\right\rangle, \left|\begin{smallmatrix}T_2\\3\end{smallmatrix}\right\rangle\right\}$ and $\left\{\left|\begin{smallmatrix}E\\1\end{smallmatrix}\right\rangle, \left|\begin{smallmatrix}E\\2\end{smallmatrix}\right\rangle\right\}$ in Eqs. (5.6.12) and (5.6.13) by symmetry projection even before introducing the potential. Now the eigenvalues follow by multiplying $\langle V^{(4)}\rangle$ by $\left|\begin{smallmatrix}T_2\\j\end{smallmatrix}\right\rangle$ or $\left|\begin{smallmatrix}E\\j\end{smallmatrix}\right\rangle$. The triply degenerate T_2 eigenvalue is

$$\left\langle \begin{matrix}T_2\\3\end{matrix}\middle|V^{(4)}\middle|\begin{matrix}T_2\\3\end{matrix}\right\rangle = \tfrac{1}{2}\left(\left\langle \begin{matrix}2\\-2\end{matrix}\right| - \left\langle \begin{matrix}2\\-2\end{matrix}\right|\right)V^4\left(\left|\begin{matrix}2\\2\end{matrix}\right\rangle - \left|\begin{matrix}2\\-2\end{matrix}\right\rangle\right)$$

$$= -8D\langle 2|\,|X^4|\,|2\rangle/(15\sqrt{14}), \tag{7.3.28a}$$

and the doubly degenerate E eigenvalue is

$$\left\langle \begin{matrix}E\\2\end{matrix}\middle|V^{(4)}\middle|\begin{matrix}E\\2\end{matrix}\right\rangle = \tfrac{1}{2}\left(\left\langle \begin{matrix}2\\2\end{matrix}\right| + \left\langle \begin{matrix}2\\-2\end{matrix}\right|\right)V^4\left(\left|\begin{matrix}2\\2\end{matrix}\right\rangle + \left|\begin{matrix}2\\2\end{matrix}\right\rangle\right)$$

$$= 12D\langle 2|\,|X^4|\,|2\rangle/(15\sqrt{14}). \tag{7.3.28b}$$

Note the $(-2:3)$ ratio of the eigenvalues. This preserves the "center of gravity" of the energy levels, since T_2 has three levels while E has only two. (This splitting was shown in Figure 5.6.3 in the Chapter 5.) In fact, the scalar ($V^{(0)} = v_0^0$) tensor operator is the only one with nonzero trace. No other tensor operator can shift the center of gravity.

Hence, the $j = 2$ example is a little too simple. The Wigner-Eckart results (7.3.28) do not predict anything interesting for the two levels E and T_2 unless one knows the value of the reduced matrix element $\langle 2\|X^4\|2\rangle$. Before we discuss formulas for the reduced matrix elements let us treat examples of crystal field splitting of $j = 3$ levels.

Setting $j_1 = j_2 = 3$ in Eqs. (7.3.23) and (7.3.24) gives the following representation of $V^{(4)}$ after using Table 7.2(f):

$$\langle V^{(4)}\rangle_{j=3} = D\langle 2\left(v_4^4 + v_{-4}^4\right)/\sqrt{70} + (2/5)v_0^4\rangle(\sqrt{7}/3)\langle 3\|X^4\|3\rangle \quad (7.3.29a)$$

$$= D\begin{pmatrix} 3 & \cdot & \cdot & \cdot & \sqrt{15} & \cdot & \cdot \\ \cdot & -7 & \cdot & \cdot & \cdot & 5 & \cdot \\ \cdot & \cdot & 1 & \cdot & \cdot & \cdot & \sqrt{15} \\ \cdot & \cdot & \cdot & 6 & \cdot & \cdot & \cdot \\ \sqrt{15} & \cdot & \cdot & \cdot & 1 & \cdot & \cdot \\ \cdot & 5 & \cdot & \cdot & \cdot & -7 & \cdot \\ \cdot & \cdot & \sqrt{15} & \cdot & \cdot & \cdot & 3 \end{pmatrix}\left(2\sqrt{7}/15\sqrt{154}\right)\langle 3\|X^4\|3\rangle. \quad (7.3.29b)$$

The eigenvectors of this $\langle V^{(4)}\rangle$ matrix can be found by symmetry projection as in Section 5.6, by direct solution of the matrix eigenvalue problem, or by inspection of multipole functions. We will use the third method now, since it has not been discussed.

From the $O_3 \supset O_h$ correlation table of (5.6.5b) it is found that ($j = 3$) splits into ($A_{2u} \oplus T_{1u} \oplus T_{2u}$). From the O_h and O_3 multipole function tables in Appendix F one easily obtains relations between polynomials of O_h and O_3. For A_{2u} one has

$$X^{A_{2u}} = xyz = -i\left(X_{-2}^3 - X_2^3\right)/\sqrt{30}\,. \quad (7.3.30)$$

For the third component of T_{1u} one has

$$X_3^{T_{1u}} = \left(x^2 - y^2\right)z = i\left(X_2^3 + X_{-2}^3\right)/\sqrt{2}\,. \quad (7.3.31)$$

Finally, for the third component of T_{2u} one has

$$X_3^{T_{2u}} = \left(x^2 + y^2\right)z = -X_0^3/10. \quad (7.3.32)$$

From this we easily deduce three normalized eigenvectors

$$|A_{2u}\rangle = \left(\left|\begin{matrix}3\\2\end{matrix}\right\rangle - \left|\begin{matrix}3\\-2\end{matrix}\right\rangle\right)/\sqrt{2}\,, \qquad \left|\begin{matrix}T_{1u}\\3\end{matrix}\right\rangle = \left(\left|\begin{matrix}3\\2\end{matrix}\right\rangle + \left|\begin{matrix}3\\-2\end{matrix}\right\rangle\right)/\sqrt{2}\,,$$

$$\text{and} \quad \left|\begin{matrix}T_{2u}\\3\end{matrix}\right\rangle = \left|\begin{matrix}3\\0\end{matrix}\right\rangle. \quad (7.3.33)$$

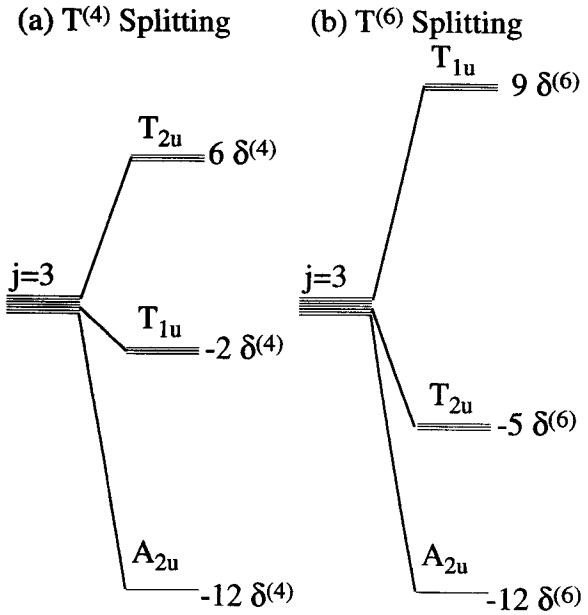

Figure 7.3.2 Octahedral tensor splitting of f-orbital levels. (a) Fourth-rank tensor splitting. (b) Sixth-rank tensor splitting.

Putting these with the $V^{(4)}$ matrix gives the following eigenvalues:

$$\langle A_{2u}|V^{(4)}|A_{2u}\rangle = -12\delta^{(4)}, \quad \left\langle \begin{matrix} T_{1u} \\ 3 \end{matrix} \middle| V^{(4)} \middle| T_{1u} \right\rangle = -2\delta^{(4)},$$

$$\text{and} \quad \left\langle \begin{matrix} T_{2u} \\ 3 \end{matrix} \middle| V^{(4)} \middle| T_{2u} \right\rangle = 6\delta^{(4)}, \tag{7.3.34a}$$

respectively, where the reduced factor is

$$\delta^{(4)} = D\left(2/15\sqrt{22}\right)\langle 3\|X^4\|3\rangle. \tag{7.3.34b}$$

From this we predict a $(12 - 2):(6 + 2) = 5:4$ splitting ratio with A_{2u} and T_{2u} levels sandwiching T_{1u}. This is indicated in Figure 7.3.2(a). One should note that this does not imply that all octahedral crystal fields will split all $(j = 3)$ levels into the order (A_2, T_1, T_2) with a 5:4 ratio. Angular-momentum levels with $j = 3$ and higher may be effected by a *sixth*-rank tensor

operator:

$$V^{(6)} = E\left[(\sqrt{8}/8)X_0^6 - (2\sqrt{7}/8)(X_4^6 + X_{-4}^6)\right]. \tag{7.3.35}$$

This is the form of the next term in the octahedral multipole expansion (5.6.28). Its representation for ($j = 3$) follows from Table 7.2(f).

$$\langle V^{(6)}\rangle_{j=3} = E\begin{pmatrix} 1 & \cdot & \cdot & \cdot & -7\sqrt{15} & \cdot & \cdot \\ \cdot & -6 & \cdot & \cdot & \cdot & 42 & \cdot \\ \cdot & \cdot & 15 & \cdot & \cdot & \cdot & -7\sqrt{15} \\ \cdot & \cdot & \cdot & -20 & \cdot & \cdot & \cdot \\ -7\sqrt{15} & \cdot & \cdot & \cdot & 15 & \cdot & \cdot \\ \cdot & 42 & \cdot & \cdot & \cdot & -6 & \cdot \\ \cdot & \cdot & -7\sqrt{15} & \cdot & \cdot & \cdot & 1 \end{pmatrix} \times \langle 3\|X^6\|3\rangle/(4\sqrt{462}). \tag{7.3.36}$$

This gives a different set of eigenvalues

$$\left\langle A_{2u}\middle|V^{(6)}\middle|A_{2u}\right\rangle = -12\delta^{(6)}, \quad \left\langle \begin{matrix}T_{1u}\\3\end{matrix}\middle|V^{(6)}\middle|\begin{matrix}T_{1u}\\3\end{matrix}\right\rangle = 9\delta^{(6)},$$

$$\text{and} \quad \left\langle \begin{matrix}T_{2u}\\3\end{matrix}\middle|V^{(6)}\middle|\begin{matrix}T_{2u}\\3\end{matrix}\right\rangle = -5\delta^{(6)}, \tag{7.3.37a}$$

where

$$\delta^{(6)} = E\langle 3\|X^6\|3\rangle/(4\sqrt{462}). \tag{7.3.37b}$$

A pure $V^{(6)}$ makes the T_{1u} level move into the high position as shown in Figure 7.3.2(b). A 1:2 splitting ratio results for the three levels (A_2, T_2, T_1).

An eighth-rank $V^{(8)}$ octahedral scalar operator exists but cannot have any effect on a ($j = 3$) level. (Its matrix must be zero, since $C^{383}_{q\,m\,n} = 0$.) However, another scalar operator is not needed. The fourth- and sixth-rank octahedral operators $V^{(4)}$ and $V^{(6)}$ are sufficient in combination to cause any ordering or splitting of the A_2, T_2, and T_1 sublevels of the $j = 3$ manifold. In fact there are three O_h scalar operators $V^{(6)}$, $V^{(4)}$, and $V^{(0)}$, but the $V^{(0)}$ only shifts the center of gravity. This is one more example of the parameter theorem in Section 6.4. The number (6.4.11) of independent scalar operators is exactly the number needed to determine all eigenvalues and eigenvectors subject to the constraints of symmetry.

At this point it may be instructive to review the counting of multipole functions and operators which was introduced in Section 5.6.C. Also the treatment of $j = 4$, 5, and 6 octahedral levels should be examined. The analyses for $j = 5$ and 6 are complicated by the fact that octahedral species

T_1 or T_2 are repeated. Then the T_1 or T_2 eigenvectors are not determined totally by symmetry constraints.

For high j the number of repeated species can be large. For $l = j = 50$ one predicts from Eqs. (5.6.5b) and (5.6.6) that 12 T_1 levels and 13 T_2 levels will appear. Since high values of angular quanta are common in molecular spectra it is important to learn how to deal with them. In Section 7.4 we will discuss some efficient methods for analyzing high-j states. The methods are based upon the theory of level clusters and induced representation bases which was introduced in Section 4.3.

Related problems involve very high crystal potentials which cause splittings which are comparable to or greater than the spacing between j levels. A large enough crystal potential could mix states of different angular momentum (j) strongly enough to make j a useless quantum number. This happens in the theory of ions tunneling in solids. The theory of level clusters can be useful then, too.

D. Evaluation of Reduced Matrix Elements

It is possible to use the Wigner-Eckart theorem while treating the reduced matrix elements as undetermined constants. One may derive some information without knowing the values of these constants. Also, the constants can be fitted using experimental results, and then the tensor analysis can be used to predict further results. These approaches require the we know only the basic symmetry properties of the system being studied.

However, in order to compute the numerical value of a reduced matrix element one must define the involved operators and states in more detail. So far we have not assumed much about anything except symmetry properties. It did not matter whether the ($j = 2$) states treated in Eqs. (7.3.28) were d orbitals of one electron in hydrogen or D orbitals made of over 100 electrons in mendelevium. For the Wigner-Eckart theorem it was only important that the states belonged to symmetry irrep $\mathscr{D}^2$ while the operators belonged to irreps $\mathscr{D}^4$ and $\mathscr{D}^{A_{1g}}$ of O_3 and O_h. We now compare the splitting of ($j = 2$) orbitals for one electron with those for two electrons.

(a) Single-Electron Orbitals in Potential Fields Let us assume a single-electron orbital state with a wave function of the form

$$\left\langle r\theta\phi \middle| \begin{matrix} l \\ m \end{matrix} \right\rangle = R_l(r)Y_m^l(\theta\phi),$$

where $R_l(r)$ is the radial wave function and Y_m^l are spherical harmonics. Let us compute the matrix elements for the general potential field multipole

expansion:

$$\left\langle \begin{matrix} l' \\ m \end{matrix} \middle| V \middle| \begin{matrix} l \\ m \end{matrix} \right\rangle = \sum_{kq} A_{kq} \left\langle \begin{matrix} l' \\ m \end{matrix} \middle| X_q^k \middle| \begin{matrix} l \\ m \end{matrix} \right\rangle$$

$$= \sum_{kq} A_{kq} \int d\phi \int d\theta \sin\theta$$

$$\times \int r^2\, dr\, R_{l'}^*(r) Y_{m'}^{l'*}(\theta\phi) r^k \sqrt{\frac{4\pi}{2k+1}}\, Y_q^k(\theta\phi) R_l(r) Y_m^l(\theta\phi).$$

This integral can be written in terms of angular and radial integrals:

$$\left\langle \begin{matrix} l' \\ m \end{matrix} \middle| V \middle| \begin{matrix} l \\ m \end{matrix} \right\rangle = \sum_{kq} A_{kq} \langle r^k \rangle \sqrt{\frac{4\pi}{2k+1}} \int d\phi \int d\theta \sin\theta Y_{m'}^{l'*}(\theta\phi) Y_q^k(\theta\phi) Y_m^l(\theta\phi), \tag{7.3.38a}$$

where the radial integral is denoted by

$$\langle r^k \rangle = \int_0^\infty r^2\, dr\, |R_l(r)|^2 r^k. \tag{7.3.38b}$$

In the angular integral it is convenient to replace the spherical harmonics Y_m^j by irrep components $\mathscr{D}_{mo}^j$ using Eq. (5.5.65):

$$\sqrt{\frac{4\pi}{2k+1}} \int d\phi \int \sin\theta\, d\theta Y_{m'}^{l'}(\theta\phi) Y_q^k(\theta\phi) Y_m^l(\theta\phi)$$

$$= \frac{\sqrt{(2l'+1)(2l+1)}}{4\pi} \int d\phi \int \sin\theta\, d\theta \mathscr{D}_{m'0}^{l'}(\phi\theta 0) \mathscr{D}_{q0}^{k*}(\phi\theta 0) \mathscr{D}_{m0}^{l*}(\phi\theta 0). \tag{7.3.39}$$

It is useful to get the integral into the form of Eq. (7.2.25) by including the third Euler-angle integral $(1/2\pi) \int d\gamma$. This can be added without any change when all the body quantum numbers are zero. Then the following results for the potential matrix:

$$\left\langle \begin{matrix} l' \\ m' \end{matrix} \middle| V \middle| \begin{matrix} l \\ m \end{matrix} \right\rangle = C_{qmm'}^{k\, l\, l'} \left(\sum_{k,q} A_{kq} \sqrt{\frac{2l+1}{2l'+1}}\, C_{000}^{kll'} \langle r^k \rangle \right). \tag{7.3.40a}$$

This in turn gives the reduced matrix elements of the multipole functions.

$$\langle l' \| X^k \| l \rangle = \sqrt{\frac{2l+1}{2l'+1}}\, C^{kll'}_{000} \langle r^k \rangle = \sqrt{2l+1}\,(-1)^{k-l} \begin{pmatrix} k & l & l' \\ 0 & 0 & 0 \end{pmatrix} \langle r^k \rangle. \tag{7.3.40b}$$

For the crystal splitting example in Eq. (7.3.28) we would need the reduced matrix element

$$\langle 2 \| X^4 \| 2 \rangle = \sqrt{\frac{2}{7}}\, \langle r^4 \rangle. \tag{7.3.40c}$$

For hydrogen the radial integral can be shown to be [see K. Bockaster, *Phys. Rev. A* 9, 1087 (1974)]

$$\begin{aligned} \langle r^4 \rangle &= (a_0)^4 \frac{n^4}{8} \{63n^4 - n^2[70l(l+1) - 105] \\ &\qquad + 15(l-1)l(l+1)(l+2) - 20l(l+1) + 12\} \\ &= (a_0)^4 \frac{63n^4}{8} (n+1)(n-1)(n+2)(n-2) \qquad (\text{for } l = 2). \end{aligned}$$

The hydrogen values are often used for approximate theories of other atoms.

(b) Two-Electron Orbitals in Potential Fields We shall now compare the splitting due to a cubic crystal field of a two-electron $L = 2$ level ($d^2\,{}^1D$) with that of the one-electron orbital ($d^1\,{}^2D$). This amounts to a comparison of two separate applications of the Wigner-Eckart theorem and two different reduced matrix elements. For the two-electron case we need energy matrix elements such as

$$\langle [d^2]^2_{M'} \Big| \overset{\text{total}}{X^4_q} \Big| [d^2]^2_M \rangle = C^{4\,2\,2}_{qMM'} \langle [d^2]2 \| \overset{\text{total}}{X^4} \| [d^2]2 \rangle, \tag{7.3.41a}$$

where the perturbation

$$\overset{\text{total}}{X^4_q} = \overset{\text{electron 1}}{X^4_q} + \overset{\text{electron 2}}{X^4_q} \tag{74.3.41b}$$

is a sum of individual electron operators. For one electron we have

$$\left\langle d^1 \; \begin{matrix} 2 \\ M' \end{matrix} \middle| X^4_q \middle| d^1 \; \begin{matrix} 2 \\ M \end{matrix} \right\rangle = C^{4\,2\,2}_{qMM'} \langle 2| \, |X^4| \, |2\rangle, \tag{7.3.42}$$

which is the same as Eq. (7.3.41a) except for the reduced matrix element. So we must compare the reduced matrix elements.

For the sake of generality let us evaluate the matrix element of a general multipole operator X_q^k between general mixed configuration $|[l_1 l_2]L\rangle$ states instead of pure $|l^2 L\rangle$ configuration states.

$$\left\langle [l_1 l_2]_M^L \middle| \overset{\text{total}}{X_q^k} \middle| [l_1' l_2']_{M'}^{L'} \right\rangle = \left\langle [l_1 l_2]_M^L \middle| \overset{\text{electron 1}}{X_q^k} \middle| [l_1' l_2']_{M'}^{L'} \right\rangle + \left\langle [l_1 l_2]_M^L \middle| \overset{\text{electron 2}}{X_q^k} \middle| [l_1' l_2']_{M'}^{L'} \right\rangle. \quad (7.3.43)$$

Treating the first term by the Wigner-Eckart theorem gives

$$\left\langle [l_1 l_2]_M^L \middle| \overset{\text{electron 1}}{X_q^k} \middle| [l_1' l_2']_{M'}^{L'} \right\rangle = C_{qM'M}^{k\,L'\,L} \langle [l_1 l_2] L || \overset{\text{electron 1}}{X^k} || [l_1' l_2'] L' \rangle. \quad (7.3.44)$$

However, we can use the fact that each two-electron state is a coupling of the form

$$\left| [l_1' l_2']_{M'}^{L'} \right\rangle = \sum_{m_1' m_2'} C_{m_1' m_2' M'}^{l_1'\, l_2'\, L'} \left| \begin{matrix} l_1' \\ m_1' \end{matrix} \right\rangle \left| \begin{matrix} l_2' \\ m_2' \end{matrix} \right\rangle \quad (7.3.45)$$

of single-electron states. Inserting these on the left of Eq. (7.3.44) gives

$$\sum_{m_1 m_2} \sum_{m_1' m_2'} C_{m_1 m_2 M}^{l_1\, l_2\, L} C_{m_1' m_2' M'}^{l_1'\, l_2'\, L'} \left\langle \begin{matrix} l_1 \\ m_1 \end{matrix} \middle| \left\langle \begin{matrix} l_2 \\ m_2 \end{matrix} \middle| \overset{\text{electron 1}}{X_q^k} \middle| \begin{matrix} l_1' \\ m_1' \end{matrix} \right\rangle \middle| \begin{matrix} l_2' \\ m_2' \end{matrix} \right\rangle = C_{qM'M}^{k\,L'\,L} \langle [l_1 l_2] L || \overset{\text{electron 1}}{X^k} || [l_1' l_2'] L' \rangle. \quad (7.3.46)$$

Now $\overset{\text{electron 1}}{X_q^k}$ only acts upon the state vectors of electron (1). Hence one may apply the Wigner-Eckart theorem again just for it:

$$\left\langle \begin{matrix} l_1 \\ m_1 \end{matrix} \middle| \left\langle \begin{matrix} l_2 \\ m_2 \end{matrix} \middle| \overset{\text{electron 1}}{X_q^k} \middle| \begin{matrix} l_1' \\ m_1' \end{matrix} \right\rangle \middle| \begin{matrix} l_2' \\ m_2' \end{matrix} \right\rangle = \left\langle \begin{matrix} l_1 \\ m_1 \end{matrix} \middle| \overset{\text{electron 1}}{X_q^k} \middle| \begin{matrix} l_1' \\ m_1' \end{matrix} \right\rangle \left\langle \begin{matrix} l_2 \\ m_2 \end{matrix} \middle| \begin{matrix} l_2' \\ m_2' \end{matrix} \right\rangle = C_{qm_1' m_1}^{k\,l_1'\,l_1} \langle l_1 | \overset{\text{electron 1}}{X_q^k} | l_1' \rangle \delta_{l_2 l_2'} \delta_{m_2 m_2'}. \quad (7.3.47)$$

By substituting this last result into Eq. (7.3.46) and using orthonormality [Eq.

(7.2.21)] to bring $C^{k\,L'\,L}_{qM'M}$ to the left-hand side, we obtain

$$\left(\sum_{m_1m_2}\sum_{m_1'm_2'}\sum_{qM'} C^{k\,l_1'\,l_1}_{qm_1'm_1} C^{l_1\,l_2\,L}_{m_1m_2M} C^{k\,L'\,L}_{qM'M} C^{l_1'\,l_2\,L'}_{m_1'm_2M'}\right)\langle l_1 \| \overset{\text{electron 1}}{X^k} \| l_1'\rangle$$
$$= \langle [l_1l_2]L \| \overset{\text{electron 1}}{X^k} \| [l_1'l_2']L'\rangle. \tag{7.3.48}$$

The combination of coupling coefficients in the parentheses appears many times in angular-momentum calculations. Up to a factor and a phase it is equal to the RACAH $6j$ coefficient (see Appendix F)

$$\sum_{\substack{m_1,m_2,m_3\\ m_{12},m_{23}}} C^{j_1\,j_2\,j_{12}}_{m_1m_2m_{12}} C^{j_{12}\,j_3\,J}_{m_{12}m_3M} C^{j_1\,j_{23}\,J}_{m_1m_{23}M} C^{j_2\,j_3\,j_{23}}_{m_2m_3m_{23}}$$
$$= (-1)^{j_1+j_2+j_3+J} \times \sqrt{(2j_{12}+1)(2j_{23}+1)} \begin{Bmatrix} j_{12} & j_1 & j_2 \\ j_{23} & j_3 & J \end{Bmatrix}. \tag{7.3.49}$$

The two-particle calculation requires the numerical values of the $6j$ coefficient. By combining Eqs. (7.3.48) and (7.3.49) one obtains

$$\langle [l_1l_2]L \| \overset{\text{electron 1}}{X^k} \| [l_1'l_2']L'\rangle$$
$$= (-1)^{k+l_1'+l_2+L} \sqrt{(2l_1+1)(2L'+1)} \begin{Bmatrix} l_1 & k & l_1' \\ L' & l_2 & L \end{Bmatrix} \langle l_1 \| \overset{\text{electron}}{X^k} \| l_1'\rangle. \tag{7.3.50a}$$

By a similar analysis for electron (2) we find

$$\langle [l_1l_2]L \| \overset{\text{electron 2}}{X} \| [l_1'l_2']L'\rangle$$
$$= (-1)^{k+l_2'+l_1+L} \sqrt{(2l_2+1)(2L'+1)} \begin{Bmatrix} l_2 & k & l_2' \\ L' & l_1 & L \end{Bmatrix} \langle l_2 \| \overset{\text{electron 2}}{X} \| l_2'\rangle. \tag{7.3.50b}$$

Summing these two with the values of momenta for our example gives

$$\langle [22]2| \, |X^4| \, |[22]\rangle = 2\sqrt{5\cdot 5} \begin{Bmatrix} 2 & 4 & 2 \\ 2 & 2 & 2 \end{Bmatrix} \langle 2| \, |X^4| \, |2\rangle$$
$$= \tfrac{4}{7}\langle 2| \, |X^4| \, |2\rangle = 0.57\langle 2| \, |X^4| \, |2\rangle. \quad (7.3.50)_x$$

This shows that the crystal field effect on a two-d-particle $L = 2$ level is 57% that of a single-electron state with the same radial and angular numbers.

7.4 ROTATIONAL LEVEL SPLITTING FOR HIGH J: SEMICLASSICAL ANGULAR MOMENTUM MECHANICS

Rotational or orbital mechanics of atomic electrons in anisotropic potentials is analogous to the quantum mechanics of molecular rotation, and it was first studied in early days of quantum theory. Bethe described the splitting of orbital levels by anisotropic crystalline fields having point symmetries ranging from octahedral (O) to orthorhombic (D_2).

In modern formalism the crystal field orbital eigensolutions are found by first expressing the Hamiltonian H in terms of irreducible (Racah-Wigner) tensors T, and then diagonalizing a representation of H in an orbital basis $\{ \cdots |n, L, N\rangle \cdots |n', L', M'\rangle \cdots \}$. The Wigner-Eckart theorem gives the representation of each tensor component as a product of coupling or Clebsch-Gordan coefficients and reduced radial matrix elements:

$$\langle n', L', M'|\mathbf{T}^k_q|n, L, M\rangle = C^{kLL'}_{qMM}\langle n'L'\|T^k\|nL\rangle. \qquad (7.4.1)$$

The remainder of the problem (and most of the numerical labor) involves truncating the basis, summing the operators, and matrix diagonalization.

Molecular rotations in a vacuum may be described analogously using anisotropic Hamiltonians. In the simplest cases the rotational Hamiltonians are conveniently expressed as polynomials of angular momentum operators J_x, J_y, and J_z defined with respect to the molecular frame. Pure rotational Hamiltonians conserve J and cannot couple rotational states $|J, K\rangle$ and $|J', K'\rangle$ having different J values. This makes the rotational analysis simpler than the external crystal field problem since numerical diagonalization is limited to treating individual $(2J + 1)$ dimensional block matrices. Even so, heavy molecules tend to have high J. For example, SF_6 spectra with $J = 150$ and higher can be resolved, and so the numerical problem still may be quite formidable.

However, for high-J states it is possible to make approximations. It turns out that for high symmetry the diagonal ($K = K'$) contributions to the tensor matrix elements are dominant, and for high J and K they can be approximated by an asymptotic expression for the Clebsch-Gordan coefficients in terms of a Wigner rotation matrix or a Legendre polynomial. (Here we take the reduced matrix factor to be unity.)

$$\langle J, K|T^k_0|J, K\rangle = C^{kJJ}_{0KK} \cong D^k_{0,0}(0, \Theta_{JK}, 0) = P_k(\cos\Theta_{JK}). \quad (7.4.2a)$$

The polar angle Θ_{JK} is that of the angular-momentum cones introduced in Chapter 5. (Recall Figures 5.4.4, 5.5.3, and 5.5.4.)

$$\cos\Theta_{JK} = K/[J(J+1)]^{1/2}, \qquad K = J, J-1, J-2, \ldots . \quad (7.4.2b)$$

The approximation (7.4.2a) is valid in the limit that J and K are both large

compared to the tensorial rank ($K \gg k$). The angle Θ_{JK} is the apex half-angle of a cone with a slant height of $\sqrt{[J(J+1)]}$ and altitude of K. The cone is the locus of the quantum angular-momentum vector J subject to the constraints $\langle \mathbf{J} \cdot \mathbf{J} \rangle = [J(J+1)]$ and $\langle J_z \rangle = K$ imposed by the state $|J, K\rangle$. The cone angle Θ_{JK} is a measure of the quantum uncertainty (ΔJ_x) or (ΔJ_y) of transverse components for that state.

The possible motion of a classical angular-momentum J vector can be displayed using a rotational energy (RE) surface. RE surfaces are radial plots of rotational energy as a function of the direction of the J vector in the body frame for a constant magnitude $|\mathbf{J}| = \sqrt{[J(J+1)]}$ of angular-momentum. The classical J vector, while fixed in the laboratory frame, follows a trajectory in the body-frame which conserves both energy E and magnitude $|J|$ of J.

Each classically allowed J trajectory is a topography line on an RE surface, that is the intersection of an RE surface for a given $|J|$ with an energy sphere for a given E. Examples of RE surfaces for D_2 and O symmetric molecules are shown in the following sections. Furthermore, we shall see the quantum eigenvalues can be related to special "quantizing" J trajectories and that these can be approximated by the intersection of the angular momentum cones with the RE surface.

A. Rigid Rotors ($D_\infty \supset D_2$ symmetry)

(a) Rotational Energy Surfaces The Hamiltonian for a rigid rotor or top is

$$H = AJ_x^2 + BJ_y^2 + CJ_z^2. \tag{7.4.3}$$

[Recall Eq. (5.5.53).] The rotational energy (RE) surface of this Hamiltonian follows if we substitute classical body-frame angular-momentum components

$$J_x = -\langle J \rangle \sin\beta \cos\gamma, \qquad J_y = \langle J \rangle \sin\beta \sin\gamma, \qquad J_z = \langle J \rangle \cos\beta, \tag{7.4.4a}$$

where the J magnitude is constant:

$$\langle J \rangle = \sqrt{J(J+1)} \cong J + \tfrac{1}{2}. \tag{7.4.4b}$$

The resulting energy expression

$$E = J(J+1)\left[A \sin^2\beta \cos^2\gamma + B \sin^2\beta \sin^2\gamma + C \cos^2\gamma\right] \tag{7.4.5}$$

is plotted radially in Figure 7.4.1 as a function of body-frame polar coordinates of azimuth ($\phi = -\gamma$) and polar angle ($\theta = \beta$) for the J vector. These

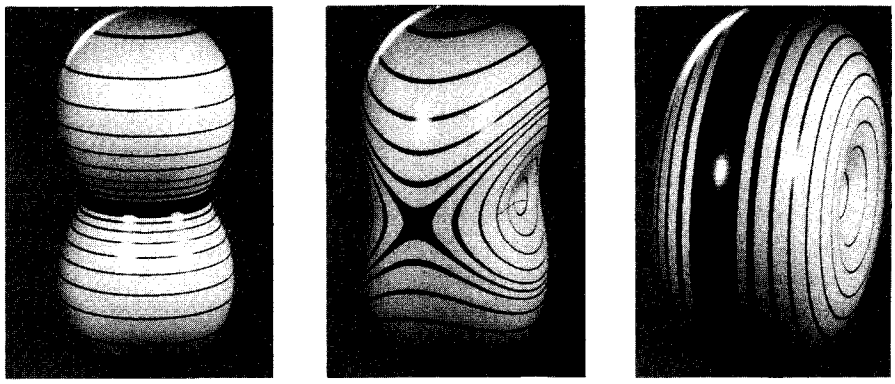

(a) (b) (c)

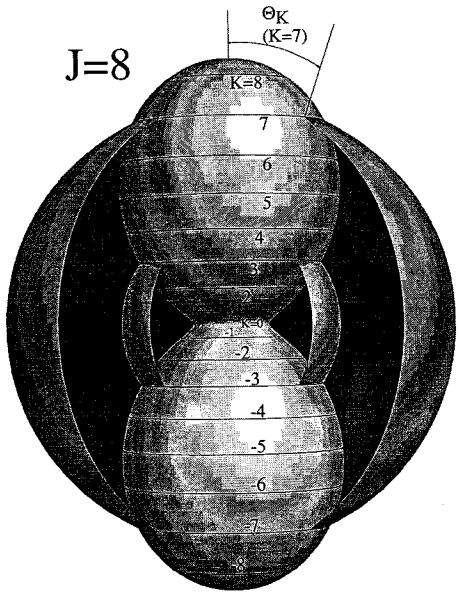

(d)

Figure 7.4.1 Rotational energy (RE) surfaces for rigid rotors. (a) Prolate symmetric top ($A = 0.2$, $B = 0.2$, $C = 0.6$). (b) Rigid asymmetric top ($A = 0.2$, $B = 0.4$, $C = 0.6$). (c) Oblate symmetric top ($A = 0.2$, $B = 0.6$, $C = 0.6$). (d) Prolate symmetric top with $J = 10$ quantum energy levels.

angles are two of the three Euler angles (α, β, γ) as explained in Section 5E(b).

Three examples of rigid top RE surfaces are shown in Figure 7.4.1 for the cases of (a) a prolate symmetric top ($A = B < C$), (b) an asymmetric top ($A < B < C$), and (c) an oblate symmetric top ($A < B = C$). Each surface contains 21 contour lines corresponding to the same number of quantum

energy levels belonging to $J = 10$ ($2J + 1 = 21$). These are labeled in Figure 7.4.1(d) which is an expanded view of Figure 7.4.1(a). They are quantizing J-phase paths in the sense that the following Bohr quantization condition is satisfied:

$$\int J_z \, d\gamma = hK, \qquad K = J, J-1, J-2, \ldots . \tag{7.4.6}$$

Some J paths may be hidden behind a surface. However, time reversal symmetry requires that for each $\mathbf{J}$ on a K path there must be an equivalent path containing $-\mathbf{J}$ or $-K$.

(b) Tensor Operator Mechanics To understand the quantum mechanics better it helps to rewrite the Hamiltonian in terms of tensor operators or as an operator multipole expansion. The multipole functions,

$$T_q^k = D_{0q}^k(0, \beta, \gamma)^* = \sqrt{\frac{4\pi}{2k+1}} \langle J \rangle^k Y_q^k(\gamma, \beta) \tag{7.4.7}$$

are analogous to the spatial multipole functions defined in Eq. (5.6.17). Examples of quadrupole tensor functions are

$$T_0^0 = \mathbf{J} \cdot \mathbf{J} = \langle J \rangle^2 = \left(J_x^2 + J_y^2 + J_z^2\right), \tag{7.4.8a}$$

$$T_0^2 = \tfrac{1}{2}\langle J \rangle^2 (3\cos^2 \beta - 1) = \tfrac{1}{2}\left(2J_z^2 - J_x^2 - J_z^2\right), \tag{7.4.8b}$$

$$\left(T_2^2 + T_{-2}^2\right) = \langle J \rangle^2 \frac{\sqrt{6}}{2} \sin^2 \beta \cos 2\gamma = \frac{\sqrt{6}}{2}\left(J_x^2 - J_y^2\right). \tag{7.4.8c}$$

From this one can construct the tensor operator expression for the rigid rotor Hamiltonian:

$$H = \frac{A+B+C}{3} T_0^0 + \frac{2C-A-B}{3} T_0^2 + \frac{A-B}{\sqrt{6}}\left(T_2^2 + T_{-2}^2\right) \tag{7.4.9}$$

Only the first term survives for a spherical top ($A = B = C$). The symmetric tops ($A = B \neq C$) have the first two terms.

The asymmetric tops ($A \neq B \neq C$) have all three. The resulting energy expression obtained from Eq. (7.4.8) and (7.4.9) is

$$E = J(J+1)\left[\frac{A+B+C}{3} + \frac{2C-A-B}{6}(3\cos^2 \beta - 1) + \frac{A-B}{2} \sin^2 \beta \cos 2\gamma\right]. \tag{7.4.10}$$

The preceding multipole expansion is equal to the polynomial expression (7.4.5) but has some quantum mechanical advantages over the first one. Tensor multipole operator expressions like (7.4.9) provide matrix elements immediately via the Wigner-Eckart theorem (7.3.20a) in terms of Clebsch-Gordan coefficients and reduced matrix elements. Only one reduced matrix $\langle J\|T^2\|J\rangle$ is a problem here, the scalar element of (7.4.8a) is elementary,

$$\langle J\|T^0\|J\rangle = J(J+1).$$

The tensor element is found by evaluating the easiest component $\left\langle {}^{J}_{K}\middle|T^2_0\middle|{}^{J}_{K}\right\rangle$ by elementary means which gives

$$\begin{aligned}\left\langle {}^{J}_{J}\middle|T^2_0\middle|{}^{J}_{J}\right\rangle &= \left\langle {}^{J}_{J}\middle|\tfrac{1}{2}\left(3J_z^2 - J_x^2 - J_y^2 - J_z^2\right)\middle|{}^{J}_{J}\right\rangle \\ &= \tfrac{1}{2}\left(3J^2 - J(J+1)\right) = \tfrac{1}{2}(2J^2 - J). \qquad (7.4.11)\end{aligned}$$

Then the Wigner-Eckart theorem and CG formulas give

$$\left\langle {}^{J}_{K}\middle|T^2_0\middle|{}^{J}_{J}\right\rangle = C^{2JJ}_{0JJ}\langle J\|T^2\|J\rangle = \frac{2(2J^2 - J)}{\sqrt{(2J+3)(2J+2)2J(2J-1)}}. \qquad (7.4.12)$$

Solving gives the desired reduced matrix element:

$$\langle J\|T^2\|J\rangle = \sqrt{(2J+3)(2J+2)2J(2J-1)}\,/4. \qquad (7.4.13)$$

Still one might wonder why we deal with tensor operators when J polynomials seem simpler. The reasons for using tensor operators become clearer when comparing the work involved with higher-degree polynomials and corresponding high-rank tensors. Manipulating and computing matrix elements for fourth- or sixth-degree polynomials can be extremely laborious while fourth- or sixth-rank tensors use the same Wigner-Eckart analysis as the T^2 example above.

(c) Symmetric Top Energy Levels ($J = 10$ Example) The trajectories on the RE surface for $A = B = 0.2$ and$C = 0.6$ [see Figures 7.4.1(a) and 7.4.1(d)] are precisely the ones that correspond to exact quantum energy levels for $J = 10$. If the cone-angle cosine formula (7.4.2b) is substituted into the tensor RE surface energy expression (7.4.10) for $A = B$ one obtains

$$E = J(J+1)\left[\frac{2B + C}{3} + \frac{C - B}{3}\left(3\frac{K^2}{J(J+1)} - 1\right)\right], \qquad (7.4.14)$$

$$E = BJ(J+1) + (C - B)K^2. \qquad (7.4.15)$$

This is the exact symmetric top quantum energy level equation. [Recall Eq.

(5.5.52).] This is an example in which the cone-angle tensor matrix element approximation (7.4.2) gives an exact result. The angular-momentum cones exactly define the quantizing J trajectories shown in Figure 7.4.1a. The same applies to the oblate symmetric top surface shown in Fig. 7.4.1c.

We consider now the asymmetric top for which the J trajectories are more or less distorted from the circular shapes they enjoy in the symmetric case.

(d) Asymmetric Top Energy Levels ($J = 10$ Example) This J-inversion symmetry and the D_2 rotational symmetry of top Hamiltonian (7.4.3) or (7.4.9) combine to give (at least) a D_{2h} symmetry to the RE surface regardless of the symmetry of the rotor which it models. The simplest rigid molecule having the surface shown in Figure 7.4.1(b) would be a bent XY_2 structure like the water molecule.

It is evident that every path on the asymmetric surface in Figure 7.4.1b belongs to a mirror image pair of trajectories with the exception of one path. The exceptional path is the x-shaped separatrix curve which crosses the saddle points on the $\pm y$ axes. The separatrix divides the surface into regions containing two different kinds of trajectory pairs. One kind of trajectory pair encircles the high-energy regions centered on the $\pm z$ axes or C axis. These paths are distorted versions of the paths for the prolate top shown in Figure 7.4.1a. The other pairs encircle the low-energy valley regions around the $\pm x$ axes or A axis, and they are distorted versions of the oblate symmetric top paths in Figure 7.4.1(c).

The separation of regions is manifested in the quantum level spectrum which is shown in the lower center portion of Figure 7.4.2. Here the lower energy quasioblate pairs of trajectories are each identified with quasidegenerate or "clustered' pairs of energy levels below the separatrix level at 44 cm^{-1}. Similarly, the quasiprolate pairs are indicated in the high-energy region on the right-hand side of Figure 7.4.2. The levels belonging to each pair are indicated inside magnifying circles which give D_2 symmetry labels for each level and the magnitude of the splitting between each pair.

The fine structure splitting is the intercluster frequency splitting such as the 150 GHz splitting between the lowest two pairs. This is approximately the frequency of classical precession or the wobbling frequency for the J vector to go once around the lowest energy path. The intracluster splitting such as the 26 kHz splitting of the A_1B_1 pair in the lowest circle is called *superfine structure*. This corresponds to the frequency of a purely quantum mechanical tunneling process between equivalent pairs of semiclassical paths. If the molecule was set initially into a localized nonstationary state with J wobbling around the lowest ($K = 10$) path near the $+x$ axis, then it would gradually evolve into a similar motion around the equivalent ($K = -10$) path near the $-x$ axis after which it would return and (more or less) repeat the whole process at rate of 26 kHz.

The cluster doublets are the angular momentum analogs of inversion doublet levels of a two-well oscillator potential discussed in Chapter 2.

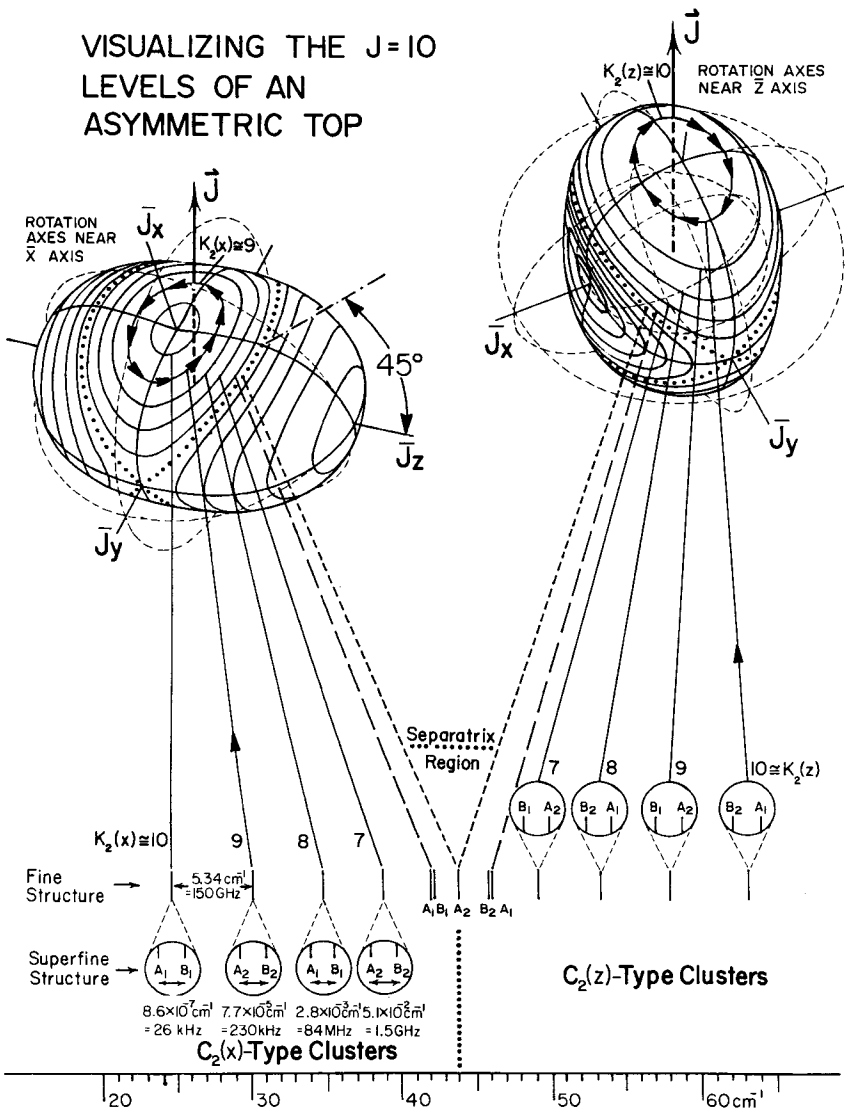

Figure 7.4.2 $J = 10$ asymmetric top energy levels and related RE surface paths ($A = 0.2$, $B = 0.4$, $C = 0.6$). Clustered pairs of levels are indicated in magnifying circles which show superfine splittings.

(Recall Figure 2.12.7.) The stationary A_1 or B_1 eigenstates are, respectively, symmetric or antisymmetric combinations of two separate but equivalent wave functions localized on separate but equivalent paths. The degree of separation or localization is given by the superfine level splitting or tunneling rate. This rate varies exponentially with the magnitude of a path integral between the points of closest approach of the separate semiclassical paths.

For the highest K trajectories which have the greatest separation the precessional motion is more than a million times faster than the tunneling motion. However, near the separatrix the tunneling rate or superfine splitting increases enormously while the classical precession rate or fine structure splitting actually decreases. In this region wave functions cannot remain localized very long, and the distinction between classical and purely quantum motion is blurred.

A classical rotor is always located at just one point on a single phase trajectory at each instant. The quantum rotor, on the other hand, can have nonzero probability spread over many different paths at once. In fact its wave function must be spread out in order to belong to a single irreducible representation such as A_1 or B_1 of the global symmetry group D_2. In order to make a wave function localized on just one trajectory one must add (or subtract) A_1 and B_1 waves. A combination of the two $K = \pm 10$ waves will still have a well defined 0-mod 2 (labeled 0_2) symmetry with respect to the local symmetry subgroup $C_2(x)$ which contains only x-axis rotation. This because $K = 10$ and $K = -10$ are even numbers. The combination states form a space belonging to the induced representation $0_2(\text{of } C_2(x)) \uparrow D_2$ of the global D_2 symmetry induced by the even representation 0_2 of the local symmetry $C_2(x)$. The even induced representation is indicated by the first column of the $D_2 \supset C_2(x)$ correlation table in the left-hand side of Figure 7.4.3. The table gives the D_2 species in the even and odd induced representa-

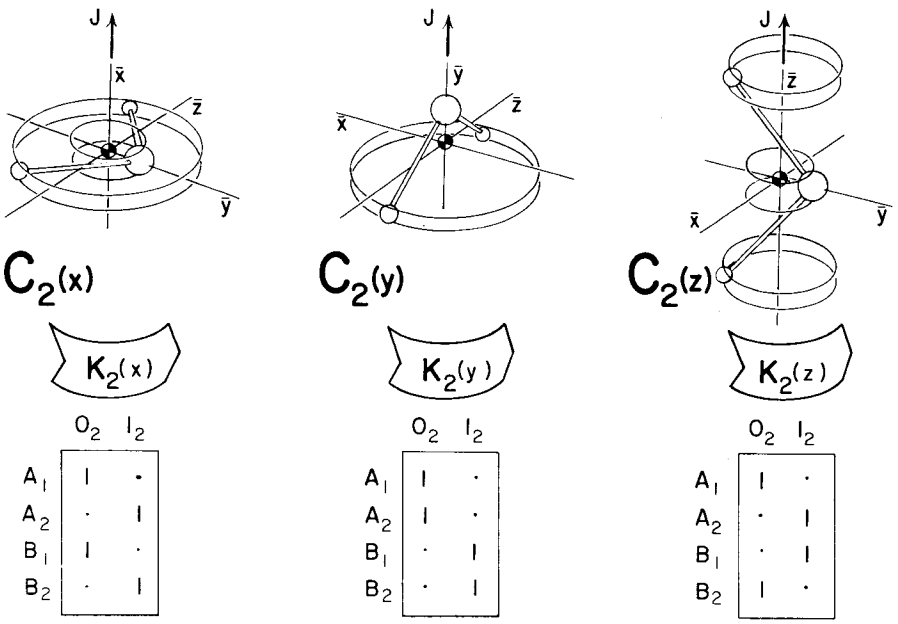

Figure 7.4.3 Correlations between the asymmetric top symmetry D_2 and three dynamical subgroups $C_2(x)$, $C_2(y)$, and $C_2(z)$.

tions according to the Frobenius reciprocity theorem:

$$0_2(\text{of } C_2(x)) \uparrow D_{2^-} = A_1 \oplus B_1, \tag{7.4.16a}$$

$$1_2(\text{of } C_2(x)) \uparrow D_2 = A_2 \oplus B_2. \tag{7.4.16b}$$

The even (odd) induced representation labels the even-K (odd-K) clusters which lie below the separatrix in Figure 7.4.2. The clusters above the separatrix have a local symmetry $C_2(z)$, and the clusters corresponding to this region are labeled according to the columns of the $D_2 \supset C_2(z)$ correlation table shown in the right-hand part of Figure 7.4.3.

Sketches of the classical motion correspond to the locally C_2 symmetric trajectories. The $C_2(x)$ motion corresponds to an XY_2 rotating on its side like a boomerang, while $C_2(z)$ motion is like a spinning crankshaft. The $C_2(y)$ motion is around the classically unstable saddle point, and hence no $C_2(y)$ level clusters appear in the spectrum. One should note that the phase portraits describe the precession or "rotation of rotation" rather than rotation itself. Precessionless rotation of a rigid body would occur only if the J vector were precisely localized on one of the principle axes; however, this is not possible for a quantum rotor.

Quantum uncertainty prohibits pure rotation without precession because the transverse components cannot be exactly zero. The transverse components are minimum for the $K = J$ states which have the least cone angle Θ_{JJ}. This corresponds to minimum angular-momentum uncertainty or angular zero-point motion. States with lower z-component quanta $K = J - 1$, $J - 2, \ldots$ have higher uncertainty angles Θ_{JJ} according to Eq. (7.4.2b). The states $|J, K\rangle$ are eigenstates of the symmetric top ($A = B$) Hamiltonian, and each angular-momentum cone exactly intersects the corresponding semiclassical path on the symmetric top RE surface in Figure 7.4.1(a).

For the asymmetric top in Figure 7.4.1(b) the Θ_{JJ} cones only approximate their corresponding semiclassical trajectories. Asymmetric top trajectories are distorted or "squeezed" so that the projection of J on the local axis of quantization oscillates around the K value which labels each path. The classical precession becomes more and more nonuniform as K decreases and the separatrix is approached. This corresponds to the mixing of more of the states $|J, K \pm 2\rangle$, $|J, K \pm 4\rangle$, and so on into the dominant $|J, K\rangle$ component of the asymmetric top eigenstate. The global and local symmetries for the symmetric top are continuous groups O_2 or $D_{\infty h} \supset R_2$ while the asymmetric top has only a discrete set of symmetries $D_2 \supset C_2$. Hence, one cannot expect the K value to be strictly conserved or the $\pm K$ degeneracy to be perfectly maintained in the latter.

However, the extent of breakdown of R_2 symmetry or K conservation is not necessarily related to the splitting of the cluster doublets. K conservation and cluster splitting are separate phenomena associated with different regions of the RE phase space; the former depends upon the shape of the

phase paths, and the latter depends upon the height of the pass or saddle region between the equivalent paths. Furthermore, the symmetry properties of the clusters should be associated with a C_2 induced representation and not an R_2 irreducible representation. This point will be amplified by examples involving the higher octahedral symmetry in the following section.

Another point which arises in the study of higher symmetries concerns the ordering of clusters and the symmetry species inside them. The species ordering in Figure 7.4.2 consists of a repetition of the sequence $A_1B_1A_2B_2$ through the entire spectrum. This remarkably uniform ordering can be related to the number of wave function nodes occurring along and between the semiclassical paths. This sort of ordering was introduced in Chapter 2.

(e) Level Correlation Between $C_2(x)$ and $C_2(z)$ Symmetry The coefficients A, B, and C determine the symmetry of the rotor Hamiltonian (7.4.3) and its RE surface. The surface represents a rotor that is prolate-symmetric ($A = B < C$) in (a) of Figure 7.4.1, asymmetric ($A < B < C$) in (b), and oblate-symmetric ($A < B = C$) in (c). The two extreme symmetric rotor cases have levels labeled by different $R_3 \supset R_2$ subgroup chains. The prolate case is labeled by $R_2(z)$ and the oblate case by $R_2(x)$. The intermediate asymmetric case is labeled using finite subgroup chains $R_3 \supset D_2 \supset C_2$. Furthermore different subgroups are appropriate for different levels; the levels below the separatrix belong to $C_2(x)$ and those above belong to $C_2(z)$.

In Figure 7.4.4 the $J = 10$ and $J = 20$ levels are plotted as a function of parameter B which ranges between the prolate ($B = 0.2$ cm^{-1}) and oblate ($B = 0.6$ cm^{-1}) cases. Coefficients $A = 0.2$ cm^{-1} and $C = 0.6$ cm^{-1} are fixed. One can see that most $J = 10$ symmetric top doublets tend to stick together for most values of B and even more so for $J = 20$. The $J = 10$ levels in Figure 7.4.2 lie above the point $B = 0.4$ in the $J = 10$ plot of Figure 7.4.4.

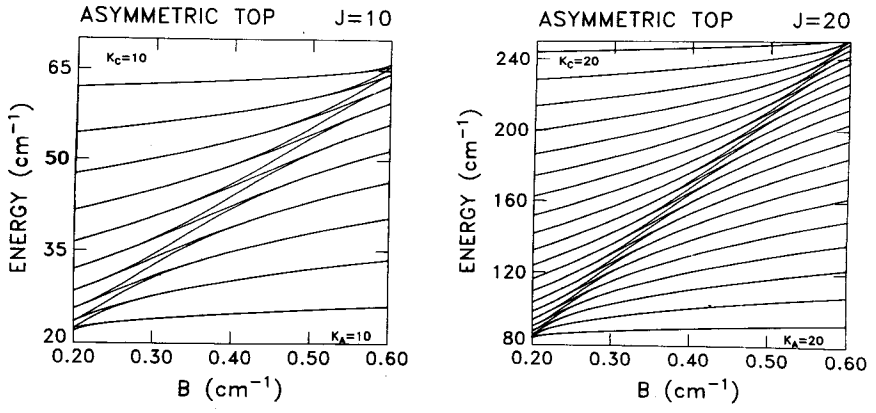

Figure 7.4.4 Rigid rotor energy levels correlations for angular momentum $J = 10$ and $J = 20$.

The separatrix region of the levels in the center of Figure 7.4.2 is the transition region where doublets split and trade levels in Figure 7.4.4. The separatrix or transition region appears to be a small fraction of the $J = 10$ spectrum and even smaller part for $J = 20$.

The doublets in the upper left-hand part of Figure 7.4.4 above the transition region belong to $C_2(z)\uparrow D_2$ induced representations while those in the lower right-hand part belong to $C_2(x)\uparrow D_2$ labeled doublets.

This correlation plot should be compared to the lattice level correlation diagrams in Figure 2.12.5. The latter involves a correlation between bands of doublets of levels belonging to $C_n(z)\uparrow D_n$ induced representations and n-fold degenerate clusters or bands of levels belonging to $C_2(x)\uparrow D_n$ representations. For $n = 2$ the plot in Figure 2.12.5 is more closely analogous to the one in Figure 7.4.4. Then the A_1, A_2, B_1 and B_2 levels (which are the band boundaries plotted in Figure 2.12.5) are the only levels allowed; the E-type levels do not exist for $n = 2$. The transition region occurs at the top of the potential barriers.

By analogy the asymmetric top spectral transition region occurs at the top (or bottom) of the saddles on the RE surface. The saddle points are on the $\pm y$ axes and rise linearly with the coefficient B of J_y^2. Certain of the transition levels are seen to rise rapidly and quasilinearly in Figure 7.4.4 while their doublet partners seen to sail right through the transition region. Wave symmetry determines which of the D_2 species are most sensitive to the y-axis saddle. The correlation table in Figure 7.4.3 for the $C_2(y)$ symmetry shows that only A_1 and A_2 are symmetric (0_2). Therefore only they have wave antinodes and substantial amplitudes on the saddles, and it is therefore A_1 and A_2 levels that "divorce" their partners in the transition region.

Outside the transition region the pairs of levels mostly stick together to form quasidegenerate tunneling doublets. One exception is the $K = \pm 1$ doublet near the lower left-hand side of Figure 7.4.4. It splits immediately, that is, to first order. This is analogous to the first order splitting observed in Figure 2.12.5. Symmetry allows nonzero matrix elements between this pair of states. In this case it is matrix element $\langle K = 1|T_2^2|K = -1\rangle$ and its conjugate that cause the $K = \pm 1$ doublet to split.

B. Semirigid Spherical Tops [Octahedral (O) Symmetry]

We now consider the high-J eigenvalues of octahedrally symmetric tensor Hamiltonians. The fourth-rank tensor Hamiltonian,

$$H = BT_0^0 + 4t_{044}\left[T_0^4 + \sqrt{\frac{5}{14}}\left(T_4^4 + T_{-4}^4\right)\right] \tag{7.4.17}$$

has the same form as the one introduced in Eq. (7.3.25). Its polynomial form

$$H = B\mathbf{J}^2 + 10t_{044}\left(J_x^4 + J_y^4 + J_z^4 - \tfrac{3}{5}\mathbf{J}\right)^4 \tag{7.4.18}$$

was introduced in Eqs. (5.6.28) and (5.6.30). It is known as the Hecht Hamiltonian after K. T. Hecht who first applied it to the analysis of methane (CH_4) spectra taken by E. Plyler in 1960. The Hamiltonian describes rotation-vibrational distortion of molecules having tetrahedral (T_d) as well as octahedral (O_h) symmetry. Changing the sense of rotation ($\mathbf{J} \rightarrow -\mathbf{J}$) should give a rotor state with the same energy so all rotors must have only pure rotational energy operators of even rank. The third-rank tetrahedral invariant $J_xJ_yJ_z$ is forbidden to appear alone.

(a) Rotational Energy Surfaces We now express the Hecht Hamiltonian (7.4.17) in terms of body polar angles as was done in the preceding section for the asymmetric rotor. The polynomial

$$E = B\langle J^2\rangle + t_{044}\langle J^4\rangle(35\cos^4\beta - 30\cos^2\beta + 3 + 5\sin^4\beta\cos 4\gamma)/2 \tag{7.4.19}$$

has the form of the harmonic polynomial functions in Eq. (5.6.29). The resulting RE surface is shown in Figure 7.4.5a for positive centrifugal distortion constant t_{044}. This constant is around 5 Hz for SF_6 and is positive for most octahedral XY_6 molecules. It is greatly exaggerated for the figure so that the hill and valleys are clearly visible.

In an octahedral XY_6 molecule rotation about the four-fold XY radial bond axes generally has the highest energy for a given J value since these

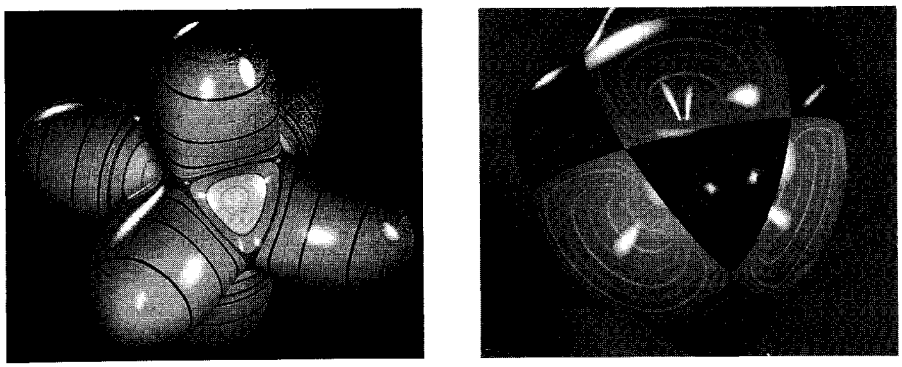

(a) (b)

Figure 7.4.5 Semirigid rotor RE surfaces with O_h symmetry. (a) $t_{044} > 0$. (b) $t_{044} < 0$.

bonds are stretched relatively little by a longitudinal centrifugal force. However, transverse forces which arise during rotation about the three-fold symmetric axes in between the bonds can bend the molecule relatively easily. Hence, the three-fold symmetry axes lie in RE surface valleys in Figure 7.4.5a while the four-fold (x, y, z) axes are on peaks. For tetrahedral XY_4 or cubic molecules the sign of t_{044} is negative as it is for the surface in Figure 7.4.5(b).

(b) Spherical Top Energy Levels (J = 30 Example) The RE topography lines correspond to quantizing J trajectories and to level clusters in the

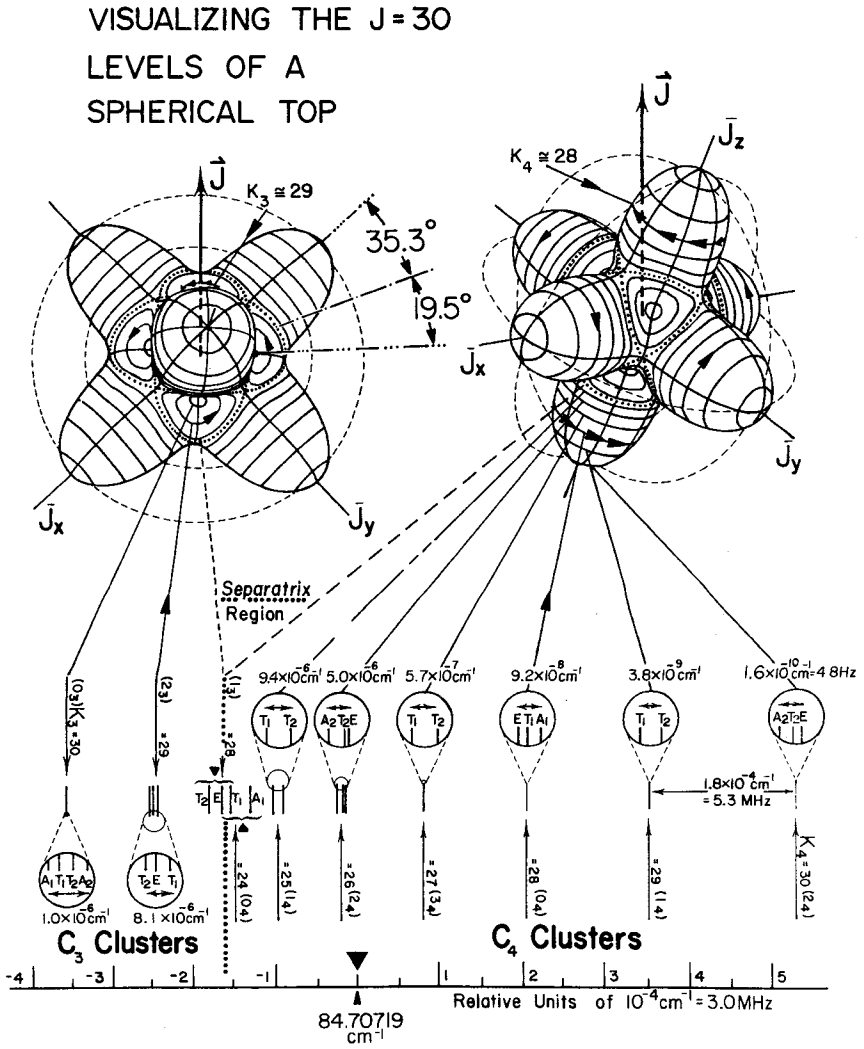

Figure 7.4.6 $J = 30$ octahedral rotor levels and related RE surface paths.

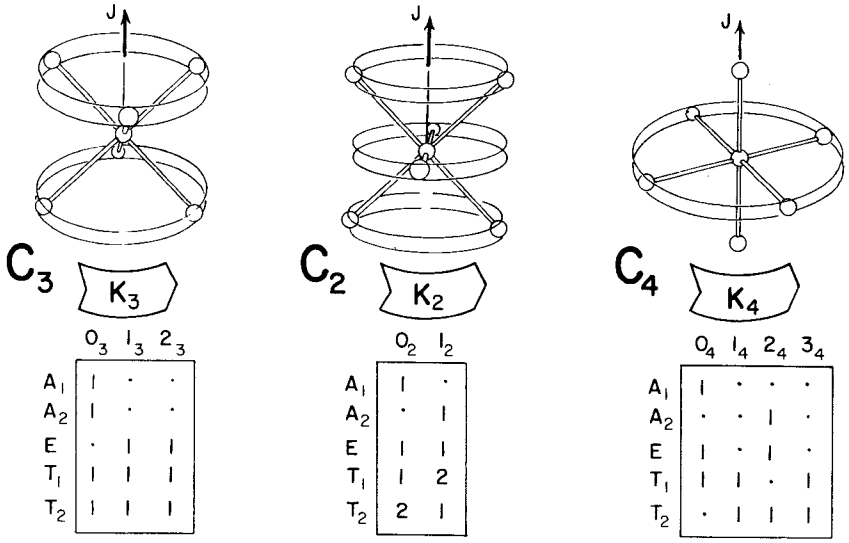

Figure 7.4.7 Different choices of rotation axes for octahedral rotor corresponding to local symmetry C_3, C_2, and C_4. Tables correlate global octahedral symmetry species with the local ones.

energy spectrum as shown by the diagram of the $J = 30$ levels of SF_6 in Figure 7.4.6. This spectrum contains clusters of six and eight rotational levels which are analogous to the rigid rotor doublet clusters in Figure 7.4.2. Above the separatrix region there are repeating sextets (T_1T_2), (A_2T_2E), (T_1T_2), or (A_1T_1E) composed of clustered singlet (A_1 or A_2), doublet (E), or triplet (T_1 or T_2) octahedral symmetry species. Below the separatrix there are two octets $(A_1T_1T_2A_2)$ and (T_2ET_1). Each set of six or eight clustered levels can be related to the same number of semiclassical J trajectories on the RE surface in Figure 7.4.5 or 7.4.6.

Each set of six rotational levels belongs to one of the C_4 induced representations $0_4 \uparrow O$, $1_4 \uparrow O$, $2_4 \uparrow O$, or $3_4 \uparrow O$ depending upon whether the effective K value is 0, 1, 2, or 3 modulo 4 for the corresponding set of fourfold symmetric semiclassical trajectories. The correlation tables in the lower right-hand part of Figure 7.4.7 tell which O species belong to each K_4 cluster and to each set of trajectories. For example, the minimum uncertainty trajectory has $J = K = 30$ and corresponds to the highest energy $2_4 \uparrow O$ or (A_2T_2E) cluster in Figure 7.4.5.

The highest energy semiclassical trajectories are very close to the intersection of the RE surface with the $K = 30$ angular momentum cone which has half-angle $\Theta_{30\,30} = \cos^{-1}(30/\sqrt{(30)(31)} = 10.3°$. A series of $J = 30$ angular momentum cones are drawn for $K = 30$ down to $K = 24$ in Figure 7.4.8. The next highest $1_4 \uparrow O$ or (T_1T_2) cluster corresponds to six trajectories which are

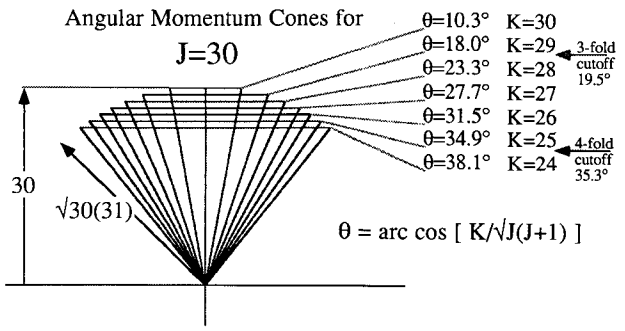

Figure 7.4.8 Quantum angles momentum cone cross sections for $J = 30$ and $K = 30, 29, \ldots, 24$.

localized to within about $\Theta_{30\,29} = 18°$ of their respective four-fold symmetry axes. This sequence of clusters ends when $\Theta_{30\,K}$ approaches the angle 35.3° between the separatrix and the four-fold axes. The $J = 30$ cutoff value is $K_4 = \sqrt{(30)(31)}\cos 35.3° = 24.9$ or about 25 as shown in Figure 7.4.8. This corresponds to a weak (T_1T_2) cluster just above the separatrix in Figure 7.4.6.

Since the eight three-fold symmetric valley regions of the RE surface are smaller there are fewer clusters associated with the C_3 induced representations. There is only a 19.5° angle between the separatrix and the three-fold axes. Hence, the $J = 30$ cut-off value is $K_3 = \sqrt{(30)(31)}\cos 19.5° = 28.7$ or about 29 as indicated in Figure 7.4.8. This allows just two $J = 30$ clusters on the three-fold symmetry side of Figure 7.4.6 corresponding to the induced representations $0_3 \uparrow O = (A_1T_1T_2A_2)$ for $K = 30$ and $2_3 \uparrow O = (T_2ET_1)$ for $K = 29$.

Two C_3 clusters and five or six C_4 clusters are visible in the infrared spectra of tetrafluorosilane (SiF_4) and cubane (C_8H_8) which is shown in Figure 7.4.9. The spectra are actually due to transitions between level clusters on lower and upper RE surfaces corresponding to ground and vibrationally excited states, respectively. However, the spectra are simply scaled copies of the pure rotational level patterns since the upper and lower RE surfaces have almost the same shape apart from a scale factor. Note that fine structure spectra outside of the separatrix region is relatively insensitive to the J value in that $P(30)$, $P(31)$, and $P(32)$ are quite similar. Note the similarity of $J = 30$ fine structure patterns for quite different molecules having tetrahedral, cubic, and octahedral shapes.

With higher resolution the superfine and even the hyperfine spectral structure can be studied. The hyperfine patterns are very sensitive to the J and K values as well as the detailed structure of the molecule. The number of Pauli-allowed nuclear spin states depends upon the type of arrangement of nuclei, and this affects the relative peak heights for the clusters.

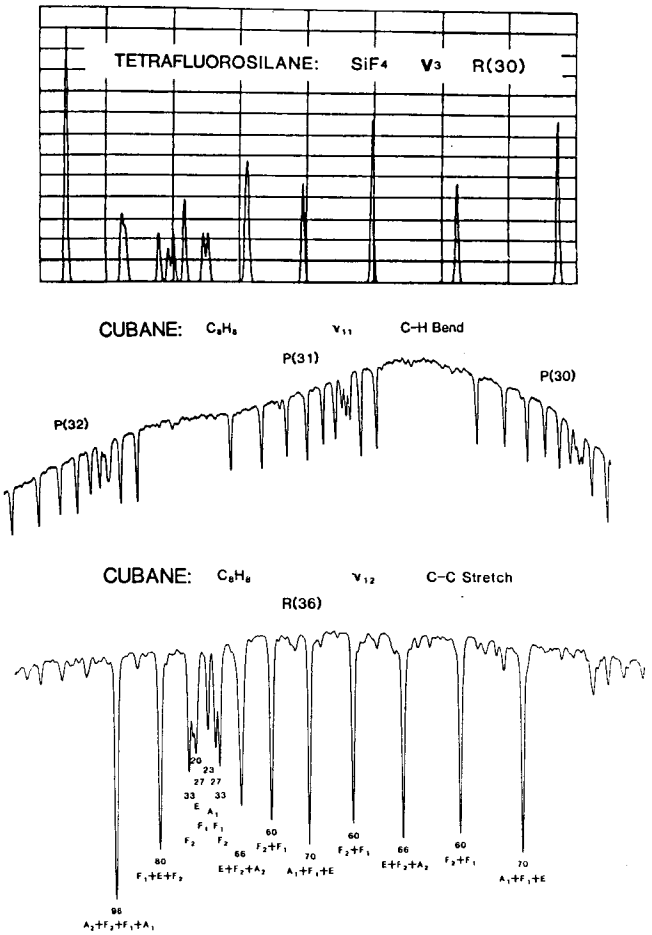

Figure 7.4.9 Infrared spectra showing fine structure clusters. Tetrafluorosilane (SiF_4) spectrum from a ν_3 $R(30)$ transition ($J = 30 \rightarrow 29$). [After C. W. Patterson, R. S. McDowell, N. G. Nereson, B. J. Krohn, J. S. Wells, and F. R. Peterson, *J. Mol. Spectrosc.* **91**, 416 (1982).] Cubane (C_8H_8) spectrum from ν_{11} $P(30)$, $P(31)$, and $P(32)$, transitions; cubane (C_8H_8) spectrum from ν_{12} $R(36)$, transition. [After A. S. Pine, A. G. Maki, A. G. Robiette, B. J. Krohn, J. K. G. Watson, and Th Urbanek, *J. Am. Chem. Soc.*, **106**, 891 (1984).]

However, the superfine structure of intracluster splitting depends only on the shape of the RE surface in the neighborhood of the saddle points. A tunneling factor S can be approximated by an exponential of a phase integral across the saddle region. (Note the rapid decrease of the superfine splitting from about one Megahertz down to just 4.8 Hz as K_4 goes from 25 up to 30 in Figure 7.4.6.) While the magnitude of the splitting may vary by many

orders, the splitting patterns have the following invariant form. The first of these was derived before Eq. (4.3.28),

$$\begin{array}{lll} \mathbf{0}_4 \uparrow O: & \mathbf{1}_4 \text{ or } \mathbf{3}_4 \uparrow O: & \mathbf{2}_4 \uparrow O: \\ \Delta E(A_1) = 4S, & \Delta E(T_2) = 2S, & \Delta E(E) = 2S, \\ \Delta E(T_1) = 0, & \Delta E(T_2) = 2S, & \Delta E(T_2) = 0, \\ \Delta E(E) = -2S, & & \Delta E(A_2) = -4S. \end{array} \tag{7.4.20}$$

The patterns for C_3 clusters can be derived using similar arguments,

$$\begin{array}{ll} \mathbf{0}_3 \uparrow O: & \mathbf{1}_3 \text{ or } \mathbf{2}_3 \uparrow O: \\ \Delta E(A_2) = 3S, & \Delta E(T_1) = 2S, \\ \Delta E(T_2) = S, & \Delta E(E) = 0, \\ \Delta E(T_1) = -S, & \Delta E(T_2) = -2S. \\ \Delta E(A_1) = -3S. & \end{array} \tag{7.4.21}$$

The splitting ratios and ordering hold if tunneling occurs only between nearest neighboring trajectories. The patterns (7.4.20) and (7.4.21) are seen magnified in Figure 7.4.6.

In addition there is an overall ordering that is maintained throughout the fine structure spectrum of Figure 7.4.6 as there was in the case of the asymmetric top. From Figure 7.4.6 one observes the following repeated sequence (recall Figure 5.6.9)

$$0_1 \uparrow O = (A_1T_1T_2A_2T_2ET_1T_2ET_1). \tag{7.4.22}$$

Taken together this would be the largest possible cubic cluster. It contains just the O regular representation. Giant clusters like (7.4.22) or the C_2 clusters half this size are possible if stable semiclassical orbits are localized around low symmetry points. This occurs for octahedral tensor combination of sixth, eighth, and higher ranks.

(c) Level Correlation between C_3 and C_4 Symmetry So far we have considered only the lowest order rotational tensors which exhibit the symmetries D_2 of the rigid rotor and O_h of the semirigid cubic or octahedral rotor. We consider now the effect of the sixth-rank normalized octahedral tensor operator introduced in Eq. (7.3.35),

$$T^{[6]} = (1/\sqrt{8})\left[T_0^6 - (\sqrt{7}/\sqrt{2})(T_4^6 + T_{-4}^6)\right]. \tag{7.4.23}$$

This will be added in varying amounts to the normalized fourth-rank tensor,

$$T^{[4]} = (\sqrt{7}/\sqrt{12})\left[T_0^4 - (\sqrt{5}/\sqrt{14})(T_4^4 + T_{-4}^4)\right], \qquad (7.4.24)$$

introduced in Eqs. (7.3.25) and (7.4.17). A sixth-rank centrifugal distortion may be necessary in the presence of anharmonic and other higher order effects. The magnitude of the $T^{[6]}$ contribution would vary according to a higher power of J than that of $T^{[4]}$ and might be significant at higher J values. Here the magnitudes of their respective contributions are varied artificially through an angle parameter ν in a combination which maintains the overall normalization.

$$T^{4,6}(\nu) = T^{[4]} \cos\nu + T^{[6]} \sin\nu. \qquad (7.4.25)$$

The exact quantum ($J = 30$)-eigenvalues for this mixed [4, 6]-rank tensor operator are plotted as a function of the mixing angle ν in Figure 7.4.10. The plot begins on the left-hand side ($\nu = 0$) with a scaled copy of the $T^{[4]}$ level spectrum in Figure 7.4.6 and ends on the right-hand side ($\nu = \pi$) with the same spectrum inverted. Between these limits the level clusters become completely reorganized.

Certain values of the ν parameter in Figure 7.4.10 are marked (b), (c), (d), and (e). At these values the RE surface of the combination tensor (7.4.25) is

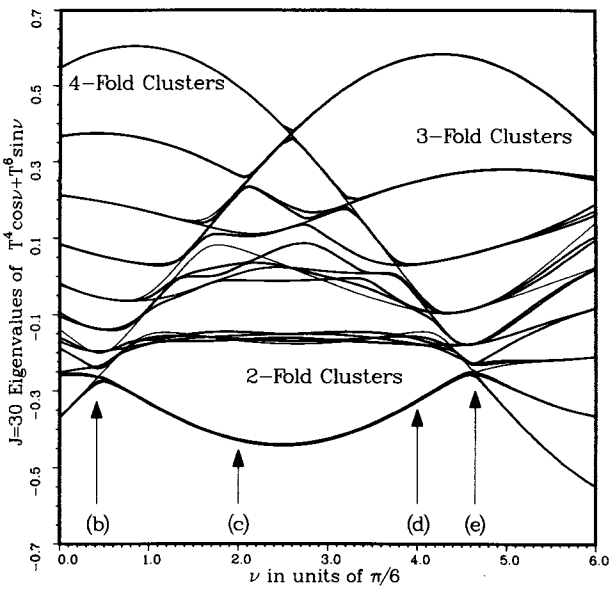

Figure 7.4.10 $J = 30$ eigenvalues of varying mixtures of fourth- and sixth-rank tensors. ($\nu = 0$) corresponds to levels in Figure 7.4.6.

drawn in Figure 7.4.11. The RE surface function used for $T^{[4]}$ is as follows. (Recall (7.4.19)]

$$E^{[4]}(\beta,\gamma) = (7/12)^{1/2}(9/4\pi)^{1/2}(35\cos^4\beta - 30\cos^2\beta + 3 + 5\sin^4\beta\cos 4\gamma)/8 \tag{7.4.26}$$

For $T^{[6]}$ the RE function is as follows,

$$E^{[6]}(\beta,\gamma) = (1/8)^{1/2}(13/4\pi)^{1/2}(231\cos^6\beta - 315\cos^4\beta + 105\cos^2\beta - 5 - 21\sin^4\beta(11\cos^2\beta - 1)\cos 4\gamma)/16. \tag{7.4.27}$$

The tensors $T^{[r]}$ and RE functions $E^{[r]}$ have a spherical harmonic normalization factor $([2r + 1]/4\pi)^{1/2}$ that was not included in the previous definition (7.4.19). This factor is used here to slightly enhance the effect of the sixth-rank tensor for this particular example. Also, the $|J|^r$ factors are deleted in (7.4.26) and (7.4.27) so that the higher rank tensor effects are not J dependent.

The eigenlevels marked by (b) in Figure 7.4.10 correspond to the RE surface drawn in Figure 7.4.11(b). The latter shows that the separatrix has taken over the regions that formerly held C_3 symmetric trajectories, and only C_4 trajectories remain. (Note that these are equally spaced contours and are not quantized paths.) The result is the destruction of C_3 clusters in the spectrum which is composed almost entirely of C_4 clusters above the (b) point in Figure 7.4.10.

Beyond this point a remarkable new type of cluster is formed. Just above the points marked (c) and (d) in Figure 7.4.10 lie two clusters which contain twelve levels each. These correspond to trajectories which encircle 12 equivalent valleys which lie on the C_2 symmetry axes in Figures 7.4.11(c) and 7.4.11(d). The symmetry species within each of these clusters are exactly the ones contained in the C_2 correlation table in the center of Figure 7.4.7. The lowest cluster in Figure 7.4.10 would correspond to $K = 30$ and hence to the even local symmetry or 0_2 column of the C_2 table which contains species A_1E, T_1, and $2T_2$. The next cluster has $K = 29$ and contains the five species A_2, E, $2T_1$, and T_2 listed in the odd column 1_2. The superfine splittings between these five levels are actually visible in the scale of Figures 7.4.10. As ν changes the levels as seem to change order within this cluster. This is the result of competition between tunneling mechanisms.

Between the (b) and (d) points in Figure 7.4.10 there is another phenomenon which occurs in the upper energy levels. There are a number of crossings or Fermi-like resonances between accidentally coinciding C_3 and C_4 clusters. This is because there are two kinds of mountains on the RE surfaces in Figures 7.4.11(c) and 7.4.11(d): the C_4 mountains which are

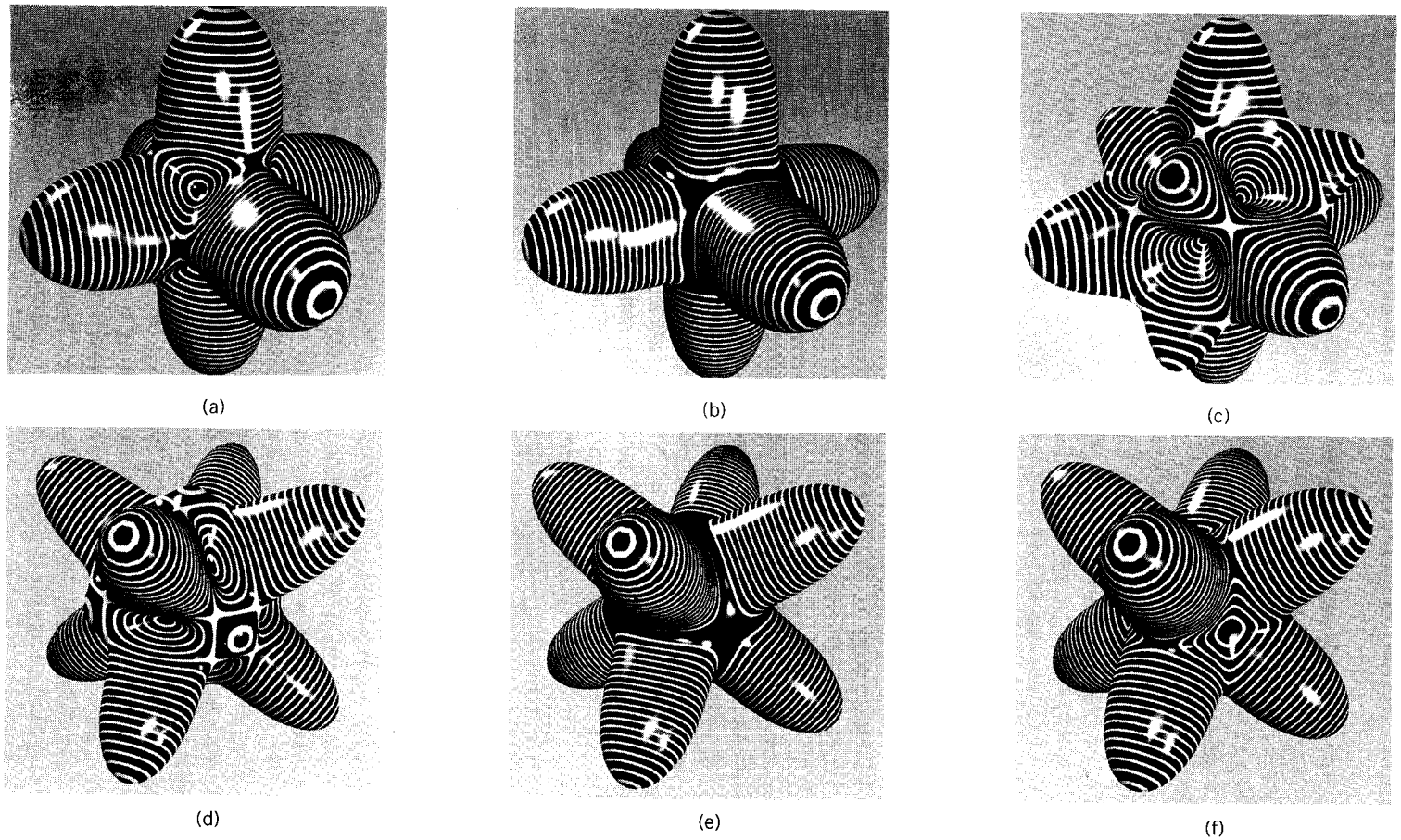

Figure 7.4.11 *RE* surfaces corresponding to selected ν values in Fig. 7.4.10. (a) $\nu = 0.0$, (b) $\nu = 0.4\ (\pi/6)$, (c) $\nu = 2.0\ (\pi/6)$, (d) $\nu = 4.0\ (\pi/6)$, (e) $\nu = 4.6\ (\pi/6)$, (f) $\nu = 5.0\ (\pi/6)$.

shrinking and C_3 mountains which are growing with ν. For certain values of ν, quantizing paths on one type of mountain are bound to be in resonance with different kinds of paths on the other. The result is an extraordinary kind of tunneling in which eigenfunctions are delocalized over both kinds of paths at once and a peculiar sort of hybrid superfine structure occurs in the eigenlevels.

The spectral region containing the unusual fine structure is bounded on the right-hand side by the (e) point in Figure 7.4.10 which corresponds to the RE surface in Figure 7.4.11(e). At this point the eight C_3 mountains dominate the surface geometry entirely and the eigenlevels are composed entirely of very strong C_3 clusters of eight levels each. The final 7.4.11(f) shows the situation at $\nu = 5.0(\pi/6)$ where the C_4 trajectories begin to return. Now they are occupying the valleys.

7.5 ROTATING SPINOR SYSTEMS AND TWO-DIMENSIONAL OSCILLATOR ANALOGIES

We consider now some physical applications of rotation group theory, spinor algebra, and $U(2)$ operators. Various analogies which use rotational coordinates lead to insight into rotational and vibrational dynamics.

So far we have introduced two physical examples of two-state systems. These were spin-$\frac{1}{2}$ states (Sections 1.1.A and 5.5.A) and the NH_3 inversion states (Section 2.12.B). A third and much older example involves optical polarization or the two-dimensional oscillator, and this will be introduced in this section. The three physical examples are each represented in two different ways by Figures 7.5.1(a) and 7.5.1(b), and the polarization example is shown in the central figure.

We shall discuss two ways to describe two-state systems such as a spin-$\frac{1}{2}$ electron. The first way, as shown in Figure 7.5.1(a1) uses a complex two-dimensional (spin-up and spin-down) space which is a basis of the fundamental representation of the unitary group $U(2)$. A second way, shown in Figure 7.5.1(b1), uses a real three-dimensional (S_x, S_y, S_z) space which is a basis for the vector representation of the rotation group $R(3)$. The spinor space may be less familiar than the vector space, since the latter is more like the one in which we live, and it is easier to visualize a real vector **S**. This spin vector **S** is a nearly complete description of the spin state; however, it turns out to be double valued in the following sense. A 180° three-space rotation of a spin-up vector to spin-down ($R(180°)\mathbf{S} = -\mathbf{S}$) corresponds to only a 90° rotation in the spinor 2-space. A "full" 360° rotation in the 3-space is only a 180° rotation in the 2-space, i.e., $|\text{spin-up}\rangle$ goes into *minus* $|\text{spin-up}\rangle$.

Spinor spaces therefore provide a more complete, though possibly less intuitive description of the two-state system. As explained in Section 5.5.A, the spinor algebra and geometry lead to simpler and more powerful compu-

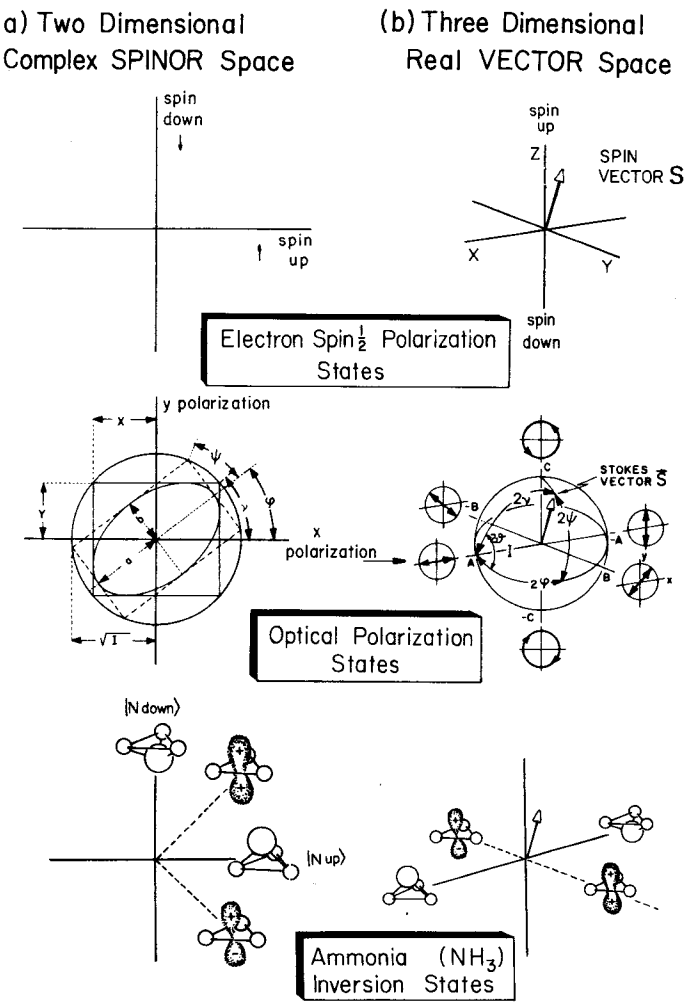

Figure 7.5.1 Two descriptions of three famous examples of two-state systems. (a) The spinor description involves complex vectors in a two-dimensional space. (b) The vector description involves real vectors in a three-dimensional space.

tational aids. To improve the intuitive value of the spinor description it helps to consider the optical polarization formalism developed by Poincaré and Stokes in the last century. In this theory the spinor bases correspond to oscillating x and y components of an electric vector. One can also picture various orbits of a two-dimensional coupled oscillator in the spinor space, and this helps greatly to understand its structure. It also helps to have a corresponding 3-space which is now labeled (ABC) instead of (xyz) in Figure 7.5.1(b2).

A key to making any of these pictures useful is to have a convenient system of coordinates for the 2-space and 3-space. Standard rotational coordinates such as Euler angles and axis angles described in Section 5.3 will be used as described below.

A. Euler-Angle Definition of Spinor States

Spinor or spin-$\frac{1}{2}$ states span the basis for the fundamental representation of SU(2), and for every pair of spinor states $|\psi\rangle$ and $|\psi'\rangle$ there exists a unitary operator R which maps one state into the other ($|\psi\rangle = R|\psi'\rangle$). A one-to-one mapping between the states and operators can be established by fixing one of the states, say, $|\psi'\rangle = |1\rangle$, and labeling all states by the mapping operator ($|R\rangle = R|1\rangle$). If the operators are labeled by Euler angles ($R = R(\alpha, \beta, \gamma)$), then so are the states

$$|\psi(\alpha, \beta, \gamma)\rangle = R(\alpha, \beta, \gamma)|1\rangle.$$

The standard Euler coordinate definition of rotation operators involves an ordered product of rotations by α, β, and γ around the x, y, and z axes, respectively, as explained in Sections 5.3 and 5.5.E:

$$R(\alpha, \beta, \gamma) = R(\alpha \cdot \cdot)R(\cdot\beta \cdot)R(\cdot\cdot \gamma). \tag{7.5.1}$$

This leads to the following explicit representation of a general spinor as a mapping of the spin-up state $|1\rangle = \begin{pmatrix} 1 \\ 0 \end{pmatrix}$:

$$\begin{aligned} \begin{pmatrix} \psi_1 \\ \psi_2 \end{pmatrix} &= \begin{pmatrix} e^{-i\alpha/2} & 0 \\ 0 & e^{i\alpha/2} \end{pmatrix} \begin{pmatrix} \cos(\beta/2) & -\sin(\beta/2) \\ \sin(\beta/2) & \cos(\beta/2) \end{pmatrix} \begin{pmatrix} e^{-i\gamma/2} & 0 \\ 0 & e^{i\gamma/2} \end{pmatrix} \begin{pmatrix} 1 \\ 0 \end{pmatrix} \\ &= \begin{pmatrix} e^{-i\alpha/2} & \cos(\beta/2) \\ e^{i\alpha/2} & \sin(\beta/2) \end{pmatrix} e^{-i\gamma/2}. \end{aligned} \tag{7.5.2}$$

A 3-space mechanical model of the expected spin vector of this state is shown in Figure 7.5.2. The figure displays the expectation values in the state $|\psi(\alpha, \beta, \gamma)\rangle$ of the Pauli spin angular-momentum operators

$$\begin{aligned} J_x = \sigma_x/2 \quad & J_y = \sigma_y/2 \quad & J_z = \sigma_z/2 \\ = \begin{pmatrix} 0 & \frac{1}{2} \\ \frac{1}{2} & 0 \end{pmatrix} \quad & = \begin{pmatrix} 0 & -i/2 \\ i/2 & 0 \end{pmatrix} \quad & = \begin{pmatrix} \frac{1}{2} & 0 \\ 0 & -\frac{1}{2} \end{pmatrix}. \end{aligned} \tag{7.5.3}$$

From the figure it is seen that the first Euler angle (α) is the relative phase between components ψ_1 and ψ_2, and it is represented by the azimuthal angle of the $\langle J \rangle$ vector. The second Euler angle (β) is the arc-cosine of the relative

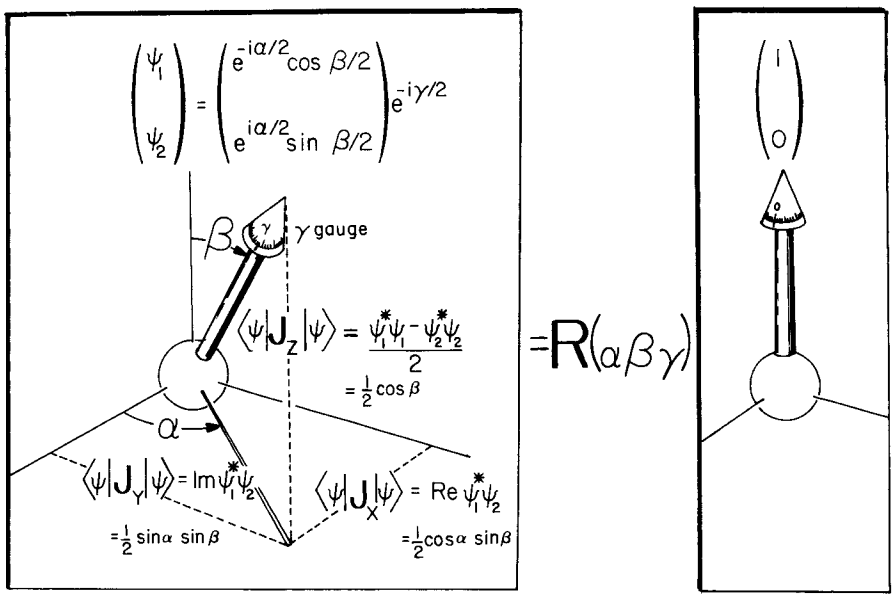

Figure 7.5.2 Detailed relation between spinor state and spin vector. The relation is based upon the fact that all spinor states are rotations of the spin-up state. Euler angles and the mechanical goniometer in Figure 5.3.1 provide a complete description of the pure spinor state.

population ($|\psi_1|^2 - |\psi_2|^2$), and it is represented by the polar angle of the $\langle J\rangle$ vector. The third Euler angle (γ) is (-2) times the overall phase or gauge of the state $|\psi(\alpha, \beta, \gamma)\rangle$, and it corresponds to the twist of the rigid body whose axis defines the direction of the $\langle J\rangle$ vector in Figure 7.5.2. In the quantum theory of spin this third coordinate is often superfluous. However, for classical applications this angle will help to define the phase of an orbit and should not be ignored. The γ angle is indicated by a dial or gauge in Figures 7.5.2 and 5.3.1.

B. Axis-Angle Definition of Spinor Operators

The general $U(2)$ group operator may be expressed in terms of a single exponential

$$U = U(\omega_0, \omega_x, \omega_y, \omega_z) = e^{-ih},$$

involving a combination of Pauli operators $\sigma = 2J$

$$h = \omega_0 1 + \omega_x J_x + \omega_y J_y + \omega_z J_z = \omega_0 + \frac{\omega_x}{2}\sigma_x + \frac{\omega_y}{2}\sigma_y + \frac{\omega_z}{2}\sigma_z,$$

which has the matrix form

$$\begin{pmatrix} h_{11} & h_{12} \\ h_{21} & h_{22} \end{pmatrix} = \omega_0 \begin{pmatrix} 1 & 0 \\ 0 & 1 \end{pmatrix} + \frac{\omega_x}{2} \begin{pmatrix} 0 & 1 \\ 1 & 0 \end{pmatrix} + \frac{\omega_y}{2} \begin{pmatrix} 0 & -i \\ i & 0 \end{pmatrix} + \frac{\omega_z}{2} \begin{pmatrix} 1 & 0 \\ 0 & -1 \end{pmatrix}. \tag{7.5.4}$$

An important example of this is the time evolution operator

$$U(t) = e^{-iHt} \tag{7.5.5a}$$

for the autonomous (H_{ij} = constant) Schrödinger equation $i|\dot{\psi}\rangle = H|\psi\rangle$, or

$$i\frac{\partial}{\partial t} \begin{pmatrix} \psi_1 \\ \psi_2 \end{pmatrix} = \begin{pmatrix} H_{11} & H_{12} \\ H_{21} & H_{22} \end{pmatrix} \begin{pmatrix} \psi_1 \\ \psi_2 \end{pmatrix} \tag{7.5.5b}$$

for a two-level system such as a spin-$\frac{1}{2}$ moment in a magnetic field. The expansion (7.5.4) reduces the solution

$$|\psi(t)\rangle = U(t)|\psi(0)\rangle \tag{7.5.5c}$$

to an exponential expression

$$\begin{aligned} |\psi(t)\rangle &= e^{-i\omega_0 t} e^{-i(\omega_x J_x + \omega_y J_y + \omega_z J_z)t} |\psi(0)\rangle \\ &= e^{-i\omega_0 t} e^{-i\boldsymbol{\omega}\cdot\mathbf{J}t} |\psi(0)\rangle, \end{aligned} \tag{7.5.5d}$$

which involves an overall phase which evolves at the angular rate

$$\omega_0 = (H_{11} + H_{12})/2 \tag{7.5.5e}$$

and an SU(2) rotation with angular velocity $\boldsymbol{\omega}$ whose three Cartesian components are

$$\begin{aligned} \omega_x &= 2\,\mathrm{Re}\,H_{21} & \omega_y &= 2\,\mathrm{Im}\,H_{21} & \omega_z &= H_{11} - H_{22} \\ &= \omega\cos\phi\sin\theta, & &= \omega\sin\phi\sin\theta, & &= \omega\cos\theta. \end{aligned} \tag{7.5.5f}$$

In the second line of (7.4.5f) the polar coordinates of the rotational "crank" axis are defined according to Figure 7.5.3(a). The azimuthal angle (ϕ), polar angle (θ), and total rotational angle (ωt) are valid parameters of SU(2) operations $R[\phi, \theta, \omega t]$, and as such they are an alternative to the Euler angle labeling $R(\alpha, \beta, \gamma)$. (We use brackets to denote axis-angle parameters, and parentheses to denote Euler angles.)

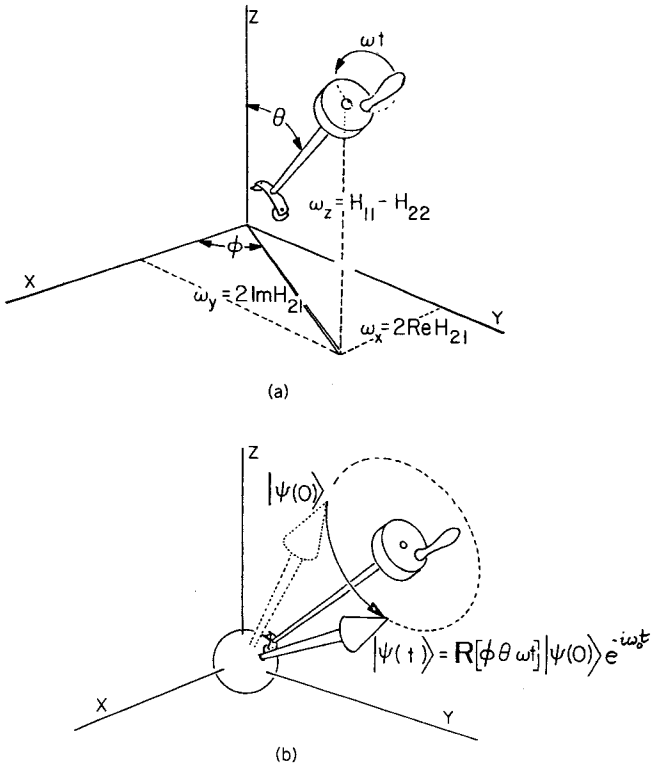

Figure 7.5.3 Mechanical crank analog for Hamiltonian matrix. (a) Components of Hamiltonian determine the direction (ϕ, θ) and rate of turn (ω) of the crank. (b) Effect of Hamiltonian is represented by mechanical analog rotation around crank axis, to within an overall phase.

Generally, it is physically more convenient to label states or rotational position with Euler angles, while Hamiltonians and other operators are more intuitively labeled by axis angles. In any case it is easy to convert one labeling into the other, as explained in Section 5.5.A. Then the time evolution (7.5.5d) is reduced to a product of the Hamiltonian rotation $R[\phi, \theta, \omega t]$, the overall phase factor, and the rotation operator in the initial state definition,

$$|\psi(0)\rangle = R(\alpha(0), \beta(0), \gamma(0))|1\rangle. \tag{7.5.6}$$

The final-state Euler angles are defined by the first line in the following:

$$\begin{aligned} |\psi(t)\rangle &= R(\alpha(t), \beta(t), \gamma(t))|1\rangle \\ &= R[\phi, \theta, \omega t]R(\alpha(0), \beta(0), \gamma(0))|1\rangle e^{-i\omega_0 t} \\ &= R[\phi\,\theta, \omega t]R(\alpha(0), \beta(0), \gamma(0) + 2\omega_0 t)|1\rangle, \end{aligned} \tag{7.5.7}$$

and they would follow from the group product in the last line.

The mechanical 3-space representation of the rotation is indicated in Figure 7.5.3(b). The resulting precessional motion corresponds to the well-known Rabbi-Ramsey-Schwinger or Feynman-Vernon-Hellwarth picture of two-state evolution. The complexity of this dynamics is shown in Figure 5.3.5.

C. Rotational Angle Parameters for a Two-Dimensional Harmonic Oscillator

The spinor components of an autonomous two-state Schrödinger equation (7.5.5b) of the form

$$i\frac{d}{dt}\begin{pmatrix}\psi_1\\ \psi_2\end{pmatrix} = \begin{pmatrix}A & B-iC\\ B+iC & D\end{pmatrix}\begin{pmatrix}\psi_1\\ \psi_2\end{pmatrix} \tag{7.5.8}$$

may be replaced by separate equations for the real parts ($x_j \equiv \operatorname{Re}\psi_j$) and imaginary parts ($p_j = \operatorname{Im}\psi_j$) of the spinor components;

$$\begin{aligned}\psi_1 &= x_1 + ip_1 & \psi_2 &= x_2 + ip_2\\ &= \sqrt{I}\,e^{-i(\alpha+\gamma)/2}\cos\beta/2 & &= \sqrt{I}\,e^{-i(\gamma-\alpha)/2}\sin\beta/2.\end{aligned} \tag{7.5.9}$$

(An arbitrary but constant normalization factor $\sqrt{I}$ has been included for this discussion.) The resulting equations,

$$\begin{aligned}\dot{x}_1 &= Ap_1 + Bp_2 - Cx_2 = \frac{\partial H_c}{\partial p_1},\\ \dot{x}_2 &= Bp_1 + Dp_2 + Cx_1 = \frac{\partial H_c}{\partial p_2},\\ -\dot{p}_1 &= Ax_1 + Bx_2 + Cp_2 = \frac{\partial H_c}{\partial x_1},\\ -\dot{p}_2 &= Bx_1 + Dx_2 - Cp_1 = \frac{\partial H_c}{\partial x_2},\end{aligned} \tag{7.5.10a}$$

are identical to those of a two-dimensional classical coupled Coriolis harmonic oscillator with the Hamiltonian

$$H_c = \frac{A}{2}(p_1^2 + x_1^2) + \frac{D}{2}(p_2^2 + x_2^2) + B(p_1p_2 + x_1x_2) + C(x_1p_2 - x_2p_1). \tag{7.5.10b}$$

By exploiting the Euler and axis-angle relations one may label in an intuitive way all possible harmonic Hamiltonians H_c as well as all their

possible initial conditions and resulting phase-space trajectories. The phase-space motion can be related though the Euler angles to a precessing rigid top (Figure 7.5.2), and the Hamiltonian can be related through axis angles to a crank [Figure 7.5.3(a)] which rotates the top.

Expansion of (7.5.9) gives the Euler coordinates for each point in phase space,

$$x_1 = \sqrt{I}\cos\left(\frac{\alpha+\gamma}{2}\right)\cos\left(\frac{\beta}{2}\right), \qquad p_1 = -\sqrt{I}\sin\left(\frac{\alpha+\gamma}{2}\right)\cos\left(\frac{\beta}{2}\right),$$
$$x_2 = \sqrt{I}\cos\left(\frac{\gamma-\alpha}{2}\right)\sin\left(\frac{\beta}{2}\right), \qquad p_2 = -\sqrt{I}\sin\left(\frac{\gamma-\alpha}{2}\right)\sin\left(\frac{\beta}{2}\right). \tag{7.5.11a}$$

These expressions include the normalization or amplitude factor

$$\sqrt{I} = \left(x_1^2 + p_1^2 + x_2^2 + p_2^2\right)^{1/2} = \left(\psi_1^*\psi_1 + \psi_2^*\psi_2\right)^{1/2}. \tag{7.5.11b}$$

The quantity I is the total intensity or probability in the two-level quantum system and is therefore a constant of motion for the classical system, as well.

A combination of (7.5.5f) and (7.5.8) leads to an axis-angle parametrization of the oscillator Hamiltonian.

$$\begin{aligned} \omega_x &= \omega\cos\phi\sin\theta & \omega_y &= \omega\sin\phi\sin\theta & \omega_z &= \omega\cos\theta \\ &= 2B & &= 2C & &= A - D \\ & & \omega_0 &= (H_{11} + H_{12})/2 & & \\ & & &= (A + D)/2. & & \end{aligned} \tag{7.5.12}$$

This relates the angular velocity vector $\boldsymbol{\omega}$ with its axis angle (ϕ, θ), angular rate of turn ω, and overall phase rate ω_0 to the four Hamiltonian constants A, B, C, and D. The oscillator Hamiltonian can also be related to a rotor Hamiltonian using angular-momentum variables obtained from the expected J values displayed in Figure 7.5.2:

$$\begin{aligned} \mathcal{J}_x &= \langle\psi|J_x|\psi\rangle = \mathrm{Re}\,\psi_1^*\psi_2 = x_1x_2 + p_1p_2 = (I/2)\cos\alpha\sin\beta, \\ \mathcal{J}_y &= \langle\psi|J_y|\psi\rangle = \mathrm{Im}\,\psi_1^*\psi_2 = x_1p_2 - x_2p_1 = (I/2)\sin\alpha\sin\beta, \\ \mathcal{J}_z &= \langle\psi|J_z|\psi\rangle = (\psi_1^*\psi_1 + \psi_2^*\psi_2)/2 = \left(x_1^2 - x_2^2 + p_1^2 - p_2^2\right)/2 \\ &= (I/2)\cos\beta, \\ 2\mathcal{J}_0 &= \langle\psi|1|\psi\rangle = \psi_1^*\psi_1 + \psi_2^*\psi_2 = x_1^2 + x_2^2 + p_1^2 + p_2^2 = I. \end{aligned} \tag{7.5.13}$$

The resulting classical variables $\mathcal{J}_a$ are combinations of density matrix

components $\psi_i^* \psi_j$ of the two-level quantum problem. The classical Hamiltonian in these variables is the following:

$$H_c = B\mathcal{J}_x + C\mathcal{J}_y + \frac{A-D}{2}\mathcal{J}_z + \frac{A+D}{2}\mathcal{J}_0 \tag{7.5.14a}$$

$$= \frac{\omega_x}{2}\mathcal{J}_x + \frac{\omega_y}{2}\mathcal{J}_y + \frac{\omega_z}{2}\mathcal{J}_z + \omega_0 J_0 \tag{7.5.14b}$$

$$= \Omega_x \mathcal{J}_x + \Omega_y \mathcal{J}_y + \Omega_z \mathcal{J}_z + \omega_0 \mathcal{J}_0. \tag{7.5.14c}$$

These are the action-angle forms ($H = \Sigma \dot{\theta} J_\theta$) for the classical oscillator and rotor. It should be noted that the angular velocities Ω_α of the classical oscillator are each half of the corresponding components ω_α for the rotor analogy. A factor of 2 is a common feature of spin-vector mappings and will be discussed further in the following.

The rotor Hamiltonian (7.5.14a) describes a rigid spin-moment body with no mass subject to torques applied by a magnetic field. A rigid massive body will have additional quadratic terms $\mathcal{J}_x^2$, etc., and this is analogous to an anharmonic oscillator in rotor-oscillator mapping. This will be discussed later. Nonrigid rotors have still higher-order terms in the angular momentum.

The coordinates conjugate to the momenta $\mathcal{J}_a$ ($a = x$, y, or z) are nonholonomic, i.e., the differentials $d\theta_a = \omega_a\, dt$ are not exact. Since the Euler angles are manifestly holonomic coordinates, it is better for many purposes to use the momenta $\{\mathcal{J}_\alpha, \mathcal{J}_\beta, \mathcal{J}_\gamma\}$ conjugate to these coordinates. Relations between the Euler momenta and the Cartesian quantities are given in Section 5.5.E [Eq. (5.5.83)].

D. Polarization Ellipsometry Coordinates

The classical description of pure states of optical polarization is equivalent to that of a two-dimensional oscillator. The relevant physical quantities in ellipsometry are the x and y electric field strengths defined by

$$E_x = \mathrm{Re}\,\langle x|\Psi\rangle, \qquad E_y = \mathrm{Re}\,\langle y|\Psi\rangle, \tag{7.5.15a}$$

which are the linear polarization amplitudes for a two-component state vector

$$|\Psi\rangle = |x\rangle\langle x|\Psi\rangle + |y\rangle\langle y|\Psi\rangle. \tag{7.5.15b}$$

The two real quantities E_x and E_y are analogous to the oscillator coordinates x_1 and x_2, respectively, in (7.5.9).

An equivalent description of the same state involves circular polarization amplitudes and bases; i.e.,

$$|\Psi\rangle = |r\rangle\langle r|\Psi\rangle + |l\rangle\langle l|\Psi\rangle, \tag{7.5.16a}$$

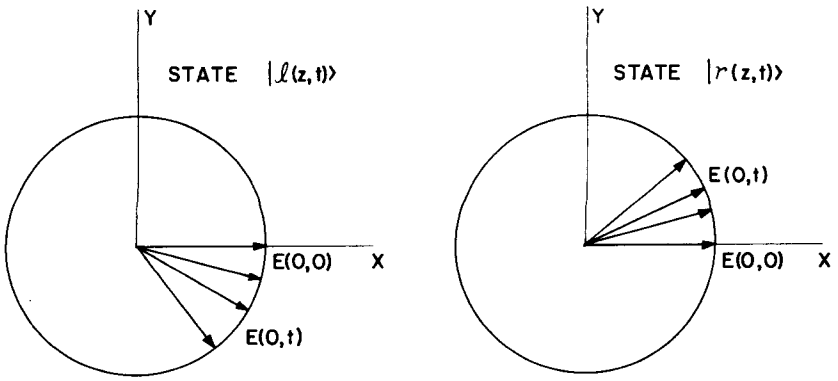

Figure 7.5.4 Circular polarization base states. States $|l\rangle$ and $|r\rangle$ are characterized by right-handed and left-handed time evolution of the E vector.

where

$$|r\rangle = (|x\rangle + i|y\rangle)/\sqrt{2}, \qquad |l\rangle = (|x\rangle - i|y\rangle)/\sqrt{2} \tag{7.5.16b}$$

represent unit states of right-handed and left-handed circular polarization, respectively. One can visualize these states by noting that the state $|\gamma\rangle = e^{i(kz-\omega t)}|r\rangle$, for example, describes a right-hand or counterclockwise circular time evolution of the electric vector, as shown in the right-hand portion of Figure 7.5.4. Linear and circular polarization bases each give rise to different but equivalent sets of ellipsometry parameters which are conveniently related to Euler angles.

In terms of linear polarization bases the general state may be written as follows:

$$|\Psi\rangle = \left(Xe^{-i\vartheta}|x\rangle + Ye^{i\vartheta}|y\rangle\right)e^{-i\theta}. \tag{7.5.17}$$

According to (7.5.15) the resulting electric vector components are

$$E_x(\vartheta, \nu, \theta) = X\cos(\vartheta + \theta), \tag{7.5.18a}$$

$$E_y(\vartheta, \nu, \theta) = Y\cos(\vartheta - \theta), \tag{7.5.18b}$$

where we define

$$X = \sqrt{I}\cos\nu, \tag{7.5.18c}$$

$$Y = \sqrt{I}\sin\nu. \tag{7.5.18d}$$

This represents an ellipse trapped in a horizontal box of dimensions $2X$ by $2Y$, as shown in Figure 7.5.5. The angle between the box diagonal and the x

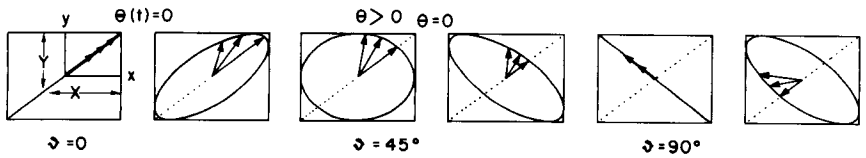

Figure 7.5.5 Examples of $\mathbf{E}\ (\vartheta, \nu, \theta)$-vector paths for various ϑ values. [Angle $\nu = \tan^{-1}(Y/X)$ is fixed.] Overall phase angle θ determines position on the elliptical orbit.

axis is ν [see also Figure 7.5.1(b2)], and the angle ϑ determines the orientation and aspect ratio of the ellipse inside the box. Overall phase θ determines the position of the electric vector on the elliptical orbit.

In terms of circular polarization bases a polarization state may be written as follows:

$$|\Psi\rangle = (Re^{-i\varphi}|r\rangle + Le^{i\varphi}|l\rangle)e^{-i\Phi} \tag{7.5.19}$$

According to (7.5.15) and (7.5.16b) the electric vector components are

$$E_x(\varphi, \psi, \Phi) = (a\cos\Phi)\cos\varphi - (b\sin\Phi)\sin\varphi, \tag{7.5.20a}$$

$$E_y(\varphi, \psi, \Phi) = (a\cos\Phi)\sin\varphi + (b\sin\Phi)\cos\varphi, \tag{7.5.20b}$$

where we define

$$a = (R + L)/\sqrt{2} = I\cos\psi, \tag{7.5.20c}$$

$$b = (R - L)/\sqrt{2} = I\sin\psi. \tag{7.5.20d}$$

This represents an ellipse trapped inside a tipped box of dimension $2a$ by $2b$ where a and b are the semimajor and minor axes of the ellipse, as shown in Figure 7.5.6. The angle between the box diagonal and the major axis is ψ [see also Figure 7.5.1(b2)]. The angle φ determines the orientation of the box and its ellipse with respect to the x axis. Overall phase Φ determines the position of the electric vector on the ellipse.

The expectation values of the Pauli momentum operators define a three-dimensional vector which is called the POINCARÉ-STOKES vector. We shall use the letters (A, B, C) to label its Cartesian components since (x, y) are already being used to label the spinor 2-space. Also, the axis of quantization, which is usually labeled by z, will be the C axis for the description based upon circular polarization and the A axis for the description based upon linear polarization. Still other axes will be used in descriptions of "local modes" in later discussions.

By relating right and left circular polarization with spin-up and spin-down, respectively, in the polarization-spin-$\frac{1}{2}$ analogy one is lead to the usual

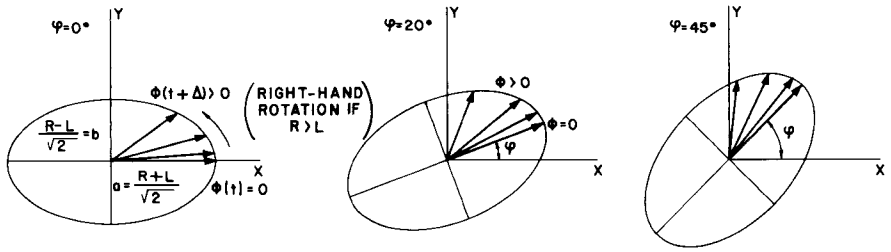

Figure 7.5.6 Examples of $\mathbf{E}\ (\varphi, \psi, \Phi)$-vector paths for various φ values. [Angle $\psi = \tan^{-1}(b/a)$ is fixed.] Overall phase angle Φ determines position on the elliptical orbit.

ordering $(x \to A, y \to B, z \to C)$ for the three Cartesian components. The three Pauli operators may be represented in the usual way in the $\{|r\rangle, |l\rangle\}$ basis as follows:

$$C(\sigma_A) = \begin{pmatrix} \langle r|\sigma_A|r\rangle & \langle r|\sigma_A|l\rangle \\ \langle l|\sigma_A|r\rangle & \langle l|\sigma_A|l\rangle \end{pmatrix} = \begin{pmatrix} 0 & 1 \\ 1 & 0 \end{pmatrix},$$

$$C(\sigma_B) = \begin{pmatrix} 0 & -i \\ i & 0 \end{pmatrix}, \qquad C(\sigma_C) = \begin{pmatrix} 1 & 0 \\ 0 & -1 \end{pmatrix}. \tag{7.5.21}$$

This then implies a different representation for the same operators in the linear $\{|x\rangle, |y\rangle\}$ basis using transformation (7.5.16b):

$$L(\sigma_A) = \begin{pmatrix} \langle x|\sigma_A|x\rangle & \langle x|\sigma_A|y\rangle \\ \langle y|\sigma_A|x\rangle & \langle y|\sigma_A|y\rangle \end{pmatrix} = \tfrac{1}{2}\begin{pmatrix} 1 & 1 \\ i & -i \end{pmatrix} C(\sigma_A) \begin{pmatrix} 1 & -i \\ 1 & i \end{pmatrix}$$

$$= \begin{pmatrix} 1 & 0 \\ 0 & -1 \end{pmatrix},$$

$$L(\sigma_B) = \begin{pmatrix} 0 & 1 \\ 1 & 0 \end{pmatrix}, \qquad L(\sigma_C) = \begin{pmatrix} 0 & -i \\ i & 0 \end{pmatrix}. \tag{7.5.22}$$

The diagonal form of σ_A indicates a choice of A-axis quantization with the permuted ordering $(x \to B, y \to C, z \to A)$ in the assignment of Pauli operators.

Points in the (A, B, C) space are identified easily by the expectation values $\langle\psi|\boldsymbol{\sigma}|\psi\rangle$ in the desired representation. This leads to relations between elliptical shape angles (φ, ψ), (ϑ, ν), and the respective Euler angles. In the

circular representation one derives

$$\langle\Psi|\sigma_A|\Psi\rangle = \overbrace{Re^{-i\varphi}Le^{i\varphi}}^{*}\begin{pmatrix}0 & 1\\ 1 & 0\end{pmatrix}\begin{pmatrix}Re^{-i\varphi}\\ Le^{i\varphi}\end{pmatrix} = 2RL\cos 2\varphi = (a^2 - b^2)\cos 2\varphi,$$

$$\langle\Psi|\sigma_B|\Psi\rangle = \overbrace{Re^{-i\varphi}Le^{i\varphi}}^{*}\begin{pmatrix}0 & -i\\ i & 0\end{pmatrix}\begin{pmatrix}Re^{-i\varphi}\\ Le^{i\varphi}\end{pmatrix} = 2RL\sin 2\varphi = (a^2 - b^2)\sin^2\varphi,$$

$$\langle\Psi|\sigma_C|\Psi\rangle = \overbrace{Re^{-i\varphi}Le^{i\varphi}}^{*}\begin{pmatrix}1 & 0\\ 0 & 1\end{pmatrix}\begin{pmatrix}Re^{-i\varphi}\\ Le^{i\varphi}\end{pmatrix} = R^2 - L^2 = 2ab. \qquad (7.5.23)$$

These values are equal to the corresponding linear representation values:

$$\langle\Psi|\sigma_A|\Psi\rangle = \overbrace{Xe^{-i\vartheta}Ye^{i\vartheta}}^{*}\begin{pmatrix}1 & 0\\ 0 & -1\end{pmatrix}\begin{pmatrix}Xe^{-i\vartheta}\\ Ye^{i\vartheta}\end{pmatrix} = X^2 - Y^2,$$

$$\langle\Psi|\sigma_B|\Psi\rangle = \overbrace{Xe^{-i\vartheta}Ye^{i\vartheta}}^{*}\begin{pmatrix}0 & 1\\ 1 & 0\end{pmatrix}\begin{pmatrix}Xe^{-i\vartheta}\\ Ye^{i\vartheta}\end{pmatrix} = 2XY\cos 2\vartheta,$$

$$\langle\Psi|\sigma_C|\Psi\rangle = \overbrace{Xe^{-i\vartheta}Ye^{i\vartheta}}^{*}\begin{pmatrix}0 & -i\\ i & 0\end{pmatrix}\begin{pmatrix}Xe^{-i\vartheta}\\ Ye^{i\vartheta}\end{pmatrix} = 2XY\sin^2\vartheta. \qquad (7.5.24)$$

Combination of these results with the box-angle definitions (7.5.18) and (7.5.20) yields the following ellipsometry relations:

$$\begin{aligned}
&\text{(Circular)} && \text{(Linear)}\\
\langle\Psi|\sigma_A|\Psi\rangle &= I\cos 2\psi\cos 2\varphi && = I\cos 2\nu,\\
\langle\Psi|\sigma_B|\Psi\rangle &= I\cos 2\psi\sin 2\varphi && = I\sin 2\nu\cos 2\vartheta,\\
\langle\Psi|\sigma_C|\Psi\rangle &= I\sin 2\psi && = I\sin 2\nu\sin 2\vartheta,\\
\langle\Psi|\Psi\rangle &= I = a^2 + b^2 && = X^2 + Y^2. \qquad (7.5.25)
\end{aligned}$$

Each of the angles in these relations is indicated on the (ABC) vector diagram in Figure 7.5.1(b) as well as in the spinor diagram. For each angle in the spinor diagram there is a corresponding double angle in the vector diagram. For example, linear polarization states on the AB equator of the vector diagram ($\psi = 0 = \nu$) are characterized by an azimuthal angle 2φ where φ is the inclination angle for the major axis of polarization in a spinor diagram. A complete vector revolution $2\varphi \to 2\varphi + 2\pi$ corresponds to only a half-revolution of the spinor picture. This is due to the fact that such a revolution maps a polarization state into one that is π out of phase. That spinor states require 4π rotations around any axis in the vector 3-space in order to have no change is seen more easily in the optical polarization analogy. The idea that a vector is a square of spinors (in the outer product sense) is relevant. The amplitude scale for spinors is $\sqrt{I}$, while for vectors it is I in Figure 7.5.1.

By choosing the C axis to be the "z direction" of quantization one picks the following angles:

$$\alpha = 2\varphi, \qquad \beta = \frac{\pi}{2} - 2\psi, \qquad \gamma = 2\Phi, \tag{7.5.26}$$

to be the Euler azimuthal, polar, and overall phase angles, respectively. This choice favors circular polarization and is convenient if there is a strong Coriolis component or Zeeman field in a vibrational model. If instead one chooses the A axis, then the angles

$$\alpha = 2\vartheta, \qquad \beta = 2\nu, \qquad \gamma = 2\theta \tag{7.5.27}$$

are the Euler angles. This choice favors linear x and y polarizations and is convenient if there are well-defined normal-mode states $|x\rangle$ and $|y\rangle$ in the vibrational model.

E. Generalized Lissajous Trajectories and Related Dynamics

(a) Examples of Rotation and Oscillation Dynamics The vectorial or three-space description complements the spinorial or two-space picture. While the latter displays more detail the former may be more efficient. Each elliptical trajectory in the 2-space corresponds to a single direction or quasispin vector ($\mathbf{S} = \mathbf{J}$) in the 3-space. This vector only moves if the ellipse changes in size, shape, or orientation.

Consider, for example, the solution to an isotropic oscillator equation (7.5.10) with constants $A = D$ and $B = 0$ for which a Coriolis force ($C \neq 0$) is present. The Coriolis term,

$$C(x_1 p_1 - x_2 p_1) = Cl_z \tag{7.5.28}$$

in Eq. (7.5.10) describes the effect of adding a magnetic field to a charged oscillating mass or a Foucault pendulum in a rotating frame. The $\mathbf{S}$ vector will precess around the $\boldsymbol{\omega}$ vector $(\omega_x, \omega_y, \omega_z) = (0, 2C, 0)$ according to Eq. (7.5.12). If we use linear polarization bases $|x_1\rangle \equiv |x\rangle$ and $|x_2\rangle \equiv |y\rangle$ for which the z axis of quantization is the A axis then the following coordinate identification is appropriate,

$$\begin{aligned}(\omega_A, \omega_B, \omega_C) &= (\omega_z, \omega_x, \omega_y) = (A - D, 2B, 2C) \\ &= (0, 0, 2C) \quad \text{for } A = D \text{ and } B = 0. \end{aligned} \tag{7.5.29}$$

An example of the resulting motion is displayed in Figure 7.5.7(a). This involves precession of an ellipse with constant shape angle ψ but variable orientation angle φ. The rotation around the C axis proscribed by (7.5.29) is called *Faraday rotation* of polarization. The states $|r\rangle$ or $|l\rangle$ of pure circular

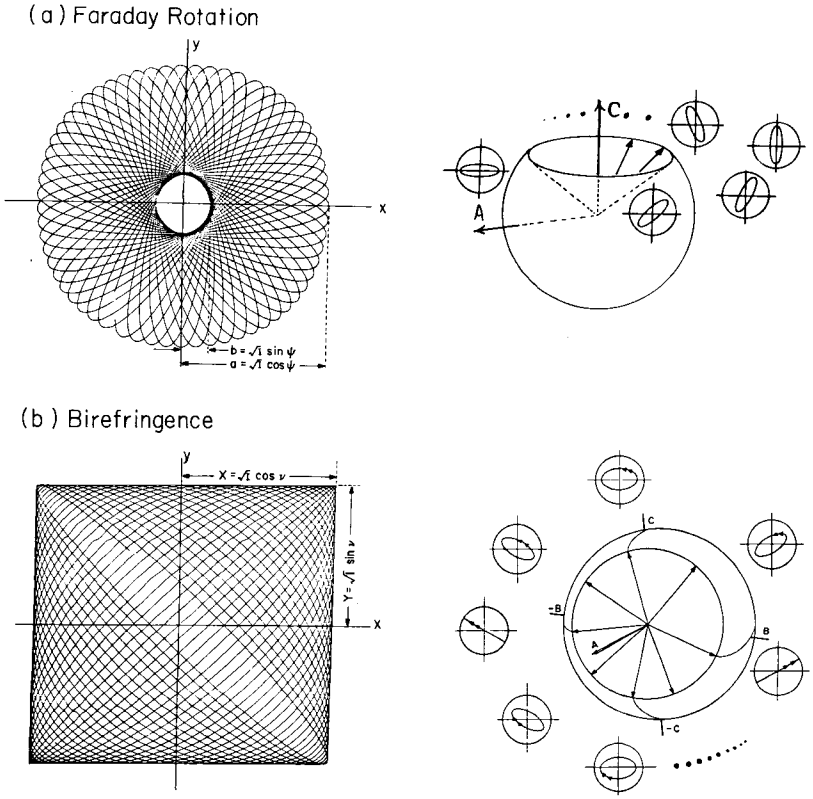

Figure 7.5.7 Analog computer plots of two famous examples of optical activity. (a) Faraday rotation or circular dichroism corresponds to constant $\psi = \tan^{-1}(b/a)$. (b) Birefringence corresponds to constant $\nu = \tan^{-1}(Y/X)$. Note that a small amount of birefringence is present in Figure 7.11(a); i.e., ψ oscillates slightly. Pure Faraday rotation is difficult to achieve on an analog computer.

polarization ($\psi = \pm\pi/4$) correspond to **S** vectors parallel or antiparallel to $\boldsymbol{\omega} = 2C\hat{\mathbf{e}}_C$, and so they represent fixed points in the ABC-vector space for the pure Coriolis Hamiltonian. All other states experience a precession of their principal directions of polarization by angle φ [recall Figure (7.5.6)] while their **S** vectors maintain a constant angle $(\pi/2 - 2\psi)$ with the C axis and rotate by 2φ around it.

A very different type of motion is that of nondegenerate $|x\rangle$ and $|y\rangle$ modes ($A \neq D$) which are uncoupled ($B = 0$) and Coriolis free ($C = 0$). Then the crank vector lies along the A axis:

$$(\omega_A, \omega_B, \omega_C) = (A - D, 0, 0). \tag{7.5.30}$$

An example of the resulting motion is displayed in Fig. 7.5.7(b). The ellipse

deforms and vibrates continuously but remains inside a box of constant diagonal angle ν. (Recall Figure 7.5.5.) The **S** vector maintains a constant angle 2ν with the A axis while rotating by 2ϑ around it. The states $|x\rangle \equiv |x_1\rangle$ and $|y\rangle = |x_2\rangle$ of pure horizontal or vertical polarization represent fixed points in each case since the **S** vector lies along the $+A$ or $-A$ axis ($\nu = 0$ or $\pi/2$). Motion of mixed $|x\rangle$ and $|y\rangle$ states such as is shown in Figure 7.5.8(b) is known as a *birefringence* in polarization optics.

S vectors on the $\pm B$ axis ($2\varphi = \pm\pi/2$) correspond to $\varphi = \pm 45°$ polarization states or equal-mixture states $(|x\rangle \pm |y\rangle)/\sqrt{2}$. If $|x\rangle = |x_1\rangle$ and $|y\rangle = |x_2\rangle$ correspond to two-particle normal mode states of A_1 and A_2 symmetry, respectively, then the ($\varphi = \pm 45°$) mixtures correspond to local mode states in which one particle is oscillating while the other is at rest. The Hamiltonian described by the A vector (7.5.30) will rotate an **S** vector from the $+B$ axis along the BC plane to the $-B$ axis and back to $+B$. During this time the oscillating particle gives all its energy to the one that was stationary and just as quickly takes it all back but suffers a phase shift of π. This is called a "half-beat" in a resonant energy transfer process. (Recall that **S** has to go around *twice* to return the state exactly.) Maximum power transfer occurs each time the **S** vector passes the $\pm C$ axis. Then the phase of the driving particle is $\pi/2$ ahead of the driven particle which has the same amplitude. This corresponds to a circular trajectory in the (x_1, x_2) space if **S** were to remain fixed on C. (Recall Figure 7.5.4.)]

The oscillator half-beat frequency is given by the magnitude of the ω vector (7.5.30).

$$\begin{aligned}\omega_{\text{half-beat}} = |\boldsymbol{\omega}| &= \left[\omega_A^2 + \omega_B^2 + \omega_C^2\right]^{1/2} = 2\Omega_{\text{beat}} \\ &= \left[(A - D)^2 + 4B^2 + 4C^2\right]^{1/2} \\ &= A - D \quad \text{for } B = 0 = C. \end{aligned} \tag{7.5.31}$$

This corresponds to the quantum frequency difference between the two-level eigenfrequencies. It is the Rabi frequency in rotating wave version of the two-level problem. The average value of the eigenfrequencies is given by Eq. (7.5.12):

$$\omega_0 = (A + D)/2. \tag{7.5.32}$$

This corresponds to the classical oscillator orbit or carrier frequency, that is, the angular rate at which one elliptical trajectory is orbited if the ellipse is constant. In quantum theory this overall frequency rate is unimportant for an isolated system.

(b) Oscillator Tori and Lissajous Trajectories Trajectories for oscillator Hamiltonians for arbitrary $\{\omega_A, \omega_B, \omega_C\}$ generally appear to form on

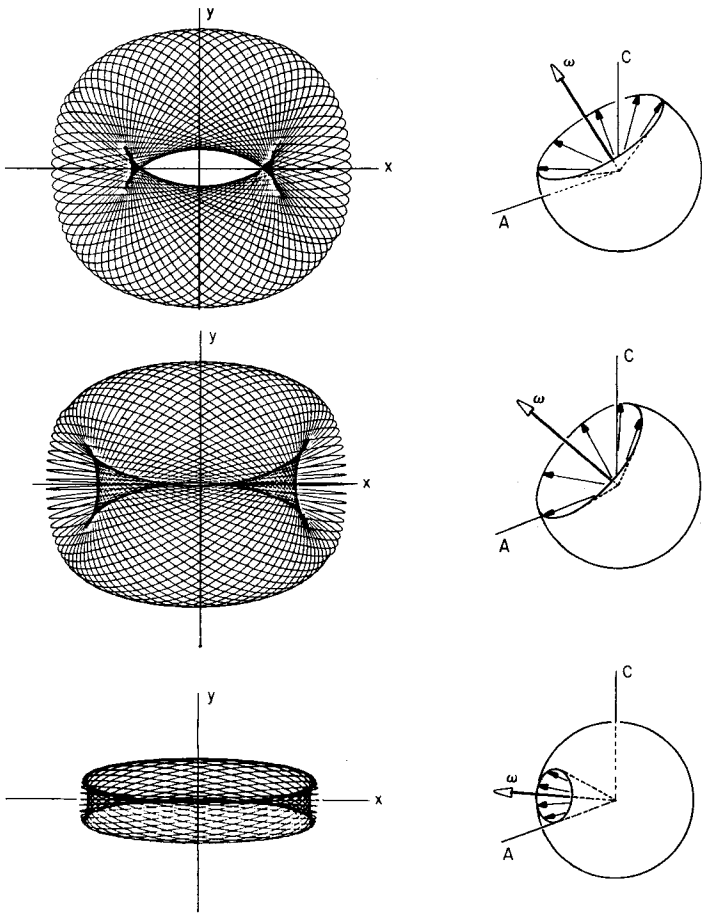

Figure 7.5.8 Evolution of states for various mixtures of A and C components.

toroidal surfaces. Three examples of trajectories with various amounts of birefringent ($\omega_A \neq 0$) and Coriolis ($\omega_C \neq 0$) or Faraday motion are shown in Figure 7.5.8. More detailed views of the oscillator tori are exhibited in Figures 7.5.9 and 7.5.10 using stereo drawings of their phase space, and these will be discussed shortly. We consider first the connection between the oscillator tori and the rotor vectors **S** and **ω**.

Figure 7.5.9 Stereograms of oscillator phase 4-space trajectories for one mixture of ω_A and ω_C components. The 3-space quasispin vector picture of each trajectory is sketched in the upper right-hand corner of each figure. Ratio of high and low eigenfrequencies is $N_H{:}N_L = 2:1$. (a) Spin vector is about 40° from H end of ω-crank vector. (b) Spin vector is perpendicular to ω vector. (c) Spin vector is about 60° from L end of ω-crank vector. (d) Spin vector is about 40° from L end of ω-crank vector.

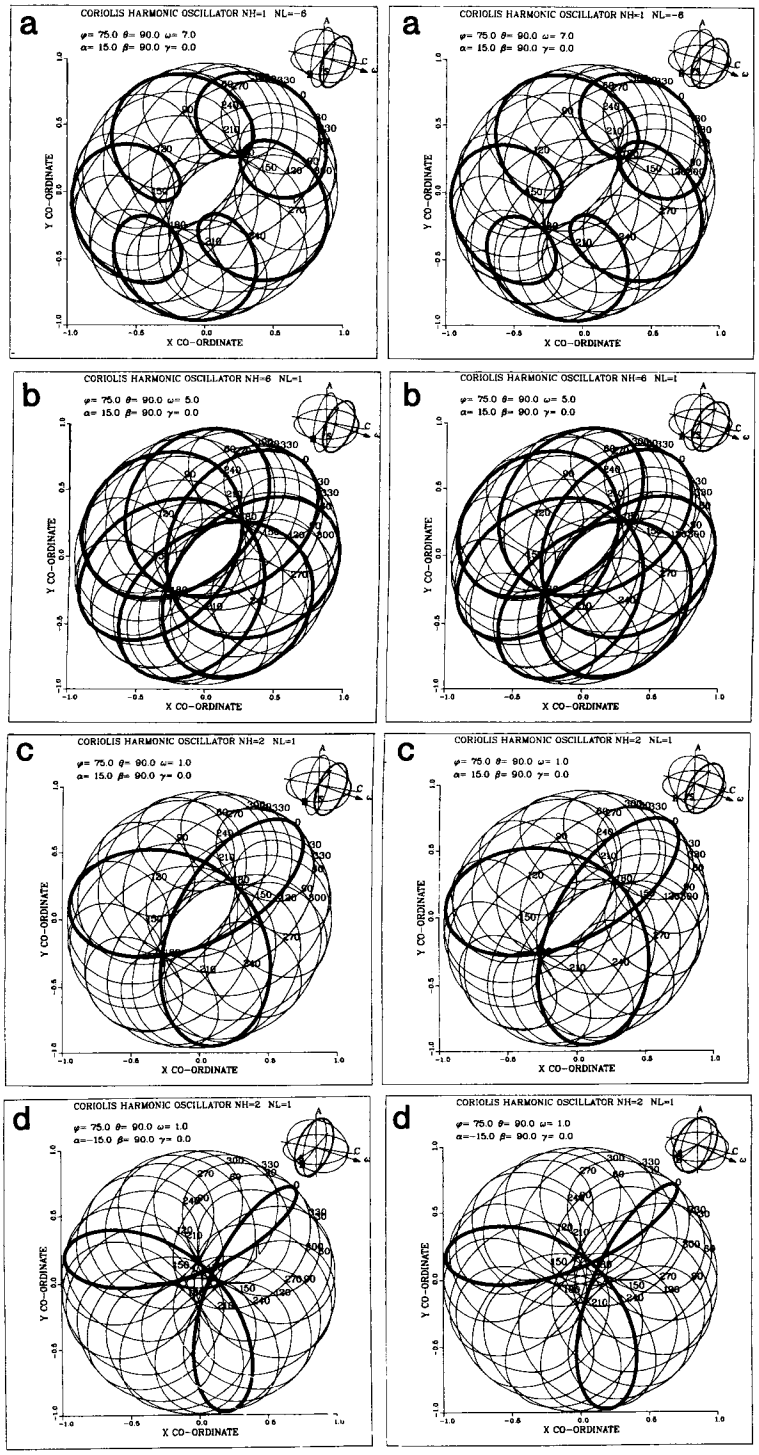
a
CORIOLIS HARMONIC OSCILLATOR NH=1 NL=-6
φ= 75.0 θ= 90.0 ω= 7.0
α= 15.0 β= 90.0 γ= 0.0
Y CO-ORDINATE
X CO-ORDINATE
b
CORIOLIS HARMONIC OSCILLATOR NH=6 NL=1
φ= 75.0 θ= 90.0 ω= 5.0
α= 15.0 β= 90.0 γ= 0.0
Y CO-ORDINATE
X CO-ORDINATE
c
CORIOLIS HARMONIC OSCILLATOR NH=2 NL=1
φ= 75.0 θ= 90.0 ω= 1.0
α= 15.0 β= 90.0 γ= 0.0
Y CO-ORDINATE
X CO-ORDINATE
d
CORIOLIS HARMONIC OSCILLATOR NH=2 NL=1
φ= 75.0 θ= 90.0 ω= 1.0
α=-15.0 β= 90.0 γ= 0.0
Y CO-ORDINATE
X CO-ORDINATE

A family of toroidal surfaces exists for each direction $\omega_A{:}\omega_B{:}\omega_C{:}$ of the ω-crank vector. Individual tori in each family are distinguished by the direction relative to $\boldsymbol{\omega}$ of the initial pseudospin vector $\mathbf{S} = \mathbf{J}$. Its magnitude $|J| = I/2 = J_0$ [recall Eqs. (7.5.11b) and (7.5.13)] determines the amplitude scale and plays no essential role for harmonic motion. The slope of a given trajectory on a particular torus depends upon the ratio of the magnitudes $|\boldsymbol{\omega}| = \omega_{\text{beat}}$ of the crank vector and the overall phase rate ω_0. [Recall Eqs. (7.5.31) and (7.5.32).] Finally, translation of a given trajectory on a torus is achieved by varying the initial value of the third Euler angle γ.

For trajectories in Figures 7.5.7 and 7.5.8 the ratio between elliptical shape evolution rate ($|\boldsymbol{\omega}|$) and orbital rate (ω_0) is equal to a small and essentially irrational number. The trajectories are quasiperiodic and could densely cover their tori. On the other hand, trajectories in Figures 7.5.9 and 7.5.10 have comparable values for ω and ω_0. In addition the ratios ω/ω_0 are chosen to be rational so that each trajectory is absolutely periodic. The resulting closed orbits are generalized or Coriolis-Lissajous figures corresponding to a single closed curve on each torus. Standard Lissajous figures correspond to closed curves in the absence of Coriolis effects ($\omega_c \equiv 0$). Lissajous trajectories only approximate ellipses briefly (i.e., for one orbit period) if the orbital rate is much greater than the shape evolution rate. This is not the case in Figures 7.5.9 and 7.5.10.

The Lissajous figures are plotted in stereo pairs in these figures using a three-dimensional subspace $\{x, y, p_x\}$ of the four-dimensional phase space. They should be viewed with a standard stereopticon or by allowing one's eyes to relax so the left and right eye views the left-hand and right-hand image, respectively. The trajectories are bold line traces which can be seen (in stereo) to reside on surfaces which are similar to the ones which would be traced quasiperiodically by the trajectories in Figure 7.5.8. Each surface is known as an invariant torus, and from the invariance of I in Eq. (7.5.13) it is seen that these examples of tori are four-dimensional spheres. Tori are sketched as doughnut shaped objects in many works, however, the stereo views of them reveal a somewhat different geometry but the same topology.

The coordinate lines on the tori in Figure 7.5.9 are constant angle lines for a choice (θ_H, θ_L) of action-angle coordinates corresponding to the high and low frequency vibrational modes of the classical oscillator. The high and low eigenfrequencies ω_H and ω_L of the two-level quantum Hamiltonian correspond to high and low frequency modes for the classical coupled oscillators.

Figure 7.5.10 Stereograms of oscillator phase space trajectories for various mixtures of ω_A, ω_B, and ω_C and various N_H and N_L. (a) $N_H = 1$, $N_L = 6$. (b) $N_H = 6$, $N_L = 1$. (c) $N_H = 2$, $N_L = 1$. (d) $N_H = 2$, $N_L = 1$.

Suppose that these frequencies are commensurate, that is,

$$\frac{\dot{\theta}_H}{\dot{\theta}_L} = \frac{\omega_H}{\omega_L} = \left(\frac{N_H}{N_L}\right) \tag{7.5.33}$$

for integers N_H and N_L. Then the quantum transition frequency or classical half-beat frequency will be

$$\begin{aligned} |\boldsymbol{\omega}| &= \omega = \omega_H - \omega_L \\ &= \omega_L(N_H - N_L)/N_L. \end{aligned} \tag{7.5.34a}$$

The classical orbit frequency will be

$$\omega_0 = \frac{(\omega_H + \omega_L)}{2} = \frac{N_H + N_L}{N_H - N_L}\left(\frac{\omega}{2}\right). \tag{7.5.34b}$$

For a mode frequency ratio of $N_H/N_L = 2/1$ the ratio orbit and beat frequencies is $\omega_0/\Omega = 3/1$.

The orbits in Figures 7.5.9(a)–7.5.9(d) all have $(N_H, N_L) = (2, 1)$. A perfect recurrence to the initial conditions at $t = 0$ occurs at $t = \Upsilon$ when $(\theta_H, \theta_L) = (\omega_H\Upsilon, \omega_L\Upsilon) = (4\pi, 2\pi)$. During the recurrence period Υ the spin vector precesses through an angle $\omega\Upsilon = 2\pi$ according to (7.5.34a), while the overall phase or orbit angle moves through $\omega_0\Upsilon = 3\pi$ according to (7.5.34b). That is, an oscillator achieves half of a beat and three halves of an orbit per recurrence with $(N_H, N_L) = (2, 1)$. This recurrence involves two turns along the H direction of the torus and one turn along the L direction. One can clearly see the double winding of the trajectory around the H direction in the upper figure [Figure 7.5.9(a)] and the single winding around the L direction in the lower figure [Figure 7.5.9(d)]. However, the winding topology is the same for all four cases. In Figures 7.5.9(a) or 7.5.9(d) the **S** vector is closer to the H or L ends, respectively, of the $\boldsymbol{\omega}$-vector. These ends correspond to ellipses with major axes oriented horizontally or vertically, respectively. The extremal ellipses correspond to fixed points or collapsed tori.

It should be noted that the tori for nonzero Coriolis effect ($\omega_C \neq 0$) exhibit curved external caustics as well as internal caustics or holes. Often the holes are clearly evident as in Figures 7.5.9(a) or 7.5.9(d) and Figure 7.5.10(a). Stereo views show that the tori actually have two orthogonal holes which are consistent with their four-dimensional spherical topology. One hole is normal to the H direction and the other is normal to the L direction. Generally, only one hole appears unobstructed in each three-dimensional projection of the four-dimensional spheres. However, Figure 7.5.10(d) shows two osculating holes most clearly.

The trajectory rosette patterns Figures 7.5.9 and 7.5.10 are predictable from the value of ω_0 in (5.8). For $(N_H, N_L) = (1, -6)$ in Figure 7.5.10(a) the

orbit angle moves through $\omega_0 \Upsilon = -5\pi$ while for $(N_H, N_L) = (6, 1)$ in Figure 7.5.10(b) it moves through $\omega_0 \Upsilon = 7\pi$ during each recurrence period Υ. There result five curlate and seven prolate rosettes, respectively. For our original example with $(N_H, N_L) = (2, 1)$ one has $\omega_0 \Upsilon / \pi = 3$ and the same number of rosettes as shown in Figures 7.5.10(b) and 7.5.10(c).

F. Rotational Energy (RE) Surface Description of Anharmonic Vibrations

The dynamics and spectral fine structure of quantum rotors was described using the geometry of RE surface trajectories in Section 7.4 (rotational level splitting for high J). An RE surface is a radial plot of a rotor Hamiltonian $H(J_x, J_y, J_z)$ in the space $\{J_x J_y J_z\}$ of its angular momentum for a fixed value of the magnitude,

$$J = |\mathbf{J}| = \left(J_x^2 + J_y^2 + J_z^2\right)^{1/2}.$$

The classically allowed motions for each J then correspond to radial level curves or topography lines formed by the intersection of the RE surface with a sphere whose radius equals the total energy $E = \langle H \rangle$ of the motion.

Here we consider the qualitative features associated with the vibrational analogy of the RE surface dynamics. The analogy is constructed by replacing angular-momentum vector J of the rotor by the quasispin vector defined by Eq. (7.5.13). The quantum expressions for the quasispin vector result if each phasor $\psi_j = x_j + ip_j$ in Eq. (7.5.9) is replaced by the oscillator boson annihilation operator a_j, and ψ_j^* is replaced with creation operator $a_j^\dagger$ for $j = 1, 2$.

$$\begin{aligned} J_x &= J_B = \left(a_2^\dagger a_1 + a_1^\dagger a_2\right)/2, \\ J_y &= J_C = i\left(a_2^\dagger a_1 - a_1^\dagger a_2\right)/2, \\ J_z &= J_A = \left(a_1^\dagger a_1 - a_2^\dagger a_2\right)/2. \end{aligned} \tag{7.5.35a}$$

Here, the permuted Pauli ordering consistent with Eq. (7.5.29) is used. The momentum conjugate to the overall phase is the total quantum number operator:

$$J_0 = a_1^\dagger a_1 + a_2^\dagger a_2. \tag{7.5.35b}$$

The advantage of the RE surface approach is that qualitative features of the eigenvalue and eigenvector spectra can be visualized relatively easily by plotting $H(J)$ and the classical RE surface trajectories. This will be shown using harmonic and anharmonic examples of vibrational Hamiltonians.

(a) Harmonic* RE *Surfaces The harmonic oscillator Hamiltonian (7.5.10b) is a linear combination (7.5.14) of the momenta or action variables

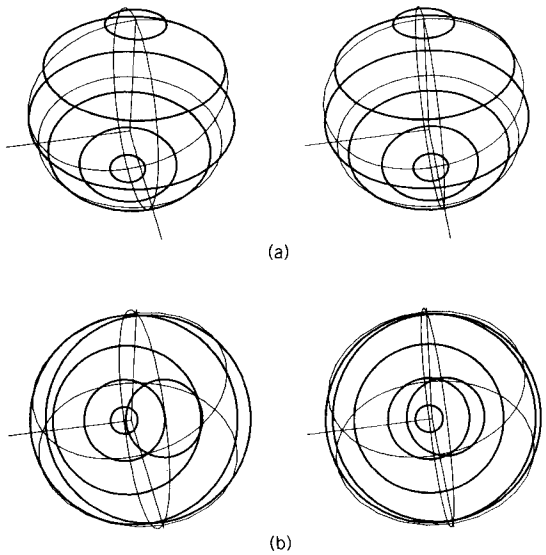

Figure 7.5.11 Quasispin RE surfaces and trajectories for harmonic coupled oscillators. (a) Coriolis free case ($C = 0$). $A = 4.0$, $D = 2.0$, $B = 0$. (b) Coriolis case ($C = 10$). $A = 4.0$, $D = 2.0$, $B = 0$.

J_m. The polar equation for the RE surface is given by substituting the Euler expressions for the momenta (7.5.13) into (7.5.14c):

$$H = (I/2)(\Omega_x \cos\alpha \sin\beta + \Omega_y \sin\alpha \sin\beta + \Omega_z \cos\beta) + J_0\omega_0, \quad (7.5.36a)$$

$$H = (I/2)\left(B \cos\alpha \sin\beta + C \sin\alpha \sin\beta + \left(\frac{A - D}{2}\right)\cos\beta\right) + J_0\omega_0. \quad (7.5.36b)$$

The (ABC) parameters are used in the second expression. The A-axis polar coordinates in (ABC) space are azimuth $\alpha = 2\vartheta$ and polar angle $\beta = 2\nu$ according to (7.5.25):

$$H = (I/4)(\omega_B \cos 2\vartheta \sin 2\nu + \omega_C \sin 2\vartheta \sin 2\nu + \omega_A \cos 2\nu) + J_0\omega_0. \quad (7.5.37)$$

The RE surface topography lines for harmonic examples with $(\omega_A, \omega_B, \omega_C) = (1, 0, 0)$ and $(1, 0, 1)$ are shown in Figures 7.5.11(a) and 7.5.11(b), respectively. The trajectories are families of parallel circles in each case. The circles are perpendicular to the axis of the ω-crank vector. The form of the RE surface is a limacon or cardioid of revolution. For large values of the constant $J_0\omega_0(\gg \omega I)$ the surface is almost the same as a

sphere displaced in the ω direction. This is the simplest type of RE surface, and the topography lines correspond to simple uniform precession around a single direction as shown in the (ABC) parts of Figures 7.5.7 to 7.5.10.

One should note that all the RE surfaces discussed so far represent Hamiltonians which had only even powers of J and were therefore invariant to J inversion $(J \rightarrow -J)$ or time reversal of the rotor. This meant that each trajectory with a clockwise direction of precession around a particular axis $(+\hat{a})$ would execute the same precession around the opposite $(-\hat{a})$ axis. In contrast, the trajectories shown in Figure 7.5.11 precess oppositely around $-\boldsymbol{\omega}$ to the way they go around $+\boldsymbol{\omega}$, that is, the vector fields of flow are all in the same direction around $\boldsymbol{\omega}$. There is no separatrix or line of fixed points on these simple RE surfaces to separate one flow field from another.

One should note also that the high-fixed points of the RE surfaces in this work are surrounded by counter-clockwise motion. (In Figure 7.5.11 $\boldsymbol{\omega}$ and $-\boldsymbol{\omega}$ are high and low points, respectively.) This is the opposite of the convention used in discussing rotors because the surfaces were drawn in the body frame in that discussion.

(b) Anharmonic* RE *Surfaces A simple model for vibrational anharmonicity includes the following perturbation operator to the harmonic oscillator:

$$a_x J_x^2 = a_x(x_1 x_2 + p_1 p_2)^2 = a_x(I^2/4)\cos^2\alpha \sin^2\beta$$
$$= a_x(a_2^\dagger a_1 + a_1^\dagger a_2)^2/4. \tag{7.5.38}$$

Anharmonic perturbations can greatly alter the classical dynamics and quantum eigensolutions.

The energy surfaces in Figure 7.5.12 show how the anharmonic perturbation (7.5.38) alters Coriolis-free harmonic normal mode dynamics described by the surface in Figure 7.5.11(a). Figures 7.5.12(a), 7.5.12(b), and 7.5.12(c) show the topography paths for increasing anharmonicity $a_x = 1.0$, 2.0, and 3.0, respectively, for harmonic values $A = 4.0$, $B = 0 = C$, $D = 2.0$, and $I = 1$. The polar equation for the surfaces in Figure 7.5.12 is

$$H = J_0\omega_0 + \left(\frac{I}{2}\right)\frac{\omega}{2}\cos\beta + a_2\left(\frac{I^2}{4}\right)\cos^2\alpha \sin^2\beta, \tag{7.5.39a}$$

where

$$\Omega = \frac{\omega}{2} = \frac{A - D}{2} \tag{7.5.39b}$$

is the true harmonic beat frequency or one-half the classical ω_{beat} frequency in Eq. (7.5.31).

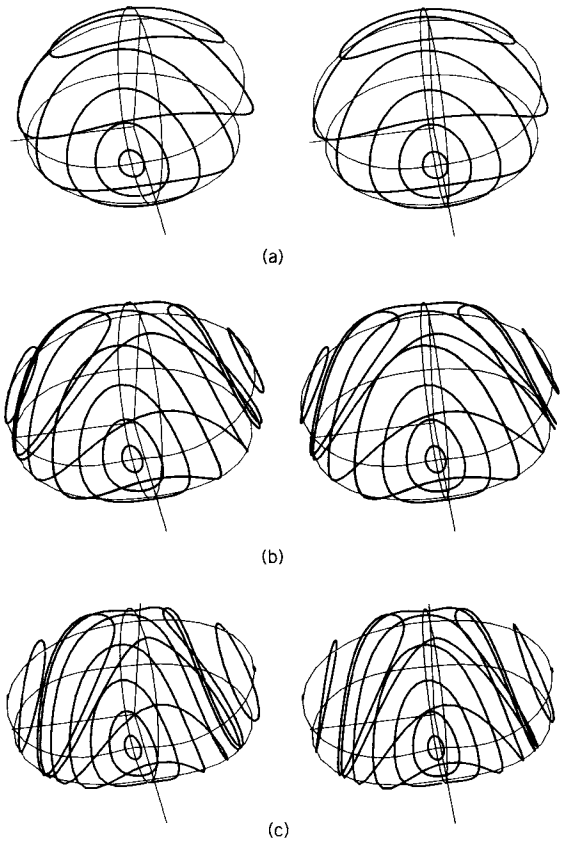

Figure 7.5.12 Quasispin RE surfaces and trajectories for anharmonic Coriolis-free coupled oscillators. (a) $a_x = 1.0$, (b) $a_x = 2.0$, (c) $a_x = 3.0$.

In Figure 7.5.12(a) one can see the first effect of the anharmonicity. The topography paths are no longer circular except in the immediate neighborhood of the normal mode fixed points. In Figures 7.5.12(b) and 7.5.12(c) one sees a more striking effect of the anharmonicity. One of the normal mode fixed points becomes an unstable saddle point at the center of a figure eight separatrix. The separatrix loops surround a pair of equivalent fixed points which move down the AB meridian away from the A point and toward the $\pm B$ axes as a_x increases. These new fixed points correspond to "local modes" and the ellipsometry of the (ABC) space immediately characterizes their trajectories. The elliptical azimuthal Euler angle is $(\alpha = 2\vartheta = 0)$ and the polar angle $(\beta = 2\nu)$ is given by solutions to

$$\frac{dH}{d\beta} = 0 = -\frac{I}{4}\omega \sin\beta + a_x \frac{I^2}{4} 2 \sin\beta \cos\beta. \qquad (7.5.40a)$$

The resulting solutions are

$$\beta = 0, \pi, \cos^{-1}(\Omega/a_x I). \tag{7.5.40b}$$

For $(\Omega/a_x I) \geq 1$ the only allowed solutions are $\beta = (0, \pi)$ which correspond to normal modes A_1 and A_2. For $a_x I > \Omega$ one mode becomes unstable and two new solutions split off. The quasispin fixed points approach the $\pm B$ axes as $a_x I$ increases. The quasispin orbits near the $\pm B$ axes correspond to oscillations in which the excitation is more or less localized on one or the other of the particles in the two-particle oscillator. This model provides a simple example of an RE surface whose form changes radically when one varies a parameter or a quantum number. The parameter of interest here is the ratio in Eq. (7.5.40) of the half-beat frequency ($\Omega = \omega/2$) to the product of the total quantum number (I) and the anharmonicity strength (a_x).

There are two properties of the RE surface trajectories in Figure 7.5.12 which are different from the ones discussed in connection with rotor motion. First, trajectories in Figure 7.5.12 have lower symmetry. Besides lacking the $(J \rightarrow -J)$ inversion symmetry mentioned previously, the double families of trajectories do not possess rotational symmetry axes at their fixed points, indeed, the fixed points are relocated by changes of the parameters. Second, the two movable stable fixed points appear suddenly, and the $\pm A$ axes are antipodal stable fixed points until $a_x I > \Omega$. Then as $a_x I$ increases, the $+A$ axis becomes an unstable fixed point while the $-A$ axis, which represents the antisymmetric mode (A_2) remains stable for all positive $a_x I$. However, the surrounding domain of stable quasi-antisymmetric trajectories becomes increasingly narrow.

The surface geometry and classical trajectories can be used to determine approximate quantum eigenvalues and wavefunctions as in the analogous rotor RE surfaces. Some qualitative observations can be made immediately. An important new feature is the emergence of equivalent pairs of localized trajectories for $a_x I \gg \Omega$. This signals the onset of a doubling or clustering in the eigenvalue spectrum, and it corresponds to pairs of local mode eigenfunctions. The doublet splitting can be related to tunneling. The quasispin ellipsometry provides a convenient visualization and computational aid for semiclassical analysis.

An advantage of the RE surface description is that it provides a more complete picture of the phase space and each point corresponds to a well defined ellipsometry or trajectory shape. Also, there exist Hamiltonians for which a simple potential curve would be an impossible or misleading description. For example, the fourth degree RE surface which has a six-maxima and eight-minima cannot be described by a simple potential curve since the minima and maxima do not belong to a single curve of section. The precise location of maxima, minima, and saddle points is essential for determining spectral properties such as clustering and tunneling.

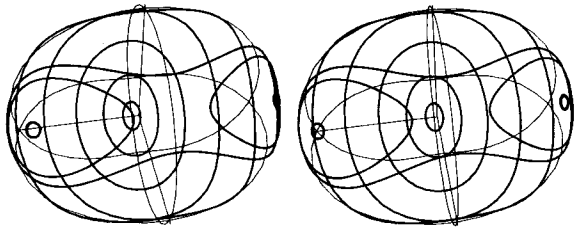

Figure 7.5.13 Quasispin RE surfaces and trajectories for Coriolis anharmonic coupled oscillators.

Finally, the RE surface picture clearly shows the effect of Coriolis terms in the anharmonic Hamiltonian. As seen in Figure 7.5.13 the addition of a nonzero C term tends to bring the local mode fixed points closer to the C axis and to each other. If the harmonic constants are varied so that $(C^2 + A^2)$ remains constant, then the harmonic Coriolis effect is equivalent to a rotation around the B axis. If the local mode points are close to the B axis (strong local mode effect), then the Coriolis effect is small. On the other hand, a large Coriolis effect could coalesce the fixed point pair near the C axis and destroy the local mode effect.

7.6 MOLECULAR ELECTRONIC STRUCTURE

We give now a brief introduction to the electronic eigenvalue problem for molecules. This is a very large and computationally intensive subject, most of which is beyond the scope of this text. Techniques and software for computing electronic structure are developing as rapidly as the computer hardware, and this is likely to continue indefinitely.

In spite of the complexity of this difficult subject there are simply concepts and guiding principles which can be shown using elementary models. We will introduce electronic structure models for the diatomic H_2^+ ion and H_2 molecule, both of which have C_2 internal point symmetry. We will also introduce some aspects of electronic structure of other symmetric molecules such as water (H_2O), ammonia (NH_3), methane (CH_4), benzene (C_6H_6), and sulfur hexafluoride (SF_6), which have C_{2v}, C_{3v}, T_d, D_6, and O_h symmetry, respectively. Symmetry analysis can help greatly to understand and calculate electronic structure.

A. Electronic Models for Diatomic Molecules

The standard electronic structure models begin with an electronic Hamiltonian in which the nuclei are point charges artificially held at fixed locations. Consider a diatomic ion with a single-electron orbiting nucleus A and

nucleus B which have charges $Z_A|e|$ and $Z_B|e|$, respectively. This would involve the following electronic Hamiltonian:

$$H_e(R_{AB}) = \frac{p_1^2}{2m} - \frac{k_A}{r_{1a}} - \frac{k_B}{r_{1b}}. \tag{7.6.1}$$

Here the electron-nuclear Coulomb potential constants are

$$k_A = \frac{|Z_A e^2|}{4\pi\varepsilon_0}, \qquad k_B = \frac{|Z_B e^2|}{4\pi\varepsilon_0} \tag{7.6.2}$$

The electronic radii r_{1a} and r_{1b} and momentum p_1 are indicated in Figure 7.6.1(a) and m is the electronic mass. For a pair of hydrogen nuclei one has $Z_A = Z_B = 1$.

To account for two electrons orbiting the same nuclei we add the kinetic energy and Coulomb interaction of the second electron with each nucleus and an electron-electron interaction energy with constant $k_{12} = (e^2/4\pi\varepsilon_0)$. (For the H_2 molecule all k's are equal.)

$$H_{e^2}(R_{AB}) = \frac{p_1^2}{2m} + \frac{p_2^2}{2m} - \frac{k_A}{r_{1a}} - \frac{k_B}{r_{1b}} - \frac{k_A}{r_{2a}} - \frac{k_B}{r_{2b}} + \frac{k_{12}}{r_{12}}. \tag{7.6.3}$$

The radii for the two-electron diatomic problem are shown in Figure 7.6.1(b).

Each of these electronic Hamiltonians treat the internuclear separation R_{AB} as a fixed parameter. The nuclear motion is found later using the following approximate nuclear Hamiltonian:

$$H_{\text{nuclear}} = \frac{P_A^2}{2M_A} + \frac{P_B^2}{2M_B} + \frac{Z_A Z_B e^2}{4\pi\varepsilon_0 R_{AB}} + E(R_{AB}). \tag{7.6.4}$$

The effect of the electrons is modeled by an expectation value of electronic energy in some electronic state $|\Psi\rangle$:

$$E(R_{AB}) = \langle\Psi|H_{\text{electron}}(R_{AB})|\Psi\rangle.$$

This is called the Born-Oppenheimer approximation. The electronic energy combined with the internuclear Coulomb potential gives a molecular bonding potential:

$$V_{\text{bond}}(R_{AB}) = E(R_{AB}) + \frac{Z_A Z_B e^2}{4\pi\varepsilon_0 R_{AB}}. \tag{7.6.5}$$

This approximation is valid only if the nuclear R_{ab} motion does not apprecia-

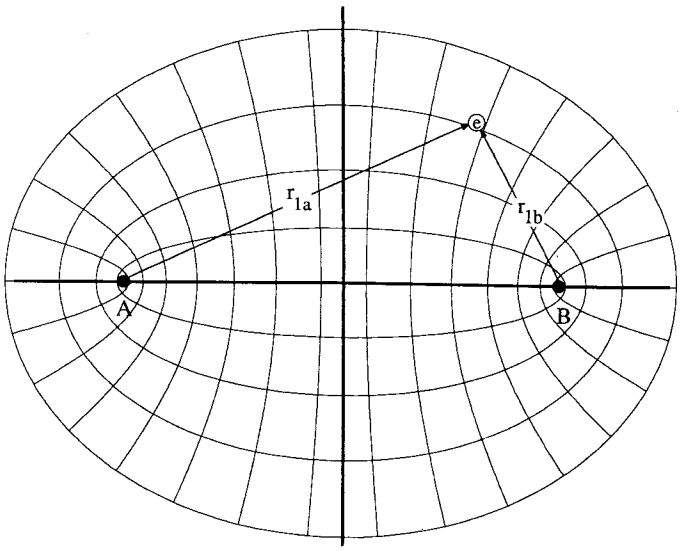

(a) H_2^+ Ion

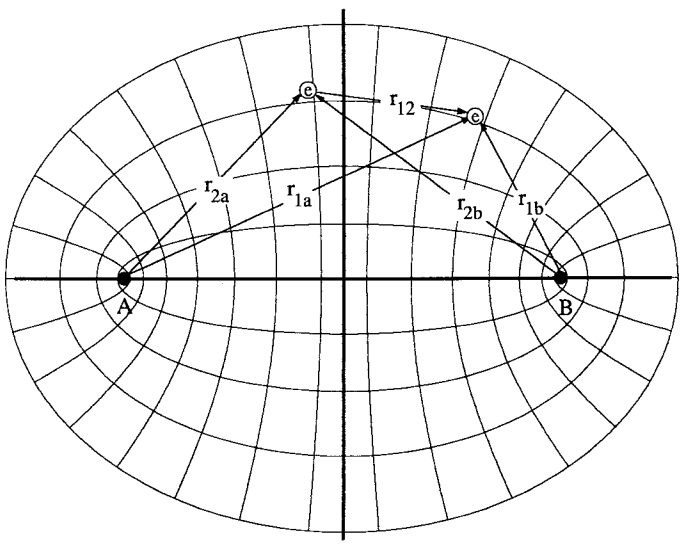

(b) H_2 Molecule

Figure 7.6.1 Coordinates for (a) hydrogen ion and (b) hydrogen molecule.

bly excite the electronic eigenstate $|\Psi\rangle$ into a combination of two or more eigenstates. In the language of Section 2.12.B the state $|\Psi\rangle$ must adiabatically follow the change in R_{ab}.

We consider now several models for electronic energy eigensolutions around a fixed pair of protons or H nuclei. With one electron we will model the bonding of an H_2^+ ion and for two electrons we will model H_2 molecular bonding.

(a) H_2^+: Atomic 1s Orbital Bonding Model The first approximation takes wavefunctions $\alpha(x)$ and $\beta(x)$ to be the lowest (1s) eigenwaves centered around position x_A or else x_B of nucleus A or B, respectively,

$$\alpha(\mathbf{x}) = (\mathbf{x}|a) = \Psi_{1s}(\mathbf{x} - \mathbf{x}_A) = \sqrt{\frac{Z_A^3}{\pi a_0^3}}\, e^{-Z_A r_a/a_0} \qquad \beta(\mathbf{x}) = (\mathbf{x}|b) = \Psi_{1s}(\mathbf{x} - \mathbf{x}_B) = \sqrt{\frac{Z_B^3}{\pi a_0^3}}\, e^{-Z_B r_b/a_0}. \tag{7.6.6}$$

We shall use parenthetical brackets $|a)$ and $|b)$ to denote these base states to remind us that they are not orthonormal. The overlap matrix $\langle \mathbf{S} \rangle$ is defined by

$$S_{ab} = (a|b) = \int d\mathbf{x}\, \alpha^*(\mathbf{x})\beta(\mathbf{x}) = \int d\mathbf{x} (a|\mathbf{x})(\mathbf{x}|b). \tag{7.6.7}$$

Wave-function overlap plays an important role in bonding theory and usually S_{ab} is *not* δ_{ab}. For the 1s states we still have normality ($(a|a) = 1 = (b|b)$) but not orthogonality ($(a|b) = (b|a) \neq 0$).

The H_2^+ bonding model reduces to a C_2 symmetric two-state system. The first state $|a)$ has the electron on nucleus A, while nucleus B is bare and vice versa for state $|b)$. A matrix representation of Hamiltonian H_e given by (7.6.1) is

$$\begin{pmatrix} (a|H_e|a) & (a|H_e|b) \\ (b|H_e|a) & (b|H_e|b) \end{pmatrix} = \begin{pmatrix} h & s \\ s & h \end{pmatrix}, \tag{7.6.8a}$$

where

$$h = \varepsilon_{1s} - k\int d\mathbf{x}\, \frac{\alpha^*(\mathbf{x})\alpha(\mathbf{x})}{r_{1b}} = \varepsilon_{1s} - \left(a\left|\frac{k}{r_b}\right|a\right), \tag{7.6.8b}$$

$$s = \varepsilon_{1s}S_{ab} - k\int d\mathbf{x}\, \frac{\alpha^*(\mathbf{x})\beta(\mathbf{x})}{r_{1b}} = \varepsilon_{1s}S_{ab} - \left(a\left|\frac{k}{r_b}\right|b\right), \tag{7.6.8c}$$

and ε_{1s} is the atomic hydrogen ground state energy value.

However, the representation basis $(|a), |b))$ does not satisfy the axioms of orthonormality and completeness given in Chapter 1. Therefore, the energy

eigenstates

$$|E\rangle = \psi_a|a) + \psi_b|b), \tag{7.6.9a}$$

which satisfy

$$H_e|E\rangle = E|E\rangle \tag{7.6.9b}$$

are not found by directly diagonalizing (7.6.8a). Instead we must convert (7.6.9) to the following generalized eigenvalue equations:

$$\begin{aligned}(a|H_e|E\rangle &= (a|H_e|a)\psi_a + (a|H_e|b)\psi_b = E[(a|a)\psi_a + (a|b)\psi_b],\\ (b|H_e|E\rangle &= (b|H_e|a)\psi_a + (b|H_e|b)\psi_b = E[(b|a)\psi_a + (b|b)\psi_b].\end{aligned} \tag{7.6.10a}$$

In matrix form this becomes

$$\begin{pmatrix}(a|H_e|a) & (a|H_e|b)\\ (b|H_e|a) & (b|H_e|b)\end{pmatrix}\begin{pmatrix}\psi_a\\ \psi_b\end{pmatrix} = E\begin{pmatrix}S_{aa} & S_{ab}\\ S_{ba} & S_{bb}\end{pmatrix}\begin{pmatrix}\psi_a\\ \psi_b\end{pmatrix}. \tag{7.6.10b}$$

The eigenvalues are roots E of a generalized secular equation

$$\det|\langle\mathbf{H}\rangle - E\langle\mathbf{S}\rangle| = 0. \tag{7.6.11}$$

For small equations like this one it is easy to invert the overlap matrix and recover a standard eigenvalue problem. The inverse of this overlap matrix is quite simple. (Let $S_{ab} = S = S_{ba}$.)

$$\begin{pmatrix}S_{aa} & S_{ab}\\ S_{ba} & S_{bb}\end{pmatrix}^{-1} = \begin{pmatrix}1 & S\\ S & 1\end{pmatrix}^{-1} = \begin{pmatrix}1 & -S\\ -S & 1\end{pmatrix}\Big/(1 - S^2). \tag{7.6.12}$$

Multiplying it by the H matrix gives a standard eigenvalue equation:

$$\frac{1}{1-S^2}\begin{pmatrix}1 & S\\ S & 1\end{pmatrix}\begin{pmatrix}h & s\\ s & h\end{pmatrix}\begin{pmatrix}\psi_a\\ \psi_b\end{pmatrix} = \frac{1}{1-S^2}\begin{pmatrix}h - Ss & s - Sh\\ s - Sh & h - Ss\end{pmatrix}\begin{pmatrix}\psi_a\\ \psi_b\end{pmatrix} = E\begin{pmatrix}\psi_a\\ \psi_b\end{pmatrix}. \tag{7.6.13}$$

The desired energy eigenvalues are the following:

$$E^+ = \frac{h + s}{1 + S}, \qquad E^- = \frac{h - s}{1 - S}. \tag{7.6.14a}$$

These correspond to symmetric and antisymmetric eigenstates:

$$|E^+\rangle = \frac{|a) + |b)}{\sqrt{2(1 + S)}}, \qquad |E^-\rangle = \frac{|a) - |b)}{\sqrt{2(1 - S)}}. \tag{7.6.14b}$$

Note that C_2 symmetry projection will give the eigenvalues directly from the

generalized eigenvalue equation (7.6.10b). Projection must diagonalize the overlap matrix as well as the H matrix. Note also that the eigenvectors are orthonormal even though the base states $|a)$ and $|b)$ are not.

The Born-Oppenheimer potentials (7.6.5) are a sum of the eigenvalues (7.6.14a) and the nuclear Coulomb potential k/R. Using (7.6.8), we have

$$V^{\pm}(R) = \frac{h \pm s}{1 \pm S} + \frac{k}{R} = \frac{\varepsilon_{1s} - k(a|1/r_b|a) \pm \varepsilon_{1s}S \mp k(a|1/r_b|b)}{1 \pm S} + \frac{k}{R},$$

$$V^{+}(R) = \varepsilon_{1s} + \frac{k}{R} - \frac{k(a|1/r_b|a)}{1+S} - \frac{k(a|1/r_b|b)}{1+S}, \tag{7.6.15a}$$

$$V^{-}(R) = \varepsilon_{1s} + \frac{k}{R} - \frac{k(a|1/r_b|a)}{1-S} + \frac{k(a|1/r_b|b)}{1-S}. \tag{7.6.15b}$$

For small S the $V^{+}(R)$ function must lie below $V^{-}(R)$ because the last term is subtracted rather than added.

To evaluate the energy eigenvalues (7.6.14a) we use confocal elliptic hyperbolic coordinates. These are also known as spheroidal coordinates. These are a generalization of the cylindrical or spherical coordinates used for one nuclear center. They are natural coordinates for a diatomic molecule which has two singularities.

Spheroidal coordinates may be defined a number of ways. The formal Cartesian transformation is

$$\begin{aligned} x &= f \sinh u \sin v \cos \phi, \\ y &= f \sinh u \sin v \sin \phi, \\ z &= f \cosh u \cos v, \end{aligned} \tag{7.6.16a}$$

where $R_{AB} = 2f$ is the distance between focal points at the nuclei, and

$$\rho = \sqrt{x^2 + y^2} = f \sinh u \sin v \tag{7.6.16b}$$

is the radius for cylindrical coordinates (ρ, ϕ, z). Constant coordinates u and v define, respectively, confocal ellipses or hyperbolas of revolution around the z axis (recall Figure 7.6.1):

$$\frac{z^2}{(f \cosh u)^2} + \frac{\rho^2}{(f \sinh u)^2} = 1, \qquad \frac{z^2}{(f \cos v)^2} - \frac{\rho^2}{(f \sin v)^2} = 1. \tag{7.6.17}$$

The semimajor axes a_e and a_h of the ellipse or hyperbola are, respectively, half the sum and differences of the electronic radii from nuclei A and B:

$$\begin{aligned} a_e &= \frac{r_{1a} + r_{1b}}{2} = f \cosh u \\ &= \frac{R_{AB}}{2} \cosh u, \end{aligned} \qquad \begin{aligned} a_h &= \frac{r_{1a} - r_{1b}}{2} = f \cos v \\ &= \frac{R_{AB}}{2} \cos v. \end{aligned} \tag{7.6.18}$$

Let the ellipsoidal coordinates μ and ν be major axes in units of nuclear separation R_{AB}:

$$\mu \equiv \frac{2a_e}{R_{AB}} = \cosh u, \qquad \nu = \frac{2a_h}{R_{AB}} = \cos v. \tag{7.6.19}$$

Then the electronic radii are given in terms of μ and ν as follows:

$$r_{1a} = \frac{(\mu + \nu)}{2} R_{AB}, \qquad r_{1b} = \frac{(\mu - \nu)}{2} R_{AB}. \tag{7.6.20}$$

The Jacobian volume element is found using (7.6.15) and (7.6.19)

$$dx\,dy\,dz = \frac{\partial(xyz)}{\partial(\mu\nu\phi)}\,du\,dv\,d\phi = \frac{\partial(xyz)}{\partial(uv\phi)}\frac{\partial(uv\phi)}{\partial(\mu\nu\phi)}\,d\mu\,dv\,d\phi$$
$$= \frac{R^3}{8}(\cosh^2 u - \cos^2 v)\,d\mu\,dv\,d\phi = \frac{R^3}{8}(\mu^2 - \nu^2)\,d\mu\,dv\,d\phi. \tag{7.6.21a}$$

If the overlap integral is converted to ellipsoidal coordinates it is simplified as follows,

$$S = \int dx\,dy\,dz\,\alpha^*(\mathbf{x})\beta(\mathbf{x}) = \frac{Z^3}{\pi a_0^3}\int_0^{2\pi} d\phi \int_1^{\infty} d\mu \int_{-1}^{1} dv\,\frac{R^3}{8}(\mu^2 - \nu^2)e^{-ZR\mu/a_0}$$
$$= \left(\frac{Z^2R^2}{3a_0^2} + \frac{ZR}{a_0} + 1\right)e^{-ZR/a_0}. \tag{7.6.21b}$$

Note that the overlap falls off exponentially as atomic number ($Z_A = Z = Z_B$) and internuclear radius $R_{AB} = R$ increase.

The other terms in the eigenvalue and Hamiltonian formulas (7.6.15) are evaluated similarly. Consider Coulomb attraction between electronic charge on nucleus A and nuclear charge B (or vice versa). The potential appears in the third term of (7.6.15):

$$-k\left(a\left|\frac{1}{r_b}\right|a\right) = -k\int d\mathbf{x}\frac{\alpha^*(\mathbf{x})\alpha(\mathbf{x})}{r_{1b}}$$
$$= -\frac{kZ^3}{\pi a_0^3}\int_0^{2\pi} d\phi \int_1^{\infty} d\mu \int_{-1}^{1} dv\,\frac{\frac{1}{8}R(\mu^2 - \nu^2)e^{-(\mu+\nu)ZR/2a_0}}{\frac{1}{2}R(\mu - \nu)}$$
$$= -\frac{k}{R} + \left(\frac{k}{R} + \frac{kZ}{a_0}\right)e^{-2ZR/a_0}. \tag{7.6.22}$$

The main contribution is $-k/R$, which lowers the atomic energy ε_{1s}. (ε_{1s} is due to the interaction of electronic charge on nucleus A and nuclear charge A.)

The crucial bonding energy is the final term in (7.6.15). It appears to be an interaction between nucleus B and the electronic "overlap charge" $\alpha^*(x)\beta(x)$:

$$\begin{aligned} k\left(a\left|\frac{1}{r_b}\right|b\right) &= -k\int d\mathbf{x}\frac{\alpha^*(\mathbf{x})\beta(\mathbf{x})}{r_{1b}} \\ &= -\frac{kZ^3}{\pi a_0^3}\int_0^{2\pi} d\phi \int_1^{\infty} d\mu \int_{-1}^{1} d\nu \frac{\frac{1}{8}R^3(\mu^2-\nu^2)e^{-uZR/a_0}}{\frac{1}{2}R(\mu-\nu)} \\ &= -\frac{kZ}{a_0}\left[1+\frac{ZR}{a_0}\right]e^{-ZR/a_0}. \end{aligned} \tag{7.6.23}$$

This term is the main difference between V^+ and V^- in (7.6.15). It represents a fundamentally quantum-mechanical effect, and quite an important one to anyone who wants their molecules to hang together! Like most quantum tunneling or resonance effects it dies off quasiexponentially with separation.

The resulting H_2^+ molecular potentials $V^+(R)$ and $V^-(R)$ reduce to the following functions of R expressed in atomic units ($a_0 = 5.3 \times 10^{-11}$ m):

$$V^{\pm}(R) = \varepsilon_{1s} + \frac{1}{R}\frac{(1+R)e^{-2R} \pm \left(1-\frac{2}{3}R^2\right)e^{-R}}{1 \pm \left(\frac{1}{3}R^2+R+1\right)e^{-R}}. \tag{7.6.24}$$

The atomic energy unit ($k/a_0 = 4.36 \times 10^{-18}$ J = 27.21 eV) is used, as well. A plot of $V^{\pm}(R)$ is shown in Figure 7.6.2.

The symmetrized (g) orbital state

$$|\sigma_g\rangle = \frac{|a) + |b)}{\sqrt{2(1+S)}} \tag{7.6.25a}$$

is called a *bonding* orbital since its potential $V^+(R)$ has a stable minimum at about 2.5 a.u. The antisymmetrized state

$$|\sigma_\mu^*\rangle = \frac{|a) - |b)}{\sqrt{2(1-S)}} \tag{7.6.25b}$$

is called an *antibonding* orbital since its potential $V^-(R)$ is repulsive and would cause the H_2^+ ion to explode. The bonding orbital concentrates electronic charge between the two nuclei, while the antibonding orbital has a

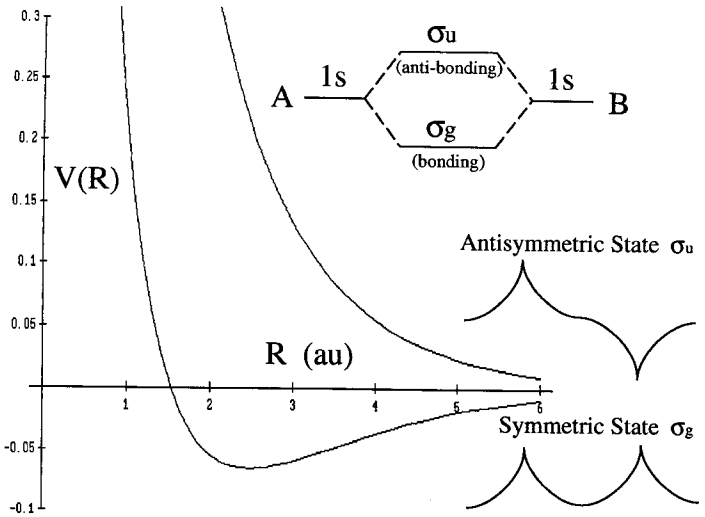

Figure 7.6.2 Antibonding and bonding states of H_2^+ with the corresponding potential curves.

node and tends to exclude charge. Both orbitals are symmetric around the z axis as their σ labels indicate. (Recall $D_{\infty h}$ labels in Section 5.)

This bonding model based upon $1s\sigma$ is qualitatively right but not the whole story. The correct value of the bonding minimum is 25% less, about 2.0 a.u., and the energy is much less, about -0.10 a.u. instead of -0.065 predicated by (7.5.24). What is missing is another quantum effect involving the uncertainty relation ($\Delta x\, \Delta p \leq \hbar$). An electron that is less confined (greater Δx) has less kinetic energy (less Δp). The H_2^+ electron can "stretch out" over two nuclei and this reduces its energy. As a result it ends up getting closer to the H nuclei and reducing the average potential energy. By using only $1s$ orbitals, this model has prevented this reduction. Exact numerical wave functions of the spheroidal coordinates (7.6.19) show this nuclear electronic concentration.

There is another important piece of physics which is left out of the rigid ($1s$) wave-function model of H_2^+: The wave on each atom cannot be polarized. To make an electronic dipole moment on one of the atoms it needs to be able to mix in some p-wave such as in a $2s2p$ superposition. This is important for modeling H^+ to H scattering potential which has a $1/R^4$ dependence at large R. Polarization of electronic orbitals plays a role in molecular bonding, as we will see later.

(b)* H_2: *Heitler-London Valence-Bond Model Suppose two electrons can occupy either of the two atomic $1s$ states $|a)$ or $|b)$, discussed in Section (a). This would yield a basis of four orbital states $|a)|a)$, $|a)|b)$, $|b)|a)$, and

$|b)|b)$. The Heitler-London model chooses to consider only the "covalent" bonding states $|a)|b)$ and $|b)|a)$ in which electrons 1 and 2 are on different nuclei. This model ignores the contribution of "ionic" bonding states $|a)|a)$ or $|b)|b)$ in which both electrons are crowded onto nucleus a or nucleus b, respectively. More complicated models show that the probability for H_2 ionic states is only a few percent.

The H_2 Hamiltonian is (7.6.3) with all k values equal. Its representation in the Heitler-London basis $\{|a)|b), |b)|a)\}$ has the following diagonal components $h_a = h_b$:

$$\begin{aligned} h_a &= \left(ab\left|\frac{p_1^2}{2m} - \frac{k}{r_{1a}}\right|ab\right) + \left(ab\left|\frac{p_2^2}{2m} - \frac{k}{r_{1b}}\right|ab\right) - \left(ab\left|\frac{k}{r_{2a}}\right|ab\right) \\ &\quad - \left(ab\left|\frac{k}{r_{1b}}\right|ab\right) + \left(ab\left|\frac{k}{r_{12}}\right|ab\right) \\ &= \varepsilon_{1s} + \varepsilon_{1s} - \left(b\left|\frac{k}{r_a}\right|b\right) - \left(a\left|\frac{k}{r_b}\right|a\right) + \left(ab\left|\frac{k}{r_{12}}\right|ab\right) \\ &= 2\varepsilon_{1s} - 2\left(a\left|\frac{k}{r_b}\right|a\right) + D, \end{aligned} \tag{7.6.26a}$$

where the last term D is called the *direct* Coulomb repulsion integral:

$$D = \left(ab\left|\frac{k}{r_{12}}\right|ab\right) = \int d\mathbf{x}_1 \int d\mathbf{x}_2\, \alpha^*(\mathbf{x}_1)\beta^*(\mathbf{x}_2)\left(\frac{1}{r_{12}}\right)\alpha(\mathbf{x}_1)\beta(\mathbf{x}_2). \tag{7.6.26b}$$

The other terms were discussed previously. Similarly, the off-diagonal component is as follows

$$\begin{aligned} h_{ab} &= \left(ab\left|\frac{p_1^2}{2m} - \frac{k}{r_{1a}}\right|ba\right) + \left(ab\left|\frac{p_2^2}{2m} - \frac{k}{r_{2b}}\right|ba\right) - \left(ab\left|\frac{k}{r_{2a}}\right|ba\right) \\ &\quad - \left(ab\left|\frac{k}{r_{1b}}\right|ba\right) + \left(ab\left|\frac{k}{r_{12}}\right|ba\right) \\ &= \varepsilon_{1s}(a|b)(b|a) + \varepsilon_{1s}(a|b)(b|a) - (a|b)\left(b\left|\frac{k}{r_a}\right|a\right) \\ &\quad - \left(a\left|\frac{k}{r_{1b}}\right|b\right)(b|a) + \left(ab\left|\frac{k}{r_{12}}\right|ba\right) \\ &= 2\varepsilon_{1s}S^2 - 2\left(a\left|\frac{k}{r_b}\right|b\right)S + E, \end{aligned} \tag{7.6.27a}$$

where the last term E is called the *exchange* Coulomb repulsion integral

$$E = \left(ab\left|\frac{k}{r_{12}}\right|ba\right) = \int d\mathbf{x}_1 \int d\mathbf{x}_2\, \alpha^*(\mathbf{x}_1)\beta^*(\mathbf{x}_2)\left(\frac{1}{r_{12}}\right)\beta(\mathbf{x}_1)\alpha(\mathbf{x}_2). \tag{7.6.27b}$$

The nonorthogonal Heitler-London representation is

$$\langle H_{e^2}\rangle_{\mathrm{HL}} = \begin{pmatrix} 2\varepsilon_{1s} - 2\left(a\left|\frac{k}{r_b}\right|a\right) + D & 2\varepsilon_{1s}S^2 - 2\left(a\left|\frac{k}{r_b}\right|b\right)S + E \\ 2\varepsilon_{1s}S^2 - 2\left(a\left|\frac{k}{r_b}\right|b\right)S + E & 2\varepsilon_{1s} - 2\left(a\left|\frac{k}{r_b}\right|a\right) + D \end{pmatrix}$$
$$= \begin{pmatrix} h_a & h_{ab} \\ h_{ab} & h_a \end{pmatrix}. \tag{7.6.28}$$

To convert this matrix to an orthogonal representation we still need to multiply it by an inverse overlap matrix similar to (7.6.12). Only now each S is replaced by S^2. The orthogonal Heitler-London representation is

$$\langle H_{e^2}\rangle_{\mathrm{OHL}} = \frac{\begin{pmatrix} 1 & -S^2 \\ -S^2 & 1 \end{pmatrix}}{1 - S^4}\begin{pmatrix} h_a & h_{ab} \\ h_{ab} & h_a \end{pmatrix}$$
$$= \begin{pmatrix} h_a - S^2 h_{ab} & h_{ab} - S^2 h_a \\ h_{ab} - S^2 h_a & h_a - S^2 h_{ab} \end{pmatrix} \Big/ (1 - S^4). \tag{7.6.29}$$

From C_2 symmetry projection (or direct diagonalization) we obtain a symmetric (g) eigenstate

$$\left|{}^1\Sigma_g^+\right\rangle = \frac{|ab) + |ba)}{\sqrt{2(1 + S^2)}}, \tag{7.6.30a}$$

with eigenvalue

$$E\left({}^1\Sigma_g\right) = \frac{h_a + h_{ab}}{1 + S^2} = 2\varepsilon_{1s} + \frac{-2(a|k/r_b|a) + D - 2(a|k/r_b|b)S + E}{1 + S^2}, \tag{7.6.30b}$$

and an antisymmetric (u) eigenstate

$$\left|{}^3\Sigma_u^+\right\rangle = \frac{|ab) - |ab)}{\sqrt{2(1 - S^2)}}, \tag{7.6.31a}$$

with eigenvalue

$$E(^3\Sigma_u) = \frac{h_a - h_{ab}}{1 - S^2} = 2\varepsilon_{1s} + \frac{-2(a|k/r_b|a) + D + 2(a|k/r_b|b)S - E}{1 - S^2}. \tag{7.6.31b}$$

The notation for singlet ($^1\Sigma$) and triplet ($^3\Sigma$) refers to the Pauli-allowed spin states with spin $S = 0$ and $S = 1$, respectively. (Recall Section 7.1.B.) The uppercase symbols Σ_g^+ and Σ_u^+ label the overall $D_{\infty h}$ symmetry of each electronic orbital.

The energy values (7.6.30b) and (7.6.31b) determine the ordering of singlet ($^1\Sigma_g$) and triplet ($^3\Sigma_g$) according to the relative magnitudes of exchange integral E and overlap factors $2(a|k/r_b|b)S$. The former tends to make the singlet higher than the triplet (as in the $1s2s$ configuration for the He atom), while the latter tends to do the opposite. In H_2 it is the latter which is larger. The Coulomb factor $(a|k/r_b|b)$ plays a decisive role in bonding the molecule H_2 as well as the ion H_2^+. It also guarantees that the ground-state H_2 electronic spin is zero.

The calculation of the two-electron integrals is very complicated even for the simple $(1s)^2$ model. We quote the results tabulated by Atkins:

$$D = \left(ab\left|\frac{k}{r_{12}}\right|ab\right) = \frac{k}{R}\left[1 - \left(1 + \frac{11R}{8} + \frac{3R^2}{4} + \frac{R^3}{3}\right)e^{-2R}\right] \tag{7.6.32a}$$

$$E = \left(ab\left|\frac{k}{r_{12}}\right|ba\right) = \frac{6k}{5R}\left[(\gamma + \ln R)S^2 - T^2E_1(4R) + 2STE_1(2R) - \left(-\frac{25R}{48} + \frac{23R^2}{24} + \frac{R^3}{2} + \frac{R^4}{18}\right)e^{-2R}\right], \tag{7.6.32b}$$

where

$$T = \left[\frac{R^2}{3} - R + 1\right]e^R, \qquad E_1(x) = \int_x^\infty du\,\frac{e^{-u}}{u}$$

and $\gamma = 0.577\ldots$ is the Euler constant. The resulting potential energy has a minimum of about $\Delta E_0 = -0.115$ a.u. at $R_0 = 1.6$ a.u. This is above the experimental value of $\Delta E_0^{\text{exp}} = -0.165$ a.u. and $R_0^{\text{exp}} = 1.4$ a.u. The discrepancy is comparable to that of the H_2^+ ion model and perhaps even a little less.

(c)* H_2: *Improved Valence-Bond Model By including the ionic states $|aa)$ and $|bb)$ one may obtain a more realistic electronic structure model. These states will be particularly important for molecules composed of dissimilar nuclei. The price for improvement is the need to calculate a 4×4 matrix

and its eigensolutions in terms of the basis $\{|aa), |bb), |ab), |ba)\}$. This time we will use a biorthogonal bra basis $\{(AA|, (BB|, (AB|, (BA|\}$ which already contains the inverse overlap matrix. The single particle bras are defined using (7.6.12):

$$(A| = (a|\mathbf{S}^{-1} = \frac{(a| - S(b|}{1 - S^2}, \tag{7.6.33a}$$

$$(B| = (b|\mathbf{S}^{-1} = \frac{(b| - S(a|}{1 - S^2}. \tag{7.6.33b}$$

These satisfy biorthonormality: $(A|a) = 1 = (B|b)$, and $(A|b) = 0 = (B|a)$. From this we get a complete set of biorthonormal two-particle bra states which satisfy $(XY|x'y') = \delta_{Xx'}\delta_{Yy'}$.

$$\begin{aligned}
(AA| &= ((aa| + S^2(bb| - S(ab| - S(ba|)/(1 - S^2)^2,\\
(BB| &= (S^2(aa| + (bb| - S(ab| - S(ba|)/(1 - S^2)^2,\\
(AB| &= (-S(aa| - S(bb| + (ab| + S^2(ba|)/(1 - S^2)^2,\\
(BA| &= (-S(aa| - S(bb| + S^2(ab| + (ba|)/(1 - S^2)^2.
\end{aligned} \tag{7.6.34}$$

$D_{\infty h}$ projection gives us two ionic and two covalent basis states of definite parity, permutational symmetry, and corresponding Pauli-allowed and spin multiplicity. The Young tableau notation on the right in the following denotes permutational symmetry by horizontal arrays of boxes and antisymmetry by vertical arrays.

$$\left|{}^1\Sigma_g^+ \text{ ion}\right\rangle = \frac{|aa) + |bb)}{\sqrt{2}} = \frac{\boxed{a}\boxed{a} + \boxed{b}\boxed{b}}{\sqrt{2}}, \tag{7.6.35a}$$

$$\left|{}^1\Sigma_g^+ \text{ cov}\right\rangle = \frac{|ab) + |ba)}{\sqrt{2}} = \boxed{a}\boxed{b}, \tag{7.6.35b}$$

$$\left|{}^1\Sigma_u^+ \text{ ion}\right\rangle = \frac{|aa) - |bb)}{\sqrt{2}} = \frac{\boxed{a}\boxed{a} - \boxed{b}\boxed{b}}{\sqrt{2}}, \tag{7.6.35c}$$

$$\left|{}^1\Sigma_u^+ \text{ cov}\right\rangle = \frac{|ab) - |ba)}{\sqrt{2}} = \begin{array}{|c|}\hline a \\ \hline b \\ \hline \end{array}. \tag{7.6.35d}$$

The symmetry-defined kets are written the same way using the uppercase-labeled bra $(AA|, \ldots, (BA|$ in place of kets $|aa), \ldots, |ba)$, respectively.

Use of ionic states means more integrals. Still the C_2 symmetry ($a \leftrightarrow b$) of the nuclei and the S_2 permutational symmetry ($1 \leftrightarrow 2$) of the electronic wave

functions reduces the number of different matrix elements to the following five which are derived in the same way as (7.6.26) and (7.6.27):

$$
\begin{aligned}
&(aa|H|aa) = (bb|H|bb) = 2\varepsilon_{1s} - 2A + C,\\
&(aa|H|ab) = (aa|H|ba) = (bb|H|ab) = (bb|H|ba) = 2S\varepsilon_{1s} - SA - B + F,\\
&(aa|H|bb) = (bb|H|aa) = 2S^2\varepsilon_{1s} - 2SB + G,\\
&(ab|H|ab) = (ba|H|ba) = 2\varepsilon_{1s} - 2A + D,\\
&(ab|H|ba) = (ba|H|ab) = 2S^2\varepsilon_{1s} - 2SB + E.
\end{aligned}
\tag{7.6.36}
$$

A set of seven $H_2(1s\sigma)^2$ integrals is listed:

$$
\begin{aligned}
A &= \left(a\left|\frac{k}{r_b}\right|a\right) = \left(b\left|\frac{k}{r_a}\right|b\right), & B &= \left(a\left|\frac{k}{r_b}\right|b\right) = \left(a\left|\frac{k}{r_a}\right|b\right),\\
D &= \left(ab\left|\frac{k}{r_{12}}\right|ab\right) = \left(ba\left|\frac{k}{r_{12}}\right|ba\right), & E &= \left(ab\left|\frac{k}{r_{12}}\right|ba\right) = \left(ba\left|\frac{k}{r_{12}}\right|ab\right),\\
C &= \left(aa\left|\frac{k}{r_{12}}\right|aa\right), & F &= \left(aa\left|\frac{k}{r_{12}}\right|ab\right),\\
G &= \left(aa\left|\frac{k}{r_{12}}\right|bb\right).
\end{aligned}
\tag{7.6.37}
$$

The H_2 Hamiltonian has nonzero matrix elements only between states (7.6.35) which have the same permutational symmetry or spin multiplicity ($2S + 1 = 1$ or 3) and parity (u or g). This leaves a 2×2 matrix involving the first two ${}^1\Sigma_g$ states (7.6.35a) and (7.6.35b) and diagonal elements for ${}^1\Sigma_u$ and ${}^3\Sigma_u$ states. A real symmetric H_2 Hamiltonian has only five independent matrix elements.

Unfortunately, the biorthogonal basis used here does not give a symmetric Hamiltonian. Instead it uses lopsided matrix elements such as the following:

$$
\begin{aligned}
\left\langle {}^3\Sigma_g \,\mathrm{cov}\middle|H\middle|{}^3\Sigma_g \,\mathrm{cov}\right\rangle &= [(AB|H|ab) - (AB|H|ba) - (BA|H|ab)\\
&\qquad + (BA|H|ba)]/2\\
&= (AB|H|ab) - (AB|H|ba)\\
&= 2\varepsilon_{1s} + \frac{-2A + 2SB + D - E}{1 - S^2}.
\end{aligned}
\tag{7.6.38}
$$

When these matrix elements are expanded using (7.6.34) as in the following:

$$
\begin{aligned}
(AB|H|ab) = [&-S(aa|H|ab) - S(bb|H|ab) + (ab|H|ab)\\
&+ S^2(ba|H|ab)]/(1 - S^2)^2,
\end{aligned}
\tag{7.6.39}
$$

a non-Hermitian representation results:

$\lvert {}^1\Sigma_g \text{ ion}\rangle$	$\lvert {}^1\Sigma_g \text{ cov}\rangle$	$\lvert {}^1\Sigma_u \text{ ion}\rangle$	$\lvert {}^3\Sigma_u \text{ cov}\rangle$
$2\varepsilon_{1s} + \dfrac{-2A + 2SB}{(1 - S^2)} + \dfrac{(1 + S^2)(C + G) - 4SF}{(1 - S)^2}$	$\dfrac{-2B + 2SA}{(1 - S^2)} + \dfrac{2(1 + S^2)F - 2S(D + E)}{(1 - S^2)^2}$	0	0
$\dfrac{-2B + 2SA}{(1 - S^2)} + \dfrac{2(1 + S^2)F - 2S(C + G)}{(1 - S^2)^2}$	$2\varepsilon_{1s} + \dfrac{-2A + 2SB}{(1 - S^2)} + \dfrac{(1 + S^2)(D + E) - 4SF}{(1 - S)^2}$	0	0
0	0	$2\varepsilon_{1s} + \dfrac{-2A + 2SB + C - G}{1 - S^2}$	0
	0	0	$2\varepsilon_{1s} + \dfrac{-2A + 2SB + D - E}{1 - S^2}$

(7.6.40)

You might expect the second diagonal matrix element in (7.6.40) to correspond to the Heitler-London eigenvalue (7.6.30b) just as the fourth diagonal element in (7.6.40) equals (7.6.31b). However, the matrix element $\langle {}^1\Sigma_g \text{ cov}|H|{}^1\Sigma_g \text{ cov}\rangle$ in (7.6.40) contains ionic contributions due to the nonorthogonality of our basis. These are not present in (7.6.30b) and so there is no simple correspondence.

(d)* H_2: *Molecular Orbital Model If the preceding discussion makes you uneasy about the use of nonorthogonal valence-bond orbital bases, you may welcome a discussion of molecular orbital bases which are generally orthonormal. The simplest examples of molecular orbital (MO) states are the approximate H_2^+ (7.6.25), which we relabel below.

$$|\sigma_g\rangle = \frac{|a) + |b)}{\sqrt{2(1+S)}}, \qquad |\sigma_u\rangle = \frac{|a) - |b)}{\sqrt{2(1-S)}}. \tag{7.6.41}$$

As long as normalized states $|a)$ and $|b)$ are related by some C_2-like operation $\mathbf{i}$,

$$|b) = \mathbf{i}|a), \qquad |a) = \mathbf{i}|b), \tag{7.6.42}$$

then the MO states will be orthonormal for all values of overlap S with $|S| < 1$. This is guaranteed by the C_2-projection orthogonality ($\mathbf{P}^u\mathbf{P}^g = 0$) as discussed in Chapter 2.

Thus one may choose a variety of trial MO states by redefining $|a)$ or $|b)$. Wave $(\mathbf{x}|a) = \alpha(\mathbf{x})$ may be a polarized mixture of $1s$, $2s$, and $2p$ orbitals, for example, to increase the electronic charge in the overlap region. Or one can simply vary the nuclear charge number Z to fatten $\alpha(x)$ until energy is minimized.

Molecular orbitals are used for heteronuclear diatomic molecules such as LiH or HCI and for polyatomic molecules. XY-diatomic molecular orbitals may have the orthogonal broken-symmetry form

$$|\sigma 1\rangle = \frac{|a) + \lambda|b)}{\sqrt{N_1}}, \qquad |\sigma 2\rangle = \frac{\lambda|a) - |b)}{\sqrt{N_2}}, \tag{7.6.43}$$

where amplitude λ depends on the relative attraction of nucleus X versus that of Y.

Given the MO states (7.5.41) we assume the H_2^+ problem is solved and consider H_2. There are four two-electron MO product states:

$$\left|(\sigma_g)^2\right\rangle = |\sigma_g\rangle|\sigma_g\rangle, \left|(\sigma_u)^2\right\rangle = |\sigma_u\rangle|\sigma_u\rangle, |\sigma_u\sigma_g\rangle = |\sigma_u\rangle|\sigma_g\rangle,$$
$$|\sigma_g\sigma_u\rangle = |\sigma_g\rangle|\sigma_u\rangle. \tag{7.6.44}$$

These are expanded below using (7.6.43) and labeled using standard spectroscopic notation. Permutation symmetrization and antisymmetrization of the latter two are needed to give Pauli-allowed states:

$$\left|{}^1\Sigma_g(\sigma_g)^2\right\rangle = |\sigma_g\rangle|\sigma_g\rangle = [|aa) + |ab) + |ba) + |bb)]/2(1+S), \quad (7.6.45a)$$

$$\left|{}^1\Sigma_g(\sigma_u)^2\right\rangle = |\sigma_u\rangle|\sigma_u\rangle = [|aa) - |ab) - |ba) + |bb)]/2(1-S), \quad (7.6.45b)$$

$$\left|{}^1\Sigma_g\sigma_u\sigma_g\right\rangle = [|\sigma_u\rangle|\sigma_g\rangle + |\sigma_g\rangle|\sigma_u\rangle]/\sqrt{2} = [|aa) - |bb)]/\sqrt{2(1-S^2)}, \quad (7.6.45c)$$

$$\left|{}^3\Sigma_u\sigma_u\sigma_g\right\rangle = [|\sigma_u\rangle|\sigma_g\rangle - |\sigma_g\rangle|\sigma_u\rangle]/\sqrt{2} = [|ab) - |ba)]/\sqrt{2(1-S^2)}. \quad (7.6.45d)$$

They may also be labeled using Young tableau notation to compare with (7.6.35):

$$\left|{}^1\Sigma_g(\sigma_u)^2\right\rangle = \boxed{g|g} = \left(\left[\boxed{a|a} + \boxed{b|b}\right]/\sqrt{2} + \boxed{a|b}\right)/(1+S)\sqrt{2},$$

$$\left|{}^1\Sigma_g(\sigma_u)^2\right\rangle = \boxed{u|u} = \left(\left[\boxed{a|a} + \boxed{b|b}\right]/\sqrt{2} - \boxed{a|b}\right)/(1-S)\sqrt{2},$$

$$\left|{}^1\Sigma_g\sigma_u\sigma_g\right\rangle = \boxed{u|g} = \left(\boxed{a|a} - \boxed{b|b}\right)/\sqrt{2(1-S^2)},$$

$$\left|{}^3\Sigma_u\sigma_u\sigma_g\right\rangle = \begin{array}{|c|}\hline u \\ \hline g \\ \hline \end{array} = \begin{array}{|c|}\hline a \\ \hline b \\ \hline \end{array} \Big/ \sqrt{(1-S^2)}. \quad (7.6.46)$$

A first approximation to MO eigenstates might involve the first $(\sigma_g)^2\ {}^1\Sigma_g$ configuration with two electrons in the lowest σ_g orbital. However, an inspection of (7.6.45a) shows that this state is 50-50 mixture of ionic and covalent base states. This is a well-known weakness of the MO bases. They generally fail to account for electronic correlations, i.e., electrons' tendency to avoid each other. [The Heitler-London approximation erred in the opposite direction by completely ignoring the ionic states $|aa)$ and $|bb)$.]

A better MO approximation is obtained by mixing the $(\sigma_g)^2\ {}^1\Sigma_g$ configuration with others. The H_2 symmetry allows it to mix with $(\sigma_u)^2\ {}^1\Sigma_g$ but not with any of the other configurations listed in (7.6.45). This is a simple example of molecular *configuration interaction* (CI) and involves the eigensolutions of the following Hamiltonian matrix:

$\left\vert {}^1\Sigma_g(\sigma_g)^2\right\rangle$	$\left\vert {}^1\Sigma_g(\sigma_g)^2\right\rangle$	$\left\vert {}^1\Sigma_u\sigma_g\sigma_u\right\rangle$	$\left\vert {}^3\Sigma_u\sigma_g\sigma_u\right\rangle$
$2\varepsilon_{1s} + \dfrac{-2A - 2B}{1+S} + \dfrac{\frac{1}{2}(C+G) + \frac{1}{2}(D+E) + 2F}{(1+S)^2}$	$\dfrac{\frac{1}{2}(C+G) - \frac{1}{2}(D+E)}{(1-S)^2}$	0	0
$\dfrac{\frac{1}{2}(C+G) - \frac{1}{2}(D+E)}{(1-S)^2}$	$2\varepsilon_{1s} + \dfrac{-2A + 2B}{1-S} + \dfrac{\frac{1}{2}(C+G) + \frac{1}{2}(D+E) - 2F}{(1-S)^2}$	0	0
0	0	$2\varepsilon_{1s} + \dfrac{-2A + 2SB + C - G}{1-S^2}$	0
0	0	0	$2\varepsilon_{1s} + \dfrac{-2A + 2SB + D - E}{1-S^2}$

(7.6.47)

To compare the H representation (7.6.47) in the molecular orbital (MO) basis with (7.5.40) in the valence-bond (VB) basis we consider extreme cases. Suppose the ionic Coulomb repulsion integrals C and G of (7.5.37) were so large that all other terms could be neglected. Then we diagonalize the MO submatrix

$$\left\langle H\left({}^1\Sigma_g\right)\right\rangle_{\mathrm{MO}} = \tfrac{1}{2}\begin{pmatrix} \dfrac{C+G}{(1+S)^2} & \dfrac{C+G}{1-S^2} \\ \dfrac{C+G}{1-S^2} & \dfrac{C+G}{(1-S)^2} \end{pmatrix} \qquad (C \text{ and } G \text{ large}) \quad (7.6.48a)$$

to get the following eigenvalues and eigenvectors (not normalized):

$$\begin{aligned} &\mathrm{mo}_1 = 0;\ |\mathrm{mo}_1\rangle = (1+S)\left|(\sigma_g)^2\right\rangle - (1-S)\left|(\sigma_u)^2\right\rangle = [|ab) + |ba)], \\ &\mathrm{mo}_2 = \frac{(C+G)(1+S^2)}{(1+S^2)^2};\ |\mathrm{mo}_2\rangle = (1-S)\left|(\sigma_g)^2\right\rangle + (1+S)\left|(\sigma_u)^2\right\rangle \\ &\quad = [|aa) + |bb)] \end{aligned} \qquad (7.6.48b)$$

The VB covalent state $|{}^1\Sigma_g\,\mathrm{cov}\rangle$ and ionic state $|{}^1\Sigma_g\,\mathrm{ion}\rangle$ show up as eigenvectors. It is reassuring to get the same eigenvalues by diagonalizing the VB submatrix from (7.6.40):

$$\left\langle H\left({}^1\Sigma_g\right)\right\rangle_{\mathrm{VB}} = \begin{pmatrix} \dfrac{(1+S^2)(C+G)}{(1+S^2)^2} & 0 \\ \dfrac{-2S(C+G)}{(1-S^2)^2} & 0 \end{pmatrix} \qquad (C \text{ and } G \text{ large}), \quad (7.6.49a)$$

which gives the following eigensolutions:

$$\begin{aligned} &vb_1 = 0; \qquad |vb_1\rangle = \left|{}^1\Sigma_g\,\mathrm{cov}\right\rangle = \frac{|ab) + |ab)}{\sqrt{2}}, \\ &vb_2 = \frac{(1+S^2)(C+G)}{(1-S^2)^2}; \qquad |vb_2\rangle = (1+S^2)\left|{}^1\Sigma_g\,\mathrm{ion}\right\rangle - 2S\left|{}^1\Sigma_g\,\mathrm{cov}\right\rangle. \end{aligned} \qquad (7.6.49b)$$

The presence of $|{}^1\Sigma_g\,\mathrm{cov}\rangle$ in the second eigenvector is an artifact of the non-Hermitian VB representation.

The opposite extreme would be to have the single-electron integrals A and B of (7.6.37) large enough to ignore the others. Then the MO submatrix in (7.6.47) is diagonal:

$$\left\langle H\left({}^1\Sigma_g\right)\right\rangle_{\mathrm{MO}} = \begin{pmatrix} 2\varepsilon_{1s} - 2\dfrac{A+B}{1+S} & 0 \\ 0 & 2\varepsilon_{1s} - 2\dfrac{A-B}{1-S} \end{pmatrix}. \quad (7.6.50)$$

The eigenvalues are just twice the single-electron potential values (7.6.15a and 7.6.15b) without the nuclear interaction term k/R. The VB submatrix in (7.6.40) gives the same values after diagonalization.

A level correlation diagram between the two extremes is sketched in Figure 7.6.3. The two ${}^1\Sigma_g$ states which are changed by configuration interaction have levels which are drawn as curves. The other two states ${}^1\Sigma_u$ and ${}^3\Sigma_u$ do not change and their levels are indicated by straight lines. The diagram is sketched to show the effects of increasing ionic Coulomb integrals C and G on the left and single-electron integrals A and B on the right. The effect of moderate direct and exchange Coulomb integrals D and E would be to push

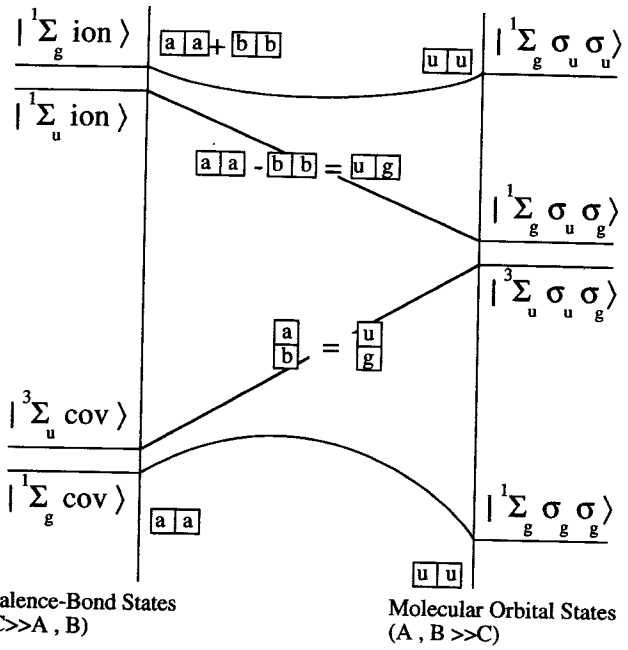

Figure 7.6.3 Sketch of level correlations between valence-bond and molecular orbital bases.

triplet ${}^3\Sigma_u$ below singlet ${}^1\Sigma_u$ on the right. Note, however, that Figure 7.6.3 is just a qualitative sketch and a template for the study of whichever parameters one chooses to vary.

B. How to "Point" Electronic Orbitals

So far we have considered scalar s waves and only sigma (σ or Σ) orbitals which have cylindrical symmetry and no component of angular momentum around the bond axis. To build up bonds for polyatomic molecules one needs to combine p, d, and f waves to make π, δ, and ϕ bonds. While σ bonds are the basic glue for most polyatomic molecules, the π bonds and higher-order waves can be important, as well.

We will explain the general method using an example of the octahedral SF_6 molecule discussed in Chapter 4. We will show how to make six equivalent orthogonal orbitals that point along the C_4 symmetric axes of an octahedron. We will apply the subgroup correlation and induced representation theory of Sections 4.2 and 4.3 and the orbital level splitting or crystal field theory of Sections 5.6 and 7.3*C*.

First we consider how some of the simplest s and p orbitals can make polyatomic molecular bonds or ligands.

(a) Elementary $s^n p^m$ Bonds The simplest orbitals which "point" are the p orbitals $\{p_x, p_y, p_z\}$. They span the real vector representation R^1 of $R(3)$ [recall (5.6.19)]:

$$\langle \mathbf{r}|p_x\rangle = \frac{-Y_1^1 + Y_{-1}^1}{\sqrt{2}} r\sqrt{\frac{4\pi}{3}}, \qquad \langle \mathbf{r}|p_y\rangle = i\frac{Y_1^1 - Y_{-1}^1}{\sqrt{2}} r\sqrt{\frac{4\pi}{3}},$$
$$= x, \qquad = y,$$
$$\langle \mathbf{r}|p_z\rangle = Y_0^1 r\sqrt{\frac{4\pi}{3}},$$
$$= z. \tag{7.6.51}$$

A combination wave function of the form

$$\chi(\mathbf{r}) = a_0\langle \mathbf{r}|s\rangle + a_x\langle \mathbf{r}|p_x\rangle + a_y\langle \mathbf{r}|p_y\rangle + a_z\langle \mathbf{r}|p_z\rangle \tag{7.6.52}$$

is a wave with a "finger" or *ligand* which points at an atom with coordinates (a_x, a_y, a_z). The relative amount a_0 of the scalar s wave $\langle r|s\rangle = Y_0^0 f(r)$ determines the degree of polarization or pointing and can be used to adjust normalization and orthogonality with other waves.

A famous example of a set of hybrid molecular orbitals based on (7.6.52) is the set of methane (CH_4) σ bonds which point from carbon to the H atoms located at tetrahedral points (1, 1, 1) (1, −1, −1), (−1, 1, −1), and

$(-1, -1, 1)$, respectively, which form T_d symmetry (recall Figure 4.1.5):

$$\begin{aligned}
|C_1\rangle &= \big(|s\rangle + |p_x\rangle + |p_y\rangle + |p_z\rangle\big)/2,\\
|C_2\rangle &= \big(|s\rangle + |p_x\rangle - |p_y\rangle - |p_z\rangle\big)/2,\\
|C_3\rangle &= \big(|s\rangle - |p_x\rangle + |p_y\rangle - |p_z\rangle\big)/2,\\
|C_4\rangle &= \big(|s\rangle - |p_x\rangle - |p_y\rangle + |p_z\rangle\big)/2.
\end{aligned} \tag{7.6.53}$$

This is called the sp^3 hybrid set, since one part $|s\rangle$ and three parts $|p\rangle$ are used to make each state. Carbon's ground configuration is $2s^2 2p^2$. (Recall Figure 7.1.2.) To make states (7.6.53), one $2s$ electron must be moved to a $2p$ orbit. The $2s$-$2p$ energy increase is made up by reduced electronic Coulomb repulsion and localization in order for CH_4 to be stable.

The simplest planar bonding orbitals for H_2O and other XY_2 molecules have the following hybrid form:

$$\begin{aligned}
|X_1\rangle &= \lambda|s\rangle + a\cos\phi|p_x\rangle + a\sin\phi|p_y\rangle,\\
|X_2\rangle &= \lambda|s\rangle + a\cos\phi|p_x\rangle - a\sin\phi|p_y\rangle,\\
|X_3\rangle &= \lambda'|s\rangle - a'|p_x\rangle.
\end{aligned} \tag{7.6.54}$$

This gives two bonds at angle $\pm\phi$ with the x axis and a third pointing along the $-x$ axis. For the first two to be orthonormal we must have

$$\lambda^2 + a^2 = 1, \qquad \lambda^2 + a^2\cos^2\phi - a^2\sin^2\phi = 0.$$

Solving gives

$$a^2\sin^2\phi = \frac{\sin^2\phi}{1-\cos 2\phi} = \frac{1}{2}, \qquad \lambda^2 = 1 - a^2 = \frac{\cos 2\phi}{\cos 2\phi - 1}. \tag{7.6.55}$$

The angle 2ϕ between the first two bonds must be at least $90°$ in order for the solutions to be useful. At $2\phi = 90°$ there are two orthogonal p waves and no s-wave admixture ($a = 1$, $\lambda = 0$). The third wave must satisfy the following to be orthogonal to the other two:

$$\lambda' = \sqrt{\frac{1+\cos 2\phi}{1-\cos 2\phi}}, \qquad a' = -\sqrt{2}\lambda = -\sqrt{\frac{-2\cos 2\phi}{1-\cos 2\phi}}. \tag{7.6.56}$$

For a molecule with bond angle $2\phi = 90°$ we have only two vector ligands and a separate orthogonal scalar wave. We indicate these states in the following using notation $(s^{\lambda^2}p^{a^2})$, where the exponents are the probabilities

for each orbital:

$$|X_1(p^1)\rangle = \frac{1}{\sqrt{2}}|p_x\rangle + \frac{1}{\sqrt{2}}|p_y\rangle,$$

$$|X_2(p^1)\rangle = \frac{1}{\sqrt{2}}|p_x\rangle - \frac{1}{\sqrt{2}}|p_y\rangle,$$

$$|X_3(s^1)\rangle = |s\rangle. \tag{7.6.57}$$

The atomic configuration for these states is $|x_1 p\rangle$, $|x_2 p\rangle$, and $|x_3 s\rangle$. The third wave is 100% s.

For a molecule with bond angle $2\phi = 120°$ we have three equivalently polarized ligands which could form a C_{3v} symmetric bonding. Each of these is a balanced sp^2 atomic configuration:

$$|X_1(s^{1/3}p^{2/3})\rangle = \frac{1}{\sqrt{3}}|s\rangle + \frac{1}{\sqrt{6}}|p_x\rangle + \frac{1}{\sqrt{2}}|p_y\rangle,$$

$$|X_2(s^{1/3}p^{2/3})\rangle = \frac{1}{\sqrt{3}}|s\rangle + \frac{1}{\sqrt{6}}|p_x\rangle - \frac{1}{\sqrt{2}}|p_y\rangle,$$

$$|X_3(s^{1/3}p^{2/3})\rangle = \frac{1}{\sqrt{3}}|s\rangle - \frac{2}{\sqrt{6}}|p_x\rangle. \tag{7.6.58}$$

Finally, a T-shaped molecule with bond angle $2\phi = 180°$ could use the following sp, sp, and p configurations.

$$|X_1(s^{1/2}p^{1/2})\rangle = \frac{1}{\sqrt{2}}|s\rangle + \frac{1}{\sqrt{2}}|p_y\rangle,$$

$$|X_2(s^{1/2}p^{1/2})\rangle = \frac{1}{\sqrt{2}}|s\rangle - \frac{1}{\sqrt{2}}|p_y\rangle,$$

$$|X_3(p^1)\rangle = -|p_x\rangle. \tag{7.6.59}$$

Now the third wave is 100% p.

Let us see how an XY_2 molecule like H_2O might be bonded. We will put one electron in each of the X_1 and X_2 states so each may form a σ-pair bond with an electron from one of the Y atoms. We will put two electrons in the X_3 state to make an inert ^1S pair since it will not be used for bonding. This is called a "lone pair." There is another lone pair composed of the third p_z orbital perpendicular to the xy plane which we have ignored. (It is used for π bonding in molecules like ethylene and acetylene.) This soaks up a pair

of electrons, too. So the atomic orbital configuration needed is the following:

$$x_1x_2x_3^2p_z^2 = (s^{\lambda^2}p^{a^2})(s^{\lambda^2}p^{a^2})(s^{2\lambda'^2}p^{2a'^2})p^2$$
$$= s^{2\lambda^2+2\lambda'^2}p^{2a^2+2a'^2+2}. \tag{7.6.60}$$

We use (7.6.55) and (7.6.56) to give the exponents in terms of the bonding angle 2ϕ:

$$x_1x_2x_3^2p_z^2 = s^{2/(1-\cos 2\phi)}p^{(4-6\cos 2\phi)/(1-\cos 2\phi)}$$
$$= \begin{cases} s^2p^4, & \text{for } 2\phi = 90°, \\ s^1p^5, & \text{for } 2\phi = 180°. \end{cases} \tag{7.6.61}$$

Atomic oxygen has a ground configuration of s^2p^4. If it stayed that way for H_2O the water bonding angle would be 90° instead of the observed 104°. The observed value corresponds to a bonding configuration of $s^{1.61}p^{4.39}$. Apparently, H_2O gains more energy by increasing its bond angle than it loses by raising 20% of the $2s$ population into a $2p$ orbital.

(b) π Bonds An example which appears to use the sp^2 model bond states (7.6.58) is the ethylene molecule C_2H_4 sketched in Figure 7.6.4(a). The angle between adjacent H atoms is close to 120°. However, C_2H_4 has additional stability due to the overlap between carbon "lone-pair" p orbitals perpendicular to each CH_2 plane. Their overlap is greatest when the CH_2 triangles are aligned. This gives a torsional stability to the complex which the $\sigma(sp_x)$ bond could never supply. The bond formed by an adjacent parallel p orbitals is called a π bond.

In the linear molecule C_2H_2 (acetylene) sketched in Figure 7.6.4(b) both transverse p orbitals participate in π bonds. These together with the $\sigma(sp)$ orbitals form what is called a triple bond.

The 120° sp^2 bonding combined with π bonds plays a role in quite a number of hydrocarbons. First among these are the *trans* and *cis* structures of butadiene C_4H_6 shown in Figure 7.6.5(a) and 7.6.5(b) and the well-known benzene molecule C_6H_6 shown in Figure 7.6.5(c). The structural pictures are generally drawn with the double bond localized between alternating pairs of carbon atoms. In fact, the π bonds tend to be delocalized and spread out over the carbon chains. This is called *conjugation* of π bonds and provides additional stability to the hydrocarbons.

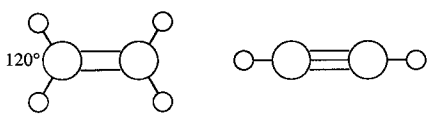

(a) C_2H_4 (b) C_2H_2

Figure 7.6.4 Examples of sp^2 bonding (a) Ethylene, (b) acetylene.

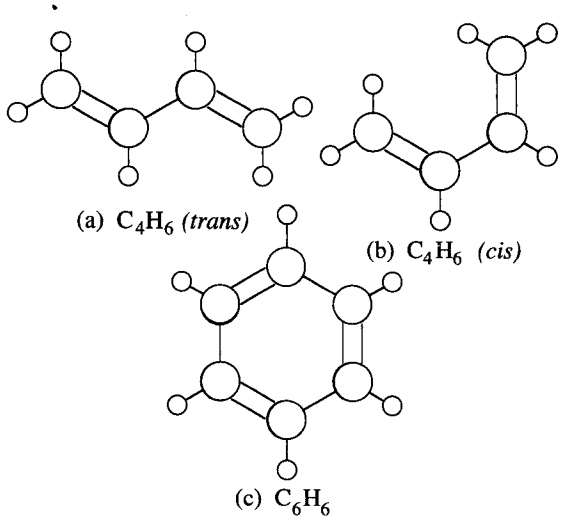

Figure 7.6.5 More examples of sp^2 bonding (a) *trans*-butadiene, (b) *cis*-butadiene, and (c) Benzene.

The increase in stability can be estimated using the Hückel model of conjugated bonds. The Hückel approximation uses a basis of n equivalent π orbitals; one on each of the n C atoms. The Hamiltonian is assumed to have only diagonal matrix elements and off-diagonal matrix elements between nearest-neighbor carbons only. The diagonal matrix elements are all equal to H and off-diagonal matrix elements equal to $-S$. This is precisely the form of the C_n symmetric tunneling problem discussed in Section 2.12 [recall (2.12.23)] and again in Section 3.6 (recall Figure 3.6.5).

For C_6H_6 the symmetry is $C_6 \subset C_{6v} \subset D_{6h}$ and the energy levels are given by (2.12.25), which is now repeated:

$$\varepsilon_k = H - 2S \cos k_n \left(k_n = \frac{2\pi k}{n}; k = 0, \pm 1, \ldots, \leq \frac{n}{2} \right).$$

The π levels labeled A_1, E_1, E_2, B_1 have energies

$$\begin{aligned} \varepsilon_0^{A_1} &= H - 2S, \\ \varepsilon_1^{E_1} &= H - S, \\ \varepsilon_2^{E_2} &= H + S, \\ \varepsilon_3^{B_1} &= H + 2S. \end{aligned}$$

Given one electron for each π bond the orbitals will take one spin ($\uparrow \downarrow$) pair in A_1 and two pairs in E_1 for a total energy of $2(H - 2S) + 4(H - S) = H - 8S$. If the bonds had been three localized double bonds (recall Figure 7.6.5) the energy would be $6H - 6S$, so the conjugation gains $2S$ of stability.

The butadiene π orbitals can be modeled in the same way using a trick discussed in Problem 2.7.4. n-equivalent atoms in an open chain can be imagined to occupy one side of a $2n + 2$-member closed ring. [The n standing sine wave solutions will be eigensolutions of the n-atom chain.] The four butadiene π orbitals will use the middle four levels of a C_{10} symmetric ring.

$$\varepsilon^{E_1} = H - 2S\cos(2\pi/10) = H - S(1 + \sqrt{5})/2,$$
$$\varepsilon^{E_2} = H - 2S\cos(4\pi/10) = H - S(\sqrt{5} - 1)/2,$$
$$\varepsilon^{E_3} = H - 2S\cos(6\pi/10) = H + S(\sqrt{5} - 1)/2,$$
$$\varepsilon^{E_4} = H - 2S\cos(8\pi/10) = H + S(1 + \sqrt{5})/2.$$

One $\uparrow\downarrow$ pair of electrons goes in each of the lowest two states E_1 and E_2. (Neither level is degenerate now since only sine waves are allowed.) This yields an energy of $4H - 2\sqrt{5}\,S$. Two pairs of localized π bonds would have had energy $4H - 4S$ so the conjugated bonds are $(2\sqrt{5} - 4)S = 0.047S$ better.

(c) Octahedral Bonding The s and p waves can bond no more than four atoms to a central one. Molecules like XY_6 need higher-order waves. We discuss some general symmetry techniques for setting up complex bonding configurations.

The local symmetry of each bond is the first thing to consider. If we desire to place bonds along each tetragonal (C_4) axis of octahedron then C_4 or C_{4v} is the relevant local symmetry group. If we desire σ bonds then their local symmetry belongs to the 0_4 irrep of C_4 or $A' = A_1$ irrep of C_{4v}. Since σ bonds are axially symmetric they belong to the scalar irreps.

If we need to install a pair of $\pi_{\pm 1}$ bonds on each C_4 axis then we would use the $1_4 \oplus 3_4$ irreps of C_4 or the E irrep of C_{4v} to locally label each wave state. The π pair of p_x and p_y transform like x and y bases of the E irrep of C_{4v}.

Next we use the induced representation bases to label the set of equivalent orthonormal bond states that we imagine exist on each C_4 axis. The σ bonds span a six-dimensional $0_4 \uparrow O$ representation induced to octahedral group O or $A' \uparrow O_h$. The π bonds span a 12-dimensional $(1_4 \oplus 3_4)\uparrow O$ or $E \uparrow O_h$ representation.

According to the Frobenius reciprocity theorem described in Section 4.3C the columns of the $C_4 \subset O$ or $C_{4v} \subset O_h$ correlation tables give the octahedral irreps that belong to each induced representation. The first (0_4) column of the table of (4.2.42b) gives

$$0_4 \uparrow O = A_1 \oplus T_1 \oplus E, \tag{7.6.62a}$$

and this is corroborated by the first A' column of (4.2.46c):

$$A' \uparrow O_h = A_{1g} \oplus T_{1u} \oplus E_g. \tag{7.6.62b}$$

The latter includes the inversion-parity labels for the three O_h symmetry species that comprise an XY_6 σ-bonding model.

A π-bonding model of XY_6 would involve the $E \uparrow O_h$ states in the last column of (4.2.46c):

$$E \uparrow O_h = T_{1g} \oplus T_{2g} \oplus T_{1u} \oplus T_{2u}. \tag{7.6.63}$$

The O_h parity labels are particularly important here to distinguish pairs of O irreps.

The final step is the correlation of whichever O_h species we just found with angular-momentum states J^p and the corresponding $O(3)$ species. The columns of (5.6.5b) provide an infinite set of all the atomic orbital states that could possibly contribute to the bonding orbital in question:

$$\begin{aligned}
(A_{1g} \text{ of } O_h) \uparrow O(3) &= O^+ \oplus 4^+ \oplus 6^+ \oplus \cdots = s_g \oplus g_g \oplus i_g \oplus \cdots, \\
(T_{1u} \text{ of } O_h) \uparrow O(3) &= 1^- \oplus 3^- \oplus 2(5^-) \oplus \cdots = p_u \oplus f_u \oplus 2h_u \oplus \cdots, \\
(E_g \text{ of } O_h) \uparrow O(3) &= 2^+ \oplus 4^+ \oplus 6^+ \oplus \cdots = d_g \oplus g_g \oplus i_g \oplus \cdots.
\end{aligned} \tag{7.6.64}$$

As a first approximation we take only the first contributions for each species. In this case we make the singlet A_{1g} using an s wave, the triplet T_{1u} using three p_u waves, and the doublet E_g using two d_g waves. That will be an sp^3d^2 atomic configuration of six octahedrally coordinated ligand orbitals. Later you may find it desirable to "sharpen up" the p ligands with an f_u^3 or h_u^3 configuration, or add some g_g to the s_g and d_g states. If so, the correlation table tells what will work.

The calculation of the states in the octahedral sp^3d^2 configuration follows the steps outlined. The induced representation is labeled and reduced according to Sections 4.3.A and 4.3.B. The resulting A_1 state (4.3.20), E states (4.3.22), and (4.3.23), and T_1 states (4.3.27a)–(4.3.27c) are tabulated backwards so as to give the desired six ligand states $\{|1\rangle, \ldots, |6\rangle\}$

$$\begin{aligned}
|1\rangle &= \frac{1}{\sqrt{6}}|A_1\rangle + \frac{1}{\sqrt{3}}|E,1\rangle + \frac{1}{\sqrt{2}}|T_1,z\rangle, \\
|2\rangle &= \frac{1}{\sqrt{6}}|A_1\rangle + \frac{1}{\sqrt{3}}|E,1\rangle - \frac{1}{\sqrt{2}}|T_1,z\rangle, \\
|3\rangle &= \frac{1}{\sqrt{6}}|A_1\rangle - \frac{1}{2\sqrt{3}}|E,1\rangle + \frac{1}{2}|E,2\rangle + \frac{1}{\sqrt{2}}|T_1,x\rangle, \\
|4\rangle &= \frac{1}{\sqrt{6}}|A_1\rangle - \frac{1}{2\sqrt{3}}|E,1\rangle + \frac{1}{2}|E,2\rangle - \frac{1}{\sqrt{2}}|T_1,x\rangle, \\
|5\rangle &= \frac{1}{\sqrt{6}}|A_1\rangle - \frac{1}{2\sqrt{3}}|E,1\rangle - \frac{1}{2}|E,2\rangle + \frac{1}{\sqrt{2}}|T_1,y\rangle, \\
|6\rangle &= \frac{1}{\sqrt{6}}|A_1\rangle - \frac{1}{2\sqrt{3}}|E,1\rangle - \frac{1}{2}|E,2\rangle - \frac{1}{\sqrt{2}}|T_1,y\rangle.
\end{aligned} \tag{7.6.65}$$

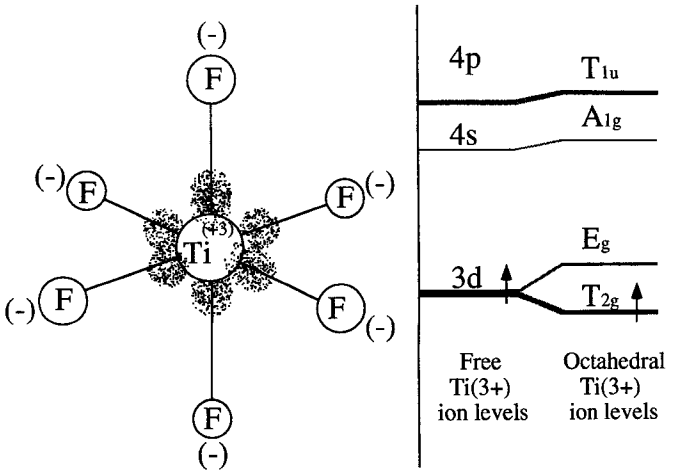

Figure 7.6.6 Octahedral crystal field splitting of 3d level of Ti^{3+} ion.

Finally, one approximates each A_1, E, or T_1 state using combinations of atomic orbitals allowed by correlations such as (7.6.64). For the simplest sp^3d^2 configuration we use combinations as derived in Section 5.6; see (5.6.15d) and (5.6.15e) for E states and the p-orbital relations (7.5.51):

$$
\begin{aligned}
|A_1\rangle &= |s_0^0\rangle, \\
|E,1\rangle &= |d_0^2\rangle = \big(2|d_{z^2}\rangle - |d_{x^2}\rangle - |d_{y^2}\rangle\big)/\sqrt{6}, \\
|E,2\rangle &= \big(|d_2^2\rangle + |d_{-2}^2\rangle/\sqrt{2} = \big(|d_{x^2}\rangle - |d_{y^2}\rangle\big)/\sqrt{2}, \\
|T_1,x\rangle &= \big(-|p_1^1\rangle + |p_{-1}^1\rangle\big)/\sqrt{2} = |p_x\rangle, \\
|T_1,y\rangle &= \big(i|p_1^1\rangle - i|p_{-1}^1\rangle\big)/\sqrt{2} = |p_y\rangle, \\
|T_1,y\rangle &= |p_0^1\rangle = |p_z\rangle.
\end{aligned}
$$

For an example of octahedral electronic structure theory we consider a $[Ti^{3+}(Ion^-)_6]$ ionic complex. The Ti atom has a $3d^24s^2$ valence configuration so the ion Ti^{3+} has a single d electron. Suppose it is surrounded by an octahedron of negatively charged ions as in Figure 7.6.6.

If the electrons on the negative ions do not overlap appreciably with the Ti d electron we imagine that latter undergoes a crystal field splitting as described in Section 5.6 (recall Figure 5.6.3). This would be a ground-state spin doublet and orbital triple configuration of $^2t_{2g}$ as shown on the right-hand side of Figure 7.6.6. The magnitude of this splitting was calculated in Section 7.3 [recall (7.3.28)].

If there is electronic overlap, as indeed there must be if the complex is bound, then a more sophisticated molecular orbital picture is needed. This is

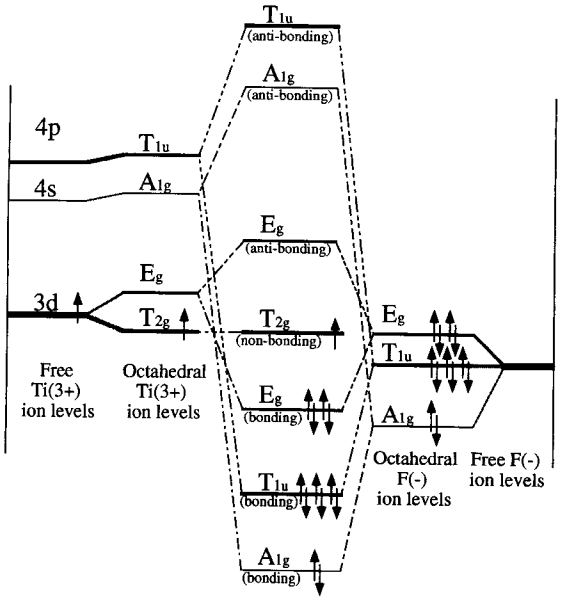

Figure 7.6.7 Bonding and antibonding molecular orbital levels for $[TiF_6]^{3+}$ complex.

sketched in Figure 7.6.7. Here we imagine a coupling between certain combinations of the six σ orbitals and the Ti atomic orbitals of the same symmetry. The six σ orbitals span the induced representation $A' \uparrow O_h = A_{1g} \oplus T_{1u} \oplus E_g$ discussed in the preceding section. Each state from the latter interacts with the nearest Ti level belonging to the same irrep to form a pair of bonding and antibonding orbitals.

Six ($\uparrow \downarrow$) pairs of electrons are needed to give the most stable σ bonding arrangement. If another electron is available it would go in the T_{2g} nonbonding level. From there it could be excited to the antibonding orbitals E_g, A_{1g} of T_{1u} which lie above it. In this sense the picture in Figure 7.6.7 is qualitatively similar to the one in Figure 7.6.6, which neglects the bonding altogether. Inclusion of the electronic bonding structure is necessary to predict the optical and magnetic properties of these complexes.

ADDITIONAL READING

Most of the references given at the end of Chapter 5 treat angular momentum Clebsch-Gordon coefficients and the Wigner-Eckart theorem. In addition there is a well-known text which introduces the idea of the irreducible density operators.

U. Fano and G. Racah, *Irreducible Tensorial Sets* (Academic, New York, 1959).

The derivation of raising and lowering operator matrix elements is the main recurring problem in applied representation theory. The following are a few references that involve $O(n)$ and $U(n)$.

I. M. Gelfand and M. L. Zetlin, *Dokl. Akad. Nauk USSR*, **71**, 101 (1950).

J. D. Louck and L. C. Biedenharn *J. Math. Phys.*, **11** 2368 (1970).

J. C. Nagel and M. Moshinsky, *J. Math. Phys.*, **6**, 682 (1965).

A. Bincer, *J. Math. Phys.*, **19**, 1173 (1978); **18**, 1870 (1977).

Tables in Clebsch-Gordon coefficients in the Wigner $3j$ form and Racah coefficients in the 6-j form are given in Rotenburg et al. from $J_1 \otimes J_2 = \frac{1}{2} \otimes \frac{1}{2}$ up to $8 \otimes 8$.

M. Rotenburg, R. Bivens, N. Metropolis, and J. K. Wooten, *The 3-j and G-j Symbols* (Technology Press, MIT, 1959).

This book usually is out of print. It is probably better to have coefficients of this sort directly available on your own computer. They can be found fairly easily in numerical or algebraic form in various packages of the *Mathematica* program which is now widely available. (See also W. J. Thompson, Computers in Physics **7**, 144 (1993).)

S. Wolfram, *Mathematica: A System for Doing Mathematics by Computer* (Addison-Wesley, Redwood City, CA, 1991).

The asymptotic behavior of Clebsch-Gordon coefficients is explained in the following paper.

K. Schulten and R. G. Gordon, *J. Math. Phys.*, **16**, 1961 (1975).

The first application of Racah tensor analysis to fine spectral structure of methane (CH_4) was by K. T. Hecht and Moret-Bailly.

K. T. Hecht, *J. Mol. Spetrosc.*, **5**, 355 (1960).

J. Moret-Bailly, *Cah. Phys.*, **15**, 237 (1961); *Cah. Phys.*, **178**, 253 (1965).

The first observation of extraordinary tensor eigenvalue degeneracy or clustering involved computer studies of fourth and sixth rank cubic crystal field operators

K. R. Lea, M. J. M. Leask, and W. P. Wolf, *J. Phys. Chem. Solids*, **23**, 1381 (1962).

Computer studies of CH_4 eigenvalues and forbidden transitions to rotational states lead to the next discovery of clustering and the first molecular examples.

A. J. Dorney and J. K. G. Watson, *J. Mol. Spectrosc.*, **42**, 1 (1972).

The most extensive numerical study of tensor eigenvalues and clustering phenomena was published by Fox, Galbraith, Krohn, and Louck.

K. Fox, H. W. Galbraith, B. J. Krohn, and J. D. Louck, *Phys. Rev. A*, **15**, 1363 (1977).

This in turn lead to a semiclassical and quantum mechanical theory for clusters and their superfine structure.

W. G. Harter and C. W. Patterson, *Phys. Rev. Let.*, **38**, 244 (1977).

W. G. Harter and C. W. Patterson, *J. Chem. Phys.*, **66**, 4872 (1977).

C. W. Patterson and W. G. Harter, *J. Chem. Phys.*, **66**, 4866 (1977).

The RE surface picture of the rotor dynamics and spectral structure was developed later. It was first applied to the levels of combined fourth- and sixth-rank tensors of cubic symmetry.

W. G. Harter and C. W. Patterson, *J. Math. Phys.*, **20**, 1453 (1979).

The semiclassical theory of RE surfaces is introduced in the following papers.

W. G. Harter, *Phys. Rev. A*, **24**, 192 (1981).

W. G. Harter and C. W. Patterson, *J. Chem. Phys.*, **80**, 4241 (1984).

A more recent review of semiclassical rotor mechanics and RE surface applications is the following.

W. G. Harter, *Computer Phys. Reps.*, **8**, 319 (1988).

Experimental observations of molecular fine structure, superfine structure, and hyperfine structure were done by developing unique spectroscopic instruments and laser devices.

CH_4:

A. S. Pine, *J. Opt. Soc. Am.*, **66**, 97 (1976).

C_8H_8:

A. S. Pine, A. G. Maki, A. G. Robiette, B. J. Krohn, J. K. G. Watson, and Th. Urbanek, *J. Am. Chem. Soc.*, **106**, 891 (1984).

SF_6:

J. P. Aldridge, H. Filip, H. Flicker, R.f. Holland, R. S. McDowell, N. G. Nereson, and K. Fox, *J. Mol. Spectrosc.*, **58**, 165 (1975).

R. S. McDowell, H. W. Galbraith, C. D. Cantrell, N. G. Nereson, and E. D. Hinkley, *J. Mol. Spectrosc.*, **68**, 288 (1977).

K. C. Kim, W. P. Person, D. Seitz, and B. J. Krohn, *J. Mol. Spectrosc.*, **76**, 322 (1979).

J. Bordé and Ch. J. Bordé, *Chem. Phys.*, **71**, 417 (1982).

The following are recent references which treat the rotor-oscillator analogy and related applications of R(3)-SU(2) coordinates.

W. G. Harter and N. dos Santos, *Am. J. Phys.*, **46**, 251 (1978).

M. E. Kellman, *J. Chem. Phys.*, **76**, 4528 (1982); *J. Chem. Phys.*, **83**, 3843 (1985); *Chem. Phys. Lett.*, **113**, 489 (1985).

K. K. Lehmann, *J. Chem. Phys.*, **79**, 1098 (1983).

W. G. Harter, *J. Chem. Phys.*, **85**, 5560 (1986).

Z. Li, L. Xiao, and M. E. Kellman, *J. Chem. Phys.*, **92**, 2251 (1990).

Two of the original papers on SU(2)-R(3) spin vector models are the following:

I. I. Rabi, N. F. Ramsey, and J. Schwinger, *Rev. Mod. Phys*, **26**, 167 (1954).

R. P. Feynman, F. l. Vernon Jr., and R. W. Hellwarth, *J. Appl. Phys.*, **28**, 49 (1957).

The following are original works on spinors, quaternions, and applications to optics:

W. R. Hamilton, *Lecture on Quaternions* (Dublin, 1853).

G. Stokes, *Proc. Soc. London*, **11**, 547 (1862).

H. Poincaré, *Theorie Mathematique de la Lumiere* (Gauthiers Villars, Paris, 1892).

There is a computer program which demonstrates the U(2)-R(3) analysis of oscillators and polarization states.

W. G. Harter, Color U(2): A Study of Classical and Quantum Resonance Phenomena, Department of Physics, University of Arkansas, Fayettevile, AR 72701.

Development of U(2) vibrational analysis as part of the vibron model is described in the following papers.

O. S. van Roosmalen, F. Iachello, I. Benjamin, R. D. Levine, and A. E. L. Dieperinh, *J. Chem. Phys.*, **79**, 2515 (1983).

O. S. van Roosmalen, I. Benjamin and R. D. Levine, *J. Chem. Phys.*, **81**, 5986 (1984).

The following article reviews the applications of semiclassical geometry and RE surfaces to other problems such as atomic diamagnetism.

T. Uzer, D. Farrelly, J. A. Milligan, P. E. Raines, and J. P. Skelton, *Science*, **253**, 42 (1991).

One of the most readable introductions to molecular electronic orbital theory is by Atkins. More advanced references are contained therein.

P. W. Atkins, *Molecular Quantum Mechanics*, 2nd edition (Oxford University Press, Oxford and New York, 1983).